Progress in Energy and Combustion Science 36 (2010) 444–509

Contents lists available at ScienceDirect

Progress in Energy and Combustion Science

journal homepage: www.elsevier.com/locate/pecs

Modeling of biomass gasification in fluidized bed

A. Gómez-Barea [a,*], B. Leckner [b]

[a] Bioenergy Group, Chemical and Environmental Engineering Department, Escuela Superior de Ingenieros, University of Seville, Camino de los Descubrimientos s/n, 41092 Seville, Spain
[b] Department of Energy and Environment, Chalmers University of Technology, S-412 96 Göteborg, Sweden

ARTICLE INFO

Article history:
Received 8 May 2009
Accepted 2 December 2009
Available online 17 March 2010

Keywords:
Gasification
Fluidized bed
Modeling
Fluidization
Simulation
Review

ABSTRACT

Modeling of biomass gasification in bubbling and circulating fluidized bed (FB) gasifiers is reviewed. Approaches applied for reactor modeling, from black-box models to computational fluid-dynamic models, are described. Special attention is paid to comprehensive fluidization models, where semi-empirical correlations are used to simplify the fluid-dynamics. The conversion of single fuel particles, char, and gas is examined in detail. The most relevant phenomena to be considered in modeling of FB biomass gasifiers are outlined, and the need for further investigation is identified. An updated survey of published mathematical reactor models for biomass and waste gasification in FB is presented. The overall conclusion is that most of the FB biomass gasification models fit reasonably well experiments selected for validation, despite the various formulations and input data. However, there are few measurements available for comparison with detailed model results. Also, validation of models with data from full-scale FB biomass gasification units remains to be done.

Contents

* Corresponding author. Tel.: +34 95 4487223; fax: +34 95 4461775.
E-mail address: agomezbarea@esi.us.es (A. Gómez-Barea).

0360-1285/$ – see front matter © 2010 Elsevier Ltd. All rights reserved.
doi:10.1016/j.pecs.2009.12.002

1. Introduction

Gasification is an important route for conversion of wastes and biomass materials to useful gaseous products: fuel gas for direct firing in thermal applications, such as kilns and boilers, co-firing in existing coal-fired boilers, gas for engines, turbines and fuel cells generating electricity, as well as raw gas for production of fuels or chemicals [1]. Gasification of biomass and waste in fluidized bed offers advantages, since fluidized beds are capable of being scaled up to medium and large scale, overcoming limitations found in smaller scale, fixed-bed designs [2]. On the other hand, the bed temperature is limited in order to avoid bed agglomeration and the gasification efficiency of a fluidized bed (FB) may be limited if part of the fuel energy remains in unconverted char. Also, if the temperature is not high enough in the gasifier, the tar in the product gas can make the process unsuitable from a technical and economical point of view [3].

Models can be helpful for gasifier design, for prediction of operation behavior and emissions during normal conditions, start-up, shutdown, change of fuel and load, and to alleviate the type of problems mentioned above. The modeling may be undertaken with different aims: the field of interest ranges from preliminary design of an industrial process to complex simulation of a unit. Experiments, especially at large scale, are often expensive and complicated; modeling can save time and money, and it can support preparation and optimization of experiments to be undertaken in a real system. The tools available for modeling of FB gasifier (FBG) reactors are the more or less simplified equations for conservation of mass, energy and momentum, complemented by boundary conditions, constitutive relationships, and terms expressing the sources and sinks of the system. To determine the latter, rate laws for the conversion processes are needed, chemical as well as physical. Thermodynamic data are useful for estimation of properties and thermal data as well as reaction products by equilibrium assumptions.

1.1. Existing surveys

There is a great amount of reviews on modeling of thermochemical fuel conversion. Most of this literature is focused on the behavior of particles: pyrolysis, combustion and gasification of coal [4–14] and specifically on biomass [15–17]. In contrast, only a few reviews have been devoted to survey gasification in FB on the reactor level and not many deal with biomass gasification in FB [24–29]. Most available reviews of this type are oriented towards coal combustion in fixed and/or fluidized beds [4,18–24] and coal gasification in FB [24–28].

There are many similarities between modeling of combustion and gasification in FB, for instance, in fluid-dynamics, devolatilization, oxidation of volatiles, and in char conversion and

Notations

A pre-exponential factor, units see tables; area, m^2
A_m area per unit of mass, m^2/kg
a_b area to volume ratio in a bubble, m^{-1}
a decay constant, clustering-flow, m^{-1}; ash content of fuel, kg ashes/kg fuel fed; coefficients
Ar Archimedes number, –
b geometry coefficient: 0 for flat plate, 1 for cylinder, 2 for sphere; combustible content of fuel, kg combustibles/kg fuel fed
Bi_m Biot modulus for mass transport, $Bi = h_m R/D_{eff}$, –
Bi_h Biot modulus for heat transport, $Bi = hR/\lambda_{eff}$, –
c concentration, $kmol/m^3$
c_p specific heat, kJ/(kg K)
C dimensionless concentration, –
D diffusion or dispersion coefficient, m^2/s
D_t diameter of the bottom bed, m
d_b bubble size, m
d_p solid particle size, m
Da Damköhler number (see Table 6 for definitions), –
Dr drying number, –
Pe Péclet number Pe = ReSc, –
$E_{a/py}$ activation energy, activation energy of pyrolysis, kJ/kmol
E_∞ Elutriation rate (elutriation flux above the transport disengaging height), $kg/(m^2\ s)$
F mass flow rate, kg/s
$F(),f()$ functions
f dimensionless factor in Table 2, –; mass exchange term, $kg/(m^3\ s)$
f_{bex} bed expansion factor, –
g acceleration of gravity, m/s^2
g_o stoichiometric flue gas from complete combustion, kg gas/kg combustibles
G mass flux, $kg/(m^2\ s)$
H riser height, m; specific enthalpy, kJ/kg
H_x height of the bottom zone, m
H_u lower heating value kJ/kg
h vertical coordinate, m; heat transfer coefficient, $kW/m^2\ K$; specific enthalpy, kJ/kg
h_m solid-to-gas mass transfer coefficient, m/s
h_{b-e} bubble to emulsion heat transfer coefficient, $kW/(m^2\ K)$
k_{b-e} bubble to emulsion mass transfer coefficient, s^{-1}
k_b back-flow ratio, –; transfer coefficient, –
k_f fragmentation constant, s^{-1}
k kinetic coefficient, various units
K decay constant in transport zone, m^{-1}; reaction coefficient, Table 10; permeability m^2;
K_{att} attrition constant, –
L_e equivalent length, m
ℓ_o stoichiometric oxygen demand, kg oxygen/kg combustibles
m mass, kg; class of particle, –
MM molecular mass, kg/kmol
n number, –; order of reaction, –
Nu Nusselt number, $Nu = hx_o/\lambda_g$, –
N_t number of holes in distributor
p pressure, Pa ; distribution function
P fragmentation probability, –
Pr Prandtl number, $Pr = \mu_g/\rho_g\alpha_g$, –
q heat rate, kW/m^3
Q_{loss} heat loss rate, kW
R Radius, m; gas constant, 8315 J/(kmol K) = 8.315 kJ/(kmol K) = 8.315×10^{-3} kJ/(mol K)
$R_{j,i}$ rate of reaction of species i in reaction j, $kmol/(m^3\ s)$
$R_{py/hi/he/dry}$ rate of pyrolysis, internal heating, external heating and drying, s^{-1}
$\Re$ reaction rate for a size class m,l, kg/s
r rate of reaction, $kg/(m^3\ s)$
$r_{m/A/v}$ char reactivity per unit of mass (s^{-1}), surface ($kg/(m^2\ s)$) or volume ($kg/(m^3\ s)$)
$r_{gg,i}$ net rate of production of i in gas-gas reactions per unit of gas volume, $kg/(m^3 s)$
$r_{gs,m,i}$ net rate of production of i in gas-solid reactions per unit of k-solid volume, $kg/(m^3 s)$
$r_{m,p}$ char reactivity per unit of mass of a single particle, s^{-1}
$r_{m,e/s}$ char reactivity per unit of mass of a single particle evaluated at emulsion/surface, s^{-1}
$r_{m,e0}$ initial char reactivity per unit of mass of a single particle evaluated at emulsion, s^{-1}
Re Reynolds number, $u_g\ x_o\rho_g/\mu_g$, –
$Re_{p,mf/t}$ particle Reynolds number at mf or terminal velocity, $u_{mf/t}\ d_p\rho_g/\mu_g$, –
Sc Schmidt number, $Sc = \mu_g/\rho_g D_g$, –
S source of a transported property per unit of volume, unit of transported property/$(m^3\ s)$
Sh Sherwood number of species i, $Sh = h_m x_o/D_{gi}$, –
T temperature, K
t time, s
$\boldsymbol{U}$ dimensionless velocity, –
U_w overall bed to surroundings heat transfer coefficient, $W/(m^2\ K)$
u, $\mathbf{u}$ velocity, m/s
w moisture content of fuel, kg moisture/kg fuel fed
V volume, m^3
x_0 characteristic length, m
x mass fraction, kg/kg
x_{py} degree of pyrolysis conversion, kg/kg
X dimensionless size, –; mass concentration, –; local conversion, –
Y volume concentration, –

Greek letter

α thermal diffusivity, m^2/s; coefficient, –
$\Gamma_{m,l}$ rate of attrition of particle m from at level l, kg/s
Δu velocity difference, m/s
δ coefficient, –
ε volume concentration or porosity, m^3/m^3
ζ distribution coefficient,-
η efficiency, –; effectiveness factor, –
θ dimensionless temperature;–
Φ conversion function, –
Λ gravimetric stoichiometric coefficient, –
λ thermal conductivity, kW/(mK); air ratio, amount of air burned/stoichiometric air;–
ν stoichiometric coefficient,–; dynamic viscosity, kg $(s\ m)^{-1}$; coefficients in Table 7;
$\nu_{i,j}$ stoichiometric coefficient of i species in reaction j
ξ part of fuel, kg fuel/kg fuel converted
ρ mass concentration or density, $kg\ m^{-3}$
σ_m volume fraction occupied by solids m, m^3/m^3; factor, –
τ time, s
$\tau_{Rf/ch}$ residence time of the fuel/char in the reactor, s

ϕ	particle sphericity, –
φ	transported property; gas produced by gasification of char, kg gas/kg char; shrinkage factor, –
Ψ	factor accounting for particle–particle interaction, –; coefficient Eq. (104), -; parameter in Table 9, –
Ω	factor, –

Subscripts

A	related to surface
a	active
av	average
B	bottom zone, bed (bottom bed)
b	bubble, back-flow, burned
bex	bed expansion
b–e	bubble–emulsion
br	rising bubble
b-w	bed-wall
c-w	core-wall
c	core, carbon (char)
ch	char
dev	devolatilization
e	emulsion, external, equivalent
ev	evaporation
eff	effective
ent	entrainment
ext	external
exp	experimental
fs	feed stream
F	freeboard
f	fuel
g	gas
g–g	gas–gas
g–s	gas–solid
h	horizontal, radial, thermal
H	horizontal
he	external heating
hi	internal heating
in	inlet, entering the system, inert
i	species, internal
j	counter
k	phase
int	intrinsic
l	particle size level of a particle size distribution
lg	light gases
m	type of solid, mass transfer
mf	minimum fluidization
ng	net (gas) flow
0	reference value, initial, at the top of the riser ($h = H_0$), superficial
out	outlet, leaving the system
rec	recycling stream
p	solid particle
py	pyrolysis, volatiles
r	reaction
s	solid, surface
sep	separator
sp	species
SRMR	steam reforming of methane
v	vertical, visible (applied to velocity and flow), volume
V	vertical
t	terminal (applied to velocity), tar
T	total
th	throughflow
u	unburned
w	wall, water (moisture)
X_m	limiting moisture content
x	at bed surface (height of bottom zone)
∞	above the transport disengaging heigth, at bulk conditions

Abbreviations

Abbreviations related to specific aspects are found in Tables 1 and 9, and in Fig. 18, and are not repeated here.)

BBM	black-box model
BFB	bubbling fluidized bed
BFBG	bubbling fluidized bed gasifier
CFB	circulating fluidized bed
CFBG	circulating fluidized bed gasifier
CFDM	computational fluid-dynamic model
FB	fluidized bed
FBG	fluidized bed gasifier/gasification
FBBG	fluidized bed biomass gasifier
FM	fluidization model
ID	inner diameter
HM	Hamel's model
SSM	Souza-Santos model
TGA	thermo-gravimetric analyzer
WGSR	water–gas shift reaction

comminution processes. With caution, therefore, most of the modeling elements from FB combustor models can be utilized in models of FB biomass gasification (FBBG). There are differences, though, such as in the mode of conversion of the char particles and in the amount of heat transferred to surfaces.

Despite the different physical and chemical properties of biomass and coal, there are no conceptual differences between the fuels with respect to model structure and mathematical description of the process [25]. However, once the model structure is set, there are a number of processes and parameter values that have to be obtained for the specific fuel: composition of volatiles, fuel reactivity and others. Essentially, biomass fuels have a higher portion of oxygen and volatiles (and sometimes, water), and the nature of the ash differs substantially from that of coal. The ash may have a strong impact on the operation of an FB gasifier, because agglomeration and sintering of bed material have to be avoided. In conclusion, the elements of the mathematical description of coal gasification in FB are transferable, with some caution, to biomass.

Different types of model can be developed, from complex non-isothermal, three-dimensional models, taking the fluid dynamics and thermal behavior of the FB into account, to simpler black-box or zero-dimension models, where mass and heat balances are made over the entire gasifier to predict gas composition. In some cases, especially when detailed information is required, the solution of a model is carried out by computational fluid-dynamics (CFD) techniques. The choice of a model depends on the objectives and the experimental information available. Advanced models are, in principle, more useful, since the information obtained from them is wider. However, this is only true if reasonable and realistic input data are available. Otherwise, simpler models could be appropriate for application if one is aware of their limitations. In some cases, black-box models with some empirical constraints are enough for preliminary predictions. Models of this type are, for example, those based on equilibrium relationships complemented by experimental correlations: the so-called pseudo-equilibrium models [30].

1.2. Types of gasifier

There are three types of gasifier: fixed or moving bed, fluidized bed, and entrained flow. Among these designs there are variations, such as spouted bed, draught tube, internally circulating fluidized bed gasifier, etc.

The fixed-bed designs are basically updraft (countercurrent) or down-draft (cocurrent). In updraft gasifiers, the fuel bed moves downwards and the gasification agent flows from the bottom upwards (updraft). As the gas leaves the reactor near the pyrolysis zone, the gas generated in updraft gasifiers has a high content of organic components (tar). The solid carbon in the fuel is almost completely converted into gas and tar. Updraft gasifiers can be used for wet fuels and are relatively insensitive to the fuel size. On the other hand, in cocurrent gasifiers, the fuel and gasification agent flow in the same direction and the gas leaves the reactor near the hottest zone, which makes the tar concentration much lower than in updraft gasifiers. The maximum size of these units is limited to a few MW fuel power because of the problem of maintaining a regular conversion front in a wide fixed bed.

Fluidized bed gasifiers have a number of advantages over fixed beds, especially with regard to mixing, reaction rates, and the possibility of being built in sizes far above those of fixed-bed gasifiers. The two types, bubbling (BFBG) and circulating (CFBG), differ in the sense that the latter type is always built with recirculation of particles. Recycling of fines leads to a greater efficiency of carbon conversion by increasing the residence time of particles. It is a generic solution that can be applied even if the bed is called a bubbling bed gasifier, as demonstrated, for example, by the high temperature Winkler process for lignite gasification [31]. Fig. 1 shows the main characteristics of the two types of FBG that will be analyzed in this work. CFBG is taller and provided with a continuous solids recycling system for re-injection of particles into the bed (particle separator, return leg and seal). CFBG operates with higher superficial velocities, typically in the range of 2–5 m/s, whereas the velocity in the BFBG is only 0.5–2 m/s, maintaining the ratio of fuel-to-fluidization gas. Therefore, for the same cross-section, the gasifier is fed with higher fuel flow rate in a CFBG than in a BFBG. The entrainment of material from the bottom bed and the recycling in CFBG increase the solids flow as well as the gas–solids contact time in the freeboard.

For large-scale systems (>400 MW_{th}), the entrained-flow gasifier with liquid ash removal is an attractive alternative. This is because the high temperature employed allows production of a gas that is almost free from tar with nearly complete carbon conversion, thus removing the two main drawbacks of FBG systems [32]. In addition, the usually lower melting point of biomass ash makes slagging operation possible at lower temperature, keeping the oxidant demand low compared to entrained-flow gasification of coal. However, there are a few drawbacks associated with processing of biomass in this application: the difficulties of economical particle size reduction of some biomasses and the corrosion of the reactor lining caused by the aggressive nature of molten slag from biomass. Furthermore, there are inherent limitations in size of equipment caused by restrictions in the quantities of biomass that can be delivered to a plant [33]. These reasons have prevented the introduction of entrained-flow gasification for biomass up to date. As a result, it seems that in the short term, most processes for biomass and waste gasification at medium and large scale will use FB designs [33].

The gasification concepts can be grouped into two approaches, depending on the way the heat for gasification is provided to the gasifier: autothermal and allothermal gasification. In autothermal or direct gasification, the heat is released by partial oxidation of the fuel in the gasifier itself. The partial oxidation can be carried out using air or oxygen. Steam can also be added to these oxidants. Air gasification produces a low heating value gas (4–7 MJ/Nm^3) suitable for nearby boiler, engine or turbine operation. Oxygen gasification produces a medium heating value gas (10–18 MJ/Nm^3) suitable for pipeline distribution and as a basis for synthesis of liquid biofuels. Allothermal or indirect gasification uses steam as gasification agent and obtains the heat necessary for gasification from a source outside of gasifier itself. This concept allows generating gas of medium heating value (14–18 MJ/Nm^3), rich in hydrogen, without the need for oxygen.

There are two concepts of indirect gasification, depending on whether heat is supplied from internal or external sources. Fig. 2a shows a scheme that illustrates three ways of supplying heat to the gasifier in indirect gasification: by external heat or by internal recirculation of gas and char. In external indirect gasification, the heat is delivered from an external source like in plasma or solar

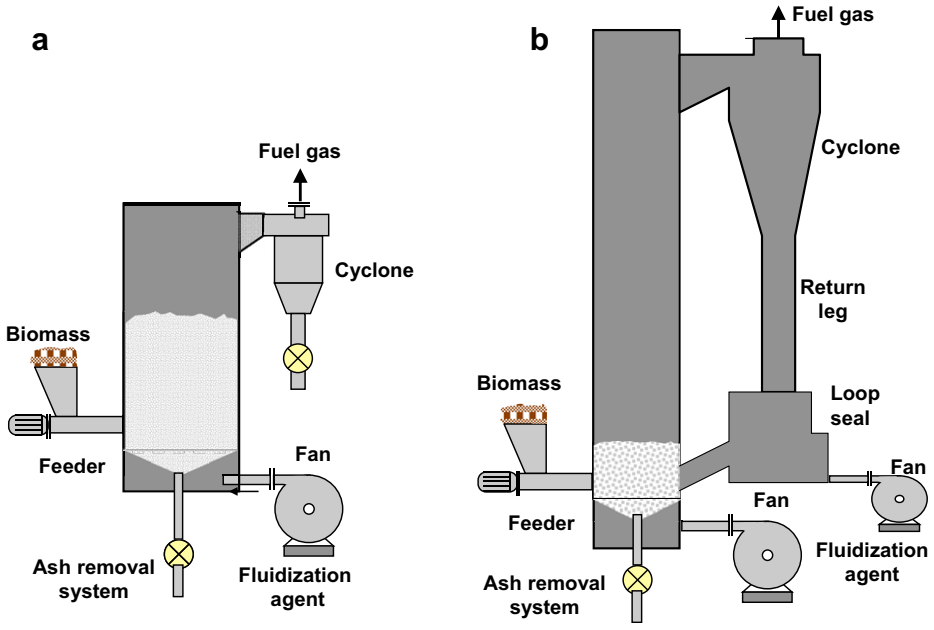

Fig. 1. The two types of FBG: (a) Bubbling FBG; (b) Circulating FBG.

gasification. In indirect internal gasifiers, the energy originates from the process itself. Indirect internal gasifiers are grouped as char-indirect gasifiers and gas-indirect gasifiers, depending on the type of internal energy source: char or gas, as indicated by the recirculation streams in Fig. 2a. A char-indirect gasifier (Fig. 2b) consists of two separate reactors: an FB steam devolatilizer that produces the product gas and an FB combustor that burns the residual char to provide heat for the drying and devolatilization. Bed material is circulated between the two reactors to transfer heat to the gasification. In a gas-indirect gasifier the heat is provided by recirculation of a fraction of the combustible gas. The hot combustion products are led through heat transfer tubes in the bed of the gasifier. External indirect gasification has not been commercially interesting, probably due to the economic limitations and technical problems related to erosion of the heat-transfer tubes. In contrast, indirect internal char gasifiers are currently offered commercially [34,35]. They have proven good performance and scalability, producing a gas of up to 18 MJ/Nm^3 with high proportion of hydrogen. Internal recirculation of gas is sometimes made in gasifiers (whether direct or indirect), to maintain the bed temperature when the fuel moisture is high. However, it seems not to be feasible to recirculate gas to maintain the overall process autothermal.

1.3. Conversion processes

A gasifying biomass particle undergoes a series of conversion processes: initially drying and devolatilization, subsequently oxidation of volatiles and char, and finally, char gasification by carbon dioxide and steam. Fuel particles are affected by shrinkage and primary fragmentation, occurring immediately after injection of the fuel particles into the bed as a consequence of thermal stresses and internal pressures caused by the release of volatiles. Secondary and percolative fragmentation and attrition of char particles take place together with char conversion. The movements in the bed distribute the char and the devolatilizing fuel particles throughout the bed, establishing a gas environment where these solids are converted. Fig. 3 presents a description of the processes occurring in an FBBG.

There are, at least, two levels of description in the analysis of fuel conversion in an FB: the particle and the reactor levels. Fig. 3 presents schematically the processes, further treated below, that should be included in the mathematical description, identifying the level of observation at which each process occurs: the bed level with its bubble and emulsion phases, the particle level with release of gases and gasification of char, and, finally, the gas phase reactions where the water–gas shift reaction plays an important role. Some processes strongly interact between one level and another. For instance, the heat and mass transport to a particle occurs on the particle level, but their rates are determined by the fluid-dynamics of the bed (reactor level) and by the fuel reactivity, both in case of devolatilization and char conversion. These processes are included in the source terms of the conservation equations and are treated by submodels during execution of numerical calculations. The description on the particle level includes particle size and biomass properties, such as density and thermal conductivity. These parameters affect the time of devolatilization and composition of volatiles [17]. On the reactor level various factors are considered: residence time (mass inventory in an FB), boundary conditions, like fuel feed points and feed rate, freeboard size, fluidization velocity, and their effects on solids elutriation, solids and gas mixing, segregation, etc. [24].

The two levels of description are connected by the boundary conditions for heat, mass and species transport. The heat-transfer coefficient establishes the heating rate of the solid particles, the rate of volatiles release, the yields of char, tar and gas, and the composition of the product gas. Different heat-transfer coefficients are found when biomass is top-fed or fed in-bed, due to the different environments under which devolatilization takes places [36]. The movement of a solid particle in an FB depends on mixing and segregation caused by the fluid-dynamics of the bed. In the typical case of FBBG, the presence of large biomass particles in a sand-like bed, may lead to segregation of (flotsam) particles in the (jetsam-rich) system [37,38]. The importance of an intermediate level, the so-called meso-scale, to obtain reliable prediction of the fluid-dynamics in multiphase reactors has been demonstrated [39], but this level of description is out of the scope of the present work.

1.4. Types of reactor model

Any comprehensive model of fuel conversion in FB is based on a description of the gas–solid processes, occurring inside the reactor, by applying mass, species, heat, and momentum balances, including formulation of the source and sink terms, boundary conditions and constitutive relationships for each phase [7,40]. An overall impression from existing modeling work is the complexity of the processes of biomass gasification in FB. A great number

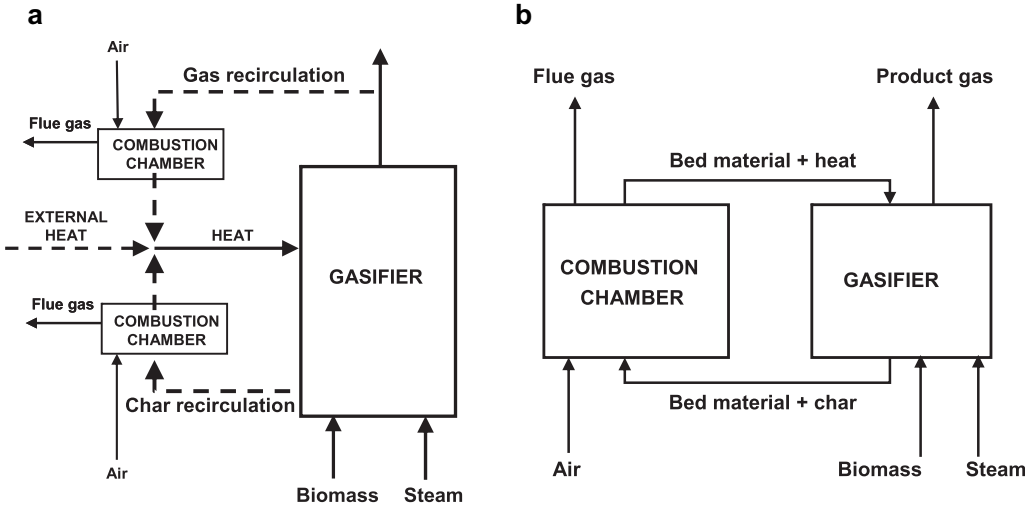

Fig. 2. (a) Indirect gasification indicating the three options to supply heat to the gasifier: internally (by gas and char burning) and externally (by external supply of heat). (b) Example of indirect internal gasifier where the heat is generated by char burning.

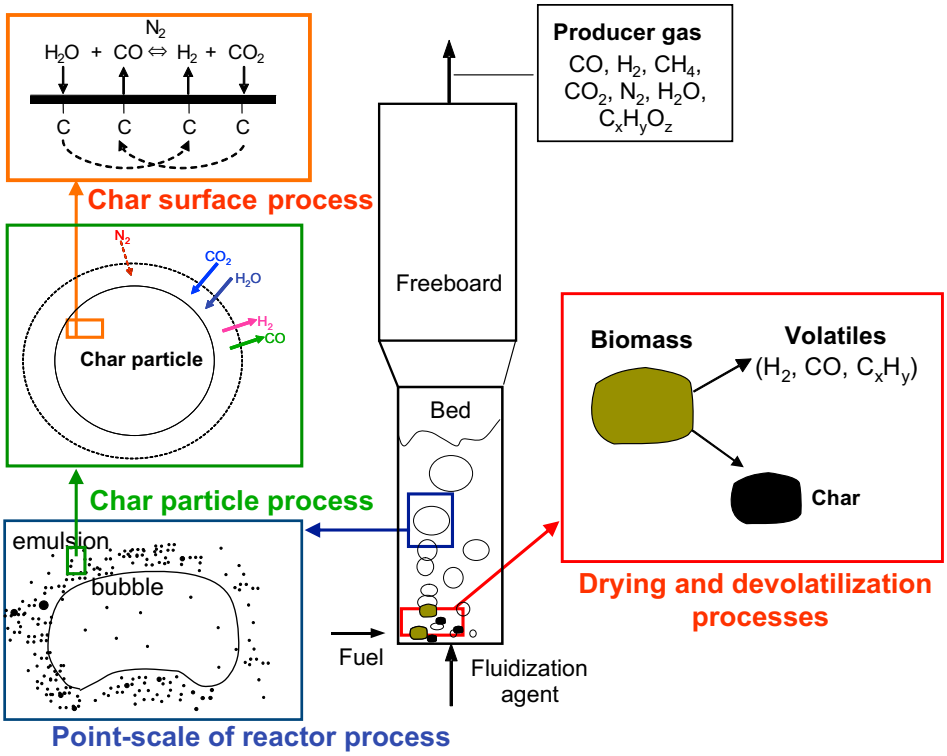

Fig. 3. Description of processes in an FBBG.

of interacting chemical and physical processes take place simultaneously. As a consequence, rigorous analysis of an FB gasifier is a problem of considerable theoretical and computational difficulty. Therefore, it is unlikely that a fundamental, universal model to represent and simulate all types of FBBG will be established in the near future [10,27]. In modeling FBG, simplifications have to be introduced to obtain reasonable and tractable models. An understanding of the processes may lead to the development of semi-empirical models for specific sets of conditions. Judicious identification of the governing phenomena in order to establish reasonable simplifications is a key task in modeling of FBG.

The closest representation of the real process is a balance on the transported variables formulated and solved for each phase k (gas and solids and their i components): density, momentum, and enthalpy (ρ_k, $\rho_{k,i}$, u_k, and h_k, in general terms, φ). The balance of the conserved variables φ over a fixed element (eulerian formulation) of reactor volume can be written in the following form (somewhat simplified, especially in the case of momentum), applicable to any reactor type: the accumulation of φ is due to the net difference between the rates of change by convection and dispersion and to generation and consumption, S, per unit volume:

$$\frac{\partial \varphi_k}{\partial t} + \mathrm{div}(\mathbf{u}_k \varphi_k) = \mathrm{div}(D_{\varphi_k} \mathrm{grad}\varphi_k) + S_{\varphi,k} \quad (1)$$

The boundary conditions for mass, species, and enthalpy include fuel feed points, gas inlet ports, and non-permeability of the reactor walls. For momentum, the formulation is more complex [40], but the boundary conditions are essentially the velocities of gas and particles at the boundaries of the computational domain. More complete and detailed mathematical formulations of the conservation equations for gas–solid flows can be found in the literature [40,41].

The solution of a mathematical model of an FBG like that in Eq. (1), requires long time and is numerically complex. Often, semi-empirical closure laws are formulated, depending on the approach. Sometimes the turbulence of the gas phase is included, but the averaging of Eq. (1) leads to extra terms that have to be described by a turbulence model. In multiphase flows, such as in the freeboard of an FBG, the k–ε model has been used, but the degree of uncertainty is high [22,42]. In addition, the boundary conditions and the source terms are coupled to models of single particle conversion, themselves being a complex mass and heat diffusion-reaction process.

Many models have been published with different names, classifications and categories depending on the purpose. In Table 1 three groups of model are sorted according to the simplification adopted to solve the fluid-dynamics: Computational fluid-dynamics models (CFDM), fluidization models (FM) and black-box models (BBM). CFDM solves Eq. (1), making certain hypotheses for the interaction between the phases. Many of the potentially interesting CFD models (LES, DFM, …) have not been applied to FBBG. FM directly assumes that the bed consists of various phases (most often two) or regions with a predefined topology allowing transport of mass and heat between them. The momentum equation is not solved, and the fluid-dynamic pattern is described by semi-empirical correlations, establishing the dynamics of bubbles and particles in the bed, which give proper closures for chemical reactor modeling. Finally, BBM consist of overall balances over the FBG. In some cases equilibrium is assumed, whilst empirical relationships are used in other occasions. Each of the three model categories includes several models, as indicated in Table 1. FM is the best developed model up to date for FBG, consisting of a comprehensive theoretical treatment, linked with experimental observations made during the last five decades. CFD for FBG are relatively new, and in spite of offering promising expectation, much has to be added. Finally, BBM are quite useful in some cases, but the treatment is limited and the prediction capability is lower than that of FM and CFDM. Because of the considerable computational times required for CFD computations, especially when chemical reactions are involved, FM are still the most common approach.

Table 1
Main three approaches of modeling FBBG.

Name and abbreviation	Essential/Concept	Results	Advantages	Disadvantages	Types of models using this approach
Computational Fluid-Dynamic Models (CFDM)	- Momentum equation is explicitly solved - Constitutive relations and closure laws are adopted	- Detailed information of the fields in the reactor	- Useful for exploring hardware details	- Time consuming solution - Uncertainty of parameters in closure relations	DNS: Direct Numerical Simulation LES: Large Eddy Simulation DPM: Discrete Particle M TFM: Two-Fluid M EEM: Eulerian–Eulerian M ELM: Eulerian–Lagrangian M LLM: Lagrangian-Lagrangian M
Fluidization Models (FM)	- Two phases are treated: emulsion and bubble, whose topology is assumed - The momentum equation is not solved but semi-empirical relations describe gas and solid flow patterns	- Profiles of solid and gaseous species, and temperature - In some cases detailed information is obtained but less than for CFDM because of limitations due to assumed gas and solids flow patterns	- A compromise of precision and numerical complication. - Often sufficient for engineering application	- The flow structure is assumed. Limited to the range of applicability of the correlations used - Although flow details can be explained, it is not generally appropriate for hardware design	DHM: Davidson–Harrison M KLM: Kunii–Levenspiel M BEM: Bubble assemblage M CCBMM: Counter-current backmixing M
Black-Box Models (BBM)	- Overall mass and heat balance - Only global models	Amount of gas and composition of gas produced and its heating value	- Very easy to use - Few inputs	- Description is crude - No description of the process inside the reactor	HMBM: Heat and mass balance M EM: Equilibrium M TM: Thermodynamic M PEM: Pesudo-equilibrium MZM: Zone M

1.5. Scope of this work

The purpose of this work is to review reactor modeling of solid–fuel gasification in FB with special emphasis on biomass and waste materials. Modeling of bubbling and circulating FB is discussed, and methods for calculation of the fluid-dynamics and reaction processes are presented. Due to the uncertainty of the complex processes simple methods are emphasized. The focus is on comprehensive fluidization models, where semi-empirical correlations represent the fluid-dynamics. Prediction of performance by black-box models, applying simple methods, is reviewed, and their prediction ability is discussed. The computational fluid-dynamic tools applied to biomass gasification in FB are also included. Despite their increasing importance to predict the detailed behavior of chemical reactors, only a few trials have been reported to simulate FBBG. As a consequence, CFD models are only briefly surveyed here. The main chapters are devoted to modeling of reactor and source terms. A survey of published FB models for biomass and waste gasification is discussed to assess the state-of the art and identify the main topics where further research is needed. The work emphasizes the prediction of the performance of an FBBG in terms of gas composition, solid conversion and gasification efficiency. Modeling of processes, such as sintering or agglomeration, emissions of contaminants, is out of the scope of this review.

2. Reactor modeling for FBBG

2.1. Fluidization models (FM)

Most comprehensive models published in connection to FBG belong to category FM (Table 1). The reason is that FM is a compromise between BBM and CFDM: FM avoids the details of complex gas–solid dynamics but still maintains the fluid-dynamic effects by assuming a multiphase pattern in the bed. This is done by introducing two (sometimes three) regions or phases. The flow pattern of the regions is described by semi-empirical correlations. The term "phase" differs from the merely thermodynamic meaning. It is just a region with a predefined configuration (particle concentration, state of gas and solids mixing, etc). Most common FM for FBG are 1D models, but 3D models [43] also fit into this category. Therefore, no matter if the FM is formulated in one, two or three dimensions, it still needs input from fluid-dynamic knowledge computed by 'external' correlations.

Early models treated FB reactors as if the gas and solids were mixed, avoiding the multiphase nature of the bed. Classical methods of reaction engineering were applied: from the simplest completely-stirred and plug-flow reactors, to those modeling non-ideal flow and the state of micro-mixing, and further, to those accounting for a residence time distribution obtained by tracer experiments. After these first modeling efforts, it was verified experimentally that the concept of 'contact time distribution' (as a refinement of the simpler gas residence time) is a key factor for taking into account the contact time of the gas with the solid reactant [44,45]. Then, the need for a multiphase description of the process was recognized, leading to the time of effective contact in an FB. The two-phase theory of fluidization [46] made this possible. In two-phase reactor models there is a division between an emulsion and a bubble phase. In the original FM, the emulsion was assumed to contain some gas and all the solids; the gas and particles were perfectly mixed in this phase, whereas the gas phase was considered to be in plug-flow. The momentum balance is not explicitly solved, but Davidson's model [47] is used together with further semi-empirical relationships and further assumptions to estimate the division of gas flow between the phases, the fraction occupied by bubbles in the bed, the porosity and velocity of gas in the dense

phase, and the velocity and size of the bubbles (some of them are included in Table 2 and will be discussed below). The flow pattern obtained allows determination of the transport rates of heat and mass to the reacting particles and the degree of gas and solid mixing. Modifications and simplifications have been introduced over the last decades by applying FM to various reaction systems. Reviews on this matter have been published [4,26,29,44,45,48–52].

Often FB reactor models are classified by the names of the authors: Davidson–Harrison (DHM) [47], Kunii–Levenspiel (KLM) [44], but also by the main features of the model, Kato and Wen (Bubble assemblage model, BAM) [53], Fryer and Potter (Countercurrent Backmixing Model, CCBMM) [54], etc. We do not find, however, fundamental differences between one model and another; all of them are based on the estimation of the essentials of fluid-dynamics (bubble velocity and diameter, fraction of bubbles in the bed, velocity of gas in emulsion, etc) applying similar correlations. Despite minor differences, all models just mentioned are categorized in Table 1 as FM.

Originally, FM were formulated and applied to catalytic systems. For non-catalytic systems, such as solid–fuel conversion, the solid reactant is constantly consumed and solids make-up is required for steady-state operation. At any instant, the reactor contains particles that have spent different times inside the bed, having a distribution of conversion. During the course of reaction, the solid reactant in the particles is gradually affected by the operating conditions of the bed, and the density and size of the particles change from one particle-size fraction to another, depending on the concentration of the solid reactant within the particles [55,56]. The original KL model was applied for FBG of coal [57,58], the DHM has been applied (with minor modifications) up to date in most of FB coal [59–66] and biomass [67,68] gasification models. The CCBMM has been applied recently [69] to describe the movement of char in a bubbling FBBG. Despite the successful application of FM in the modeling of FBG systems, the pseudo-empirical nature of the description of the fluid-dynamics makes this approach difficult to extrapolate to conditions that differ from those where the correlations were obtained, mostly the type of solid particles, superficial velocity, and reactor diameter.

In order to focus attention on the model structure, a selection of basic fluidization concepts are presented separately in Table 2. This table contains expressions on bubble properties, critical fluidization velocities, emulsion characteristics, such as voidages, and particle elutriation rates. The quantities are further explained in the text where they are used. More information on these fluidization quantities is found in the works referred to and in the fluidization literature, for example [4,44,45,47,51], etc.

2.2. Mixing and reaction in FBBG

Fig. 4 presents typical flow patterns in FBG units, bubbling or circulating. The image shows groups of particles ascending in the suspended flow and denser wall layers flowing down, as observed in circulating beds but also to some extent in the freeboard of bubbling beds. The bottom bed is a bubbling fluidized bed, also observed in circulating systems. Graph (b) shows quantitatively the concentration of solids in different parts of a reactor. Two main zones are distinguished in both FB types: a bottom zone and a freeboard (or riser, in the CFB case). The bottom bed is a bubbling fluidized bed. The freeboard is a more dilute zone, where the solids are carried away upwards from the bed. There is a splash region between the two zones characterized by the return of the solids that were thrown up from the bed's surface. The flow structure in the freeboard is not qualitatively different in the two cases, so the sketches in Fig. 4 can represent both.

The performance of FBG, including the efficiency of carbon conversion and the tar content of the gas, may greatly depend on the movement of solids and gas in bed and freeboard. For instance, in a pilot CFB biomass gasifier, reactor conditions resulting in lack of contact between char/oxygen and tar/catalyst and an unfavorable consumption of oxygen by the devolatilization gases were identified [70]. This leads to lower char conversion and higher tar content in the product gas. Modeling of solids and gas mixing can identify the best arrangement for design and operation of the gasifier. In spite of its significance, there are few detailed measurements of gas and solid mixing in FBBG. Most of the knowledge comes from chemical FB reactors and FB boilers [71–73]. In addition to mixing there are several other factors influencing conversion, such as the residence time in the bed, as will be discussed below.

Simplification of the FBBG modeling by the identification of rate-determining processes is a useful approach, in particular the comparison between transport and conversion processes. Combination of four processes can be considered: vertical and horizontal transport (by convection and dispersion), devolatilization and char conversion. The two latter always differ in time because devolatilization is faster than char conversion; especially gasification with CO_2 and H_2O is slow. Consequently, as an approximation, devolatilization is sometimes regarded as instantaneous, assuming that the movement of the solid fuel is slower than the devolatilization. In this way, the steady-state composition of the gas released by devolatilization becomes an input to the model that can be obtained by devolatilization experiments, ideally with similar fuel particle size, temperature and heating rate. This simplification is, in fact, the same as assuming that solids mixing and char conversion are the slow, rate-controlling mechanisms in the reactor. This often holds for narrow laboratory-scale FBG, that is, as a matter of fact, the most common system analyzed.

In wider commercial reactors lateral dispersion during devolatilization may be a key issue in the distribution of gaseous species in large FB [19]. This has been experimentally verified in combustors [74,75], but it has not been reported for FBG. Only one attempt has been undertaken by 3D modeling to study the effect of maldistribution during sewage sludge gasification in a CFBG gasifier [43] where it was concluded that, due to the very fast release of volatiles and the high-volatile content in the fuel (sewage sludge), mixing of the gas around the feed port is not fast enough, and an ascending plume with highly concentrated pyrolysis gas is formed. These effects require 3D modeling, and further refinements seem to be necessary for the analysis of key processes, like the prediction of the tar content in the gas. A non-uniform biomass distribution is accompanied by steep gradients in the radial gas concentration profiles [76]. Also, large devolatilizing biomass particles rapidly move to the top of the riser [76], contributing to the tar measured in the product gas. In connection to this, large (>8 mm) char particles were found in the loop seal without being completely gasified. A population balance on devolatilizing fuel particles seems to be essential for the detailed analysis of such a case. Attempts have been made in modeling CFB biomass combustors [77] where drying and devolatilization of single biomass particles were solved simultaneously with an age population balance up to a devolatilization time t_{py}, obtained experimentally for the feed biomass distribution. No model has been found dealing with this process in FBG. In a bubbling FBBG, in contrast, the fuel particles are likely to remain in the bed most of the devolatilization time due to lower superficial velocity. and, hence, lower entrainment. Then elutriation of biomass particles during devolatilization does not play an important role [36] (while it could do so during char gasification). In general, both particle size and density are reduced during devolatilization, and that could enhance elutriation. For instance, under the operating conditions tested in [36], particles larger than 1 mm would be elutriated when their density had

Table 2
Semi-empirical fluid-dynamic correlations for the gas-flow pattern in FB.

Name of variable, Symbol	Unit	Correlation	Eq.	Ref
Rising velocity of a single bubble, u_{br}	m/s	$u_{br} = 0.711(gd_b)^{1/2}$	(96)	[47]
Bubble velocity, u_b	m/s	$u_b = u_{br} + 1.6\left(\left(u_0 - u_{mf}\right) + 1.13\, d_{b,av}^{0.5}\right)D_B^{1.35}$	(97)	[44]
		$d_{b,av} = \frac{1}{H_x}\int_0^{H_x} d_b(h)\, dh$		
Velocity at minimum fluidization, u_{mf} (Reynolds number at minimum fluidization, $Re_{p,mf}$)	m/s	$u_{mf} = \mathrm{Re}_{p,mf}\left(\frac{\mu_g}{d_p\rho_g}\right)$	(98)	
		$\mathrm{Re}_{p,mf} = \begin{cases}\left(28.7^2 + 0.0494\,\mathrm{Ar}\right)^{0.5} - 28.7 (\text{for } d_p \geq 100\ \mu\text{m}) \\ \left(33.7^2 + 0.0408\,\mathrm{Ar}\right)^{0.5} - 33.7 (\text{for } d_p < 100\ \mu\text{m})\end{cases}$	(99)	[45]
		$\mathrm{Re}_{p,mf} = \sqrt{C_1^2 + C_2\mathrm{Ar}} - C_1 (C_1 = 27.2 \text{ and } C_2 = 0.0408)$	(100)	
Voidage at minimum fluidization, ϵ_{mf}	–	$\mathrm{Ar} = \frac{1.75}{\left(\epsilon_{mf}^3\phi\right)}\mathrm{Re}_{p,mf}^2 + \frac{150\left(1-\epsilon_{mf}\right)}{\left(\epsilon_{mf}^2\phi^2\right)}\mathrm{Re}_{p,mf}$	(101)	[119,120]
Bubble size, d_b	m	$d_b = 0.54\left(u_0 - u_{mf}\right)^{0.4}\left(h + 4\sqrt{A_B}\right)^{0.8} g^{-0.2}$	(102)	[121]
Bubble size, d_b	m	$d_b = d_{bm} - (d_{bm} - d_{b0})e^{-0.3\, h/D_t} (\text{for } 0.3 < D_t < 1.3)$ $d_{b0} = 1.38\, g^{-0.2}\left[A_B(u_0 - u_{mf})/N_t\right]^{0.4}$ (perforated plate) $d_{b0} = 3.77\ g^{-1}\left(u_0 - u_{mf}\right)^2$ (porous plate) $d_{bm} = 2.59\, g^{-0.2}\left[A_B(u_0 - u_{mf})\right]^{0.4}$	(103)	[122]
Dimensionless visible velocity, ψ	–	$\psi = 1.45\ \mathrm{Ar}^{-0.18}$	(104)	[128]
Dimensionless visible velocity, ψ	–	$\psi = f\left(h + 4\sqrt{A_0}\right)^{0.4}$ $f_{SFB} = [0.26 + 0.70\exp(-3.3d_p)]\,[0.15 + (u_0 - u_{mf})]^{-1/3}$ $f_{CFB} = 0.3121 + 0.129u_0^{-1} - 16.6d_{p_b} - 2.61\cdot10^{-5}\Delta p_{ref}$	(105)	[125]
Bubble void fraction, ϵ_b	–	$\epsilon_b = \left[1 + (1.3/f)\left(u_0 - u_{mf}\right)^{-0.8}\right]^{-1}$	(106)	[125]
Bed expansion factor, f_{bex}	–	$f_{bex} = 1 + \frac{\left(1.032\left(u - u_{mf}\right)^{0.57}\rho_g^{0.083}\right)}{\left(\rho_p^{0.166}u_{mf}^{0.063}D_t^{0.445}\right)}$ $(D_t < 0.0635)$ $f_{bex} = 1 + \frac{\left(14.31\left(u_0 - u_{mf}\right)^{0.738}d_p^{1.006}\rho_p^{0.376}\right)}{\left(\rho_g^{0.126}u_{mf}^{0.937}\right)}$ $(D_t > 0.0635)$	(107)	[129]
Voidage in the emulsion phase, ϵ_e	–	$\epsilon_e = \epsilon_{mf}\left(u_e/u_{mf}\right)^{1/6.7}$	(108)	[130]
Bubble to emulsion mass transfer coefficient, k_{be}	1/s	$k_{be} = \frac{2\, u_{mf}}{d_b} + \frac{12\left(D_g\,\epsilon_{mf}\,u_b\right)^{1/2}}{\pi\, d_b^{3/2}}$	(109)	[132]
Terminal velocity,u_t(inside the Reynolds number at terminal velocity, $Re_{p,t}$)	m/s	$u_t^* = \left[18/\left(d_p^*\right)^2 + (2.335 - 1.744\,\phi)/\left(d_p^*\right)^{0.5}\right]^{-1}$ *with* $u_t^* = \mathrm{Re}_{p,t}/\mathrm{Ar}^{1/3}; d_p^* = \mathrm{Ar}^{1/3}; \mathrm{Re}_{p,t} = \left(\rho_g d_p u_t\right)/\mu_g$	(110)	[109]
Entrainment flux of particles at the bed surface ($h = H_x$), G_x	kg/(m^{2}s)	$G_x = 3.07\cdot10^{-9}A_B\, d_{b,h=H_x}\left(\rho_g^{3.5}g^{0.5}\mu_g^{-2.5}\right)\left(u_0 - u_{mf}\right)^{2.5}$	(111)	[136]
Elutriation rate constant for different particle size i (entrainment flux where $dG/dh = 0$) $G_{i,\infty} = E_{i,\infty}$	kg/(m^{2}s)	$E_{\infty,i} = 0.011\,\rho_p(1 - u_{t,i}/u_0)^2 (\text{for } u_{t,i} < u_0)$ $E_{\infty,i} = 0 (\text{for } u_{t,i} \geq u_0)$	(112)	[137]
Decay coefficients, a and K	m^{-1}	$a = 4\, u_t/u$	(113)	[139]
		$K = 0.23/(u_0 - u_t)$	(114)	

fallen below 200 kg/m^3, i.e. when devolatilization was practically completed.

In conclusion, the behavior of fuel particles and the location where they are converted in an FB depend greatly on the relative rates of mixing (fluid-dynamics) and reaction. Fuel properties, such as density, size, volatile content, and topology of the gasifier like bed diameter, aspect ratio, and number and position of the feeders can decisively influence the conversion process. The prediction of

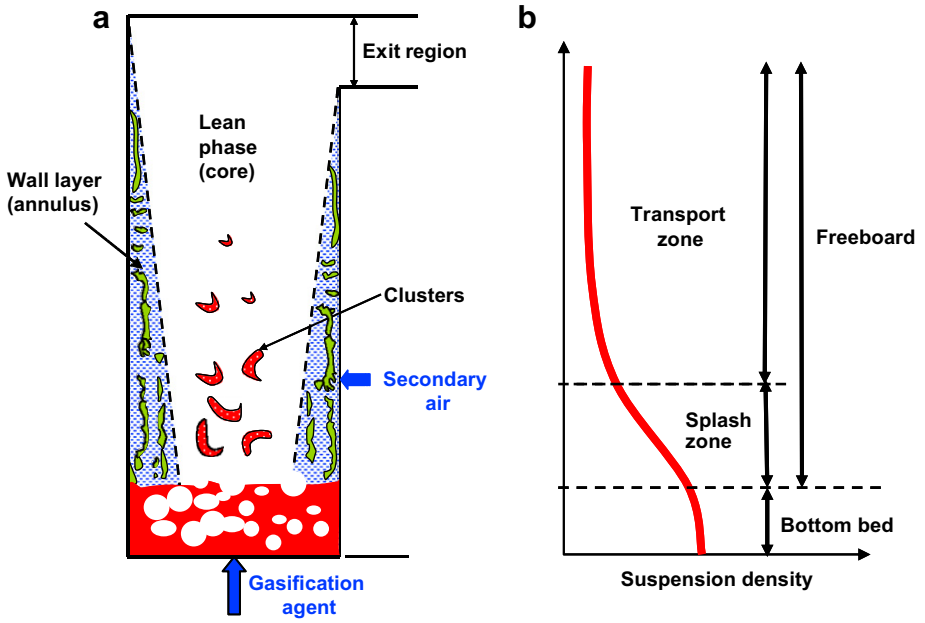

Fig. 4. (a) Characteristic flow pattern in FB units (b) simplified diagram of solids density profiles through the different zones of the FB units.

fuel-particle conversion, based on experience from laboratory and pilot-scale research plants, is of great importance for the design of full-scale units, because mixing and reaction can change significantly from one plant to another. An important question, still to be answered, is how to employ results from small-scale equipment as a support for the design of large-scale units. Most information on biomass gasification has been obtained in small FB gasifiers and this issue is extraordinarily important for modeling as a means of extrapolation.

2.2.1. The equations of mixing

Solid-solid and gas–gas mixing of species i is theoretically determined by Eq. (1), applied for transport of solids (index s) and gas (index g) in an isothermal system:

$$\frac{\partial c_{si}}{\partial t} + \mathrm{div}(\mathbf{u_s} c_{si}) = \mathrm{div}\left(D_{sV/H,i}\mathrm{grad}\ c_{si}\right) + S_{si} \tag{2}$$

$$\frac{\partial c_{gi}}{\partial t} + \mathrm{div}(\mathbf{u_g} c_{gi}) = \mathrm{div}\left(D_{gV/H,i/}\mathrm{grad}\ c_{gi}\right) + S_{gi} \tag{3}$$

These 6i (i is the number of solids and gaseous species in a 3D system) equations, with their source terms S, for concentrations $c_{s/g}$ can be solved with appropriate boundary conditions and solids and gas velocities $\mathbf{u}_{s/g}$ obtained from momentum and continuity equations. There could also be a term describing transfer between gas and solids. At steady state Eq. (1) becomes, using the dimensionless variables: $X = x/x_0$; $C_{ki} = c_{ki}/c_0$; $\mathbf{U}_k = \mathbf{u_k}/u_{k0}$ (k = solid or gas),

$$\mathrm{div}(\overline{\mathbf{U}}_k C_{ki}) = \frac{1}{\mathrm{Pe}_{ki}}\mathrm{div}(\mathrm{grad}\ C_{ki}) + \mathrm{Da}_{ki,I} \tag{4}$$

or alternatively

$$\mathrm{Pe}_{ki}\mathrm{div}(\overline{\mathbf{U}}_{\mathbf{k}} C_{ki}) = \mathrm{div}(\mathrm{grad}\ C_{ki}) + \mathrm{Da}_{ki,II} \tag{5}$$

Two main governing parameters arise in Eqs. (4) and (5). Da is the Damköhler number, expressing the ratio of the chemical reaction rate R_{ki} to the volumetric rate of transport by convection $c_0 u_{k0}/x_0$ or by diffusion $c_0 D_{ki}/x_0^2$. Consequently, $\mathrm{Da}_{ki,I} = R_{ki}x_0/(c_0 u_{k0})$ and $\mathrm{Da}_{ki,II} = R_{ki}x_0^2/(c_0 D_{ki})$, are the first and the second Damköhler numbers [78]. $\mathrm{Pe}_{ki} = \mathrm{ReSc} = x_0 u_{k0}/D_{ki}$ is the Péclet number, the product of the Reynolds and the Schmidt numbers, expressing the ratio of transport by convection and diffusion. $\mathrm{Da}_{ki,I} = \mathrm{Da}_{ki,II}/\mathrm{Pe}_{ki}$ and D_{ki} m^2/s is formally a diffusion coefficient for a solid or gaseous (k) constituent (i) in the bed. The characteristic length x_0 is selected according to the geometry of the problem under consideration (vertical and/or horizontal). The choice between Eqs. (4) and (5) depends on the dominant mechanism of mass transport. The equations are used in CFD methods and they form the basis of fluidization models, or else, only the dimensionless quantities are employed for qualitative judgments.

2.2.2. Solids mixing

The movement of solids in an FB is often described by a simplified version of Eq. (2), in which diffusion and convection are lumped into one term, called dispersion and expressed by the diffusion term only. The dispersion model usually fits data for fine particles and deep beds, i.e. chemical reactors, where small-scale mixing mechanisms are dominant [44]. A number of correlations for dispersion coefficients have been published based on the dispersion model, where the experiments have been run with Group A particles in small FB units. They have been summarized in several publications [4,44,72,79–81]. The vertical dispersion coefficient increases with superficial velocity and bed diameter. Solids transport in the wake of bubbles is essentially the reason why vertical solids mixing is one to two orders of magnitude better that horizontal mixing. Extrapolation of the dispersion coefficient for fine powder to large FBG seems to be inadequate, because such reactors use Group B particles, and there is a large-scale movement due to strong particle streams and large-scale recirculation [4,44,72,82]. When the dispersion model does not fit properly experimental data, the countercurrent mixing concept is often used. The countercurrent mixing model assumes the presence of two phases, one ascending and the other descending, with a cross flow or interchange of mass between the phases [79].

In the FB, beside the inert bed material (or sometimes solid catalyst), there is a distribution of fuel and char particles in the bed. Therefore, the movement of solids in the vessel should be described by accounting for three or more types of solids. However,

qualitatively the motion of biofuel particles can be visualized as the movement of flotsam particles in a jetsam-rich bubbling FB. As a result, experimental studies on mixing and segregation in FB have been focused on binary systems [38,79,80,83–87]. Some studies have reported time-average vertical distribution of material, finding higher concentrations of flotsam material in the upper region of the bubbling FB [38]. Higher superficial velocity may improve mixing, but biomass particles with lower density and larger size than bed particles can still be non-uniformly distributed. At a given fluidization velocity, char particles are more likely to be elutriated from the bed or to sink from the bed's surface than devolatilizing particles. This is because the jet force from escaping volatile matter tends to keep them floating, as has been observed experimentally [88,89]. A key issue in modeling FBBG is weather the fuel particles keep floating once they have reached the bed's surface or if they are forced to descend. This depends much on the behavior of segregation of a few flotsam particles in a bed of many jetsam particles. The competition between mixing and segregation has been studied experimentally in various types of particle system and superficial velocities to make this issue clearer [38,84,86,87]. A large body of low density particles (<800 kg/m^3) in a bed of glass beads (Group B) with a bulk density of 1490 kg/m^3 was observed to sweep up to the top of the bed by the bubbles and remain there [84]. Bodies of densities between 1300 and 800 kg/m^3 occasionally descended, but they were pushed back again. In a cold 2D rig the distribution of biomass particles (8 mm spherical wood) was more uniform in the vertical direction of the bed at a low superficial velocity than at a high superficial velocity [86]. Cylindrically shaped cotton stalk segregates locally in a 3D cold rig, and as gas velocity gradually increases, the bed undergoes global segregation, local mixing, global mixing and re-segregation [87], while biomass particles accumulate at the top of bed within what was called [87] partial and transient fluidization regime, promoted at the higher gas velocity.

The change of particle properties during devolatilization and other factors, such as the jet force, caused by rapid volatile release, adds further complexity to the phenomena discussed, where solids mixing and segregation were achieved with binary systems of particles, each class having fixed size and density. The relative change in size-density from the initial value has been shown to depend on the environment where the particle is immersed, especially heating rate and bed temperature. It has been found a critical size-density, at which a given particle will rise through a column [90]. Therefore, under the conditions of biomass gasification, it is better to feed at the bottom, because this prolongs the residence time of a particle in the bed during devolatilization [36]. This is so, because normally the density of the bed material is higher than that of an initial biomass particle, and the particle will tend to float from the beginning. However, the lateral dispersion is lower in the bottom part of the bed than at the top. Also the effect of the jet force caused by the release of volatiles contributes to maintaining the fuel particles at the surface during devolatilization [91,92].

In an FBG, segregation should be avoided in order to preserve the bed from problems like sintering or excessive tar emission. Based on [83], a method has been proposed to check the risk of segregation by calculation of the mixing ratio, defined as the ratio of the mass fraction of the heaviest species at the top and that at the bottom of the bed [24]. In well-mixed beds, this ratio tends to unity. Segregation is likely to occur if the ratio is equal to or below 0.5. A mixing ratio between 0.5 and 1 is desirable in order to be out of segregation problems.

The propagation of solids in the horizontal direction is crucial in large devices, characterized by aspect ratios of unity or lower (wide beds). This problem has received attention for the understanding of the maldistribution of fuel in CFB boilers firing biomass. An extensive comparison of models and dispersion correlations has been focused on modeling large FB boilers [72], although measurements of the horizontal fuel dispersion rate in FB boilers are still scarce and contradictory. Dispersion coefficients in a 100 MW$_{th}$ BFB boiler with a superficial velocity of 1.3 m/s have been reported to be in the order of 0.001–0.01 m^2/s [71], while data from hot measurements in Chalmers 12 MW$_{th}$ CFB boiler give 0.1 m^2/s [72]. Further investigation on horizontal solid mixing in large CFB boiler has been reported recently [73]. The mixing is almost perfect in the vertical direction in the bottom zone of a CFB, but the lateral mixing was found to be limited, having dispersion coefficients of about 0.1 m^2/s, corresponding to Péclet numbers of around 40 [93]. The various regions in a CFB exhibit different predominant mechanisms of solids motion and mixing [94]. In the transport zone there is a dilute, upward flow in the core and a descending motion near the wall. In the core, the behavior of the solids is similar to plug flow, whereas in the wall region there are horizontal gradients. The Péclet number of the solids movement in the core increases from 150 to 300 with increasing solids volume concentration [95]. Recent investigation in large CFB boilers allow better distinction between the flow patterns compared to lab-scale units, and results in formulae for estimation of wall-layer thickness and flow distribution [96].

To conclude, segregation of devolatilizing fuel particles and bed material has to be checked, and modeled, if found significant. In small FBG with large aspect ratio, an axial gradient of devolatilizing fuel particles may arise. A key issue for such units is the location of the fuel feed point: top or bottom. Very few experiments have been reported to clarify this issue. In large units with in-bed (bottom) feeding, lateral gradients of gaseous species may arise from non-uniform distribution of fuel. In both cases, models should be formulated to account for these effects in order to predict the gas composition and to support the improvement of tar conversion and other rate-limited processes. In addition, problems of hot spot and agglomeration can be predicted. The distribution of fuel near the feed ports can be critical to the optimization of large FBG and needs careful study [43]. In both small and large units char seems to be well-mixed because mixing is faster than char conversion in an FB gasifier, since most of char is converted by gasification. However, despite the good mixing, prediction of the entrainment of char particles by the gas is a key issue for the estimation of carbon conversion. Although char is well mixed in the bottom bed, differences in concentration and particle-size distribution may arise in the freeboard [97]. Comminution of fuel and char affects the rate of elutriation and the particle content of the gas. Validation of the models has to be done preferably by measurements in large-scale systems. Very little is known about the actual behavior of models describing gasification of biomass fuels. Values reported for fuel dispersion from large FB biomass boilers can be helpful for estimates of FBBG, since the mechanisms of solids dispersion are similar. With respect to char, measurement results from FB boilers may differ significantly from those in FBBG, because the char concentration in the bed and freeboard is greater in the latter due to the lower char conversion rates.

2.2.3. Gas mixing

The mixing of gas in an FB is promoted by fluctuations at various scales. A large-scale motion is created by the bubbles in the bottom bed. Gas dispersion is high in the splash zone, while in the freeboard the gas mixing decreases significantly all the way up to the upper part of the freeboard [98].

Gas-dispersion coefficients have been used to model gas mixing. These coefficients in the vertical and horizontal directions based on single-phase dispersion models are similar and follow similar trends to those of solid-dispersion coefficients [99]. An important question is whether estimations based on Péclet numbers obtained in laboratory-scale beds can be extrapolated to large units [100]. Reported

diffusion coefficients or Péclet numbers have been obtained from measurements at different solids flows, hold-up, gas velocities, and aspect ratios of units. In addition, various methods (models) to evaluate measurements have been used. In the bottom bed of an FB a single-phase dispersion model gives only a crude description of gas mixing. In this zone, the bubbles influence the gas residence-time distribution through the bypass of the bubble flow and the exchange between bubbles and the gas in the dense phase. Therefore, a more exact description is obtained from models that take the two-phase nature of the bed into account [99]. This is made by considering a single-phase dispersion model in the bottom bed to model the gas mixing in the emulsion phase, whereas plug-flow is usually assumed in the bubble phase. This type of model is used to represent the bottom zone in both BFB and CFB. In the freeboard of a BFB, plug flow gives reasonably good predictions for the gas motion [24]. In the freeboard of CFB a core-annulus flow structure is assumed, consisting of a lean gas-particle suspension in the centre region and a sharply separated wall zone with a denser phase moving downwards. Gas mixing can be described by dispersion in the lean phase and by mass transfer between the lean and the dense phases, as long as only primary gas is injected. With secondary gas-injection, the gas-flow pattern is affected, and the impact of the secondary gas jets should be taken into account [101]. Since the gas velocity is high in the axial direction, convection is the dominant transport mechanism. Gas mixing in the lateral direction of the freeboard is similar to that of single-phase flow [98]. For instance, the height h necessary for the gas from a point source to spread over a duct with radius R in a riser with a Péclet number of 400 [102] gives $h = 100R$. Therefore with the data used, the radial mixing is far from good [19]. Data obtained in other laboratory risers yield Pe of about 200 [99] for which h would be $50R$. However, measurements in large CFB boilers have shown that lateral gas mixing is not as limited [74].

There are few measurements on gas dispersion coefficients and concentration profiles in FBBG [70,103]. Axial and radial mixing coefficients of gas in a 500 kWth CFBB gasifier have been reported [70] as well as radial profiles for the gaseous species in the freeboard of a lab-scale CFBG unit for a variety of biomasses [103]. The gas mixing seemed not to be sufficiently effective to distribute the gas released from the devolatilizing particles, and this affected the tar content of the gas [103]. Due to the importance of the latter in FBG, both the distribution of fuel particles in the freeboard (solid mixing) and the gas mixing mechanisms have to be modeled precisely. This is still waiting to be further investigated. Detailed mathematical models supported by gas and solid dispersion coefficients could give better guidelines for design.

2.2.4. Simplified reactor models for FBBG

This section gives guidelines for the choice of simplified FBBG models based on the rates of reaction and mixing. Comparison between rates can be made in terms of the Damköhler number of the reactor (Eqs. (4) and (5)). (Here the Damköhler numbers are those of the reactor. In Section 3 Damköhler numbers are related to conversion of particles. In order not to complicate the nomenclature, the subscripts indicating "reactor" and "particle" are not shown as they formally should).

The Damköhler number of the reactor $Da_{i,V/H}$ is defined as the ratio of the i-solids' residence time in the reactor, $\tau_{Ri,V/H}$ and the time of their conversion $\tau_{Ci} = 1/R_i$, that is, $Da_{i,V/H} = \tau_{Ri,V/H}/\tau_{Ci}$. The subscript k in Eqs. (4) and (5) has been omitted because only solids are treated. Subscript i stands for the type of solid or type of solid reaction: char (ch) yielding gasification gas (gas) and fuel (f) subjected to devolatilization (py). The Damköhler number can be applied to both vertical and horizontal processes, as indicated by subscript V and H. Comparisons will be made for different situations and the Damköhler number has to be judged accordingly.

The residence time of the reacting solids in the reactor can be calculated from either the convective transport time $\tau_{Ri,V/H} = x_0/u_{i,V/H}$ or the dispersion time $\tau_{Ri,V/H} = x_0^2/D_{i,V/H}$ where x_0 is the dimension: $x_0 = d_B$ (in the horizontal direction), $x_0 = H_x$ (vertical in the bottom bed) and $x_0 = (H - H_x)$ (vertical in the freeboard). In a circulating system the transport time should be multiplied by n_{loop}, which is the number of times the reacting solid particle travels through the reactor, related to the separator efficiency, $n_{loop} = 1/(1 - \eta_{sep})$ [104]. As discussed, $D_{i,V/H}$ is an experimental dispersion coefficient for solids (it is called "dispersion coefficient" and not "diffusion coefficient" because in some tests, particularly in the dense, bubbling bed, convective features, caused by the bubbles, are included [72,73,105]).

Clearly, in a large reactor the horizontal transport may become a limiting factor and the corresponding residence time $\tau_{Ri,H} = d_B^2/D_{i,H}$ may be long in comparison to the conversion time τ_{Ci}. This is especially the case for devolatilization, whose rate is high, but it is less critical in char conversion due to the slow reactions. In this situation $Da_{py,H} >> 1$, indicating lateral maldistribution of volatiles, whereas $Da_{ch,H} << 1$, indicating that the char is already well mixed before conversion takes place to an significant extent. In a small reactor, also $Da_{py,H} << 1$ holds because of the short lateral mixing distance. In the bottom bed of a FB both convection and diffusion may contribute to the vertical transport, whereas in the freeboard, and particularly in a CFB, the convective transport of fuel and char is dominant in the vertical direction with the residence time $\tau_{Rf/ch,V} = n_{loop}(H - H_x)/u_{f/ch,V}$. $u_{f/ch,V}$ can be roughly estimated by $u_{f/ch,V} = u_0 - \psi u_{t,f/ch}$, where $u_{t,f/ch}$ is the terminal velocity of a fuel/char particle and ψ a factor accounting for the influence of particle–particle interaction on the terminal velocity of a single particle: small particles of a given size have a higher terminal velocity u_t than a single particle of the same size because of clustering effects, and large particles can be carried upwards pushed by the flow of smaller particles [106]. Models to estimate ψ have been developed [107,108]. In the vertical flow case, the residence time should be long to convert the char, $Da_{ch,V} >> 1$, which may require $n_{loop} >> 1$, hence, it depends on the efficiency of the particle separator.

In a BFBG the fraction of elutriated fuel particles from the bottom bed is low ($u_0 < u_{t,f}$ for a large portion of the fuel particles) so $u_{f,V} \to 0$. Therefore devolatilization of fuel occurs mostly in the bottom bed. Various limiting cases can be identified, to be discussed in Section 2.2.4.1. For char particles, however, $u_{ch,V}$ can be significantly higher, and the proportion of char in the freeboard can be considerable [97]. In a CFBG the fraction of elutriated fuel and char is high ($u_0 > u_{t,f/ch}$ for a large portion of the fuel/char particles). The fuel particles stay in various parts of the reactor during devolatilization: in the wall layer, in the dilute zone of the freeboard, and even in the loop seal. The char is converted in the freeboard to a great extent, since the char tends to be entrained from the bed, once generated.

A qualitative judgment of the tendency of a particle to be carried away can be made by calculation of the terminal velocity of a single particle u_t. Fig. 5 presents u_t versus particle diameter calculated by Eq. (110) in Table 2 [109] for different materials used in a CFBG [110]. At a superficial gas velocity of 5 m/s, the diagram indicates that, while silica sand of 0.5 mm would stay in the bottom bed, dolomite of 0.6–1.0 mm would remain in the bed initially, but once calcined, it could be rapidly elutriated. Biomass like wood chips would be carried away from the bottom bed for particle sizes smaller than 3 mm, whereas the char generated from this fuel could be transported for particle sizes up to 10 mm. It should be noted that the relationship for terminal velocity used here is valid for a single particle and, hence, the concept only gives a rough indication about the movement of groups of particles where various kinds of particle–particle interaction may occur.

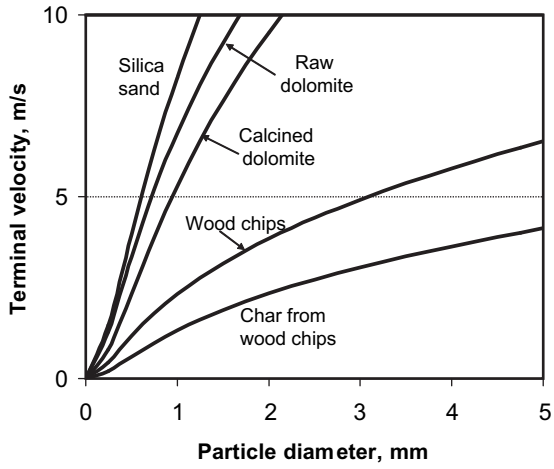

Fig. 5. Terminal velocities of single particles of various materials in a CFB biomass gasifier (calculated for air, at 850 °C and at a total pressure of 1.1 bar) as a function of particle size. Properties of solids: Silica sand (2600 kg/m^3, sphericity 0.9); Raw dolomite (2400 kg/m^3, sphericity 0.8); Calcined dolomite (1300 kg/m^3, sphericity 0.9); Wood chips (850 kg/m^3, sphericity 0.4); Char from wood chips (350 kg/m^3, sphericity 0.4).

2.2.4.1. Vertical mixing vs. devolatilization in the bottom bed. When fuel devolatilization mostly takes place in the bottom bed (i.e. when the fraction of fuel particles entrained from the bed is low, such as in BFBG and sometimes in CFBBG operated at moderate gas velocities) the identification of the location where devolatilization occurs may be helpful to simplify the reactor model. There are three possible situations, illustrated in Fig. 6: (1) when a particle stays floating on the free surface of the bed during most of the devolatilization process, Fig. 6a, (2) when the devolatilization takes place completely in the bottom part in the vicinity of the feed point, Fig. 6b, and (3) when the particle is being distributed throughout the bed as devolatilization takes place, Fig. 6c.

Fig. 6a corresponds to an under-fed FBG when the vertical transportation (segregation) of fuel particles is rapid compared to devolatilization and $Da_{py,V} << 1$. It also includes the case when the biomass is fed at the top and keep there. The devolatilization takes place on top of the bed, because it is assumed that the particles keep floating once they have reached the bed's surface, as discussed above [38,84,86,87]. This case is depicted in Fig. 6a.1. Once the devolatilization has finished at the surface of the bed, the remaining solids (char) are likely to descend in the bed. At steady state, it can be assumed that the resulting char is evenly distributed in the bed. A simplified model for this situation is presented in Fig. 6a.2. At the bottom of the bed, the amount of volatile matter in this zone is expected to be small, and hence, the airflow meets the hot char. The oxygen is consumed rapidly by the char in a short distance compared to the bed height. In the upper zone (most of the bed; the figure is not scaled) char gasification takes place. The extent of char gasification depends on the reactivity of the char and on the bed temperature. Gas-phase reactions also occur in this zone, especially the water–gas shift reaction. This zone is expected to be the source of carbon loss due to entrainment of char.

In the other limiting situation, $Da_{py,V} >> 1$, depicted in Fig. 6b.1, the devolatilization is rapid, and most of the volatiles are released in the bottom zone of the bed. This is why most FBG models have considered instantaneous devolatilization. $Da_{py,V}$ in the range of 7–14 was estimated in a lab-scale FBG [69]. After devolatilization, the biomass (already char) is carried up by the fluidizing gas to the oxidation zone, where the char is exposed to oxygen, Fig. 6b.2. The presence of combustible matter i.e. H_2, CO and CH_4 gives rise to a depletion of oxygen in a short height [24,28,59,64] due to the high rate of oxidation reactions. There is no clear evidence, however, about the main source of oxygen consumption: homogeneous reaction with CO and H_2 or char oxidation. It has been argued that the high availability of oxygen near the distributor leads to consumption of oxygen by char. However, the rate of char combustion decreases steeply and nearly ceases due to limited oxygen transfer from the bubbles to the emulsion phase and from the gas phase of the emulsion to the particle's surface. Therefore, it seems more reasonable that the oxygen is mainly consumed by volatiles [111].

In the two limiting situations exposed in Fig. 6a and b, one mechanism, either reaction or mixing is dominant, and devolatilization coupled with fluid-dynamics or a population balance over the parts of the reactor does not have to be included in a model; it is sufficient to know the accumulated release of volatile matter, using it as a boundary condition in the proper position. For instance, when the fuel is fed at the bottom, the initial composition of the gas entering the bed is given by the accumulated distribution of volatiles mixed with the fluidizing agent, ascending from the distributor. This is a common procedure applied by modelers (though only a few of them have quantified the $Da_{py,V}$ to assess this assumption), which greatly simplifies the FBBG model and also the input data required. In such a case, the overall or accumulated decomposition of a fuel particle, determined in the laboratory, is enough to model biomass devolatilization. The general case, illustrated in Fig. 6c requires complex modeling: the motion of biomass particles has to be established in each position, coupled with devolatilization and size distribution, so that the instantaneous yields of gaseous species have to be be determined. Experimental information [38,84] is helpful to establish a fluid-dynamic model to predict the distribution of devolatilizing (flotsam) particles in the bed. Fig. 6c.3 represents a typical experimental distribution of flotsam particles along the vertical axis [38]. In the extreme case when the fuel particle is well distributed throughout the bed, the devolatilization takes place uniformly in the entire bed, and again the model can be simplified assuming an evenly distributed source of gas throughout the bed.

2.2.4.2. Lateral mixing vs. devolatilization in the bottom bed. In large, wide FB, the critical condition is expressed by $Da_{py,H}$. Little has been written on lateral mixing related to FBBG, probably because most information available in this area comes from small units where this problem is absent. However, its importance during scale-up and process optimization is evident [100,112]. To illustrate this problem an example is given. The time for 90% devolatilization of a dried (7%w/w moisture) 4 mm sewage sludge particle has been measured to be about 30 s [113]. During this time, taking $D_{f,H} = 0.01$ m^2/s, a fuel particle would be transported a horizontal distance of about 0.5 m in the bed. This is more than sufficient in an small lab-scale FBG of say, 50 mm diameter, where devolatilization takes place in the entire cross-section ($Da_{py,H} = 0.008 << 1$) and one should analyze the vertical processes to find the limiting behavior, as discussed in Section 2.2.4.1, to further simplify the model. On the other hand, in an FBG with a larger bed, say 5 m in horizontal size, devolatilization takes place only in the vicinity of the feed port ($Da_{py,H} = 83 >> 1$). In intermediate cases the distribution of volatiles over the cross-section may be important, and then one has to determine the devolatilization rate, taking into account the lateral dispersion. This case has been demonstrated by the 3D simulation in Fig. 7 [43], illustrating the distribution of volatiles (CH_4, CO and H_2) near the feed point in a CFBBG of 0.5 m square cross-section for processing of dried sewage sludge. In this case, the $Da_{py,H}$ is around 0.8, taking $D_{fH} = 0.01$ m^2/s. The simulation results shown in Fig. 7a, predict steep concentration gradients of volatile species (CH_4, CO, H_2) in the horizontal direction, caused by limited radial mixing of the fuel. In Fig. 7b, the corresponding distribution in the vertical

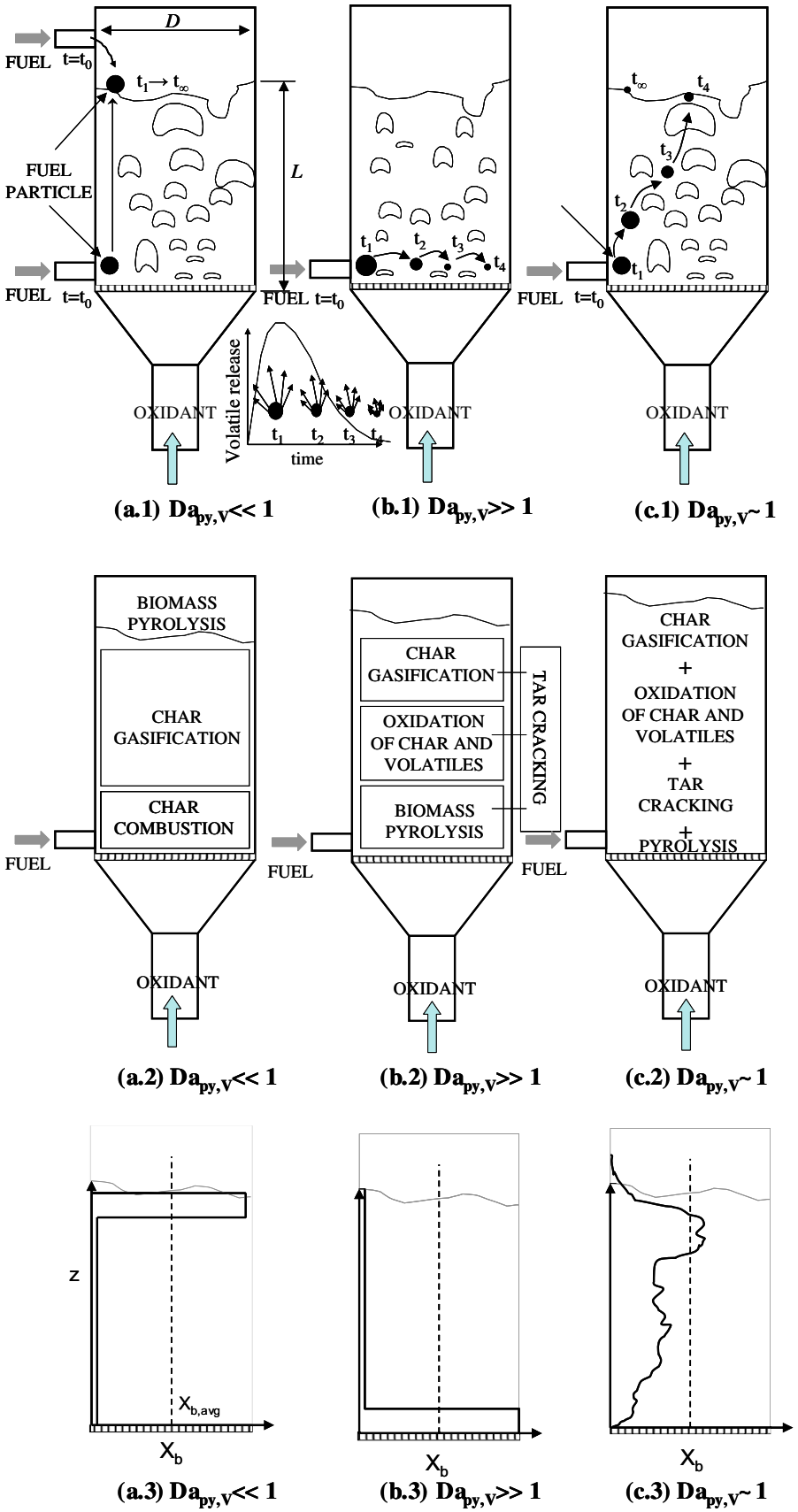

Fig. 6. (a.1)–(c.1): Possible situations according to Damköhler number $Da_{py,V}$ in a bubbling FB. (a.2)–(c.2) Models of the limiting situations (a) (b) and general case (c). (a.3)–(c.3) Models of distribution of fuel in the three cases.

direction on the *x,z*-plane is given for a cross-section in the central part of the bed. The insufficient radial gas dispersion is evident. As seen, the horizontal gas mixing is slower than the axial transport, and the gaseous components, devolatilized at the feed height, flow in streamers to higher regions. Incomplete mixing is visible up to about 10–12 m height. Parametric studies varying D_{fH} show similar behavior even at $Da_{py,H}$ around 0.1. The conclusion is qualitatively valid for various high-volatile fuels, such as biomass.

To sum up, the analysis in terms of $Da_{py,H}$ gives a rough estimate that serves as a guideline to simplify models in some cases. Estimation of the radial dispersion coefficient and the overall time of devolatilization of the biomass particles are needed for such estimates. Intermediate values of $Da_{py,H}$ should be handled with caution, since there are further phenomena to account for that can affect the results, leading to maldistribution of individual species: endogenous bubbles formed during devolatilization, ascending as plumes and bypassing the bed, different release rates of volatile components, and simultaneous homogeneous oxidation reactions. This problem can be of great significance for the tar yields in the gas. The analysis suggests that, in large units, measurements in various radial positions should be made to obtain meaningful averages. This has been undertaken in boilers [72,74], but values from FBG are missing.

2.3. Fluidization modeling

An FM consists of conservation equations applied to the various regions of the reactor. The flow pattern in each region is established by semi-empirical fluid-dynamic modeling to determine the distribution of gas species and reacting particles, the size and velocity of bubbles, and other relevant variables. A 1D isothermal model for the bed and freeboard is formulated below. Such a formulation describes with sufficient detail the parameters to be estimated and the main equations to be solved. It covers the essential features of most FBBG models published up to date. A few models have been published accounting to two-dimensional and non-isothermal effects and the presence of a particle size distribution for the solids. This is discussed later on as extensions of the basic model.

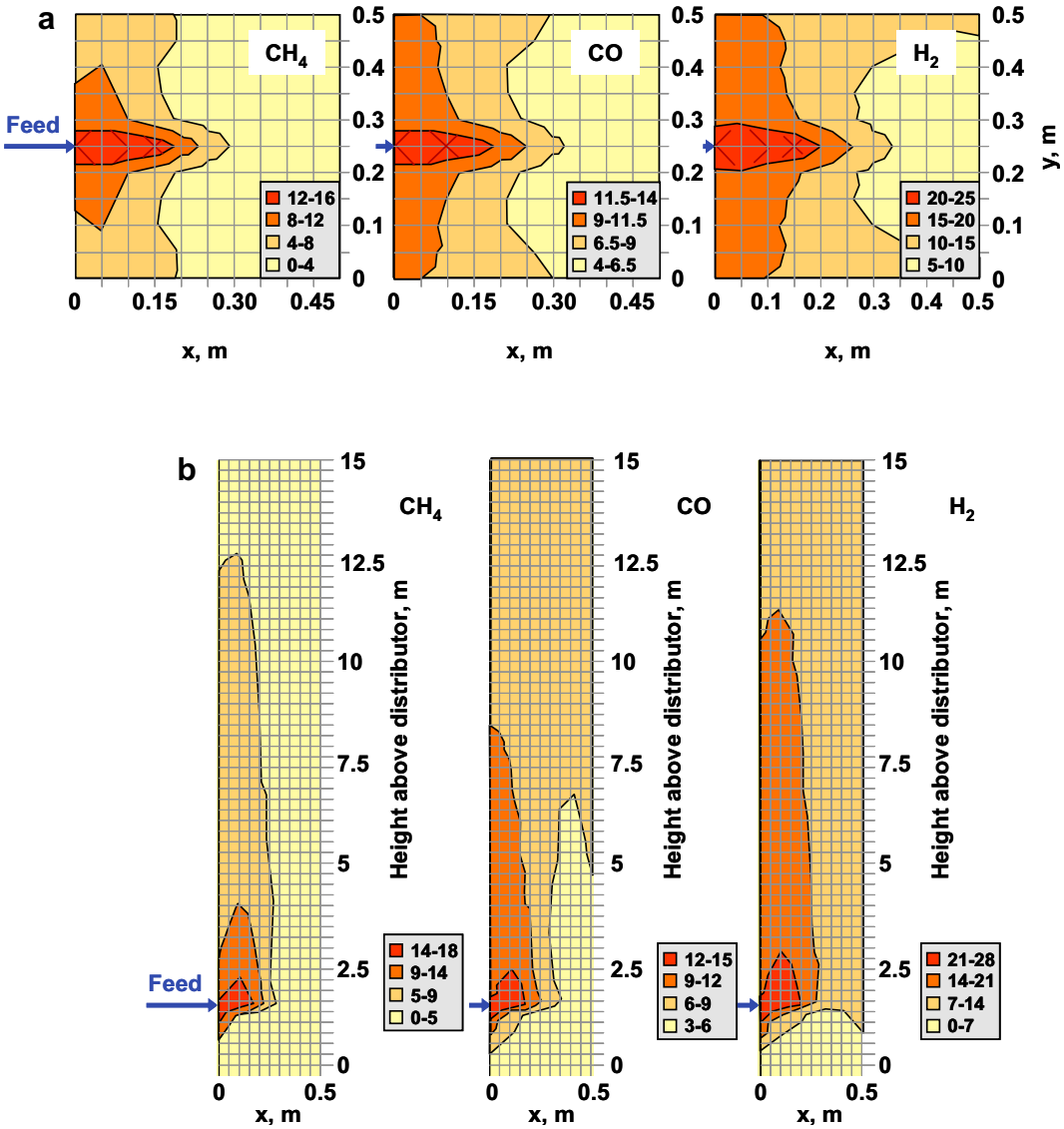

Fig. 7. Distribution of the concentrations of CH_4, CO and H_2 over the cross-section of a CFBG with 0.5 m square cross-section burning sewage sludge (a) horizontal cross-section on the feeding level z (axial coordinate)=1.5 m (b) vertical cross-section at $y = 0.25$ m (half width) (from Petersen and Werther [43]).

2.3.1. Conservation equations

Eq. (1) is applied for species i in any zone of the reactor. Assuming steady-state, one-dimensional system and neglecting diffusion, Eq. (1) can be simplified as:

$$\frac{\mathrm{d}(u\rho_\mathrm{i})}{\mathrm{d}h} = S_\mathrm{i} \tag{6}$$

In the bottom bed (index 'B'), the mass balances for gas species in the bubble (index 'b') and emulsion (index 'e') at height h are according to Eq. (6)

$$\frac{1}{A_\mathrm{B}}\frac{\mathrm{d}F_\mathrm{i,b}}{\mathrm{d}h} = \varepsilon_\mathrm{b} r^\mathrm{b}_\mathrm{gg,i} + f_\mathrm{b-e,i} \tag{7}$$

$$\frac{1}{A_\mathrm{B}}\frac{\mathrm{d}F_\mathrm{i,e}}{\mathrm{d}h} = \varepsilon_\mathrm{e}(1-\varepsilon_\mathrm{b}) r^\mathrm{e}_\mathrm{gg,i} + \sum_\mathrm{m}(1-\varepsilon_\mathrm{e})(1-\varepsilon_\mathrm{b})\sigma_\mathrm{m} r^\mathrm{e}_\mathrm{gs,m,i} - f_\mathrm{b-e,i} \tag{8}$$

The variables in Eqs. (7) and (8) are function of height h. The mass flow rates of gas i in the bubble and emulsion are $F_\mathrm{i,b} = u_\mathrm{b}\rho_\mathrm{i,b}A_\mathrm{b}$ and $F_\mathrm{i,e} = u_\mathrm{e}\rho_\mathrm{i,e}A_\mathrm{e}$. The cross-section areas in the bubble phase, A_b, and the emulsion, A_e, are related to the reactor (bottom zone "B") cross-section, A_B, by: $A_\mathrm{B} = A_\mathrm{b} + A_\mathrm{e}$. Fig. 8 shows the geometry of a differential volume $A_\mathrm{B}dh$ in the bottom zone with the main fluid-dynamic parameters, schematically represented as a bubble phase and a particle phase, the latter divided into particles and void.

The chemical reaction terms are given by

$$r^\mathrm{e/b}_\mathrm{gg,i} = \sum_{j=1}^{\mathrm{n^{e/b}_{rgg}}} R_\mathrm{j,i}\nu_\mathrm{i,j}MM_\mathrm{i} \tag{9}$$

$$r^\mathrm{e}_\mathrm{gs,m,i} = \sum_{j=1}^{\mathrm{n_{gs}}} R_\mathrm{j,m,i}\nu_\mathrm{i,j}MM_\mathrm{i} = R_\mathrm{py,fuel,i}\nu_\mathrm{i,py}MM_\mathrm{i} + \sum_{j=1}^{\mathrm{n_{rch}}} R_\mathrm{j,char,i}\nu_\mathrm{i,j}MM_\mathrm{i} \tag{10}$$

The main homogeneous (gas-gas) reactions are the oxidation of volatiles, the water–gas shift reaction and the reforming of hydrocarbons (Reactions R7–R15 in Table 3). The main heterogeneous reactions are the devolatilization (R1 in Table 3) and char–gas (mainly O_2, CO_2 and H_2O) reactions (Reactions R2–R6 in Table 3).

The term $f_\mathrm{b-e,i}$ on the right-hand side of Eqs. (7) and (8) arises from the mass exchange of species i between the bubble and emulsion phases,

$$f_\mathrm{b-e,i} = \varepsilon_\mathrm{b} a_\mathrm{b} k_\mathrm{b-e,i}(\rho_\mathrm{i,e} - \rho_\mathrm{i,b}) + f_\mathrm{ng,i} \tag{11}$$

There are two contributions in Eq. (11): the first one is driven by the difference in concentration of species i characterized by a coefficient $k_\mathrm{b-e,i}$. The second term $f_\mathrm{ng,i}$ is the transfer of gaseous species i with the net flow f_ng from the emulsion to the bubble phase

$$f_\mathrm{ng,i} = f_\mathrm{ng}\frac{\rho_\mathrm{i,e}}{\rho_\mathrm{T,e}} \tag{12}$$

f_ng results from the generation of gas by devolatilization and char reactions in the emulsion (all solids are assumed to be in the emulsion) as well as the increase in molar flow due to the homogeneous reactions in the emulsion

$$f_\mathrm{ng} = (1-\varepsilon_\mathrm{e})(1-\varepsilon_\mathrm{b})\sum_\mathrm{i}\sum_\mathrm{m}\sigma_\mathrm{m} r^\mathrm{e}_\mathrm{gs,m,i} + \varepsilon_\mathrm{e}(1-\varepsilon_\mathrm{b})\sum_\mathrm{i} r^\mathrm{e}_\mathrm{gg,i} \tag{13}$$

All gas generation is transferred to the bubble phase, or it directly forms new bubbles, i.e. endogenous bubbles [91,92]. Fig. 8 illustrates this by the arrow representing F_ng ($F_\mathrm{ng,i} = f_\mathrm{ng,i}A_\mathrm{B}\mathrm{d}h$) from the solids in the emulsion to the bubble phase. The bubble phase in Eqs. (7) and (8) then includes both exogenous bubbles coming from the distributor and endogenous bubbles generated by the reaction. Note that the exchange of species i by the excess of gas production in the emulsion phase (with the net flow) is considered instantaneous, whereas the exchange driven by the difference of species concentration is finite, characterized by $k_\mathrm{b-e,i}$.

To account for the net gas generation and the change in gas density, at any height h, the total gas flow rate $F_\mathrm{0,h}$ is updated to incorporate the increments in the flow given by $F_\mathrm{ng,h}$ (see Fig. 8)

$$F_\mathrm{0,h+dh} = F_\mathrm{0,h} + F_\mathrm{ng,h} = (F_\mathrm{e,h} + F_\mathrm{b,h}) + F_\mathrm{ng,h} = F_\mathrm{e,h+dh} + F_\mathrm{b,h+dh} \tag{14}$$

Several solids m can be part of the bed, for instance inert bed material, char and catalyst, being σ_m the volume fraction occupied by solid m ($\mathrm{m^3}$ solid $m/\mathrm{m^3}$ solids). The m-th solid subjected to gas–solid reaction with the rate $r_\mathrm{gs,m,i}$ in Eqs. (8), (10), and (13) takes into account the generation of the gaseous species i.

The mass balance for solids m in the bottom bed, assuming that the solids are perfectly mixed, is

$$F_\mathrm{m,in,B} - F_\mathrm{m,out,B} = \int_0^{H_x}\left(A_\mathrm{B}(1-\varepsilon_\mathrm{e})(1-\varepsilon_\mathrm{b})\sigma_\mathrm{m}\sum_\mathrm{i} r^\mathrm{e}_\mathrm{gs,m,i}\right)\mathrm{d}h \tag{15}$$

The flow of solids m entering the bottom bed, $F_\mathrm{m,in,B}$ consists of the solids feed and the recycling stream, if there is one. The flow of solids leaving the bed, $F_\mathrm{m,out,B}$ consists of the drainage (overflow or mechanical removal) and the net flow to the freeboard.

The mass conservation of the components in the freeboard is

$$\frac{1}{A_\mathrm{F}}\frac{\mathrm{d}(F_\mathrm{i,F})}{\mathrm{d}h} = \varepsilon_\mathrm{F} r^\mathrm{F}_\mathrm{gg,i} + \sum_\mathrm{m}(1-\varepsilon_\mathrm{F})\sigma_\mathrm{m} r^\mathrm{F}_\mathrm{gs,m,i} \tag{16}$$

where a single-phase model for the gas (plug flow) and an axial distribution of the solids in the freeboard, $\varepsilon_\mathrm{F}(h)$ are assumed. Note that $F_\mathrm{i,F}$ in Eq. (16) indicates the net flow of i in the upward direction, including the i traveling both as gas and as solid. The

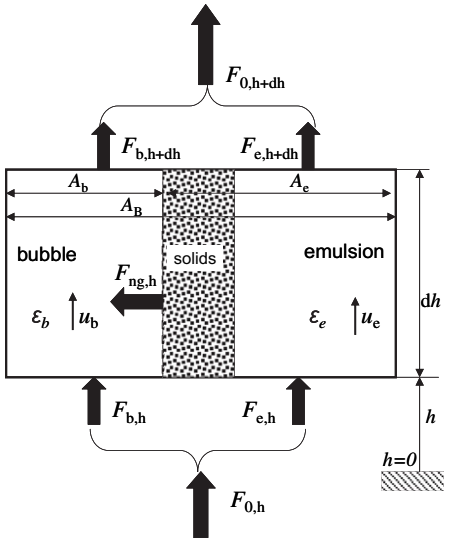

Fig. 8. Definitions of fluid-dynamic parameters in a volume element of the bottom bed.

Table 3
Main reactions in biomass gasification process.

Stoichiometry	Heat of reaction (kJ/mol)	Name	Number
Biomass → char + tar + H_2O + light gas (CO + CO_2 + H_2 + CH_4 + C_2 + N_2 + …)	>0	Biomass devolatilization	R1
Char combustion			
$C_2 + ½O_2 \rightarrow CO$	−111	Partial combustion	R2
$C + O_2 \rightarrow CO_2$	−394	Complete combustion	R3
Char gasification			
$C + CO_2 \rightarrow 2CO$	+173	Boudouard reaction	R4
$C + H_2O \rightarrow CO + H_2$	+131	Steam gasification	R5
$C + 2H_2 \rightarrow CH_4$	−75	Hydrogen gasification	R6
Homogeneous volatile oxidation			
$CO + ½O_2 \rightarrow CO_2$	−283	Carbon monoxide oxidation	R7
$H_2 + ½O_2 \rightarrow H_2O$	−242	Hydrogen oxidation	R8
$CH_4 + 2O_2 \rightarrow CO_2 + 2\,H_2O$	−283	Methane oxidation	R9
$CO + H_2O \leftrightarrow CO_2 + H_2$	−41	Water–gas shift reaction	R10
Tar reactions (**tar assumed** $C_{n\ and\ m}$)			
$C_nH_m + (n/2)\,O_2 \rightarrow nCO + (m/2)\,H_2$		Partial oxidation	R11
$C_nH_m + n\,CO_2 \rightarrow (m/2)\,H_2 + (2n)\,CO_2$		Dry reforming	R12
$C_nH_m + nHO_2 \rightarrow (m/2{+}n)\,H_2 + nCO_2$	Highly endothermic +(200 to 300)	Steam reforming	R13
$C_nH_m + (2n - m/2)\,H_2 \rightarrow n\,CH_4$		Hydrogenation	R14
$C_nH_m \rightarrow (m/4)\,CH_4 + (n - m/4)\,C$		Thermal cracking	R15

contribution of the net flow has no meaning, since solids and gas are lumped into a single component. The mass flows of solids tend to decrease at higher positions, accounted for by modeling of the entrainment and elutriation at different heights, giving $\varepsilon_F(h)$. This 1D single-flow model for the freeboard is often enough to describe the conversion in bubbling FBG. In CFBG a somewhat more complex, but still simplified, treatment is usually made by dividing the freeboard into regions as described below, based on the core-annulus model. This makes it possible to calculate the distribution, $\varepsilon_F(h)$ as well as the solids flow in the freeboard by giving a 1D formulation of a 2D flow situation (sometimes called 1.5 D models), and Eq. (16) can be used for both types of FBG.

Boundary conditions are given by the composition and flow rates of the fluidization agent and of the solids fed to the reactor. Other boundary conditions necessary for the fluid-dynamic model are discussed below. The source terms of the reacting particles, i.e. chemical reactions and gas–solid transport coefficients, are discussed in detail in Section 3. r_{gg} and r_{gs} are functions of h, and therefore the spatial distribution of particles involved in the calculations of these quantities, mainly char and devolatilizing particles, has to be known. Char is well mixed in the bottom bed, as discussed above, so a volumetric source equally distributed through the bed can be defined. On the other hand, the distribution of devolatilizing fuel particles depends on Da_{py} discussed in Section 2.2.4. For the limiting Da_{py}, described in connection to Fig. 6, the devolatilization reactions r_{gs} can be simplified by identifying sources at specific locations (Case a and b), or by assuming the release of volatiles to be well distributed in the bed (limiting case within Case c). The intermediate Da_{py} cases need further modeling of individual particles moving through the bed, as already discussed (general Case c).

In order to apply the conservation equations Eqs. (7), (8), (15), and (16) the key parameters have to be calculated from the fluid-dynamic model. In the bottom zone these parameters are: the (volume) fraction occupied by gas ε_x in the bottom bed, the fraction occupied by bubbles ε_b in the bottom bed, the fraction of gas in the emulsion phase, ε_e, the velocity of gas in the emulsion u_e, the bubble velocity u_b and bubble size d_b. The distribution of gas in the phases is computed at any height by Eq. (14). In the freeboard, the corresponding quantity is ε_F. Other variables appearing in the conservation equations, such as the coefficient of gas exchange between bubble and emulsion k_{b-e}, the specific surface of bubbles a_b, the volume fraction of solid m, σ_m, and others not explicitly written in the equations can be obtained from the variables mentioned, as will be shown in the following.

2.3.2. Fluid-dynamic modeling

This section establishes the distribution, the flow, and other properties of solids and gases in the reactor, needed to close the reactor models. The major part of the solids inventory inside an FBG is bed material (sand, dolomite, etc). The amount of char and devolatilizing particles is much less and is usually assumed not to have an influence on the gross solids flow-pattern, although its distribution throughout the reactor is given by the flow of the bed material. Therefore, the fluid-dynamics in an FBG are calculated using the properties of the inert solids. The bed material is distributed in different ways in bubbling and circulating FBG: the bottom bed contains most of the material in a BFB, whereas in a CFB the material in the bottom is about the same or less than that circulating in the freeboard. In addition, in the CFB there is some material in the external loop, i.e. in the return leg and downcomer. Depending on the operating conditions and on the geometry of the FB, different steady-state distributions are attained. Beside the superficial velocity and bed temperature, the way of operation should be known before the flow pattern can be established. The operation strategy could be such that the amount of bed material is conserved, and a constant pressure is maintained in the gasifier. To fulfill this condition, material has to be added during an increase of load and removed during a decrease of load. In the processing of fuels containing a high fraction of ash, bed material has to be removed from the bed to maintain the bed inventory. This can be made by continuous drainage or at intervals. Consistently, for low-ash fuels, bed material has to be added continuously with the fuel feed or at intervals through dedicated ports.

The literature on the flow in FB is abundant [4,44,47,114–117]. Only the most relevant estimations needed for the solution of Eqs. (7), (8), and (16) are discussed here. In the following, modeling of the two main zones, bottom bed and freeboard, is carried out separately in both bubbling and circulating FB.

2.3.2.1. Modeling of the bottom zone. Despite the observation of different time-averaged bottom bed voidages in bubbling and

circulating beds, the modeling of the two FB units is similar in fuel conversion devices, employing beds of Group B particles, provided that the correlations used are within their ranges of validity [117].

Neglecting a small influence of acceleration, the density of solids in the bottom zone at a height h is calculated by means of the pressure gradient [118]

$$\rho_p(1-\varepsilon) = \frac{1}{g}\left(-\frac{dp}{dh}\right)_h \tag{17}$$

Consistently, the amount of bed material in the bottom zone becomes

$$m_x = \int_0^{H_x} A_B \rho_p (1-\varepsilon) dh \tag{18}$$

At every height h, part of the gas flows through the emulsion phase, and the rest forms bubbles. The overall voidage is

$$\varepsilon = \varepsilon_b + (1-\varepsilon_b)\varepsilon_e \tag{19}$$

The bubble velocity is estimated [47] to

$$u_b = u_v + u_{br} \tag{20}$$

where u_{br} is the single bubble velocity in an infinite freely bed, which can be calculated according to Eq. (96) in Table 2. u_v is the visible bubble flow defined as $u_v = \varepsilon_b u_b$, which is equal to $u_v = (u_0 - u_{mf})$ according to the original two-phase theory. The velocity at minimum fluidization can be calculated by Eq. (98) where $Re_{p,mf}$ is obtained by empirical correlations [45,119] in Eqs. (99) and (100). Once u_{mf} is known, ε_{mf} is given by the Ergun equation [120], given by Eq. (101) in Table 2. The bubble size can be calculated with empirical correlations [121–124]. The two first are included in Table 2 (Eqs. (102) and (103)). There are alternative equations [4,24,44,114].

Various approaches have been followed to calculate the distribution of gas in the two phases of the bottom bed. Two main procedures are described below. Each of them has several alternatives, depending on the assumptions made and the correlations used. In the following we discuss some alternatives, indicating the most suitable models for FBBG.

2.3.2.1.1. Procedure 1. To find the fluid-dynamic parameters, some FBG models assume a constant superficial velocity through an isothermal bed without considering the effect of endogenous bubbles formed by the volatiles, which is strictly true in cold models. The solids mixing is considered even in the entire bottom bed, and the average porosity ε (or bed density ρ) independent of height above the gas distributor. This porosity is calculated by time-average pressure difference between any two axial points in the range of 0 to H_x. If the emulsion phase is assumed to be at minimum fluidization ($\varepsilon_e = \varepsilon_{mf}$), ε_b is also constant with h to be in agreement with Eq. (19).

The total fluidization flow supplied to the bottom bed, represented by the superficial velocity u_0, is divided into three parts: the flow in the emulsion phase, u_e, the visible bubble flow, u_v and the throughflow, u_{tf} [117,126,127].

$$u_0 = u_e + u_v + u_{tf} \tag{21}$$

That is, a gas flow ($u_v + u_{tf}$) does not pass through the emulsion phase. Combination of Eqs. (20) and (21) and taking into account that $u_v = \varepsilon_b \cdot u_b$, lead to the following relation for ε_b:

$$\varepsilon_b = \frac{1}{1+\frac{u_{br}}{u_v}} = \frac{1}{1+\frac{u_{br}}{(u_0-u_e-u_{tf})}} \tag{22}$$

u_{br} is estimated by Eq. (96) and u_e is usually assumed to be equal to ε_{mf}, so to determine ε_b from Eq. (22), the visible flow u_v has to be determined. This is made in terms of a dimensionless visible bubble flow, ψ [128]:

$$u_v = \psi(u_0 - u_e) \tag{23}$$

Combination of Eqs. (21) and (23) yields an expression for u_{tf} in terms of ψ:

$$u_{tf} = (1-\psi)(u_0 - u_e) \tag{24}$$

ψ is correlated with measurements and presented as correlations (Eq. (104) [128] and Eq. (105) [125] in Table 2) so u_v and u_{tf} can be determined. Eq. (105) was introduced to remove the height-dependence of ψ (and so ε_b) calculated with Eq. (104), which was in disagreement with their measurements [125]. The factor f in Table 2 is independent of height and correlated in the original model [125] to experimental data from bubbling beds in BFB units (f_{BFB}) and thereafter for CFB units (f_{CFB}) [117,125].

In summary, determination of ε_b is then made by Eq. (22), using u_v and u_{tf} given by Eqs. (23) and (24). For instance, Eq. (106) in Table 2 was obtained in [125] by using Eqs. (102) and (105) as correlations for d_b and ψ, respectively. The original two-phase theory is a particular case, where $\psi = 1$, $u_{tf} = 0$, so $u_v = (u_0 - u_{mf})$ flows through the bubble phase and u_{mf} through the emulsion. At very high fluidization velocity in CFBG for particles of Group B, the bottom-bed voidage levels out at a certain value provided that there is a sufficient amount of solids in the CFB-loop to maintain a dense bottom bed [118].

2.3.2.1.2. Procedure 2. In this method non-isothermal effects and generation of gas by reaction can be dealt with. ε is calculated through a bed expansion factor f_{bex}, defined as

$$f_{bex} = \frac{1-\varepsilon_e}{1-\varepsilon} \tag{25}$$

f_{bex} is calculated by empirical correlations such as Eq. (107) in Table 2, obtained by fitting measurements of various commercial BFB coal gasifiers [129]. It depends on height h because some of the variables appearing in Eq. (107) depend on h. Eq. (25) together with a correlation for f_{bex}, yields a relationship for ε and ε_e. Some authors assume $\varepsilon_e = \varepsilon_{mf}$. Then ε can be directly estimated by Eq. (25) and Eq. (19) gives ε_b. Others calculate ε_e by empirical correlations, such as Eq. (108) in Table 2 [130], and again, others have applied the gas conservation given by Eq. (14) to calculate F_e, once F_b has been estimated by semi-empirical correlations (such as the one presented in Eq. (20)). In this method, the two-phase theory of fluidization determines the gas split near the distributor ($h = 0$), as an initial condition, but this theory is abandoned for positions above the distributor in order to allow gas generation and temperature variation with height by Eq. (14).

2.3.2.1.3. Bubble–emulsion transfer. The coefficient of mass exchange between bubble and emulsion, k_{b-e}, has been thoroughly investigated. It has been assumed [47] that the mass is transferred by convective gas flow through the bubble and by molecular diffusion, and that there is no difference between the gas in the bubble and emulsion. An empirical correlation for k_{b-e} has been developed in analogy with mass transfer across the surface of a liquid droplet rising in another liquid, assuming that the gas in the bubble and cloud is thoroughly mixed [131]. The previous two models can be combined [44], introducing three phases, bubble, bubble cloud and emulsion, where two processes take place in series: gas exchange between bubble and cloud and between cloud and the emulsion. Experimental verification has demonstrated that models applying the convective mass transfer processes (Davidson's approach) yield excessively large values of k_{b-e}, whereas models implying that the mass transfer process is controlled by molecular diffusion [44,131] underestimate the mass transfer k_{b-e}

[4,51], mostly in the zone near the distributor where the bubble interaction is strong [132]. The previous experimental studies have been used [132] to suggest a combination of convective and diffusion processes: the clouds around the bubbles were included as part of the emulsion, resulting in Eq. (109), which is the most accepted correlation [4,44,45], since it appears to fit the measurements better that the others. Surveys on models and correlations have been published [4,24,44,45,51].

2.3.2.1.4. Discussion. As seen, there is no universal method to model the fluid-dynamics of the bottom zone of an FBG. Many correlations are identical, but the hypotheses made may vary, especially those accounting for the flow pattern in the emulsion. Most correlations have been obtained in cold rigs without considering the influence of the gas generated by reactions with solids. It is difficult to establish guidelines for choosing the correct model in each case, since the fluid-dynamic parameters have not been measured in the works where the FBG models were formulated. In most cases, only measurements of gas composition in the outlet stream are used for validation.

In an FBG, the gas flow F_0 increases with height h due to release of volatiles and gas generated by char gasification. Also temperature may affect the rise in F_0, especially near the gas distributor where a peak temperature (and so, higher u_0) can be attained [24]. In this case $d\varepsilon/dh \neq 0$ and $dp/dh \neq constant$. Some authors have provided experimental evidence that the voidage of the dense bed depends on h even in cold, non-reacting rigs [128,132,133]. Some authors [117] have argued that the gas flow through the emulsion phase, u_e, is small compared to the primary gas flow and the influence of an error due to the assumption of $\varepsilon_e = \varepsilon_{mf}$ is small. Experimental support for this statement has been published for FB combustors [125]. There is no clear evidence whether the statement applies to FB gasifiers, since the ratio of gas/solids in FBG is smaller than in combustors, whereas the ratio of gas produced to fluidization agent is larger. The latter enhances the impact on the flow pattern of the rapid release of volatiles in the form of endogenous bubbles. Only some works [91,92,134,135] deal with this question. However, these works investigated the flow pattern at minimum fluidization, which is quite far from the real situation in FBG, and quantitative extrapolation is questionable. Qualitatively, though, the conclusions in [91,92] indicate that the fluid-dynamics of FBG are greatly affected by gas produced by reaction in the form of endogenous bubbles. Without dedicated measurements, a compromise between uncertainty and simplicity is recommended: use Eqs. (7) and (8), where it is assumed that all gas generated by reactions of solids in the emulsion phase, together with the net flow generated by homogeneous reactions in the emulsion gas, is transferred to the ascending bubbles or forms new bubbles, consistent with the hypothesis that the emulsion remains at minimum fluidization. This avoids the difficult discussion on the gas-flow pattern in the emulsion, and the mass balance is fulfilled by Eq. (14).

2.3.2.2. Modeling of the freeboard. The key concept of freeboard modeling is the quantification of the entrainment of particles from the bubbling bottom zone in the form of a steady solids flow through the freeboard and further through a circulation loop back to the bed. The state in the freeboard can be regarded either as flow of particles (F), flux of particles (G), density of suspension (ρ), or as voidage (ε).

Particles are ejected by the bubbles, especially by the wake and by bubbles coalescing at the bed's surface. A fraction of the particles returns to the bed because their terminal velocity is greater than the gas velocity or because the terminal velocity is enhanced by clustering of particles. Most downflow of solids in the riser takes place along the walls. These phenomena exist in both bubbling and circulating FB. However, the importance of the backmixing of the two solids flows, i.e. a solids-clustering flow and a core/wall-layer flow in the upper part, can differ significantly between types of bed as discussed below. In BFB the superficial velocity is lower, but there is no fundamental difference in the fluid-dynamics of the freeboard in the two types of unit. The difference is in the relative contribution of the freeboard to the overall conversion processes: the amount of particles in the bed of a BFB is much higher than that in the freeboard, so most solid fuel transformations occur in the bed. In contrast, in a CFB, the particles in the bed are entrainable, so the solids circulation is larger and the significance of solids reactions in the freeboard increases: a great deal of the fuel conversion occurs there.

The development of BFB preceded that of CFB and therefore a great amount of correlations for modeling of the freeboard are based on entrainment and elutriation in BFB (mostly obtained in lab-scale cold vessels). This has been demonstrated not to be sufficiently good for the estimations of CFB units [96], and a more complex modeling is developed for CFB. Here we present separately the freeboard modeling in the two types of FBs because of historical reasons. However, it is demonstrated here how the classical modeling of BFB [44] is just a particular case of a more general model treating CFB units.

2.3.2.2.1. BFB freeboard. The entrainment rate of particles at height h, that is, the flux of particles G, can be empirically represented by [44,136]

$$G = G_\infty + (G_x - G_\infty)\exp(-a(h - H_x)) \quad (26)$$

where G_x, is the entrainment flux of particles at the surface of the dense bed ($h = H_x$) and G_∞ is the particle flux in an imaginary long column, whose height is higher than the transport disengaging height. There are few correlations for direct estimation of G_x. Eq. (111) in Table 2 presents the most widely used correlation for G_x in modeling of bubbling FB combustors and gasifiers [136]. G_∞ is estimated by empirical correlations for the elutriation rate coefficient, E_∞ (E_∞ equals the saturation carrying capacity, i.e. entrainment at heights above the transport disengaging height, i.e. $G_\infty = E_\infty$). Numerous experiments have been conducted to determine the elutriation rate constant for different particle sizes i, $E_{i,\infty}$. For a distribution of particles in the bed, E_∞ is calculated as $E_\infty = \sum E_{i,\infty} x_{i,b}$, where $x_{i,b}$ is the mass fraction of particles i in the bed. Compilation of correlations for $E_{i,\infty}$ under different operating conditions are available [4,44,90]. Many of them relate the elutriation coefficient to $u_0 - u_t$. There is a large disagreement between experimental data and correlations for specific elutriation fluxes, and these empirical correlations should be used carefully within the experimental conditions for which they have been derived. A correlation [137] for solids density from 920 to 5900 kg/m^3 in FB up to 0.9 m diameter using gas velocities up to 4 m/s, is shown in Eq. (112) (Table 2).

In accordance with the flux, a similar relationship expresses the particle density at height h (or loading $\rho = G/u_p$) as

$$\rho = \rho_\infty + (\rho_x - \rho_\infty)\exp(-a(h - H_x)) \quad (27)$$

where $\rho_x = \rho_p(1 - \varepsilon_x)$ is the cross-section average suspension density at the surface of the bed $h = H_x$ and ρ_∞ is the density above the transport disengaging height.

In summary, the fluid-dynamic modeling of the freeboard in a BFBG is given by Eqs. (26) and (27). This allows estimation of the particle flux and density profiles along the freeboard as a function of the parameters: a, ρ_∞, ρ_x, G_x, and G_∞ ($=E_\infty$). The decay coefficient a is assumed to depend on superficial velocity and to be independent of particle size. It is determined by empirical correlations, ranging from 3.5 to 6.4 m^{-1} [44]. ρ_∞ is in the order 10^{-3}–10^{-4} for

most BFBG, while ρ_x is the result of the bottom zone model developed above. For estimation of G_x, the correlation in Eq. (111) can be used as a result of available correlations and G_∞ is estimated by empirical correlations for the elutriation rate coefficient, E_∞, for instance Eq. (112) from [137]. Since there is a large disagreement between correlations for G_x and E_∞, they only should be used within the ranges of the experimental conditions for which they have been derived; otherwise dedicated experiments for a given system are recommended. This point is critical if entrainment plays a decisive role for calculation of the gasification performance, i.e. for high char entrainment with severe fragmentation, producing a great portion of elutriable char fines.

2.3.2.2.2. CFB freeboard. The freeboard of a CFB can be divided into a splash zone, a transport zone and an exit zone. Particles are thrown out of the bottom bed by bubble eruptions and/or are carried away by the gas. The bubble eruptions form a splash zone with high back-mixing of particles. Above the splash zone, sufficiently small particles are carried away by a saturated flow of gas, and the clustering back-mixing in the core of the transport zone is small. Instead, particles are transported from the core into the wall layers, where the gas velocity is smaller, and they fall downwards. This second mechanism is dominant far away from the splash zone [117,138].

The transfer of particles from the core to the wall results in a decay of the average solids density with height. In the splash zone, the concentration changes from a typical average particle volume concentration $(1-\varepsilon_x)$ at the top of the bottom bed of 0.3–0.4 to that in the transport zone, which ranges from 0.001 to 0.01 at full load operation. There is also a variation of flux and density in the horizontal direction. The vertical flow is upwards in the core and downwards at the walls. The difference in horizontal flow profiles between risers with different aspect ratios (height to diameter ratio) is notable: it is parabolic for narrow and tall risers, while the profile is flat for risers with small aspect ratio. It has been argued [139], based on a comparison of available literature data, that this difference between broad and narrow risers could depend on the fact that the profile is still developing in the broad risers, which have a small height to width ratio, whereas it is developed in risers with a large aspect ratio. It is suggested that above a certain, yet unknown height to diameter ratio, the flow of particles into the wall-layer will be compensated for by an equally large flow out of the wall-layer, and above that level the vertical particle suspension density will be constant with height.

Fig. 9 illustrates the main solids flows in the transport zone of a FB by distinghishing between the upward flow in the core, F_c, and the downward flow in the layer, F_w. The upward flow of particles in the transport zone is $F_c = G_c A_c$ where G_c is the particle flux and A_c the cross-section area of the core (index c). Due to transfer of particles between the core and the wall layer (illustrated in Fig. 9) there is a change in the ascending flow given by

$$-\mathrm{d}F_c = 2\pi R_c \mathrm{d}h(k_w\rho_w - k_c\rho_c) \tag{28}$$

where R_c is the radius of the core (a circular section is assumed), dh a height element and $k_{w/c}$ are unknown transfer coefficients related to the particle concentration $\rho_{c/w}$ in the core and wall layer. The transfer mechanisms may be deposition and diffusion, but little is known about them, so a net transfer coefficient $k_{c\text{-}w}\rho_c = k_w\rho_w - k_c\rho_c$ is introduced. The wall layer thickness is small compared to the equivalent radius of the freeboard, and integration of Eq. (28) from the top of the freeboard (index o) to a height h yields

$$G_c = \rho_o A_c(u_o - u_t)\exp(-K(h-H)) = G_{co}\exp(-K(h-H)) \tag{29}$$

where the integration has been made by defining a "decay" constant $K = 4k_{c\text{-}w}/(2R_c(u-u_t))$ assuming that the flow in the transport zone is rather dilute, so that the terminal velocity of a single particle u_t can be used to determine the slip velocity $u_p = u_o - u_t$. This allows formulating a relationship between particle flux and suspension density.

$$G_c = \rho_c(u_o - u_t) \tag{30}$$

At any height $F_w + F_c = F_{wo} + F_{co}$ holds, so the downward flow at the wall becomes

$$F_w = F_{wo} + F_{co}(1 - \exp(-K(h-H))) \tag{31}$$

Without exit effects in the riser, F_{wo} is zero and $F_{co} = GA_F$ is equal to the net solids flow, which at this height is equal to the external recirculation flow. However, most CFB have a more or less abrupt exit, and a fraction of solids fails to leave the exit. Therefore F_{wo} can be described in proportion to G as $F_{wo} = -k_b GA_F$ [140] and the flow $F_{wo} + F_{co}$ partly leaves the riser to the separator, $(1-k_b)GA_F$, and is partly reflected back from the roof, $-k_b GA_F$. Therefore the exit of the riser acts as a separator with separation efficiency $\eta_{sep} = k_b/(1+k_b)$. The wall-flow can now be written as:

$$F_w = A_F G[1 - (1+k_b)\exp(-K(h-H))] \tag{32}$$

To sum up, calculation of the solids flow is made as follows: F_c is calculated by $F_c \approx G_c A_F$, where G_c is estimated by Eq. (29) if no direct measurements are available. F_w is then calculated by Eq. (32) and k_b is estimated by measurements [139,140]. u_t is given by correlations (Table 2) and the "decay" constant K is usually correlated experimentally (Eq. (114)), as discussed below.

It is important to know how the bed material is distributed in the riser, as expressed by the vertical and horizontal density profiles. On the basis of Eq. (30), the suspension density in the core of the transport zone can be obtained from Eq. (29)

$$\rho_c = \rho_{co}\exp(-K(h-H)) \tag{33}$$

There is a relationship between the suspension density in the core ρ_c and that at the wall ρ_w in the transport zone. Therefore, it is possible to relate ρ_c to the cross-section average density $\rho_{av} = b\rho_c$ where $b \approx 2$ [141], a ratio that is rather constant over a vide range of densities, as illustrated in Fig. 10, which also shows that the suspension density of the wall layer is higher than that of the core. Eq. (33) is then

$$\rho_{av} = \rho_{avo}\exp(-K(h-H)) \tag{34}$$

with ρ_{avo} being the average density at the top. To keep the notation simple, in the following the subscript 'av' will be omitted.

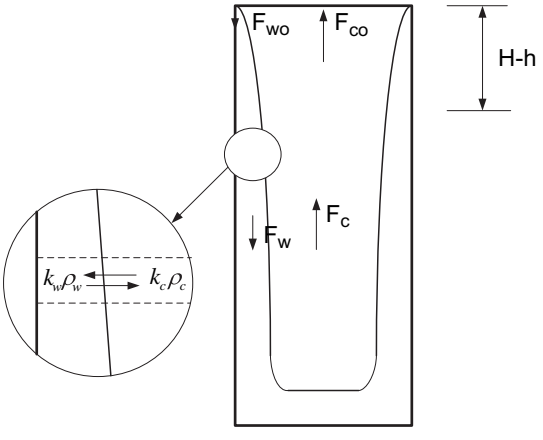

Fig. 9. Particle flows in the transport zone of an FB.

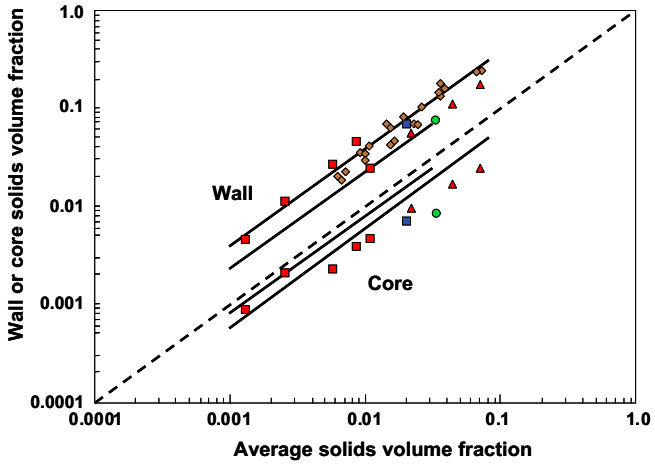

Fig. 10. Local solids volume concentrations at a plane vertical wall layer and in the core versus cross-section average solids volume concentration in a CFB. The cross-section average density ρ_{av} is about $2\rho_c$ where ρ_c is the suspension density in the core (After Zhang et al. [141] who collected data from own measurements and other sources).

Close to the bottom bed, the particle concentration is also affected by the contribution from ejection of particles by the bubbles followed by a back-flow of coarser particles (as in the bubbling FB). The corresponding density profile from the splash zone must be added to the density of the transported flux of particles, described by Eq. (34). Therefore, in the modeling of average axial density profiles through the splash zone down to the surface of the bottom bed, both mechanisms are accounted for:

$$\rho = \rho_{bx}\exp(-a(h-H_x)) + \rho_o\exp(-K(h-H)) \quad (35)$$

ρ_{bx} is obtained by applying Eq. (35) at the bed surface where the two components of particle density are assumed to coexist: $\rho_{bx} = \rho_x - \rho_{ox}$. ρ_x is given by the above mentioned bottom-bed model and ρ_{ox} is calculated by applying Eq. (34) at $h = H_x$: $\rho_{ox} = \rho_o\exp(-K(H_x - H))$. The decay constants a and K have been determined empirically [140] as indicated in Eqs. (113) and (114) in Table 2 and further illustrated in Fig. 11.

Fig. 12 shows how ρ (Eq. (35)) is obtained by summing up the two contributions. The first part of Eq. (35) is the contribution of the splash zone, caused by the particles thrown up by the movement of the bed, similar to the classical form proposed by Lewis and others, typical for the bubbling bed, shown in Eq. (27). The second part of the Eq. (35) is the contribution from the riser flow above the splash zone extrapolated to the surface of the bed. If the transport mechanism is neglected in Eq. (35), the second term vanishes and $\rho_x = \rho_{bx}$. In this case Eq. (35) equals Eq. (27), which is valid since ρ_∞ is negligibly small for both the splash zone and for the transport zone, as illustrated in Fig. 12. Hence, Eq. (35) is a general empirical representation of the fluid dynamics of the freeboard in an FB, valid for both circulating and bubbling FB units, whereas Eq. (27) is a simplification that takes into account only one mechanism of backmixing, usually applicable for bubbling units. In BFB the decay in solids concentration above the bed is a direct function of the superficial velocity as shown in Eq. (113) or by $au_0 = constant$ [44]. The influence of superficial velocity on K has also been observed in circulating systems [139]. In large scale CFB it has been found that $K \approx 1/H$ fits measurements better, suggesting that the decay mechanism depends only of the riser's height and not of the superficial velocity [138]. In [138] measurements on average suspension density were compared for various large-scale CFB boilers and the agreement of Eq. (35) compared with Eq. (27) was shown. Despite this experimental evidence, Eq. (27) instead of Eq. (35) is still sometimes used for freeboard modeling of CFB units.

To sum up, the axial density profile in the freeboard of a CFB can be represented by Eq. (35) and that of a BFB by the first part of Eq. (35) or by Eq. (27). The decay constants are obtained by Eqs. (113) and (114), Fig. 11, or by measurements. The suspension density at the top of the riser ρ_o is the most uncertain parameter. It can be estimated, though, from the circulating flux G assuming Eq. (30) to be valid if G is not measured. Alternatively, an estimate of ρ_o is obtained from pressure measurements along the riser. Clearly Eq. (30) is not valid at the walls where $u_0 < u_t$ and the particles fall down. This means that $dp/dh = -\rho g$ is difficult to interpret, and so, the determination of ρ from pressure drop measurements is uncertain. However, in a large riser this seems to be of minor importance. Finally, in the equations, the bottom bed parameters ρ_x and H_x are obtained by the bottom bed model presented above or by direct measurements.

2.3.3. Extensions

The range of validity of FM is discussed as follows. Extensions of the model deal with size distributions of different types of solids, and with multidimensional, non-isothermal and non-steady effects. Inclusion of such improvements in FBG models can be useful for more precise knowledge of the process; however, a large quantity of input data, often not available, is needed. Dedicated experiments, seldom carried out in large FBBG, are necessary for determination of some inputs and also for validation. Therefore, only when predictions with simple 1D isothermal models are not

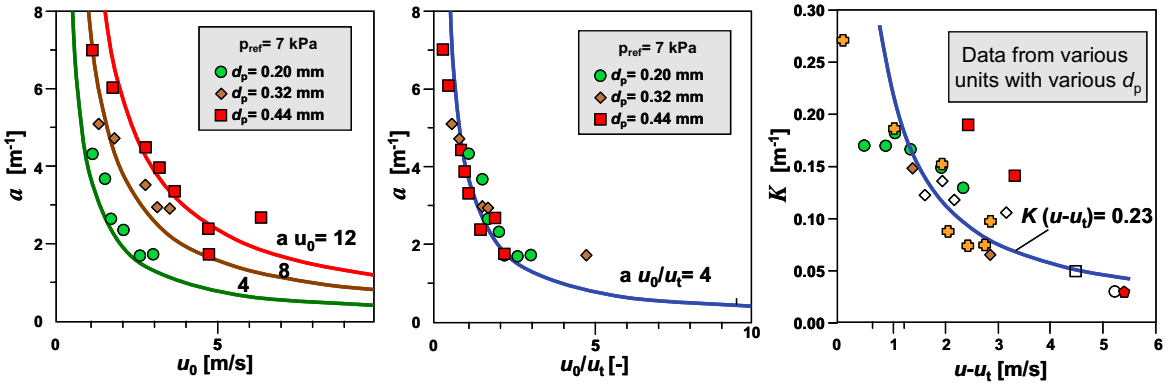

Fig. 11. Decay coefficients a and K for different bed particle sizes. (After Johnsson and Leckner [140]).

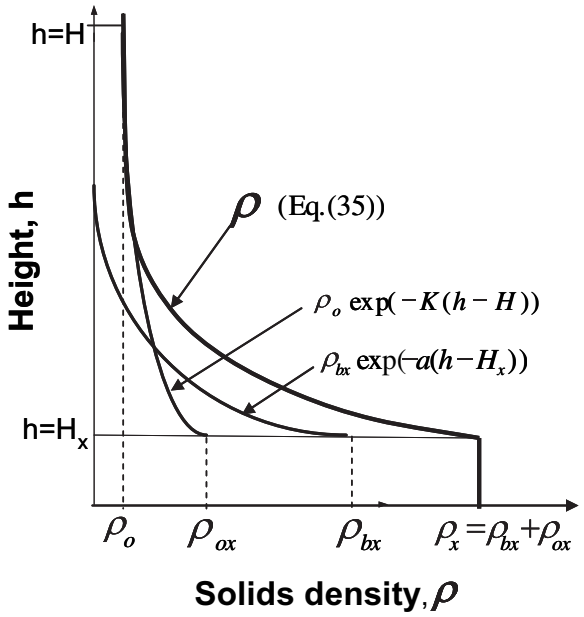

Fig. 12. Solids density profiles in an FB (thick black line is given by Eq. (34)).

sufficiently good, models including these extensions should be formulated together with consistent input data. This is further discussed in Section 4 where the capabilities of published FBBG models are compared.

2.3.3.1. Particle size distribution. In addition to the spatial distribution of solids, there is a particle size distribution. Several phenomena affect the original particle size distribution of the feed, such as gas–solid reactions, entrainment, fragmentation and generation of fines by attrition. The most common solids in FBG are inert sand, fuel, and catalyst for tar removal, such as dolomite, lime or other. Consideration of the devolatilizing fuel as an individual type of solid is important. Despite this, it is not done in most of FBG models. We have shown in connection to Fig. 6 that such a distinction should be made, at least for the choice of a simple model. In a bubbling FBG, most of the solid fuel is expected to be converted in the bottom region, and the approach that will be developed below is valid for the devolatilizing fuel particles too. In contrast, in a CFBG, when a considerable fraction of fuel is elutriable at nominal operation, an extension of this treatment should be made, as discussed in Section 2.3.3.3.

Let a particle of kind m and of size l be named as a particle of the m,l class. The flux and density relationships defined above for the freeboard (Eqs. (26), (27), (29), (32), and (35)) can be used for a particle of the m,l class at height h, provided that the corresponding mass fraction, $x_{m,l}$ is known. For instance: $G_{m,l} = Gx_{m,l}$, $\rho_{m,l} = \rho x_{m,l}$, etc. Therefore, the model developed above is directly applicable if the decay constant and boundary conditions at the surface of the bottom bed and at the top of the freeboard are formulated for a particle of the m,l class. In order to calculate the mass fraction of a particle of the m,l class at steady state in the bottom bed, a population balance for each solid m is formulated:

$$F_{m,l,in} + \Gamma_{m,gain} = F_{m,l,out} + \Gamma_{m,l,loss} + \Re_{m,l} \quad (36)$$

The sum of Eq. (36) for all sizes l yields Eq. (15). The meaning of each term in Eq. (36) can be described as follows:

- $F_{m,l,in}$ is the contribution from the feed streams $F_{m,l,fs}$ and the recirculation or recycling stream, $F_{m,l,rec}$,

$$F_{m,l,in} = F_{m,l,fs} + F_{m,l,rec} \quad (37)$$

The recycling stream $F_{m,l,rec}$, depends on the stream leaving the freeboard and the split ratio applied in a mechanical valve or similar, and on the efficiency of the particle separator (cyclone). The cyclone efficiency as a function of the main geometry parameters and operating temperature of the cyclone can be computed by various methods [142–144].

- $F_{m,l,out}$ is the loss due to forced withdrawals $F_{m,l,with}$ and to entrainment at the surface of the bed $F_{m,l,ent}$:

$$F_{m,l,out} = F_{m,l,with} + F_{m,l,ent} \quad (38)$$

The fraction m,l of particles in the n withdrawal streams is equal to that in the bottom bed $x_{m,l,b}$ as long as perfect mixing is assumed in the bed. The net entrainment at the surface of the bed, consistent with the freeboard model derived, is:

$$F_{m,l,ent} = x_{m,l,c}F_{c,x} - x_{m,l,w}F_{w,x}, \quad (39)$$

or

$$F_{m,l,ent} = x_{m,l,x}F_x - x_{m,l,\infty}F_\infty, \quad (40)$$

if the simplified model for BFB, given by Eqs. (26) and (27) is used. The fraction m,l of particles in the entrainment flow of an BFBG (1D model), is equal to that in the bottom bed $x_{m,l,b}$ as long as perfect mixing is assumed in the bed. In a CFBG, a distinction is made because both particle size distribution and composition of the downward wall-layer flow F_w differs from those in the upward flow in the core F_c and also from those in the bed.

- $\Gamma_{m,gain}$ and $\Gamma_{m,loss}$ are the gain of particles of the m,l class due to the attrition and fragmentation of particles from superior levels (size $> l$) and the loss of particles of the m,l class to inferior levels (size $< l$). The rate of production of fines by attrition and fragmentation is discussed in Section 3.
- $\Re_{m,l}$ is the consumption by chemical reaction of particles of m,l class. This term depends on the conversion model of the particle and, besides the influence of the operating conditions, it may strongly depend on the size and other physico-chemical properties of the solid. This topic is developed in Section 3.

2.3.3.2. Non-isothermal effects. In the model presented, the bed temperature is input, and the temperatures of gas and solids are assumed to be equal. Heat balances can be formulated to give a step forward in the capability of prediction of a gasifier. There are several approaches depending on the aim: (1) overall heat balance over the reactor [65], (2) overall heat balances over regions, such as bed, secondary-air injection zone, and freeboard [110], (3) distributed single-phase heat balances over the various regions without distinction of solids and bubbles in the bottom or solids and gas in the freeboard, and finally (4) distributed heat balances over the phases and along the zones of the reactor, including heat and mass transfer between bubble and emulsion, gas and solid particles, and heat transfer across the external reactor surface (to calculate the heat losses) [28,66,67,145,146]. Models of Type 4 are, in principle, the most convenient for accurate prediction, giving details of temperature profiles for solids and gas phase reactions in the phases along the height of the FBG. Extreme cases (Type 1 and Type 4 models) are formulated in the following to serve as a basis for discussion when comparing published FBG models in Section 4.

A model of Type 1, overall heat and mass balances, can be formulated as inlets = outlets + losses. For heat, this balance can be written

$$\sum_{i=1}^{n_{sp}}\sum_{j=1}^{n_{fs}} F_{i,j}H_{i,j} = \sum_{i=1}^{n_{sp}}\sum_{j=1}^{n_{os}} F_{i,j}H_{i,j} + Q_{loss} \quad (41)$$

The left-hand side is total sum of energy entering the bed: species (index i) in the feed streams (index j) including solid streams, i.e. fuel, catalyst, inert, etc and the gas feed streams, i.e. fluidization agent, secondary injection of air or oxygen, recirculated produced gas, etc. n_{fs}, n_{os} and n_{sp} are, respectively, the number of feed and outlet streams and the total number of species in the system. The right-hand side is the energy carried by gas and solid products leaving the bed, and the net heat loss from the fluidized bed to the surroundings Q_{loss}. The latter can be treated as an input parameter [65] or alternatively, it can be calculated on the basis of reactor temperature, type and thickness of insulation and dimensions of the reactor. A stream j in Eq. (41) can contain m solids, depending on the arrangement of the feed system. A recirculation stream is not included in the streams of Eq. (41) because that would be an internal stream.

In a model of Type 4, exemplified by [66], a 1D isothermal model of the phases is formulated as follows. For the gas in bubble and emulsion phases, the heat balance over a differential volume of height h in the bottom bed yields,

$$\frac{1}{A_B}\frac{d(F_bH_b)}{dh} = q_{b-e} \quad (42)$$

$$\frac{1}{A_B}\frac{d(F_eH_e)}{dh} = \sum_m (1-\varepsilon_e)(1-\varepsilon_b)\sigma_m h_{g-s,m}(T_{s,m}-T_e) + U_w(T_e-T_{ext}) - q_{b-e} \quad (43)$$

The term q_{b-e} arises from the heat exchange between the bubble and emulsion phases,

$$q_{b-e} = \varepsilon_b a_b h_{b-e}(T_e-T_b) + f_{ng,i}\bar{c}_{p,ng}(T_e-T_b) \quad (44)$$

H_e and H_b are the enthalpies of the emulsion and bubble phases including the enthalpies of all species i in respective phase:

$$H_{b/e} = \sum_i^{n_{sp}} x_{i,b/e}H_i \quad (45)$$

H_i is the enthalpy of the i species, accounting for the sensible heat and chemical energy:

$$H_i(T) = H^0_{f,i} + c_{p,i}(T-T_0) \quad (46)$$

For the gas in the bubble phase, Eq. (42) reads as follows: the enthalpy of the gas in the bubble changes due to the net rate of heat transfer from the emulsion by convection (with coefficient h_{b-e}) and to the accompanying net flux f_{ng}. In the emulsion (Eq.(43)), the enthalpy changes by the net rate of heat transfer from the solid particles (by convection with coefficient h_{gs}), the bubbles (by convection with coefficient h_{b-e} and by the net flow) and by exchange with the surroundings (with the overall heat-transfer coefficient U_w). U_w is calculated by taking into account the three mechanisms of heat transfer in series: bed to wall (with film transfer coefficient $h_{b\text{-}w}$), conduction through the solid insulation blanket and free convection caused by the environment (at T_{ext}). Correlations for estimation of h_{b-e}, h_{gs} and $h_{b\text{-}w}$ can be found in the literature [4,24,44].

Boundary conditions necessary for Eqs. (42) and (43) are simply formulated from the heat input with the gas and solids feed streams and are not explicitly written here. The boundary condition for the gas temperature at the distributor ($h = 0$) is more complex. In general, a heat balance from the gas in the plenum to the gas at $h = 0$ is formulated. A heat transfer coefficient has to be calculated for this zone, since the condition of heat transfer differs from the one in the bed [44,67]. For model estimations, a flux of heat losses can be assumed as a parameter to see the influence of this boundary condition.

For any of the m solids in the bed, the heat balance for a particle of type m is formulated in analogy with Eq. (14) as:

$$(FH)_{m,in,B} - (FH)_{m,out,B} = \int_0^{H_x} A_B(1-\varepsilon_e)(1-\varepsilon_b)\sigma_m h_{gs,m}(T_{s,m}-T_e)dh \quad (47)$$

For the freeboard, the heat balance formulation is written as:

$$\frac{1}{A_F}\frac{d(F_FH_F)}{dh} = U_w(T_F-T_{ext}) \quad (48)$$

Eq. (48) considers the solids and the gas in the freeboard as one isothermal phase, similar to the mass conservation equation, Eq. (16). As a result, the flow F_F and enthalpy H_F are the sum the heat contents of the species in the gas and in the solids at height h. The boundary condition for Eq. (48) is obtained by the flux and temperature coupled to the bottom bed model at $h = H_x$.

The solution of the model formulated gives the spatial profiles of gas species in the bubble and emulsion phases. This type of information is rarely validated by measurements (instantaneous profiles of gas in the emulsion, solids m in the emulsion and gas in the bubbles, etc, have not been measured in large FBG, and not even in small devices). As a matter of fact, this criticism also applies to the isothermal model (also in this case there is a lack of solids concentration profiles and other data). The achievement made by including non-isothermal effects in a model of Type 4, i.e. given by Eqs. (42)–(48), has not been proven to be much better than models of Type 1 given by Eq. (41).

To sum up, the Type 1 model should be formulated first, if estimation of the loss can be made. Only if sufficient input data are available, a non-isothermal formulation in the form of Type 4 model should be developed, for instance, in case heat transfer controls the rates of the mass and heat sources.

2.3.3.3. Further improvements. Further extensions are sometimes necessary when formulating FBG models. They are briefly discussed as follows:

- **Modeling the region near the distributor**. Most authors have integrated this zone into the model of the bottom zone due to the complex processes taking place there simultaneously: devolatilization of the fuel, rapid oxidation accompanied by drastic changes of temperature, concentrations, and agglomeration of bed material, etc. Some investigators explicitly modeled this region [65,147] and estimated the jet penetration and transfer coefficients for heat and mass [147]. Gas is distributed in a similar way as discussed above (application of the two-phase theory of fluidization at $h = 0$ and application of overall gas conservation consistent with the gas generation). It has been shown that the jet penetration hardly influences the process in large-scale systems, where bubble cap distributors are used, and jets are not formed, so this model seems not to be necessary for practical applications.

- **Modeling the zone near the feed port**. When modeling the source terms, the transient heating of the devolatilizing particles and the oxidation of volatiles by the entering oxygen are probably the dominant processes in this zone. This, of course, depends on the exact geometry of the feed port and the physical properties of the injected fuel. In general, despite the great importance of this region for correct operation of an FBG, modeling is not well suited to the FM approach, because many of the fluid-dynamics correlations used are based on lumped cold models (bubble size and velocity, expansion factor, throughflow, etc). In addition, very few measurements are available for validation in FBG, especially in large units [147]. It seems better to analyze this zone by means of CFD models, where fluid motion is considered in a consistent way. However, experimental verification is still necessary. Similar discussion could be made for the splash, exit and cyclone regions in FBG, especially in CFB.
- **Modeling the spatial distribution and age population of devolatilizing fuel**. When a considerable fraction of the fuel is elutriable during devolatilization, the treatment should be extended by a population balance of the devolatilizing fuel over the whole reactor. This would give the distribution of devolatilizing particles along the riser, and so, the generation of volatiles in the riser. In this case a more complex model is needed. A rational approach has been presented for combustion of biomass in a CFB [77] where two kinds of particle were distinguished: large non-elutriable fuel particles and fine fuel particles of elutriable size. The non-elutriable fuel particles were assumed to devolatilize uniformly in the bottom bed, whereas the elutriable fuel particles devolatilized all along the riser. To determine the distribution of elutriable fuel particles in the zones of the riser, an age population balance of devolatilizing fuel particles should be formulated, coupled to a kinetic model for drying and devolatilization, as discussed in Section 3. This approach has not been applied to FBG, despite the fact that the fuel distribution along the freeboard can strongly influence the composition of the product gas, specially the tar content and composition.
- **Two-dimensional modeling the freeboard**. In this work, the fluid-dynamics in the freeboard have been formulated on the basis of a 2D structure. However, once the flux of materials in the wall layer and core was estimated, a pseudo-1D formulation for the net flux and density of solids along the riser was made. Consistently, in the conservation equations for the freeboard, a single-phase 1D model was expressed by Eqs. (16) and (48). This implies that particles and gas species are evenly distributed over a section at height h of the freeboard. In addition, in Eqs. (16) and (48) the gas and solids were lumped, so no distinction was made between them. However, in CFBBG, the reacting gas environment in the wall and core has been found to be different [70,76,103]. Moreover, the particle size distributions in the wall layer and the dilute zone of the transport zone are known to be different. As a consequence, an extension by consideration of two phases in the freeboard (instead of lumping the gas and solid as in the model developed above), formulated with an explicit distinction between gas and solids and with some exchange of gas, could be necessary. In addition, different particle size distributions in the wall and core zones might need to be accounted for. This type of model, to the best knowledge of the authors, has not been published for any CFBBG, although measurements made in CFBBG suggest that it could be useful for better understanding of the performance of a reactor [70,76,77,103].

3. Modeling of the source terms

The model of mass and energy transport in the gasification reactor, Eq. (1), contains source terms that handle the production or consumption of fuel, char or gas. The development of submodels to predict these source terms is presented in this section. The thermochemical transformations of the main species C, H, and O are treated, but prediction of the fate of other minor species, such as nitrogen, sulfur, chlorine, alkali and heavy metals is not dealt with.

3.1. Chemical reactions during gasification

Fig. 13 resumes the processes occurring in an FBG. The main chemical reactions are listed in Table 3. The energy for heating the fuel to reactor temperature and for satisfying the endothermic reactions is provided by combustion of part of the fuel. Reaction R1 in Table 3 is primary pyrolysis or initial devolatilization, where char and volatiles are formed. The volatiles include non-condensable gases, such as CO_2, H_2,…, condensable volatiles (tar), and water (chemically bound and free water). After primary decomposition, a variety of gas–gas and gas–solid reactions take place: secondary pyrolysis, during which the tar may oxidize (R11), reform (R12 and R13), and further react by cracking (R15), dealkylation, deoxygenation, aromatization and formation of soot by polymerization. Primary and secondary tar conversion processes can be homogeneous and heterogeneous, occurring inside as well as outside of a particle. The tar conversion can be catalyzed by solids added to the bed (dolomite, olivine, etc) or simply by the carbonaceous surfaces in the devolatilizing particles. The light hydrocarbons (CH_4, C_{2+}) and other combustible gases (CO, H_2) may react by reactions (R7–R9), and the char may react with O_2 (R2 and R3), CO_2 (R4), H_2O (R5), and H_2 (R6). The rates of char gasification with H_2O and CO_2 are orders of magnitude lower than those of primary pyrolysis: it takes tipically a minute to gasify more than half of the char at temperatures below 900 °C [148]. In comparison, conversion of volatiles is rapid [6,7]. When pyrolysis takes place in an atmosphere containing steam and O_2, the O_2 is consumed preferentially by combustion of the volatiles, leaving steam and char. This is the main reason for the relatively low carbon conversion in FB: the absence of O_2 in most reactor zones and the sole presence of H_2O and CO_2 make it difficult to completely convert the solid char into gas at low temperature (below 900 °C) within the typical residence time of fuel in an FBG.

3.2. Outline of the modeling procedure

A biomass particle fed into the reactor becomes a source of char, gas and tar for the comprehensive reactor modeling developed above. The chemical reactions and processes should be predicted quantitatively, but due to the complexity of the conversion situation, simplifications have to be developed. How this is done by modelers, is dealt with in the following.

A scheme is developed to follow the gaseous species, tar and char, along with the conversion of a particle, and with the processes in the reactor. This leads to a distinction between primary and secondary conversion. In Fig. 14a a control volume (solid line) is extended over the particles to indicate generation, including the various process steps and products. Subsequent conversion is contained within the dashed line. Generation (primary conversion) includes devolatilization inside a particle in the absence of oxygen, whilst the subsequent conversion (secondary conversion) consists of extraparticle processes: oxidation, cracking, and reforming of the gases. Due to the fast release of volatiles, the gasifying agent surrounding the particles has only a small impact on the devolatilization itself, which then occurs in an inert atmosphere as in

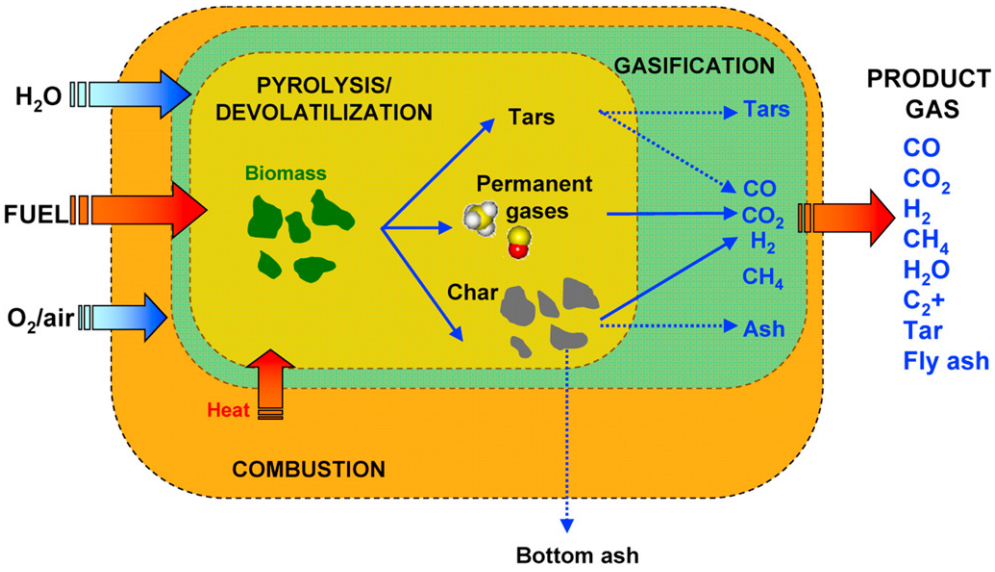

Fig. 13. Processes in a gasifier: pyrolysis/devolatilization of solid fuel and reforming/gasification of the resulting gaseous products and char.

pyrolysis. In contrast, the volatiles released from a particle are converted in the bulk gas, where the presence of oxygen and steam (just to mention the most influencing reactants), leads to oxidation and reforming reactions. Correspondingly, the conversion of a char particle is also treated in two steps. Inside the solid line in Fig. 14a, a mechanism for primary pyrolysis is represented, where char, tar and gases interact. Serial and parallel reactions take place, yielding primary gases, tar and char, represented by "1". In the secondary conversion, delimited by the dashed line, char1 reacts with gases1, such as CO_2, H_2O, and yields char2 and gases2 (CO, H_2). The interrelation between the species is not shown for the sake of clarity.

The distinction made between intraparticle/primary conversion and external/secondary conversion is not perfect. For instance, the intraparticle processes could include steam reforming of tar that may occur already in the pores of the particles. Similarly, some oxidation of char may take place, especially towards the end of devolatilization. Nonetheless, the approach can be adopted if experimental kinetics, yields, and other input data are consistent with the modeling. The approach allows decoupling of processes if their reaction times are different, and this becomes a practical and consistent way to model the complex system. The strategy of modeling is outlined in Fig. 14b, distinguishing primary ("1") and secondary ("2") char, gas species, and tar. The prediction of the yields of these species is the subject of the following sections, which are organized as follows: firstly, products from primary pyrolysis (including drying) are expressed as a model of the box within the solid line of Fig. 14b. This is done in Section 3.4. Secondary reactions, are modeled by distinguishing the following reaction processes: heterogeneous conversion of char by oxidation (with O_2) and gasification (with H_2O, CO_2) (Section 3.5), size reduction of fuel and char during conversion (Section 3.6), homogeneous reaction of light gases (oxidation, reforming, etc) (Section 3.7), tar conversion, mainly reforming and oxidation, in the form of heterogeneous and homogeneous reactions (Section 3.8). First, the boundary conditions for heat and mass transport to the particles in an FBG are discussed (Section 3.3).

3.3. Mass and heat transport at the particle scale

The heat and mass transport to, from, and inside a particle is modeled with the same equation as used for the reactor (Eq. (1)), but now applied to a particle. There are two kinds of particle in an FBG, active and non active (inert). Particles are active if they participate in the conversion processes, like fuel and char. If not, they are inactive, like inert bed material. The boundary between the emulsion phase of the bed and the active particles contained in it couples the particles to the source terms of the reactor model developed in the previous section.

The rate of heat and mass transport from the bulk gas (emulsion in an FB) to the surface of a particle immersed in the gas is calculated from the gradient in the gas at the particle surface (+s), which is given in dimensionless form by

$$\left.\frac{\partial\theta}{\partial X}\right|_{+s} = \mathrm{Nu} \tag{49}$$

$$\left.\frac{\partial C_i}{\partial X}\right|_{+s} = \mathrm{Sh} \tag{50}$$

where $X = x/x_o$, $\theta = (T - T_{g\infty})/(T_s - T_{g\infty})$ and $C_i = (c_i - c_{gi\infty})/(c_{si} - c_{gi\infty})$ are the dimensionless size of the particle, $x_o = L_e$ the equivalent particle diameter,and the dimensionless temperature and concentration of species i. $\mathrm{Nu} = h x_o/\lambda_g$ and $\mathrm{Sh} = h_m x_o/D_{gi}$ are the Nusselt and Sherwood numbers. The temperature and concentration in the gas far from the particle are $T_{g\infty}$ and $c_{gi\infty}$ and those at its surface T_s, and c_{si}. Heat and mass transfer dimensionless groups (Nu and Sh) for a fuel particle (an active particle) in a fluidized bed of passive, inert particles have been summarized [149] based on [89], in Table 4. The relationships are valid for large active particles ($d_a/d_{in} >> 1$, index 'large') or for active particles of the same size as the bed particles ($d_a/d_{in} \approx 1$, index '1'). Simple interpolation yields heat and mass transfer coefficients Nu_{in} and Sh_{in} for $d_a/d_{in} \geq 1$, which in the case of spherical particles are:

$$\frac{\left(\mathrm{Nu}_{in} - \mathrm{Nu}_{in,large}\right)}{\left(\mathrm{Nu}_1 - \mathrm{Nu}_{in,large}\right)} = \left(\frac{d_{in}}{d_a}\right)^{2/3} \tag{51}$$

$$\frac{\left(\mathrm{Sh}_{in} - \mathrm{Sh}_{in,large}\right)}{\left(\mathrm{Sh}_1 - \mathrm{Sh}_{in,large}\right)} = \left(\frac{d_{in}}{d_a}\right)^{2/3} \tag{52}$$

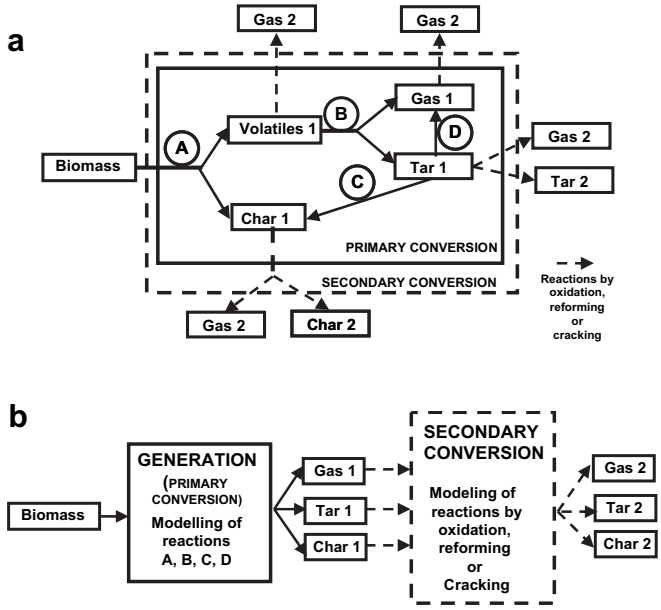

Fig. 14. Primary and secondary conversion processes. (a) Simplified model indicating primary (solid line) (resulting species indicated by "1") and secondary conversion processes (dashed line) (species indicated by "2") (b) Simplified model concept.

where $Nu_{in,large}$ and $Sh_{in,large}$ are calculated by Eqs. (115) and (116) for large particles compared to the bed particles and Nu_1 and Sh_1 by Eqs. (117) and (118) for particles of the same size as the bed material. Index *in* refers to the inert particles in the dimensionless numbers. $Nu_{in,large}$ is the maximum Nusselt number obtained at optimum fluidization velocity (at maximum transfer rate), but it is assumed to be valid also at higher velocities (this is in analogy with bed-wall heat transfer [149]). Naturally, there is no particle convection that contributes to mass transfer, so the first term of Eq. (115) is not included in Eq. (116). Small active particles (index *a*, Eqs. (119) and (120)) are entrained by the gas through the space between the larger bed particles and are assumed to behave like particles in a single-phase flow. The small particles follow the interstitial gas when their terminal velocity (u_{at}) is equal to or smaller than the gas velocity u_{mf}/ε. This gives the particle Reynolds number in the convective terms. In the disperse suspension above the dense bed the particles are small and not frequently in contact with each other; Therefore, the heat and mass transfer to such particles can be modeled as if they were single particles in a gas stream, that is, Eqs. (118) and (119) are valid.

Eqs. (49) and (50) can be formulated in terms of the gradients of T and c_i at the internal face of the particle surface ($-$s), yielding

$$\left.\frac{\partial\theta}{\partial X}\right|_{-s} = \mathrm{Bi_h} \tag{53}$$

$$\left.\frac{\partial C_i}{\partial X}\right|_{-s} = \mathrm{Bi_m} \tag{54}$$

$Bi_h = hx_0/\lambda_{eff}$ and $Bi_m = h_m x_0/D_{eff,i}$ are the Biot module for heat and mass transport, where eff denotes the effective values in the particle. If Bi_h and Bi_m are $>>1$, the external mass and heat transfer processes are rapid enough not to influence the rate of supply of mass and heat to the particles. In this case T_s, and c_{si} are equal to $T_{g\infty}$ and $c_{gi\infty}$, and the rate is determined by the internal process. When Bi_h and Bi_m are $<<1$, the opposite holds, the external rate of mass and heat transport determines the rate, so in this case accurate calculation of h and h_m is important. In the intermediate case Bi_h and $Bi_m \approx 1$, and both external and internal processes must be taken into account.

Table 4
Correlations for Nu and Sh to estimate the mass and heat transfer coefficients between gas and particles in FB [89,149].

$Nu_{in,large} = 0.85Ar_{in}^{0.19} + 0.006Ar_{in}^{0.5}Pr^{0.33}$	(115)
$Sh_{in,large} = 0.009Ar_{in}^{0.5}Sc^{0.33}$	(116)
$Nu_1 = 6 + 0.117Ar_{in}^{0.39}Pr^{0.33}$	(117)
$Sh_1 = 2\varepsilon_{mf} + 0.117Ar_{in}^{0.39}Sc^{0.33}$	(118)
$Nu_a = 2 + 0.6Re_{at}^{0.5}Pr^{0.33}$	(119)
$Sh_a = 2 + 0.6Re_{at}^{0.5}Sc^{0.33}$	(120)

In FBG as well as FB combustion, devolatilization of fuel particles is caused by thermal degradation, where heat transport plays a fundamental role, whilst the transport of mass is of secondary importance. The essential external film coefficient is then h. In contrast, for char conversion, mass transport from the gas component i in the emulsion to the char particle is the relevant process; in this case heat transfer plays a secondary role, since the thermal gradients at the particle scale are smooth, and the essential external film coefficient is h_m. Depending on the size of the fuel particles internal or external transport processes or both may be decisive together with the rate of the chemical reaction. The limiting resistances to mass and heat transport are further treated below in connection to the chemical processes.

3.4. Drying and devolatilization

The primary decomposition of the fuel into char, tar, light gases, and water can be written as:

$$\begin{aligned}\text{biomass} \rightarrow\ & \nu_{ch,1}C_{ch,1}H_{ch,1}O_{ch,1} + \nu_{t,1}C_{t,1}H_{t,1}O_{t,1} + \nu_{lg,1} \\ & (\nu_{CO,1}CO + \nu_{CO_2,1}CO_2 + \nu_{H_2,1}H_2 + \nu_{CH_4,1}CH_4 \\ & + \nu_{C_2+,1}C_{2+} + \nu_{N_2,1}N_2 + \cdots) + \nu_{H_2O,1}H_2O\end{aligned} \tag{55}$$

A model aims at predicting the rates and yields ν_i of the species released (index H_2O is water and lg represents light gases), as well as the relative amounts of tar (index t) and char (index ch). The C–O–H composition of tar and char and their chemical structures have to be known, especially that of tar, since the tar lumps contain many chemical species, generally hydrocarbons heavier than benzene. Eq. (55) is not a single reaction, but it represents several physical and chemical transformations. Consequently, the release rates of the species differ and cannot be presented by a single rate.

In the following, methods of prediction of the process outlined in Eq. (55) are reviewed. Firstly, models of the kinetics are described, where the prediction is based on a set of chemical reactions without diffusion effects. Thereafter, there is a discussion on particle models where physical aspects, such as diffusion, play a role.

3.4.1. Kinetic models

Extensive surveys of drying and pyrolysis chemistry are available [9,14,16,17,150–154]. Pyrolysis models have been reviewed recently [17]. The most important classes of model have been categorized as basic, distributed activation energy, and structural models [24].

Basic models represent pyrolysis by a single reaction (global model) or by a combination of series and parallel reactions, usually

treated as first-order and independent reactions [17,24]. The global model is the simplest representation of pyrolysis kinetics:

$$\text{biomass} \xrightarrow{k_{py}} \zeta_{py,1}\text{volatiles1} + (1-\zeta_{py,1})\text{char1} \quad (56)$$

The only parameters to be adjusted by experiments are the kinetic constant k_{py} (and reaction order if different from unity) and the coefficient of distribution between primary volatiles (volatiles1 = gases1 + tar1) and char1, $\zeta_{py,1}$. Many publications deal with kinetic parameters for the calculation of k_{py} for various fuels, but there is a great variation between the representations, probably because a number of physical and chemical factors are incorporated in one expression. Despite this fact, this type of expression has been widely used in reactor models due to its simplicity making it computationally tractable, needing only a small set of input data. In most cases, however, it does not give enough information for comprehensive modeling.

The combination of series and parallel reactions is an improvement. The kinetic scheme of primary pyrolysis in Fig. 14a, based on [24,155] includes as particular cases many of the models published [17,24]. For instance, the global model of Eq. (56) is just a limiting case, where reactions A, B, C and D in Fig. 14a are lumped into a single global reaction. Various processes that are known to be important in primary pyrolysis are considered in the figure. As seen in Fig. 14b, this prediction of primary pyrolysis comprises the rates of reaction given by reactions A, B, C, and D. Although some works have dealt with reaction networks to represent primary pyrolysis [17], the kinetics of these reactions is not well known, especially at high heating rate.

The method of distributed activation energies has been applied to fuel devolatilization [156], assuming that the number of reactions is large enough to describe the activation energy by a continuous distribution function. If first order reactions are assumed, once the distribution function is chosen, the pre-exponential factor can be found by fitting theoretical and experimental curves of volatiles released versus time. This significantly simplifies the experimental determination. Various improvements of the original work of Pitt [156] have been made, allowing the application of the method to non-isothermal conditions, as well as fitting distribution functions to represent the activation energy [5,157]. This type of model has been applied to biomass devolatilization [158], but it seems to be more suitable for coal with its complex structure than for biomass.

The models mentioned predict the amounts of tar, gas, and char released during pyrolysis, but the yields of the main gas species are not predicted. Instead, empirical correlations developed for coal [159] and experimental data for a variety of biomasses [160–163] have been used to predict the yields in reactor simulations. These correlations have been obtained for a particular set of operating conditions and type of fuel, not always similar to those to be simulated. Therefore, more fundamental data are desirable to increase the predictive capability of model simulations. Structural models have been developed to perform such predictions by accounting for the chemical constitution of the solid fuels. Structural models are derived for coal in terms of the key structures of the solid fuels: (1) functional groups (Gavalas–Cheong Model, [164,165]), (2) aromatic nuclei, bridges, and peripheral aromatic groups (DISKIN, DISCHAIN, DISRAY [166]), (3) aromatic clusters connected by weaker aliphatic and ether bridges (species-evolution/functional-group (FG) or, simply, FG model, depolymerization–vaporization–cross-linking, DVC model, and the model resulting from the combination of these two models, FG-DVC model [167]) (4) linking blocks of aromatic rings (FLASHCHAIN models [168,169] and chemical percolation devolatilization model, CPD model [170]). In general, a great deal of input is needed. A critical comparison of these models applied to coal is made in [24]. The overall conclusion is that, with the exception of the FG model, the composition of the gas released during pyrolysis is not predicted. Therefore, FBG models for coal have rarely used these models. A notable exception is the FBG models of [24] where a modified version of the FG model is applied.

During the last years efforts have been made to develop structural models also for biomass fuels. Devolatilization of biomass is significantly different from rapid coal devolatilization, primarily because the macromolecular structure and composition of biomass components contain few, if any, condensed polynuclear aromatic compounds. Biomass fuels are usually characterized in terms of the cellulose fraction plus contributions from several components, including lignin, hemicellulose, and xylan. In addition, the ash catalysis is recognized to significantly affect both yields and product release rates. An early attempt [171] to reformulate a network model for coal devolatilization into a biomass pyrolysis model was based on the FG-DVC model for coal [167]. The model reverted to a form in which the yields of tar—the most abundant product—had to be measured and introduced into the model to predict the distribution of noncondensable gases [171]. This type of input is usually not available, and the corresponding models are therefore not useful as predictive tools. There are only a few models that avoid this difficulty, describing the product distribution of primary devolatilization. The most important are the Bio-FLASHCHAIN model [172], the Bio-FG (or FG-BioMass) model [173], the Ranzi model [174] and the Bio-CPD model [175]. All these four models predict the yields of gas, tar and char, while only the first three predict the composition of the gas.

In the Bio-FLASHCHAIN model [172], pyrolysis is presented as a reaction process, consisting of three independent mechanisms: competitive chemical reactions, fragmentation statistics, and flash distillation. Fragmentation statistics determine the probability that a specific chemical reaction will release a product with a certain molecular mass during the transformation history. Flash distillation determines whether a particular fragment will enter the vapor phase or will remain susceptible to char formation in the condensed phase. These two mechanisms, in conjunction with chemical kinetics, determine the product release rates. As recognized by the author [172], the FLASHCHAIN model is more difficult to implement with biomass than with coal, because of the lack of supporting database information. The author applied a method to assign the main input parameters to various biomass fuels. Specifically, he used product distributions from cellulose and lignin to assign compositions to the lignin-like component. The Bio-FLASHCHAIN model was applied to define fuel structures based on the composition of 26 biomass samples, including hardwoods and softwoods, various grasses and agricultural residues. The parameters in the reaction mechanism for cellulose were determined by fitting the dataset to rapid devolatilization of cellulose [160]. The greatest ambiguity was recognized to be the impact of mineral catalysis during rapid heating. For the fuels investigated, the Bio-FLASHCHAIN model provides a complete description of the product distribution of primary devolatilization. Unfortunately, there is no firm empirical basis to apply the same tendencies to other biomass forms, so the calibration procedure to obtain input parameters needs more extensive validation. In addition, it is not clear how to introduce the transport process in the Bio-FLASHCHAIN model.

The Bio-FG [173] is a modification of the FG-DVC model for coal [167]. The FG-DVC model combines a functional group (FG) model for gas evolution and a statistical depolymerization, vaporization and cross-linking (DVC) model for tar and char formation. The difference in the applications to coal and biomass is that the DVC model is given less importance in the biomass version and that gas and tar evolution are described by the FG model. The tar is treated

like any other volatile species in the biomass model, and the maximum of each evolved species is fixed by the corresponding pool size. Kinetic data and pool sizes are fitted to experimental data from tests with several heating rates to be used in the models. The kinetics of each reaction is assumed to be first order with a Gaussian distribution of activation energies.

A kinetic mechanism, recently proposed [174], describes both the chemistry of biomass devolatilization and successive gas-phase reactions. Biomass is characterized in terms of three reference constituents, cellulose, hemicellulose and lignin. A multi-step kinetic model defines the rates and the stoichiometry of a few lumped reactions for each reference component. The overall devolatilization of a single biomass particle is then the combination of the decomposition of the three reference components. After this first step, all the released species in the gas phase are described with their primary propagation and decomposition reactions in the gas phase. The model is able to account for the evolution of the species in the gas phase and to predict the final products, mainly H_2, CO, CO_2, CH_4, C_2 and H_2O.

3.4.2. Particle models

In the kinetics models described above there is no influence of mass and heat transfer. However, in FBBG, the size of fuel particles is such that these effects have to be accounted for, coupled with the kinetics. For this purpose a particle model is needed to solve the diffusion equations within a single biomass particle with adequate boundary conditions, predicting the evolution with time of char, gas and tar. The composition of the main products released is, however, rarely predicted theoretically. A variety of particle models for pyrolysis have been published [17,176–187]. Despite the existence of advanced particle models, they are not frequently employed in FBG simulations. Instead, semi-empirical or simplified particle models are used (discussed below). Only in some special cases advanced particle models have been applied: the particle model of Agarwal et al. [176] was used to calculate simultaneous fuel drying and devolatilization, while the amount of volatile matter released was described by a distributed activation energy model [157]. This model was validated for the simulation of coal in FBG simulations. As the authors themselves recognized [188], a similar treatment for biomass fuels is not yet possible due to the lack of published measurements and suitable models. Also the FG-model for coal [167] adapted to biomass was applied [24], assuming a certain stoichiometry from experimental findings. Ranzi's kinetics model [174] has recently been introduced [189] in a particle model for the prediction of devolatilization of fine wood particles in a lab-scale entrained bed apparatus. However, in conclusion, there is no published model that combines a structural kinetics model with diffusion effects for FBBG conditions. Therefore, measured data are still the basic input for FBBG modeling.

3.4.3. Devolatilization measurements

The type of biomass is the first factor that has to be dealt with: due to the variations in the character of biomasses (and wastes), extrapolation of data from one biomass to another (and from coal) is questionable, even for the same operating conditions [113]. Although this fact is well known, reactor models use the devolatilization yields (gas, char and tar) from different fuels from that to be simulated.

The kinetics and yields vary widely, even for a biomass like wood, as realized early [150]. The reason for the discrepancy observed is that, besides the nature of the parent fuel, the peak temperature and the heating rate at which the fuel material is thermally decomposed influence the yield of species. The major factor affecting the heating rate and the temperature inside a particle is the particle size. Therefore, the particle size is particularly important when selecting pyrolysis measurements. Tests conducted with fine fuel particles allow determination of the intrinsic kinetics of the chemical pyrolysis, because of uniform temperature and negligible mass and heat transfer resistance throughout the fuel particle. This is the so-called kinetic regime. In contrast, for large particles the devolatilization rate tends to be limited by the internal heat transfer through the particle, depending mainly on the effective thermal conductivity. The particle is not heated isothermally, and this affects the rate of devolatilization and the product distribution. When the external surface of particles is subject to high heating rates, such as in an FB, external heat diffusion may affect the rate of devolatilization [190]. In addition, mass transfer by the release of volatiles may influence the devolatilization rate, but it usually plays a secondary role. These considerations explain why it is convenient to treat the kinetics in two groups [150]: those derived from experiments with small samples, in which the experimental conditions and diffusion effects could be closely controlled, being more appropriate for determination of kinetics, and those derived from experiments with large samples, which relate more closely to the behavior of the fuel in practical situations in FB.

Measurements have been undertaken in TGA with low or moderate heating rates, or in flash pyrolysis devices, where the heating rates are very high and the temperature range of interest is from 300 to 700 °C. Surveys of the kinetics available have been published (for instance, Table 1 in [191] and Table 3 in [17]). In FBG the temperature is higher than in flash pyrolysis and the heating rate is higher than in TGA or similar laboratory devices. As a result, biomass devolatilization studies oriented to FBG (and combustion) should be carried out in the range of 700–900 °C with heating rates in the range of 100–500 °C/s with mm-sized particles [113]. When data are taken from TGA or flash pyrolysis to represent the behavior of biomass devolatilization in FB, some correction has to be applied. Experimental kinetics of biomass devolatilization that has been commonly used for FBG models originate from several works [160–163,191–196].

In devolatilization experiments, secondary vapor reactions take place and may vary widely between test rigs. Therefore, if kinetics and distribution yields of primary pyrolysis are searched for, the residence time of the gas has to be minimized [197]. This is not always easy in FB devolatilization measurements. As a result, some authors have used an ancillary reactor to obtain primary decomposition of the fuel, while measurements in an FBG have been conducted to obtain information of the extent of secondary reactions [191]. It is difficult to distinguish between primary and secondary reactions since, for instance, secondary conversion of volatilizes already occurs in the internal pores of the devolatilizing fuel particles. In this context, consideration of the fuel particle size, the residence time of the vapor, and the type of arrangement can be required to make such a distinction. Table 3 in Ref. [17] provides data that can be useful to distinguish primary and secondary pyrolysis.

Since experiments are not perfect, most investigations describe pyrolysis by global mechanisms (apparent kinetics); particle models using such data have to be consistent with the way in which the measurements have been made. A quantitative estimation of the thermal behavior during devolatilization is dealt with in the following section by a priori calculable, dimensionless numbers.

3.4.4. Simplified particle models

Combinations of simplified hypotheses and empirical relations based on experimental data are used to characterize the rate and the composition of the gases released during devolatilization. The essential idea behind the simplified models is to estimate the time of complete devolatilization (including drying in case of wet fuels) by considering only the rate-limiting phenomena. The yields of

char and volatiles and the composition of volatiles are not predicted, but these quantities are estimated separately by mass balances and empirical relations. This two-stage modeling approach is useful in applications to FBBG if it is combined with some limiting cases for mixing and devolatilization already discussed (Section 2.2.4). In simulations where the individual yields have to be predicated in each step (Case c in Fig. 6), the simplified modeling is not valid. In such a case, advanced fuel particle models should be used.

3.4.4.1. Estimation of the time of drying and devolatilization. The rate of drying and devolatilization is described by Eq. (1) for heat and mass transport in a fuel particle [158,198]. By making these equations and boundary conditions dimensionless, dimensionless numbers describing drying and devolatilization are derived supported by the characteristic times for drying and devolatilization given in Table 5. It is assumed that the values of the physical properties of the fuel remain constant during drying and devolatilization. The devolatilization process is described by a first order reaction with a coefficient following the Arrhenius law. A simplified expression for the time of drying is given, assuming that drying is controlled by heat transfer [198]. Other assumptions and simplifications are summarized in the explanations accompanying Table 5.

The corresponding dimensionless numbers are listed in Table 6 where the previously mentioned numbers for the entire reactor are also included. Here we deal with the transformation of wet fuel where drying and devolatilization take place. Dry fuel is a limiting situation, where the time of drying is null, so it can be modeled as a particular, simpler, case. Locally, in the fuel particle, drying and devolatilization occur sequentially: first, drying at the evaporation temperature, T_{ev} and thereafter devolatilization at some temperature T_{py} between the evaporation and the ambient (much higher) temperature, T_∞. To estimate T_{py}, the condition that the reaction time and the thermal time are equal, $Da_{py} = 1$, is used. The times of drying and devolatilization are obtained from the solution of the transient heat and mass transport equations in a single particle with appropriate boundary conditions [89,183,190,198]. Such times for a variety of simple cases are listed in Tables 7.

The identification of simplified models is made by comparing the characteristic rates of drying R_{dry}, devolatilization/pyrolysis R_{py}, and external/internal heat transport $R_{he/i}$ of Table 5a using the Damköhler and the thermal Biot numbers for solid–fuels [190], defined in Table 6. The thermal Biot number, Bi_h, quantifies the thermal behavior of the fuel particles by comparing the rates of internal and external heat transport, R_{hi} and R_{he}. The Damköhler number of pyrolysis, $Da_{py,i} = R_{py}/R_{hi}$, compares the rate of the pyrolysis reaction R_{py} with the rate of internal heating of the particle, R_{hi}, whereas $Da_{py,e}$ compares R_{py} with the external heating R_{he}. (Pyle and Zaror [190] called these Pyrolysis Numbers Py and Py', defined as $Py = 1/Da_{py,i}$ and $Py' = Bi_{hi}/Da_{py,i}$). For wet solid–fuels, an additional dimensionless number, Dr_{xm}, the drying number, can be used to take the drying process into account [198]. X_m is the moisture content chosen to evaluate the drying rate, usually ranging from 10 to 20% of the initial moisture in the fuel particle [198]. The drying number Dr_{xm} compares the rate of devolatilization with that of drying. $Dr_{xm} << 1$ means that $R_{py} << R_{dry}$, and most of the moisture has been driven off before devolatilization begins in the particle. Then both processes can be considered to occur sequentially. In contrast, when $Dr_{xm} >> 1$, $R_{py} >> R_{dry}$ devolatilization and drying take place simultaneously.

For thermally fine fuel particles, $Bi_h << 1$, the rate of external heat transfer is much lower than the internal heat transport by conduction. Intraparticle gradients are negligible and the rate of external heat transfer controls the heating of the particle. If the particle is wet, Dr is small ($Dr << 1$) and drying and devolatilization occur sequentially and can be modeled separately. The total time of devolatilization (moisture included) is $t = t_{dry} + t_{py}$. The drying time t_{dry} is estimated by Eq. (121) in Table 7a and t_{py} is given from one of two limiting cases, depending on the value of $Da_{py,e}$ (evaluated at T_∞):

- If the pyrolysis kinetics are slower than the external heat transfer and, hence, limit the rate of pyrolysis process, $Da_{py,e} << 1$, the entire particle attains the surrounding temperature T_∞ before the major part of the volatiles has left the particle. The kinetic rate can then be calculated at the temperature of the surroundings T_∞, and the time t_{py} is obtained by Eq. (122) in Table 7. This is *Case 1* in Table 8.
- If the devolatilization process is limited by the external heating rate, $Da_{py,e} >> 1$, and most the volatiles are released at some T_{py} between T_0 and T_∞. t_{py} can be then estimated as the time required for heating the particle up to T_{py}, estimated by the condition $Da_{py,e} = 1$, as mentioned above. Eq. (123) in Table 7 presents t_{py} and T_{py} for this case, named as *Case 2* in Table 8.

For thermally large fuel particles, $Bi_h >> 1$, the internal temperature gradient is large and the heating of the particle is controlled by internal heat conduction. If the particle is wet, Dr becomes large, $Dr_{xm} >> 1$ so moisture evolves from the particle simultaneously with the volatiles. The reason is that drying takes place in the thermal wave penetrating into the particle, whilst devolatilization is already occurring at the external layers of the dried fuel. Then, the time for complete loss of volatiles (moisture included) of a single fuel particle is approximated by the time of drying, $t_{py} \approx t_{dry}$. The solution is obtained using the expression for $R_{dry,xm}$ given in Table 5, solved for the case $X_m \to 0$. The solution is given by Eq. (124) in Table 7 (which corresponds to $1/R_{dry,xm=0}$ with

Table 5
Characteristic rates and times of drying and devolatilization.[a]

Process	Characteristic rate	Characteristic time
Pyrolysis kinetics	$R_{py} = k_{py} = A_{py}\exp(-E_{py}/RT)$	$\tau_{py} = 1/R_{py}$
External heat transfer	$R_{he} = \frac{h}{\rho_s c_{ps} d_s}$[b]	$\tau_{he} = 1/R_{he}$
Internal heat transfer	$R_{hi} = \frac{\lambda_s}{\rho_s c_{ps} d_s^2} = \frac{\alpha_s}{d_s^2}$	$\tau_{hi} = 1/R_{hi}$
Drying[c]	$R_{dry,X_m} = (F_{ev}F_{Bi_h})R_{hi}$	$\tau_{dry,X_m} = 1/R_{dry,X_m}$
Dimensionless factors F_{ev} and F_{Bi_h} to calculate $R_{dry,Xm}$		
F_{Bi_h}	F_{ev}	$\varphi(X_m)$
$\frac{Bi_h}{(1+\varphi(X_m))\,Bi_h)}$	$4(b+1)(\frac{(1-Y_m)}{Y_m})(\frac{c_p(T_\infty - T_{ev})}{Q_{ev}})$[d]	$\begin{cases}(1-X_m) \text{ for flat plate}\\ -\ln(X_m^{1/2}) \text{ for cylinder}\\ (1/X_m^{1/3}-1) \text{ for sphere}\end{cases}$

Nomenclature: Q_{ev} is the heat of vaporization (kJ/kg); Y_m is the initial moisture, based on fuel as received; T_∞ ambient temperature; T_{ev} temperature at which the moisture is released; b the geometric coefficient: 0 for flat plate, 1 for cylinder, 2 for sphere; Bi_h is defined based on radius for spherical and cylindrical particle and on thickness for a flat particle.

[a] Characteristic rate and time are rough estimates for a single fuel particle, based on a priori known values (operating conditions and fuel properties). Table 7 presents "precise" times of drying and devolatilization. For flat geometry $R_{hi/e}$ is the based on the length of the particle.

[b] R_{he} and τ_{he} are based on particle diameter d_s (in Table 7 $R'_{he}$and τ'_{he} are used, based on particle equivalent size, $L_e = V_p/A_p$).

[c] Approximate expressions of rate and time of drying at the time when the fraction of the moisture remaining (moisture content/initial moisture content) is X_m [198]. It is assumed that drying is controlled by heat transfer to the evaporation front, and that the thermal influence of the volatile gases leaving the particle is small.

[d] The factor 4 is 1 in flat geometry.

Table 6
Definitions of some dimensionless numbers (reaction kinetics assumed to be first order).

Reactor	
Vertical mass Damköhler number = rate of reaction i/transport velocity in the vertical direction of the reactor[a]	- Fuel pyrolysis: $Da_{py,V} = R_{py}\,\tau_{f,V}$[b] - Char conversion: $Da_{ch,V} = R_{ch}\,\tau_{ch,V}$[b]
Horizontal mass Damköhler number = rate of reaction i/transport velocity in the horizontal direction of the reactor[a]	- Fuel pyrolysis: $Da_{py,H} = R_{py}\,\tau_{f,H}$[b] - Char conversion: $Da_{ch,H} = R_{py}\,\tau_{ch,H}$[b]
Single particle of characteristic dimension L_e[c]	
Thermal Biot number = external/internal heat transport rate	$Bi_h = R_{he}/R_{hi} = hL_e/\lambda_{eff}$
Mass Biot number = external/internal mass transport rate	$Bi_m = R_{me}/R_{mi} = h_mL_e/D_{eff}$
Internal thermal Damköhler number for pyrolysis = pyrolysis rate/internal heat conduction rate	$Da_{py,i} = R_{py}/R_{hi} = k_{py}\rho c_pL_e^2/\lambda_{eff}$
External thermal Damköhler number for pyrolysis = pyrolysis rate/external heat transfer rate	$Da_{py,e} = R_{py}/R_{he} = Da_{py,i}/Bi_h = k_{py}\rho c_pL_e/h$
Drying number = devolatilization rate/ drying rate (at time of moisture X_m)	$Dr_{xm} = R_{py}/R_{dry,xm} = R_{py}/R_{dry,xm}$ (see Table 5 for definition of $R_{dry,xm}$)
Internal mass Damköhler number for char conversion = reaction rate/internal mass transfer rate	$Da_{ch,i} = k_vL_e^2/D_{eff}$
External mass Damköhler number for char conversion = reaction rate/external mass transfer rate	$Da_{ch,e} = k_A/h_m$

[a] The reaction i is pyrolysis of fuel, combustion, or gasification of char.
[b] The residence time of the reacting solids "i" (i: fuel and char) in the reactor τ_{Ri} can be calculated from the convective transport time $\tau_{Ri,V/H} = x_0/u_{i,V/H}$ or the diffusion time $\tau_{Ri,V/H} = x_0^2/D_{i,V/H}$ where x_0 is the dimension: $x_0 = d_{bed}$ (horizontal), $x_0 = H_x$ (vertical in the bottom bed) and $x_0 = (H - H_x)$ (vertical in the freeboard).
[c] L_e is the equivalent length, equal to L, $R/2$, $R/3$ for flat, cylindrical and spherical geometry, respectively. In other parts of the paper Bi and Da are based on R or d instead of L_e.

$F_{Bih} = 2Bi_h/(2 + Bi_h)$ for any geometry [15,198]). This is *Case 5* in Table 8.

For an intermediate thermal behavior characterized by a finite Bi_h ($Bi_h \sim 1$) there are significant temperature gradients in the particle but also, to some extent, in the external gas layer. In addition, if the particle is wet, it is not obvious if drying and devolatilization can be considered as separate or coupled processes. The estimation of the Dr_{xm} is helpful in this case to establish simple limiting cases. On the one hand, if $Dr_{xm} >> 1$ drying and devolatilization occur simultaneously so, the same procedure as for $Bi_h >> 1$ is used, i.e. $t_{py} \approx t_{dry}$ calculated by Eq. (124) in Table 7. This case becomes equivalent to *Case 5* with regard the calculation of t_{py} and t_{dry}. On the other hand, if $Dr_{xm} << 1$, drying and devolatilization occurs sequentially, and then t_{dry} is calculated again by Eq. (122) in Table 7. To estimate t_{py}, two limiting cases can be identified, depending on the value of $Da_{py,i}$ (evaluated at T_∞)

- If the kinetics limits the process $Da_{py,i} << 1$: the particle reaches the surrounding temperature before devolatilization appreciably starts. Then t_{py} can be estimated as in *Case 1*, i.e. by Eq. (122) in Table 7.
- If the rate of internal heating controls the process $Da_{py,i} >> 1$: the reaction zone becomes narrow compared to the particle size, and the process can be regarded as a drying–devolatilization front advancing into the virgin solid at a rate determined by the velocity of propagation of the thermal wave into the

Table 7
Times of drying and devolatilization.

Time (s)

$$t_{dry} = \tau'_{he,df}\left[1 + (Y_m/(1 - Y_m))\left(c_{p,m}/c_{p,df}\right)\right]\ln(1/\Theta(T_{ev})) + \tau'_{he,df}4(b + 1)/F_{ev} \quad (121)$$

$$t_{py} = (1/k_{py}(T_\infty))\ln(1/(1 - x_{py})) \quad (122)$$

$$t_{py} = \tau'_{he,df}\ln(1/\Theta(T_{py}))$$
$$T_{py} = -\left(E_{py}/R_g\right)\ln\left(A_{py}\tau'_{he,df}\right) \quad (123)$$

$$t_{dry} = \left(\frac{\tau_{hi,df}}{F_{ev}}\right)\left(\frac{2 + Bi_h}{2Bi_h}\right) \quad (124)$$

$$t_{py} = \tau_{ih,df}\left(1/\mu_1^2\right)\ln(\mu_2/\Theta(T_{py})); \quad (125)$$

Values of μ_1 and μ_2 in Eq (125).	$0 < Bi_h < 2$	$2 < Bi_h < \infty$
μ_1	$\sqrt{\frac{(a_0Bi_h)}{(1 + Bi_h/a_1)}}$	$\frac{(a_3Bi_h)}{(Bi_h + a_4)}$
μ_2	$1 + (Bi_h/a_2)$	$\frac{(a_5Bi_h)}{(Bi_h + a_6)}$

	a_0	a_1	a_2	a_3	a_4	a_5	a_6
Plate	1	3	7	π^2	0.95	1.273	0.15
Cylinder	2	4	4	2.405	1	1.602	0.35
Sphere	3	5	3.5	π	1.1	2	0.65

Definitions and nomenclature: m: moisture; df: dry fuel; ev: evaporation; py:pyrolysis; (τ_{he}, τ'_{he} and τ_{hi} defined in Table 5); T_{py} temperature at which the volatiles are released; $\Theta(T) = (T_\infty - T)/(T_\infty - T_0)$ dimensionless temperature (0: initial, ∞ bulk gas); $x_{py} = (m_{t_0} - m_t)/(m_{t_0} - m_{t_\infty})$ degree of charring (pyrolysis conversion) (0: initial, ∞ final, after complete devolatilization).

Table 8
Identification of limiting cases and the equation for t_{dry} (wet fuels) and t_{py}.

Limiting case	Condition	t_{py}	t_{dry} (for wet fuels)	Application/Comment
1	$Bi_h << 1$ $Da_{py,e} << 1$	Eq. (122)	Eq. (121)	- Conversion of low-reactive fine fuel at relatively low T_∞ and heating rate (slow pyrolysis). Then not applicable for FBG. - Dr_{xm} becomes <<1 for wet fuel
2	$Bi_h << 1$ $Da_{py,e} >> 1$	Eq. (123)	Eq. (121)	- Conversion of high-reactive fine fuel at relatively low T_∞ and heating rate (slow pyrolysis). Then not applicable for FBG. - Dr_{xm} becomes <<1 for wet fuel
3	$Bi_h \sim 1$ $Da_{py,i} << 1$ $Dr_{xm} << 1$[a]	Eq. (122)	Eq. (124)	- Conversion of course low-reactive fuel at relatively high T_∞ and heating rate - Rarely applicable for biomass conversion in FBG
4	$Bi_h \sim 1$ $Da_{py,i} >> 1$ $Dr_{xm} << 1$[a]	Eq. (125)	Eq. (124)	- Conversion of high-reactive coarse fuel at relatively high T_∞ and heating rate - Typical situation in FBBG for dry fuels or fuels with relatively low moisture content
5[b]	$Bi_h >> 1$ $Dr_{xm} >> 1$	$t_{py} \approx t_{dry}$	Eq. (124)	- Conversion of course wet fuel at relatively high T_∞ and heating rate - Typical situation in FBBG for fuels with high moisture content

[a] For wet fuel. In the case of dry fuel the condition of Dr_{xm} is meaningless ($X_m = 0$).
[b] Only for wet fuels (there is no meaning for dry fuels).

solid. This is a shrinking core situation, limited by internal heat transport. If pyrolysis is assumed complete at T_{py} (as in Case 2), then t_{py} can be roughly determined by the time needed for the temperature at the centre to reach T_{py}. Calculation of t_{py} requires the solution of the transient energy balance with boundary conditions of finite Bi_h. Graphical solution is available [199] as a function of the Fourier (dimensionless time) and Biot numbers, which are included in textbooks [200]. However, an analytical, explicit, solution for t_{py} has not been presented up to date. Here, we present an approximate analytical solution based on recent work [201,202]. Eq. (125) in Table 7 shows such a solution for different geometries. We have called this *Case 4* in Table 8.

In fact, Eq. (125) can be used for both fine and large particles, i.e. for any Bi_h, provided that there is a T_{py} above which devolatilization is very fast compared to the heat up of the particle. For thermally fine particles, however, intraparticle temperature gradients are negligible, and Eq. (123) is simple to use for Case 2.

The discussion above, summarized in Table 8, refers to the general case of a wet fuel particle. The case of dry fuel in Table 8 is a limiting case where $Dr_{xm} << 1$, but it is meaningless to calculate Dr, since there is no moisture to evaporate. Obviously $t_{dry} = 0$, and t_{py} is calculated by the limiting cases just mentioned (Cases 1 to 4). Case 5 can only be applied for wet fuels, because t_{py} is calculated by $t_{py} \approx t_{dry}$. This is not a problem, since the counterpart of Case 5 for dry fuels is Case 4. As indicated in Table 8, Cases 4 and 5 are the most likely ones to represent the situation in an FB.

The devolatilization temperature T_{py} is based on the assumption of complete devolatilization at T_{py}, and that the main components of the biomass are virtually carbonized at this temperature [113,203]. To clarify this point, an example is given in Fig. 15, where thermal and reaction times are shown [204]. The characteristic time for pyrolysis kinetics is calculated as $1/k_{py}$ for the main components of wood: cellulose, hemicellulose and lignin, based on the kinetics from [205]. The thermal time, i.e. the time for heating up a fuel particle from initial temperature, T_0, to ambient, T_∞, is calculated for various particle sizes (6–10 mm) assuming that the heating is controlled by heat conduction. It follows from Fig. 15, that for the particle sizes indicated, the condition $Da_{py,i} >> 1$ holds approximately at $T_{py,1} > 400$ °C for cellulose and hemicellulose and at $T_{py,2} > 650$ °C for the more thermally stable lignin. For wood, the hemicellulose pyrolyzes at 225–325 °C, the cellulose at 325–375 °C, and the lignin at 300–500 °C. This shows that the rough concept of instantaneous devolatilization at T_{py} calculated by $Da_{py,i} = 1$, is a reasonable approximation for wood, having, say, 1/3 of lignin, the rest being cellulose and hemicellulose. However, for other solid–fuels, extrapolation from these conclusions have to be made with caution. For instance, for pellets made of MSW, compost, and other wastes, the thermal degradation takes place at a higher temperature than for wood [113]. The procedure is valid but T_{py} has to be estimated according to the specific thermal devolatilization behavior of the fuels concerned.

Fig. 16 presents a map of the limits of pyrolysis as a function of temperature and particle size for dry wood [206]. To construct the graphic, the chemical regime was defined by $Da_{py,i} = 0.1$, the upper limit of the thermal regime by $Da_{py,i} = 10$, and $Bi_h >> 1$, i.e. the resistance of external heat transfer is neglected. The limits are represented by hatched bands to illustrate the uncertainty of the data (the kinetics from [193] and [194] are used). As indicated in the figure, at 850 °C the kinetics of pyrolysis are limiting for particles smaller than 0.1 mm. In this case, heating up of the particle can be considered instantaneous and the particle devolatilized

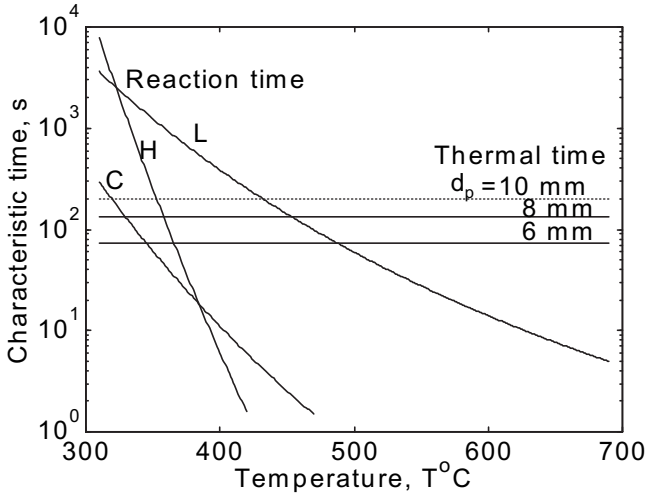

Fig. 15. Characteristic times vs temperature for dry wood pellets: Curves marked with C (cellulose), H (hemicellulose) and L (lignin) represent kinetic times. Horizontal lines are thermal times at different fuel particle diameters (d_p): 6, 8 and 10 mm. Physico-chemical properties of wood pellets from Leckner et al. [204]: thermal conductivity = 0.25 W/(mK), density = 1000 kg/m^3, moisture = 7%. Kinetics from Grønli [205]. Figure adapted from Leckner et al. [204].

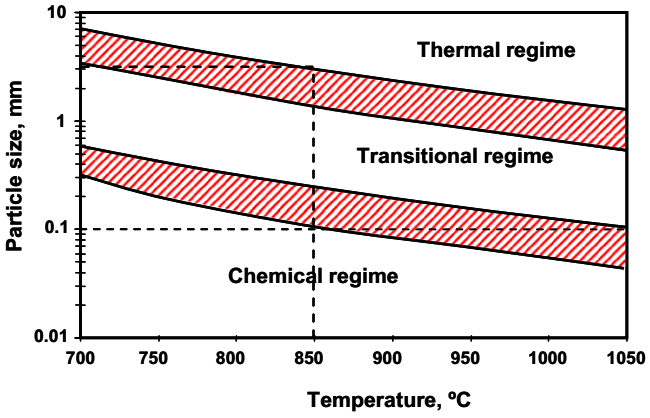

Fig. 16. Pyrolysis regimes: particle size versus temperature. Adapted from Dupont et al. [206].

isothermally (at 850 °C). In the other extreme, the thermal regime is established for particles larger than 3 mm. In FBG the fuel particle size usually ranges from 0.2 to 10 mm and the temperature from 800 to 900 °C, depending on the nature of the fuel, so the fuel is likely to be gasified in the intermediate regime, where the characteristic times of heat transfer and pyrolysis reaction are of the same order of magnitude. Therefore, none of the processes can be assumed always to be limiting [206]. For wet wood, the representation given in [198] is helpful to identify the temperature-particle size window, where drying and devolatilization are either coupled or sequential, in terms of Dr_{10}.

For intermediate values of Bi_h, Da_{py} and Dr, a more complex description is required, and therefore, more advanced particle models have to be used. In these cases, however, the time of devolatilization can be estimated semi-empirically by direct measurement of the devolatilization time, including drying, for the type of fuel and range of particle size of interest as expressed by a correlation with two coefficients a_1 and a_2 together with the characteristic dimension d_e of the fuel particle, $t = a_1 d_e^{a2}$ [187,203,207–210]. The constants have some physical meaning as can be seen from a derivation of the times of drying and devolatilization of thermally small particles or thermally large particles. The first constant, a_1, is related to the specific fuel and the second constant, a_2, to the physical process. Theoretically, a_2 approaches unity if the process is limited by the thermal process. If the process is controlled by the kinetics of devolatilization, a_2 approaches zero. For thermally large particles a_2 approaches two. These extreme cases are consistent with the limiting cases discussed. According to empirical experience for most fuels in combustion or gasification devices, the constant a_2 ends up in the region of 1.5–2 [15]. The correlations are approximate because other processes are also present, such as sintering, swelling or shrinkage of the particle, temperature dependence of the physical data and convective flows within the fuel particle, etc. In addition, most of the cases treated correspond to particles with the three standard geometries: slabs, infinite cylinders and spheres. A more complex situation arises if the pore structure and directionality are taken into account, particularly in the case of woody biomass, having its intrafibre capillaries [183]. These aspects are rarely considered in models but may have strong influence on predictions. During devolatlization a spherical isotropic particle (see Fig. 17a), the oxygen reacts with the volatiles released before it reaches the particle's surface, and the oxidation involves only volatiles without char combustion. On the other hand, for anisotropic particles with a slab-like shape, as illustrated in Fig. 17b, the oxygen can reach the upper and lower (non-porous) boundaries, where, however, the resistance to mass transfer could be high. The shape can significantly alter the predictions made on spherical-like, isotropic particles [209,158] but a variety of particle sizes and geometries can be modeled by the correlation $t = a_1 d_e^{a2}$. For first predictions, this method is reasonable.

3.4.4.2. Estimation of yields and gas composition. The prediction of the yields (accumulated) of the main volatile species is made by elemental balances completed by empirical relations. The empirical relations are estimated as function of operating conditions, type of biomass, particle size, temperature and heating rate. The remaining char after devolatilization is usually assumed to be pure carbon and its amount has to be estimated from the amount of volatiles released or given as input. This type of model has been applied to biomass reactor simulations, for instance for fixed-bed simulation [211] and also for FBBG [147]. In these models, however, there is no

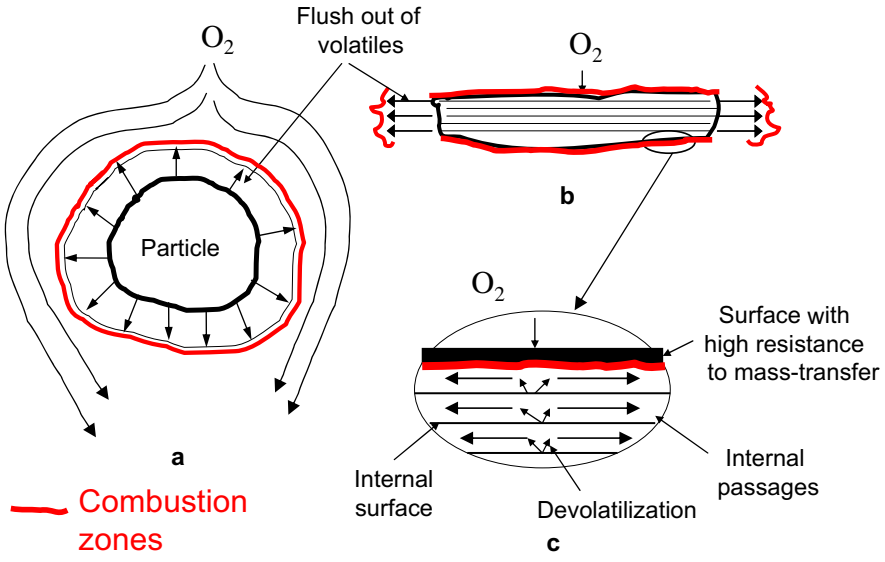

Fig. 17. Accessibility of oxygen to solid particles (char) during devolatilization. (a) Spherical isotropic particle; (b) Flat and non-isotropic particle; (c) Details of the internal process in flat non-isotropic particles with highly directional porous structure.

clear judgment on the choice of the empirical input data, their range of validity, their dependence on fuel, or their influence on the solution. Therefore, although the models are simple enough, the empirical data selected to close the balances seem case-specific. Other FBBG models [212,213] have determined the unknowns by assuming that the gas released has attained equilibrium, a simplified description that does not seem to be realistic under FBG conditions.

The model of Ref. [214] is an example of a particle model of this type where the empirical relations are discussed in detail. The influence of the choice of parameters on the solution was investigated by a sensitivity analysis, and the main influencing factors were identified. For instance, an empirical parameter for prediction of the yield of hydrocarbons was shown to depend basically on the type of biomass and particle size. Recommendations have been given for different fuels, particle sizes and other operating conditions [214,215]. Therefore, among the models of the type discussed, this model [214] seems to be sufficiently comprehensive, and in a simplified model of FBG for wood, the devolatilization can be assumed to be instantaneous. Models of this type for other biofuels are not found in literature.

3.4.5. Summary and conclusions

In drying and devolatilization, part of the fuel is converted into gases while heated in the gasifier. It is desirable to know the rate of gas release, its amount and composition. It is difficult to establish a rigorous description of the release of volatiles. The most reasonable procedure is to first identify the dominant process during devolatilization: chemical (kinetics) or physical (heat transport in and to a particle). The dimensionless numbers Bi, Da (Py) and Dr are helpful for such an identification. Simplifications are made at a loss of generality and have to be supported by empirical data. The gas composition can be estimated to some extent by molar balances on C, O, H and energy, but some additional empirical relations are needed. In simplified modeling, the total amount of volatiles can be estimated, based on a standard analysis at the cost of some accuracy. Time of devolatilization can be readily estimated by simple expressions, allowing the choice of reactor model by comparing it with the time of solids mixing.

3.5. Chemical conversion of char

As discussed in Section 3.1 (Fig. 13) the char particles in a FBG are generated after rapid devolatilization of the fuel. The char mainly consists of ash and carbon. Chemical conversion of char occurs by reactions with O_2 (R2 and R3), CO_2 (R4), H_2O (R5) and, in much minor proportion, with H_2 (R6). At steady state, an FBG contains a distribution of char particles with different sizes and degrees of conversion. The rate of char conversion is influenced by variables, such as temperature, partial pressure of the gasifying reactants and the products, particle size, porosity, and mineral content of the char, some of which vary with time due to chemical conversion and attrition. This section examines the chemical conversion of char particles, and in Section 3.6 the influence of fragmentation and attrition is dealt with. Emphasis is given to the representation of char reactivity data from the laboratory with a single-particle model to be included in FBG models. Conversion models for gas–solid non-catalytic reactions with a single gas reactant are first reviewed. Char combustion (char–O_2) and gasification (char–H_2O, CO_2, H_2) are then treated, paying attention to the characteristics of these reactions in an FBG, looking for simplifications. Simplified predictions are presented rather than surveying advanced particle models. More fundamental analyses can be found in reviews [6,7,10,20,216].

3.5.1. Reactivity of char

The reactivity of a char sample at time t is defined as:

$$r_m = -\frac{1}{m_c}\frac{dm_c}{dt} = \frac{1}{(1-x_c)}\frac{dx_c}{dt} \quad [kg/(kg\ s)] \tag{57}$$

where m_c and x_c are the mass of carbon contained in the sample and its conversion at time t, this latter defined as

$$x_c = 1 - \frac{m_c}{m_{c0}} \tag{58}$$

By studying the effect of concentration ρ of the reactant gas (O_2, H_2O, CO_2 or H_2) and the temperature T in the laboratory, the rate of the char–gas reaction can be determined by Eq. (57). For instance, assuming a kinetic law, often of nth order,

$$r_m = k_m \rho^n \quad [kg/(kg\ s)] \tag{59}$$

the kinetic coefficient k_m and the order of reaction n can be obtained by reactivity experiments. According to the classical plot of r vs. $1/T$, some regimes can be distinguished [6]. Regime I, the kinetic regime, is free of diffusion effects. In Regime II pore diffusion controls and in Regime III diffusion in the external boundary layer is rate controlling. If the experiments are conducted in the kinetic regime (Regime I), the concentration and temperature of the gas in all surface sites on the particle are the same as in the bulk gas and the reactivity determined is the true reactivity. The char particle is uniformly converted, the profiles of conversion are flat, and the overall conversion of the particle x_c is the same as the local conversion X in any interior location.

The reactivity can also be defined per unit of reacting surface:

$$r_A = k_A \rho^n \quad \left[kg/\left(m^2\ s\right)\right] \tag{60}$$

The rate coefficient k_A (as well as k_m) is related to temperature via an Arrhenius expression of the form $k_A = A\exp(-E_a/RT)$ where A is a pre-exponential factor, E_a an activation energy and R the gas constant. Eq. (60) expresses global n-th order kinetics, valid for certain operating conditions. It is a simplified representation of a more complex surface process, usually described by the Langmuir–Hinshelwood equation [6]. To relate r_m and r_A, the total reacting surface area per unit of mass A_m (m^2/kg) is introduced:

$$r_m = A_m r_A \tag{61}$$

A distinction is sometimes made between the internal ($A_{m,i}$) and external ($A_{m,e}$) areas of a particle, so that $A_m = A_{m,i} + A_{m,e}$. The change in reactivity during conversion is described by the variation of A_m, while k_A is assumed to depend on temperature and concentration only. The surface changes continuously during conversion due to pore enlargement and pore coalescence [217]. The form of variation depends on the char and operating conditions. A practical way to describe this variation is to relate A_m to a reference state of conversion ("0"), using a structural profile $f(X)$,

$$A_m = A_{m0} f(X) \quad \left[m^2/kg\right] \tag{62}$$

$f(X)$ takes into account the variation of the total reacting surface in relation to the initial (or reference) surface. Empirical expressions for $f(X)$ have appeared in the literature for a variety of chars, valid for specific ranges of operating conditions. Expressions for $f(X)$ have also been developed from structural models, describing the change of the pore system during conversion. These models provide a theoretical basis for $f(X)$, where parameters appearing in $f(X)$ can be interpreted in terms of the porous structure, but their values are

normally obtained experimentally. Table 9 gives some models of $f(X)$, employed to express char conversion reactions.

For the development of particle models, it is sometimes useful to express the reactivity per unit of volume

$$r_v = \rho_c r_m = \rho_c A_m r_A = k_v \rho^n \left[\mathrm{kg}/\left(\mathrm{m}^3\ \mathrm{s}\right)\right] \quad (63)$$

The local change in carbon density with conversion is represented by

$$\rho_c = \rho_{c0}(1 - X) \quad (64)$$

where ρ_{c0} is the initial density of the char. The so-called intrinsic reactivity r_{int} is equal to r_A, the reactivity based on the reacting surface. The other two reactivities r_m and r_v depend on the reacting area and the local density of carbon, as seen in Eq. (63). However, the three are true reactivities, provided that they are determined by measurements within the kinetic regime [6].

Table 10 shows the relationships between the reactivities and kinetic coefficients. The kinetic coefficients K in Table 10 are common in literature for non-catalytic gas–solid reactions, because they are useful in separating conversion caused by physical and chemical factors. The coefficients K can be normalized to surface, mass and volume: K_A, K_{m0}, and K_{v0} (see units in Table 10). Note that K_A is not related to any state of conversion; it is independent of conversion.

Eq. (57), expressed in the form

$$\frac{dX}{dt} = K_{m0} f(X)(1 - X) \quad (65)$$

is a standard way to correlate non-catalytic gas–solid reaction measurements. Various proposals of $f(X)$, listed in Table 9, are useful for making an a-priori choice of $f(X)$ to fit empirical kinetic parameters using Eq. (65). The local conversion X has been used in Eq. (65) because $X = x_c$ in experiments carried out in the kinetic regime. Often, Eq. (65) is applied outside of the limits of the kinetic regime, producing data that are difficult to scale-up. Sometimes this is done intentionally, by employing the char size in the range of interest in the final application. In such a case, X is not equal to x_c and Eq. (65) is merely a way to obtain dx_c/dt for reactor modeling, avoiding the solution of a char particle model.

Char reactivity depends on the parent fuel and on the form of preparation, especially the heating rate and peak temperature [228,229]. The reactivity of coal chars varies widely depending on the rank of the parent coal. Variation between chars derived from biomasses is even more significant, due to the differences in the nature of the biomass fuels. Biomass chars vary greatly in porosity, directionality, and catalytic activity. Therefore, caution should be exerted in applying expressions from one char to another [25]. Despite this, it is typical to use kinetics from coal when modeling biomass systems. For instance, Langmuir–Hinshelwood kinetics obtained by [230] for coal chars were used to model char gasification of sewage sludge in a CFB [43,231]. The same assumption was adopted in another biomass model [232] where char kinetics for gasification of coal in a jetting FB gasifier [233] were employed. In this case, the authors accounted for the possible deviation and arbitrarily introduced an empirical correction factor (from 1 to 10).

The influence of the form of char generation on the char reactivity has been studied [229,234,235,236]. FB reactors (also laminar flow (drop tube) or entrained flow, having conditions that are as similar as possible to FB) should be used to generate the char, and preferably, also to measure the char–gas reactivity without inetermidiate cooling. However, physical interaction like mass transport can lead to misinterpretations of the intrinsic kinetics [234]. This is the reason why most experimental data with O_2, CO_2 and H_2O have been measured using TGA, fixed bed or similar devices, where it is easier than in an FB to ensure that the experiments are really carried out in the kinetic regime.

The reactivity of lignocellulosic chars with O_2, H_2O and CO_2 has been recently reviewed [216]. Extensive collection of char kinetics of various coals and chars from biomasses and wastes are also available [6,228]. The kinetics measured by different researchers using similar biomass fuels have been compared and discussed [216,226,234]. In the following detailed aspects and specific references addressing modeling aspects on kinetics of char are reviewed.

3.5.2. Reactivity of a single char particle

The reactivity of a single char particle may differ from the data obtained from a particular laboratory test, depending on size of the particle and operating conditions. A model of a single particle is then required. The intrinsic reactivity obtained in the laboratory is still valid, but two aspects have to be taken into consideration: (1) porous char particles may be subjected to variations in local gas concentration and temperature, and thus, there may be profiles of these quantities, $\rho(r)$ and $T(r)$, in the particle and in the boundary layer surrounding the particles; (2) there may be a conversion profile within the particle, $X(r)$, depending of the conversion history, and then the global (particle) conversion x_c may differ from the local conversion X. Assuming a continuum description of the porous solid particle, i.e. that the local variations of reacting surface and carbon density inside the particles are given by Eqs. (62) and

Table 9
Main structural or empirical models applied to char gasification kinetics.

Name of model	Abbreviation	$f(X)$	Parameters	Ref.
Uniform conversion model	UCM	1	–	[218]
Shrinking models or grain model[a]	SCMs (SUPM and SUCM) GM	$(1-X)^{-1/3}$	–	[211,219]
Random pore model	RPM	$(1-\Psi\ln(1-X))^{1/2}$	Ψ	[217]
Extended random pore model[b]	ERPM	$(1-\Psi\ln(1-X))^{1/2}(1+(cx)^p)$	Ψ, c, p	[220]
Simons model	SM	$(X+\alpha(1-X))^{1/2}$	α	[221]
Johnson model	JM	$(1-X)^{-1/3}\exp(\alpha X^2)$	α	[222]
Dutta model	DM	$1 \pm 100\cdot X^{\gamma\cdot\beta}\exp(-\beta\cdot X)$	γ, β	[223]
Gardner model	GM	$\exp(a X)$	a	[224]
Modified volumetric model	MVM	$a^{1/b}b[-\ln(1-X)]^{(b-1)/b}$	a,b	[225]
Empirical potential model	EPM	$(1-X)^{\alpha}$	α	[6]
Polynomial model	PM	$\sum_{i=1}^{n} a_i X(1-X)^i$	a_i	[226,227]

[a] The two Shrinking models of Fig. 18 (cases (b) and (c), i.e. SUPM and SUCM) have the same $f(X)$ in the chemically-controlled regime.
[b] This model is an extension of the random pore model for biomass char.

Table 10
Definition of various intrinsic reactivity and kinetic coefficients.

Definition	Units
Intrinsic reactivity, r	
$r_A = K_A$	kg/(m^2 s)
$r_m = K_{m0} f(X)$	kg/(kg s)
$r_v = K_{v0}(1-X) f(X) = K_{v0} F(X)$	kg/(m^3 s)
Kinetic coefficient, K	
$K_A = k_A \rho^n$	kg/(m^2 s)
$K_{m0} = k_A \rho^n A_{m0} = A_{m0} K_A$	kg/(kg s)
$K_{v0} = \rho_{c0} k_A \rho^n A_{m0} = \rho_{c0} K_{m0} = \rho_{c0} A_{m0} K_A$	kg/(m^3 s)

(64), the reactivity of a single char particle $r_{m,p}$ can be calculated by integration of the volumetric reactivity r_v throughout the volume of the particle V_p:

$$r_{m,p}(x_c(t)) = -\frac{1}{m_{c,p}} \frac{dm_{c,p}}{dt} = \frac{1}{m_{c,p}} \int_{V_p(t)} r_v(t,\Omega) d\Omega = \frac{\rho_{c0} A_{m0}}{m_{c,p}} \int_{V_p(t)} k_A \rho^n (1-X) f(X) d\Omega \quad (66)$$

To obtain $\rho(r,t)$, $T(r,t)$, and $X(r,t)$, from the condition in the bulk gas, i.e. in the emulsion in an FB, the conservation equation for the gas species involved in the reaction and the energy equation have to be solved inside the char particle and its boundary layer. Furthermore, the carbon balance has to be solved at any position within the char. This problem has been treated for a variety of situations [237,238] for single char-particles. However, the solutions are not used in FBG models, probably because of numerical difficulties. Therefore, tractable models should be formulated for implementation in reactor codes. The solutions of advanced particle models, such as [237], could support the development of simplified treatments.

To derive Eq. (66), it was assumed that $f(X)$, obtained by experiments in the kinetic regime using fine-sized samples, is applicable locally in a macroscopic char particle. This approach presumes that the largest length scale of the solid structure (pore, grain, etc) is much smaller than the characteristic length associated with the concentration gradients. At the same time the particles have to be fine enough to avoid diffusion effects in kinetic experiments, but they should be much larger than the microstructure of the solid. An example let show if these requirements are accomplished in practical applications: experiments with fine char particles of 50–100 μm yield the kinetics of a char particle at any conversion, i.e. $f(X)$, k_A and n. These data is then used to compute the conversion rate of a 5 mm char particle. The equations comprising the particle model are numerically integrated using a grid of 10 points to capture the spatial gradients of ρ, T and X, i.e. the grid size is then 0.5 mm. The char structure is typically represented by its pore size, in the range of a few nanometers. Since this value is much smaller than the grid size, the conditions for application of Eq. (66) are fulfilled. The main advantage of this formulation is that the reaction rate is formulated on a volumetric basis allowing easier mathematical treatment of diffusion effects; however, the local variation of A_g, i.e. $f(X)$, can still be described by heterogeneous structural models obtained experimentally under kinetically-controlled conditions [234].

A useful method to make a char-particle model tractable is in to employ a particle effectiveness factor:

$$\eta_p(x_c) = \frac{r_{m,p}(x_c)}{r_{m,e}(x_c)} \quad (67)$$

$r_{m,e}$ is the conversion rate of a particle exposed to the emulsion conditions of the bed, where the concentration and temperature of the gas are known, while $r_{m,p}$ is the actual (observed) conversion rate of the particle. Obviously, η_p changes with time, and thus, it should be calculated at each degree of conversion as emphasized in Eq. (67). η_p can be estimated by separating the effect of the external and the internal resistances. For this purpose, two effectiveness factors, external and internal, η_e and η_i, are defined

$$\eta_e(x_c) = \frac{r_{m,s}(x_c)}{r_{m,e}(x_c)} \text{ and } \eta_i(x_c) = \frac{r_{m,p}(x_c)}{r_{m,s}(x_c)} \quad (68)$$

where the subscript "s" denotes the conditions of the external surface of the particle, so $r_{m,s}$ is the reactivity of a particle exposed to the conditions at the particle's surface (not a priori known). η_e is the ratio of the intrinsic reaction rate, evaluated at the surface, and the rate under emulsion conditions, i.e. it accounts for the drop in concentration and temperature in the boundary layer of the particle, whereas η_i is the ratio of the actual rate and the intrinsic rate evaluated for surface conditions.

The use of η_p, η_i, η_e is useful when prediction of these quantities can be determined by simple methods. This provides a short-cut method for estimation of $r_{m,p}$, avoiding the solution of a particle model and Eq. (66). The particle effectiveness factor is calculated as $\eta_p = \eta_i \eta_e$, and $r_{m,p}$ is obtained from $r_{m,e}$ and η_p by applying Eq. (67). How to do this for combustion and gasification of char in an FBBG is shown in the following sections. First, a survey is given of the models describing the modes of conversion of a single char particle.

3.5.3. Conversion models for single char particles

Fig. 18 shows various ways to represent the conversion of char. As the reaction proceeds, there is a change of the mass of carbon depending on the operating conditions and char type, leading to a decrease of the particle's size and/or density. A spherical particle, undergoing continuous conversion, has been assumed for simplicity in Fig. 18. Cases (a), (b) and (c) are the classical models, representing extreme behavior, whereas Cases (d) and (e) represent more general modes of char conversion.

In the uniform conversion model (Case a: UCM) the reaction takes place throughout the char particle and the internal fields of gas species and temperature are smooth during the entire process, $\eta_i \approx 1$. Distinction between particle and local conversion is not needed ($X \approx x_c$). If the external resistance is small, $\eta_e \approx 1$, so that $\eta_p \approx 1$, the rate of gasification of a single char particle can be calculated directly from the intrinsic reactivity evaluated for emulsion conditions.

In the surface reaction models (Cases b and c) the reaction is fast and takes place as soon as the reactant gas has reached the external surface of the particle. The useful kinetic coefficient is k_A, and there is no need for a complex description of the development of the internal area, since the reaction surface is A_e. Two cases are distinguished, depending on the ash behavior during conversion. In the shrinking unreacted particle model (Case b: SUPM) the ash formed peels off instantaneously. Then, the particle shrinks during conversion due to the chemical reaction, and the instantaneous size of the particle is correlated with its conversion. This relation is shown in Fig. 18 for a spherical char particle. In the shrinking unreacted core model (Case c: SUCM) the reaction occurs at the surface of the core whose radius decreases with time as the reaction proceeds. The particle size, however, is preserved because the ash remains attached to the particle and becomes an additional resistance to mass and heat transfer. This resistance grows with the thickness of the ash layer and depends on the effective mass and heat transfer coefficients. The SUPM and SUCM models are sharp-interface models [239] and are usually applicable to non-porous chars.

Extension to porous char can be handled with progressive models (PM). Two representative progressive models, with

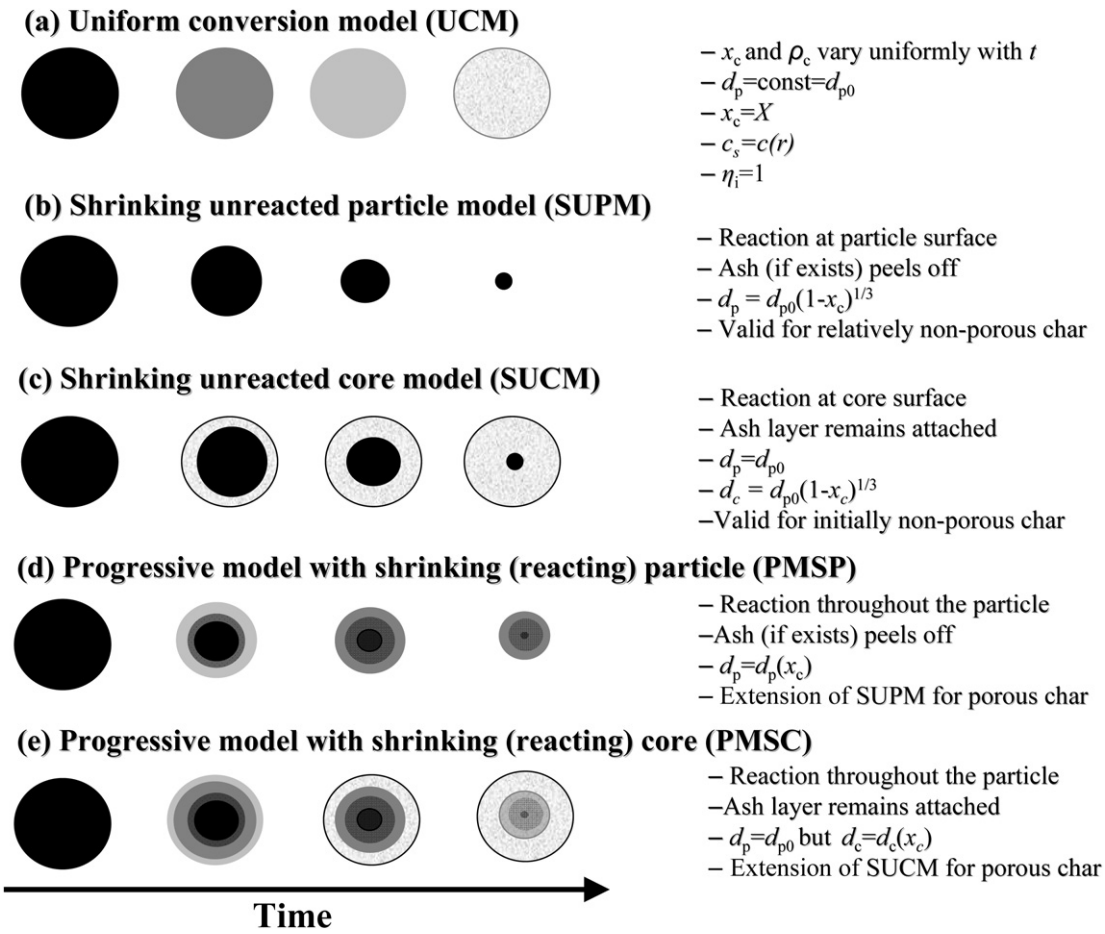

Fig. 18. Single char-particle conversion models. Black is the color of carbon, no conversion; white is the ash color, full conversion. Intermediate colors are intermediate states. Models (a)–(c) are the classical ones. Types (d) and (e) are extensions of (b) and (c) for porous char, allowing reaction to take place within the shrinking core/particle, showing an extreme behavior of the ash formed. Alternative names are: Homogeneous model (Cases a). Sharp-interface or Surface-interface model (Cases b and c) [239]. Case (d) and (e) are sometimes called finite-reaction-zone models [239]. Souza-Santos [24] used Exposed-core model or Ash segregated model for cases b and d and Unexposed-core model for cases c and e.

shrinking particle (PMSP) and with shrinking core (PMSC), are shown as Cases (d) and (e) in Fig. 18. In these models the reaction takes place in a reaction zone, which grows inwards during the course of reaction. The difference between the two models is in the behavior of the ash, which is removed in the case of the PMSP, whereas it is maintained in the PMSC. In the PMSC, it is assumed that an external shell of ash (free from carbon, $X = 1$) is formed at some time. From that time on, the reaction zone detaches itself from the surface of the particle and begins to move inwards. The effective diffusion coefficient of mass and heat in the ash layer may differ from that of the reaction zone. Some models have been formulated, extending the above PM by considering two parts within the reaction zone: a zone that is permeable to the reactant gas with a volumetric reaction and an unreacted core, impermeable to the gas [240].

Mathematical description of Cases (a)–(c) is found in classical textbooks [241]. Mathematical treatment for the progressive models, Cases (d) and (e), has been reviewed thoroughly [24,43,239,242–244]. In all models of Fig. 18, the boundary layer treatment is similar, because it is the first step for the gas diffusion, treated as a series process. It is emphasized that the limiting models in Fig. 18 (Cases a–c) provide simple relations: the size is kept constant in the UCM, whereas the density remains constant in the SUPM and the SUCM, in the latter model, the density of the core. The solution of progressive models, in contrast, is more difficult and numerical integration is needed to establish the conversion of the particle, the location of the moving core, or its shrinkage with time. These relations may be altered by attrition as discussed below.

Aiming at simplification of the mathematical treatment of the particle models, macroscopic empirical models describe the variation of density, particle size and reactivity in terms of overall particle conversion x_c by adjusting some parameters. The change in size and density of char during conversion can be empirically described by,

$$d_c(t) = d_{c0}(1 - x_c)^{\delta} \tag{69}$$

$$\rho_c(t) = \rho_{c0}(1 - x_c)^{\alpha} \tag{70}$$

Then, the reactivity of a particle per unit volume $r_{v,p}$ can be written

$$r_{v,p} = \rho_{c0}(1 - x_c)^{\alpha-1}\frac{dx_c}{dt} \tag{71}$$

Since Eq. (58) holds for the particle mass at any time t, the two coefficients α and δ are related: $1 = 3\delta + \alpha$. For the UCM (Case a in Fig. 18), consistent values of the coefficients are $\delta = 0$ and $\alpha = 1$, so that $r_{v,p} = \rho_{c0}dx_c/dt$. For the SUPM (Case b in Fig. 18) $\delta = 1/3$ and $\alpha = 0$, so that $r_{v,p} = \rho_{c0}(1 - x_c)^{-1}\, dx_c/dt$. In between these two limiting cases, the empirical macroscopic models claim to describe the process by judicious extrapolation of α and δ, and (δ,α) should hold in the ranges (0,1) and (1/3,0). Obviously, the macroscopic models given by Eqs. (69–71) provides a short-cut

method for the calculation of $r_{v,p}$, but the degree of approximation is uncertain. Nevertheless, the macroscopic models are widely used because they are helpful to develop empirical particle models by adjusting the values of α and δ for the operating conditions of interest (type and size of char, temperature, and gaseous concentration). A more rational basis for calculation is provided by formulating char particle models in a simplified way. This is done in the following.

3.5.4. Evaluation of the combustion reactivity of a single char particle

Advanced particle models are developed for combustion conditions [183,245,246]. The models of char combustion in FB combustors and gasifiers share some features but differ in others. The temperature of a char particle in an FB combustors can be significantly higher (50–100 °C) than the average bed temperature [247]. In contrast, the temperature difference between the char particles and the bed is small in an FBG, due to the simultaneous endothermic and exothermic reactions [25,59,219]. This allows assuming isothermal conversion in an FBBG even for the combustion reaction.

During char combustion it has been experimentally verified for a large number of chars that the reaction is so rapid that it occurs in a thin layer. Therefore, sharp-interface reaction models are often adopted (Case b and c in Fig. 18). The SUPM is likely to be the closest representation for combustion of low-ash biomass char, such as wood in an FB, since the abrasion by bed material enhances the removal of ash from the particles. For high-ash chars, such as sewage sludge, it has been demonstrated that the SUCM better represents the behavior, because the ash remains attached during the whole conversion [248]. The use of sharp-interface reaction models greatly simplifies the solution, because the surface where the reaction takes place can be directly correlated with x_c as indicated in Fig. 18. This is the reason why char reactivity for combustion is usually based on a reacting external surface. A description of the internal surface and the pore development during conversion is not necessary in any of these cases.

For first-order kinetics with respect to the gas, the reactivity of a single particle according to the SUPM and SUCM has been presented in classical text-books. For instance for char particles with spherical geometry [241]:

$$r_{m,p} = \frac{6}{d_{p0}\rho_{c0}} \frac{\rho_e}{\left(\frac{1}{\Lambda h_m} + \frac{1}{k_A}\right)} \quad \text{for SUPM} \tag{72}$$

$$r_{m,p} = \frac{6}{d_{p0}\rho_c} \frac{\rho_e}{\frac{1}{\Lambda h_m} + \frac{d_{p0}(d_{p0}-d_c)}{2\Lambda D_{ash} d_c} + \frac{1}{k_A}\left(\frac{d_{p0}}{d_c}\right)^2} \quad \text{for SUCM} \tag{73}$$

Λ is the gravimetric stoichiometric coefficient, defined as $\Lambda = MM_c/(MM_G \nu_G)$, and ν_G is the stoichiometric coefficient of the gas in the char–gas reaction, i.e. according to the stoichiometry Carbon + ν_G Gas → Products. In the SUPM the density ρ_c remains constant during conversion, whereas the size d_p and the mass transfer coefficient h_m change with conversion. The evolution of d_p and h_m with x_c are known, as indicated in Fig. 18 by the relation of $d_p(x_c)$. In the SUCM d_p keeps constant $d_p = d_{p0}$ but the position of the core d_c (see the law of change in Fig. 18) and the particle density change with x_c according to Eq. (64). Therefore, $r_{m,p}$ can be calculated as a function of x_c. The corresponding Eqs. (72) and (73) expressed as a function of x_c, the integrated t–x_c expressions, as well these relations for other geometries are available [241].

However, the reaction order for combustion of biomass and coal char at atmospheric pressure is in the interval of 0.5–1 [6,77,216,249,250]. Analytical expressions for nth order kinetics have been obtained here for general nth order kinetics, summarized in Table 11, where the solution of $r_{m,p}$ is expressed in the general form:

$$r_{m,p} = r_{m,e0}\,(1-x_c)^{-1/3}\,\eta_p(x_c) \tag{74}$$

$r_{m,e0}$ being the reactivity at $t = 0$ ($x_c = 0$) evaluated for emulsion conditions given in Table 11. Eqs. (72) and (73) can be obtained from Eq. (74) as particular cases for $n = 1$.

The relatively large particle size and high reactivity of the char in an FBG usually make the rate of char combustion controlled by external diffusion (Regime III). In this regime, the reactivity of a single particle, no matter the order of reaction of the kinetics, is

$$r_{m,p} = \frac{\Lambda h_m \rho_e}{L_e \rho_{c0}} \quad \text{(for SUPM)} \tag{75}$$

$$r_{m,p} = \frac{\Lambda h_m \rho_e}{L_{e0} \rho_c} \quad \text{(for SUCM)} \tag{76}$$

which are particular cases of Eq. (72) or Eq. (73) when the reactivity of the char is high compared to the rate of diffusion to the external surface (the sum of external and ash diffusion if the ash is kept attached, i.e. SUCM). Eqs. (75) and (76) have been expressed in term of L_e, the equivalent particle diameter, given by the ratio of particle external surface and volume ($d_p/6$, $d_p/4$ for spherical and cylindrical particles and half-width in a flat particle). Variation of L_e with x_c is given by $L_e = L_{e0}(1-x_c)^{1/3}$.

Owing to the gas-film diffusion control for practical operating conditions in FB combustion, models of single char-particles have been focused on the solution of the mass transport in the boundary layer instead of inside the particle; various gas-film models have been developed: single, double and continuous film

Table 11
Model for the combustion reactivity of a single char spherical particle in an FBBG (nth order kinetics, surface model (SUPM or SUCM) and isothermal conditions) $r_{m,p} = r_{m,e0}(1-X_c)^{-1/3}\eta_p(x_c)$ (Eq. 74).

	SUPM	SUCM
$r_{m,e0}$	$(6k_A\rho_e^n)/(\rho_{c0}d_{p0})$	
η_p	$(1-\mathrm{Da}_{ch}\eta_p)^n = \begin{cases} [(((1-n)\mathrm{Da}_{ch})^{1/n}+1)^n + n\mathrm{Da}_{ch}]^{-1} & 0<n\le 1 \\ 2n[(2n)^{1/n}-1+(1+2n\mathrm{Da}_{ch})^{1/n}+1]^{-n} & 1<n<2.7 \end{cases}$	
Da_{ch}	$\mathrm{Da}_{ch,e0}(1-x_c)^{\xi}\begin{cases}\xi = 1/3 & \text{for Sh} \propto \text{const} \\ \xi = 1/6 & \text{for Sh} \propto \mathrm{Re}^{1/2}\end{cases}$	$\mathrm{Da}_{ch,e0}(1-x_c)^{2/3} + \mathrm{Da}_{ch,i0}((1-x_c)^{1/3}-(1-x_c)^{2/3})$
$\mathrm{Da}_{ch,e0}$	$(k_A\rho_e^{n-1})/(h_{m0}\Lambda)$	
$\mathrm{Da}_{ch,i0}$	–	$(k_A\rho_e^{n-1}d_{p0})/(2D_{ash}\Lambda)$

models [6,251]. All these models can be represented by a single film and a global reaction characterized by a factor θ,

$$C + \theta O_2 \rightarrow 2(1-\theta)CO + (2\theta - 1)CO_2 \quad (77)$$

θ can be obtained as a function of temperature and other parameters [252]. Values of θ in the range of 0.8–0.9 have been used for char combustion in FBG, fitting well measurements with lignite coal [253] and sewage sludge [231]. In modeling of char combustion in FB combustion, θ is a key factor [254], but in FBG models it plays a secondary role and influences the solution only weakly. This is because the final gas composition from the gasifier is determined by the water–gas shift reaction and char gasification rather than char combustion [111]. This is another great difference between char combustion in an FB gasifier and in a combustor.

When the reaction takes place in a finite zone (and not in a sharp interface as assumed in the derivation of Eq. (74)) the treatment becomes more difficult. However, such a case is not likely to occur during char combustion in FBBG, although it can be handled with the method presented below for char gasification.

In summary, combustion of biomass char in FBBG takes place on the external area of the particle, linking directly d_p (or d_c) and x_c. An isothermal SUPM (Case b in Fig. 18) with external diffusion control is considered to be a good representation of the process, and then $r_{m,p}$ can be calculated by Eq. (75). For fine chars with high reactivity at high temperature, Regime II can be established and $r_{m,p}$ should be calculated by Eq. (74). Eqs. (72) and (73) should be used only with first order kinetics.

3.5.5. Evaluation of the gasification reactivity of a single char particle

The reactions of char with CO_2, H_2O and H_2, are much slower than with oxygen for the conditions of FBG. The char remains a considerable time in the bed (from a few minutes to around an hour) to be converted. Then the reactants have time to diffuse into the particles, the reactions take place inside the particle to a greater extent than during combustion, and the interior surface changes significantly (internal area and degree of catalytic effect). A model capturing the local carbon conversion, reaction area, and gas conditions (concentration and temperature) is, therefore, essential. Gasification is most likely to proceed in Regime II, and Eq. (74) is not a useful model because the reaction does not occur on the external surface only. A formulation of the kinetics expressing the volumetric consumption of carbon inside the char particle is appropriate. A variety of advanced particle models have been published to calculate $r_{m,p}$ during gasification of char from coal [237,238,255,256] and from biomass [227]. These models have solved the multicomponent mass diffusion of species in both the external layer and in the interior of the particle, considering non-isothermal effects and that particle properties vary with time. The models provide an understanding of the process, but they are not used for reactor simulation due to the complexity of the calculations. Instead, models of kinetics without transport effects are often employed in reactor calculations [211,257].

Here a way to calculate $r_{m,p}$ for FBBG is presented, accounting for both transport and kinetics effects. The model is simplified, based on experimental observations made during normal operation of an FBBG, as well as on theoretical aspects learnt from advanced particle models. The following simplifications are made:

a. At usual temperatures, the rate of char hydrogenation (R6 in Table 3) is slow in atmospheric gasifiers, and methane formation can be disregarded. Then, three reactions participate in char gasification: char–CO_2, char–H_2O, and the water–gas shift reaction, the latter being rapid compared to the other reactions [238].
b. Temperature is nearly uniform in the bed and in the particles, and isothermal conditions are assumed [219,237,238].
c. The high diffusivity of hydrogen leads to nearly uniform concentration of this gas throughout the char particles [238,255], whereas this may not be the case with other gases.
d. The dependence of the char reactivity on the concentrations of the reactants CO_2 and H_2O and on the temperature of char can be represented by nth-order kinetics. It is known that Langmuir–Hinshelwood kinetics is a more general description based on surface mechanisms, especially when inhibition by the products (CO and H_2) must be taken into account [226,258]. However, at near-atmospheric pressure and low partial pressures of CO and H_2 experimental results are rather well correlated with an order of reaction between 0.4 and 0.7. Kinetic parameters based on a model involving nth-order kinetics have been surveyed [216,226,258]. Despite wide variation of the activation energy, the reaction order was found to be within the range of 0.4–0.7 for most chars. Assumption of a first order reaction can lead to substantial error, and a particle model has to handle nth-order kinetics.
e. Fig. 19 shows the evolution profiles of conversion of X during char particle conversion for (a) rapid and (b) slow reactions. For rapid reactions, such as char combustion (Fig. 19a), the conversions X and x_c differ significantly: the external layers have $X = 1$, while $X = 0$ in the interior of the particle. This leads to the surface interface models shown in Fig. 18. In contrast, for slow reactions, such as char gasification with CO_2 and H_2O, the conversion profiles are more similar to those shown in Fig. 19b. In low-temperature gasifiers (such as FBBG), the char is mainly converted by CO_2 and H_2O due to the lack of O_2 in most reactor space. An important conclusion is that, at any time, X and x_c do not differ much, simplifying the reaction-diffusion problem in a char particle.
f. The reactions of char with CO_2 and H_2O can be added into one single reaction. This is based on the study [228] where the reaction rate was found to depend on the concentrations of H_2O and CO_2 in a similar way; the rate of the reaction with H_2O is greater (twice) than with CO_2 [25,219,228,259]. Some authors considered the rates to be identical [260]. Others have omitted one of the reactions or did not consider the $CO_2 + C$ reaction directly [259] because of the large difference in rates observed for coal chars. For simulation of an FBG operated with wood, the reactivity of the char with H_2O has been considered to be twice that with CO_2 [219]. In any case, the ratio of the two reaction rates can be obtained from measurements [261] and may be assumed constant during conversion. In this way, only one reaction is explicitly taken into account [104].

Based on assumptions (a) to (f), a simple char particle model can be developed. The procedure is to estimate an effectiveness factor for the particle η_p through its interior η_i and exterior η_e counterparts, defined in Eq. (68). The detailed derivation of the equations and the way to obtain the necessary information from experiments has been published [234]. The solution of the isothermal mass transfer problem in the boundary layer and within the char particles under pseudo-steady-state can be written as a function of η_e and η_i as:

$$\eta_e = \left(1 - Da_{ch,e}\eta_i\eta_e\right)^n \quad (78)$$

$$\eta_i = \frac{\tanh\left(\eta_e^{(n-1)/2n} Da_{ch,i}^{1/2}\right)}{\eta_e^{(n-1)/2n} Da_{ch,i}^{1/2}} \quad (79)$$

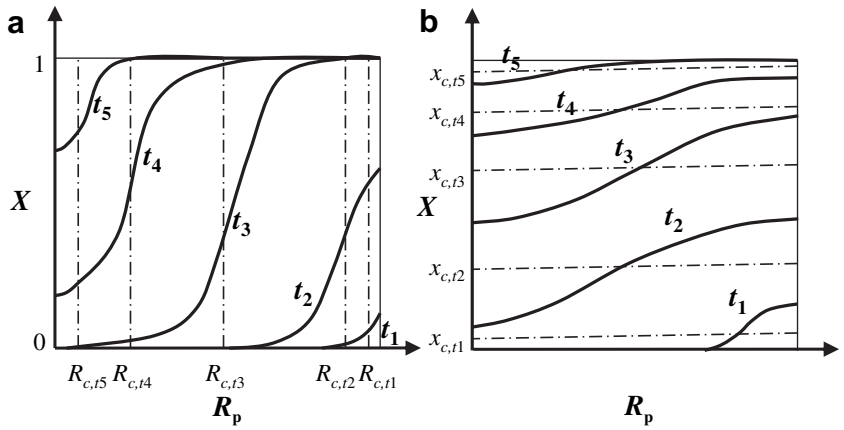

Fig. 19. Typical local conversion (X) vs. particle radius (R_p) at various times (from t_1 to t_5) within a char particle during: (a) combustion and (b) gasification. Dotted lines in graph (a) represent the position of the core ($R_{c,t1}$–$R_{c,t5}$) at different times if a surface interface model (surface reaction) is assumed (see cases b and c in Fig. 18). Dotted lines in graph (b) represent the particle conversion ($x_{c,t1}$ to $x_{c,t5}$).

For known $Da_{ch,e}$ and $Da_{ch,i}$, Eqs. (78) and (79) provide two coupled non-linear equations for η_e and η_i. Once η_p is determined ($\eta_p = \eta_e\,\eta_i$), $r_{m,p}$ is estimated as

$$r_{m,p} = r_{m,e0}\, f(x_c)(1-x_c)\eta_p(x_c) \tag{80}$$

$r_{m,e0}$ being the reactivity evaluated at initial conversion in the emulsion:

$$r_{m,e0} = A_{m0}k_A\rho_e^n = k_{m0}\rho_e^n \tag{81}$$

$Da_{ch,e}$ and $Da_{ch,i}$ are defined in Table 12. $Da_{ch,e}$, the external Damköhler number of the particle for char gasification, is the ratio of the reaction rate to the external diffusion rate. $Da_{ch,i}$ the internal Damköhler number (Thiele modulus squared), is the ratio of the reaction rate to the internal diffusion rate. Both $Da_{ch,e}$ and $Da_{ch,i}$ are computed for the conditions in the emulsion phase and they depend on conversion. $Da_{ch,e0}$ and $Da_{ch,i0}$ are the corresponding values at the initial conversion. As seen in Table 11, for char gasification, $Da_{ch,e}$ and $Da_{ch,i}$ are defined with the volumetric kinetic constant k_v to take into account the change in internal surface of the char particle. In combustion, where the reaction occurs only at the surface, the kinetics constant is based on the surface, k_A. The factors λ_e and λ_i in Eqs. (126) and (127) (Table 12) result from the variation of the particle's properties and k_v (volumetric kinetic coefficient), L_e (equivalent length), h_m (mass transfer coefficient) and D_{eff} (effective diffusivity), vary with conversion x_c. The change of D_{eff} with x_c is given by the empirical equation $g(x_c)$ in Table 12. The change of particle size with x_c is estimated by a model like Eq. (69) with an equivalent length L_e, given in Eq. (133), containing the adjustable parameter δ. δ is difficult to predict theoretically because it not only depends on the mode of chemical conversion of the char but also on attrition and secondary fragmentation. Therefore, δ needs to be obtained experimentally [261]. Eq. (79) is strictly valid for first-order kinetics in a slab. However, it can be shown [262] that it is a reasonable approximation for any geometry (characterized by an equivalent size L_e) and reaction order, n.

The simplified method is valid for relatively low $Da_{ch,i}$, which corresponds to a situation like the one depicted in Fig. 19b. The precise value of $Da_{ch,i}$, up to which the approximate model yields reasonable results depends on the operating conditions and the way in which the intrinsic reactivity varies with x_c (that is, on the nature of the biomass and the form of preparation of the char). This case can be seen as an extension of a UCM, where some pore-diffusion effects may exist without being dominant; this case can be useful for char gasification in FBG.

Note the similarity between Eqs. (74) and (80): $r_{m,e0}$ are demonstrated to be equal if proper relations between the kinetic coefficients are used, $k_{v0} = \rho_{c0}A_{m0}k_A = \rho_{c0}k_{m0}$ together with the variation of size and density during conversion for SUPM and SUCM, i,e, sharp interface models. The function $(1-x_c)^{-1/3}$ is used for char combustion (sharp interface models) whereas $f(x_c)(1-x_c)$ for gasification (homogeneous model).

3.5.6. Evaluation of the effective reactivity in a FBG

The overall reactivity in the bed, $r_{m,b}$ is calculated taking into account the mass distribution of conversion of the char particles in the bed $p_b(x_c)$, each having the reactivity $r_{m,p}(x_c)$,

$$r_{m,b} = \int_{\forall\, x_c} r_{m,p}(x_c)p_b(x_c)\mathrm{d}x_c \tag{82}$$

Most FBG models assume that $r_{m,b}$ can be approximated by $r_{m,p}(x_{c,b})$, i.e. the reactivity evaluated at the average conversion in the bed, $x_{c,b}$. To assess this approximation, a factor Ω is introduced [262], measuring the discrepancies between $r_{m,b}$ and $r_{m,p}(x_{c,b})$,

$$\Omega = \frac{r_{m,b}}{r_{m,p}\left(x_{c,b}\right)} \tag{83}$$

Table 12
Relationships and parameters for the calculation of the single char particle model given by Eqs. (78) and (79) (all resulting quantities in the table are dimensionless).

$$Da_{ch,e}(x_c) = Da_{ch,e0}\lambda_e(x_c) \tag{126}$$

$$Da_{ch,i}(x_c) = Da_{ch,i0}\lambda_i(x_c) \tag{127}$$

$$Da_{ch,e0} = \left(L_{e,0}k_{v,0}\rho_e^{n-1}\right)\Big/\left(h_{m,0}A\right) \tag{128}$$

$$Da_{ch,i0} = \left((n+1)/2\left(L_{e,0}^2k_{v,0}\rho_e^{n-1}\right)\right)\Big/\left(D_{eff,0}\Lambda\right) \tag{129}$$

$$\lambda_e(x_c) = \begin{cases} f(x_c)(1-x_c)^{1+(3/2)\delta} & \left(\text{for } Sh\propto\text{const}\right) \\ f(x_c)(1-x_c)^{1+2\delta} & \left(\text{for } Sh\propto Re^{1/2}\right) \end{cases} \tag{130}$$

$$\lambda_i(x_c) = \left(f(x_c)/g(x_c)\right)(1-x_c)^{1+2\delta} \tag{131}$$

$$g(x_c) = D_{eff}(x_c)/D_{eff,0} = \left(\varepsilon(x_c)/\varepsilon_0\right)^{\kappa} = \left[1+\left((1-\varepsilon_0)/\varepsilon_0\right)x_c\right]^{\kappa} \tag{132}$$

$$L_e(x_c)/L_{e,0} = (1-x_c)^{\delta} \tag{133}$$

When $\Omega \approx 1$, the distribution of conversion has a small impact on the average reactivity in the bed, then population balance is not necessary, and $r_{m,b} = r_{m,p}(x_{c,b})$ as investigated in [262–265]. In general, Ω depends on $f(X)$ and $\eta_p(x_c)$. Since the contribution of char combustion to the overall conversion of char is low under FBBG conditions, the population balance seems not to be necessary for the modeling of a hypothetical char combustion zone with a distribution of char particles. This can be easily quantified. For the particular case of SUPM ($f(x_c) = (1 - x_c)^{2/3}$) $\Omega > 0.95$ at $x_{c,b} < 0.4$ has been reported [262]. Therefore, to estimate the char conversion by combustion in an FBBG, it is sufficient to assume $\Omega \sim 1$ and to calculate $r_{m,p}$ with Eq. (74). A population balance may be needed to evaluate the overall char gasification rate, since most of the char is consumed by gasification reactions. The difference between $r_{m,b}$ and $r_{m,p}(x_{c,b})$ has been analyzed by the curves of Ω vs. $x_{c,b}$ from the extended random pore model (ERPM) (Table 9) for different values of the parameters ψ, c and p [265], representing a variety of biomass chars [220]. The main conclusion is, that to model the gasification of char in an FBBG working with an $x_{c,b}$, say, in the range of 0.6–0.9, a population balance should be included. In FBBGs operating at so low temperature that the char conversion is below 0.5, a population balance does not seem to be necessary. However, the case of FBBG attaining high char conversion is the one wished to be simulated, since it yields higher efficiency. Therefore, consideration of the population balance is needed for optimization of FBBG.

3.6. Comminution of solid particles

Fuel size is reduced by shrinkage during devolatilization, by primary fragmentation, secondary and percolative fragmentation of char, and fines generation by attrition (see Fig. 20). The comminution can differ from one fuel to another, but it is difficult to infer attritability from fuel properties, so it has to be characterized by experiments [266,267]. The processes to be discussed are visualized in a CFBBG in Fig. 21.

Thermal stresses or release of volatile gases inside fuel particles exerting high internal pressure may break the particles into fragments. This phenomenon, called primary fragmentation, is indicated as Process 1 and 2 in Fig. 20. In addition, owing to the high mass loss during devolatilization, the shrinkage of the fuel particles may be significant. During the subsequent char convertion in Regime I or II, the pores increase in size, weakening the carbon bonds inside the char. When a bridge is too weak to withstand the hydrodynamic forces on the char, a fragment is formed. This process is called secondary fragmentation, visualized as Processes 3, 4 and 5 in Fig. 20. Sometimes (usually in Regime I), all internal bridges may collapse suddenly, giving rise to the special type of secondary fragmentation known as percolative fragmentation. Experimental evidence [97] states that percolative fragmentation is the main mechanism of fines generation during char circulation in the freeboard of an FBG, probably a consequence of the highly porous char generated from beech. Although this feature has not been studied for many types of biomass, it seems to be a distinctive feature of biomass char compared to coal char [268,269]. The fragments produced by secondary fragmentation are an order of magnitude larger than the attrited carbon fines. The fragmented char particles may also experience further division into finer particles in an FB due to the abrasive action of the bed material. It has been shown [267] that the contribution of char conversion of fines in the freeboard is up to 70% of the conversion attained in the bottom bed at 700 °C, whereas this value decreased to about 10% at 900 °C. Therefore, char conversion in the freeboard of a BFB should be considered in models operating at low-temperature gasification with high char concentration suffering attrition.

A survey of attrition of carbons, mainly coal and char, during FB combustion has been presented [266]. Significant differences have been observed between biomass and coal and between different types of biomasses with respect to attrition and fragmentation [268,269]. Primary fragmentation is extensive for tyre-derived fuel, whilst attrition by abrasion plays an important role during combustion of bituminous coal and biomass. The intrinsic reactivity of biomass fuels is so high that extensive afterburning of attrited fines overcomes elutriation. The conversion of granulated sludge is characterized, in contrast, by the formation of a coherent ash skeleton throughout fuel conversion, though primary ash particles may undergo extensive attrition beyond burn-off. These features warrant high carbon conversion of this type of fuel in FBG. An investigation of FB combustion of three biomasses [269] showed that the conversion of fines occurred essentially by percolative fragmentation, accounting for 25–45% of the fixed carbon consumption. Compared to the amount of work published on attrition of coal and biomass in FB combustors, very little information is available on attrition of biomass in FBG [97].

Inclusion of fragmentation and attrition in the population mass-balances given in Eq. (36) is rather complex, demanding detailed knowledge of the mass-flow rates at different particle sizes, i.e. the model of terms Γ_m in Eq. (36). An additional consequence of the generation of finer pieces of solids is that they may affect the time–temperature history of the reacting solids because of substantial overheating of fine particles (which heat up higher during burning due to their smaller size) with respect to the average temperature of the bed [270]. This feature, in combination with the large alkali content of some biomass fuels, may increase the fuel's propensity to agglomerate [271].

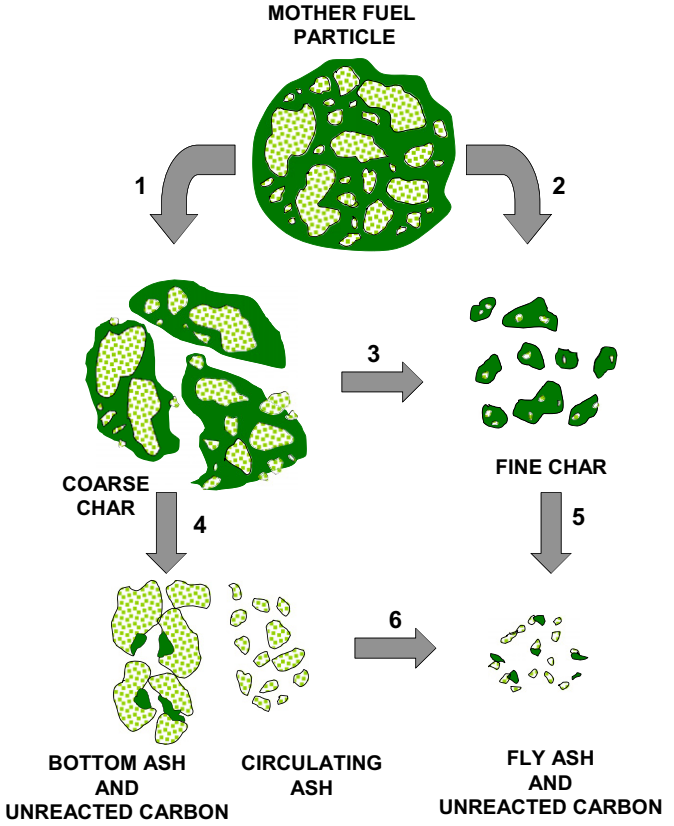

Fig. 20. Comminution of fuel and char during conversion in an FB. The main processes are identified by numbers and arrows indicate the progress of time: 1,2: Primary fragmentation of mother fuel-particle. 3: secondary fragmentation of coarse char. 4 Conversion and secondary fragmentation of coarse char. 5: Conversion and attrition of fine char. 6: Attrition of char and ash.

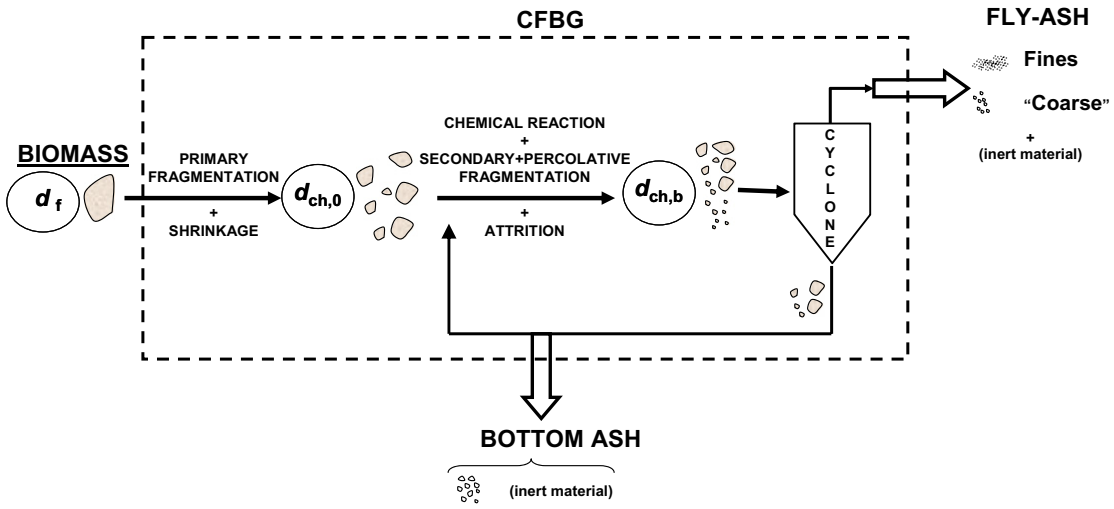

Fig. 21. Particle transformation in a CFBG.

3.6.1. Modeling of comminution of fuel and char

Due to the complexity of the process and to the variation of the properties of biomass fuels, detailed modeling of comminution in FBBG is still a nascent field. Therefore it is out of the scope of this review, although a great deal of work has been published for FB combustion. Here, a qualitative description is given of the key quantities, showing the essentials of comminution modeling and the type of input necessary for first estimates. Thereafter, a simplified treatment is dealt with, giving rough quantitative expressions that could be used in reactor codes.

Primary fragmentation changes the particle size distribution of the char and its average diameter. Therefore, modeling should be focused on the determination of these quantities, although few models can predict them with sufficient accuracy. The fragmentation probability is sometimes related to the maximum overpressure within a particle, created during rapid heating, as estimated by Darcy's law:

$$p_{\max} = \frac{\rho_f}{\rho_{py}} x_{py} \frac{1}{t_{py}} \frac{L^2}{2K} \tag{84}$$

where K is the permeability of the particle, ρ_f and ρ_{py} the densities of the particle and of the volatiles released, and x_{py} the mass fraction of volatile matter in the fuel. $p_{\max}$ should be compared with a mechanical failure criterion to establish whether breakage of the slab occurs or not under the action of internal overpressure.

It has been experimentally verified that the probability for large fuel particles to break up during devolatilization is high, whereas small particles do not undergo fragmentation. Theoretical quantification of this fact is made in terms of a fragmentation probability P_f [266,272], defined as the probability of a particle of certain size d_f to fragment during devolatilization. Complex models have been developed to calculate P_f on the basis of internal stress [266]. Simpler models of P_f has expressed it as $P_f = 1 - \exp(-k_f\, t_{py})$, where the fragmentation rate constant was $k_f = 0.11\ s^{-1}$. The time at which primary fragmentation occurs is not well known. However, calculations assuming fragmentation, either at the beginning or at the end of the devolatilization period, show that the influence is small on the distribution of volatiles at the end of the devolatilization process [29]. Therefore, its calculation seems to be of secondary concern. In fact, primary fragmentation is almost instantaneous, because the devolatilization time is much shorter than the time of char conversion, so that the two processes can be considered to occur in series. The number and size distribution of the fragments, in contrast, must be predicted; they have a major impact on the FBG performance. Recent advanced models attempt to quantify these variables [185,186] by taking into account the thermal stress caused by the release of volatiles. One of these models predicts the possibility of fragmentation, timing of fragmentation and its location within the wood particle in an FB combustor. This type of model supports characterization of fragmentation patterns, but it is too complex to be used in reactor codes, and it needs several input parameters.

During char gasification, secondary fragmentation changes the number and size of the char particles. The knowledge on secondary fragmentation of char is even more uncertain than that of primary fragmentation. Experiments aiming at characterization of fragmentation patterns result in an empirical expression of the dependence of the size d_{ch} on conversion x_c during fragmentation [267]. Percolative fragmentation generates fines and is claimed to be a dominant mechanism in biomass gasification [267]. Percolation, modeled for coal [273] requires definition of a percolation threshold. For coals, this threshold generally is at a high degree of conversion (>90%). Little is known about the behavior of biomass in this respect.

Production of fines from coarse particles by abrasion with other particles is enhanced by combustion or gasification. The attrition rate in an FB is [274,275]:

$$\frac{dm_{att}}{dt} = K_{att} \Delta u \frac{m_{ch}}{d_{ch}} \tag{85}$$

$\Delta u = u_0 - u_{mf}$ the velocity difference in a BFB and the slip velocity $u_0 - u_t$ in a CFB. K_{att} is the dimensionless attrition constant, determined experimentally for a variety of chars and solids [26] and roughly independent of the type of fluidization [275]. Also, friability coefficients Θ_m are taken from literature for first estimates for various solids in the bed [276] quoted in [24]. For char, sand and other materials used in FB various friability coefficients have been reported [24,277].

A simplified treatment of FB combustion of coal char [278] and of biomass char [269] can be extended to FB gasification. Primary fragmentation and particle shrinkage, considered to be instantaneous, affect the size distribution of char and reduce its average diameter (see Figs. 20 and 21). The relationship between the original fuel size, d_f and the average size of the fragments of char after devolatilization, $d_{ch,0}$ can be formulated as $d_{ch,0}/d_f \approx (\varphi/n_1)^{1/3}$, where $\varphi = \rho_f Y_{ch}/\rho_{ch}$ is a shrinkage factor, and n_1 and Y_{ch} number of fragments and yield of char after primary fragmentation [269]. The

average diameter of the char in the bed, $d_{ch,b}$ (see Fig. 21), is assumed to be the result of two independent processes, one accounting for chemical reaction, yielding the fictitious size $d_{ch,1}$, and the other accounting for fragmentation and attrition, yielding the fictitious size $d_{ch,2}$. $d_{ch,1}$ is calculated as if chemical reaction were the only process reducing the size of the char, so $d_{ch,1} \approx \sigma d_{ch,0}$ [278], σ being a factor that depends on the mode of conversion. $d_{ch,2}$ has been shown [268] to be related to $d_{ch,0}$ by $d_{ch,2} \approx d_{ch,0} \cdot n_{2,m}^{-1/3}$, where $n_{2,m} = (1+n_2)/2$, with n_2 being a multiplication factor determined experimentally [269]. Now, assuming that the relations for $d_{ch,1}$ and $d_{ch,2}$ could be used for the real, coupled case, the average char size in the bed, $d_{ch,b}$, is related to the initial fuel size, d_f, by the approximate relation:

$$\frac{d_{ch,b}}{d_f} \approx \left(\frac{\varphi}{n_1 n_{2,m}}\right)^{\frac{1}{3}} \sigma \tag{86}$$

The change in size caused by generation of fines from attrition was neglected in the treatment above. In biomass chars peripheral percolative fragmentation dominates rather than mechanical attrition. This leads to a negligible influence from the fines generation during conversion of coarse char on the mean diameter of the char particles in the bed, and this phenomenon can be treated just as an enhancement of the rate of conversion [269,279]. Hence percolative fragmentation only affects the calculation of the total carbon consumption rate in the overall carbon mass-balance. The carbon consumption-rate can be simply evaluated by increasing the char conversion-rate calculated in the absence of fines generation, by a factor $(1+\alpha)$ [279,280]. The factor α can be determined by measurements under the operating conditions of interest. In fact, this approach is based on the assumption that char conversion is confined to a region close to the particle surface, which is valid for FB combustion, which is usually controlled by boundary layer diffusion. However, the assumption is questionable for FBG and should be verified for the conditions to be modeled.

To sum up, for the estimation of the average particle size in the bed $d_{ch,b}$, one has to measure n_1, n_2, φ. σ should be estimated according to the mode of conversion of the particle by a simple solid population balance, assuming no attrition and no outlet streams (no overflow/drainage, or elutriation). For combustion of char according to the shrinking-core model controlled by gas-film diffusion, σ ranges between 0.78 and 0.80 [278]. For a char conversion model, such as that presented in gasification reactors, σ can vary more, depending of the reaction order and the effectiveness factor. It is expected that n_1 and φ do not change from combustion to gasification due to the difficulty of oxygen to penetrate the front created by volatiles during devolatilization. In contrast, $n_{2,m}$, can be different under oxidizing conditions due to the possible enhancement of fragmentation and attrition by oxygen. Table 13 gives experimental values of the main quantities defined here for three biomasses [269].

Table 13
Parameters for fragmentation modeling and calculation results (after Scala et al. [269]).

Fuel	n_1	n_2	φ	d_1/d_0	$d_{ch,0}/d_f \approx (\varphi/n_1)^{1/3}$	$d_{ch,b}/d_f$ (from Eq. (86))
Pine seed shells	1.6	1.5	2.0	0.72	0.68	0.50
Wood chips	3.5	2.2	2.3	0.59	0.50	0.34
Olive husk	1.04	1.0	1.3	0.91	0.90	0.72

3.6.2. Comminution for other solid particles

For inert material and catalysts, attrition can be characterized by abrasion and the description is easier. Eq. (85) can be used with an attrition constant for the solid material. In the case of a catalyst that decomposes thermally in the bed, such as carbonate rock (dolomite, lime, etc), changes in physical properties have to be taken into account during the heating time until it is calcined to CaO or MgO. Under standard operation conditions the time of calcination is in the order of a minute [44], suggesting that this time is short compared to the solids residence time in the bed. Much work available from the modeling of sorbents for desulphurization of coal in FB combustion units [19,281,282] can be applied in FBBG modeling. There are a few measurements in this field [283], providing attrition and elutriation constants for a variety of catalysts. However, so far, they have not been applied in FBG codes.

3.7. Kinetics of homogeneous reactions

Combustion and reforming of volatile species may have a great impact on the outlet gas composition, carbon conversion and gasification efficiency. The homogeneous combustion of volatiles determines the behavior in the so-called flaming pyrolysis zone [284], a high-temperature zone (particularly in fixed-bed gasifiers) where the biomass is rapidly devolatilized and partly oxidized. The rates of the homogeneous combustion reactions have a strong impact on the behavior of FBG of high-volatile fuels like some low-rank coals and biomasses [59,111]. The reforming of volatiles such as tar, light hydrocarbons and the WGSR (i.e. the steam reforming of CO) determine the final gas composition and the extent of carbon conversion. These reactions may be catalyzed to a great extent by the sand, char or catalyst in the bed [285].

One could imagine that the kinetics of the homogeneous combustion and reforming reactions are well known, but this is not the case. The reactions between the stable chemical species involved in the homogeneous reactions are a complex combination of several elementary reactions. In particular, the reactions between oxygen and CO, H_2 and hydrocarbons comprise chain mechanisms with elementary steps of stable and unstable chemical species (for instance, radicals). Most work in the area of combustors and gasifiers uses global reactions, i.e. the reaction resulting after combination of the elementary reactions. Therefore, in most kinetics used in reactor modeling, the concentration exponents are not equal to the respective stoichiometric coefficients. In addition, some expressions include concentrations of species that do not take part explicitly in the stoichiometry of the global reaction, for example, the effects of water vapor on the oxidation of CO, of catalytic or poisoning species, such as HCl, on some oxidation reactions, or of some metals in the ash acting as catalysts over the solid–fuel particles, etc. In FBBG, the solids can strongly interfere with the rates of reaction. The quenching of radicals in the dense phase may determine the concentration of intermediate species, and so the observed reaction rate. As a result, the rate of these reactions in the bubble and the emulsion can differ significantly. This has been evidenced experimentally, for instance, during visualization of volatiles combustion in FB combustion, where the rate of volatiles oxidation is frozen by radical quenching in the dense phase and the combustion of volatiles is only observed within the bubbles [286]. Despite such evidence, this is rarely addressed in the reactor models.

There is a great amount of work on the kinetics of homogeneous reactions. Some authors have analyzed the difference in the kinetics available in the literature, especially for the homogeneous oxidation of CO [21,24,287,288]. The numerical expressions of selected reactions are presented in Table 14, where the kinetic parameters are given for the oxidation of CO, H_2, CH_4 and the steam reforming of CH_4 and CO. There is a great variation between the expressions for the same reaction. In Fig. 22 the Arrhenius graph ($\ln k$ vs. $1/T$) for the CO oxidation is represented by various kinetics that have been used in models over the years [21,287–292], pointing out

the large discrepancies between one set of kinetics and another. The kinetics of hydrogen is very fast and some authors have simply considered it instantaneous [289] or kinetics parameters have been assigned to obtain very high reaction rate [295]. Haslam [296] studied the simultaneous combustion of H_2 and CO, showing that the ratio of the rate constants for these two reactions is 2.86 between 900 and 1500 °C (see Table 14).

The homogeneous oxidation and steam reforming of CH_4 are much slower than the oxidation of CO and H_2 (see Table 14). It can be concluded that, in absence of catalytic effects, the concentration of methane is expected to remain constant after the devolatilization and oxidation in an FBBG. This fact has been assumed in FBBG models over the years to simplify the gasification process, as will be discussed in Section 4.3. However, the reforming of CH_4, as well as the WGSR, as discussed below, are known to be catalyzed by solids in an FBG. The effect of coal ash on the rate of steam reforming of methane and WGSR has been quantified [285]. The impact of solids has been taken into account in a few FBG models. Hamel [28,188] used the kinetics data determined by Chen et al. [285] for the steam reforming of CH_4 and the WGSR to simulate coal and biomass gasification in an FBG. Weimer and Clough [59] and Yan et al. [285] considered the catalytic effects of char on the rates of these two reactions in the gas of the emulsion of coal FBG. The kinetics have to be chosen with caution because the composition of the ash and char (and so their catalytic activity) depend greatly on the parent fuel (especially the amount of iron, calcium and alkali). A factor was used in [285] to adjust the catalytic activity depending on the char. When a commercial catalyst is added to the bed, the rates are typically an order of magnitude higher than the reactions over ash and char [285], which has to be taken into account.

After analyzing models and kinetics from literature, a concern with regard to the WGSR arises: is this reaction controlled by kinetics or equilibrium? The attainment of WGSR equilibrium is questionable, especially in lab-scale FB in the usual temperature range of operation (800–900 °C) if no in-bed catalyst is used. In these devices, the temperature of the gas in the freeboard is usually significantly lower than in the bed. In large-scale systems, however, with sufficiently tall freeboard and insulated walls, the equilibrium of the WGSR is expected to be reached if the temperature is maintained above 800–850 °C. There is no quantitative evidence on this issue, though, since most of the FBG tests have been carried out in small units with large heat loss or with the air ratio decoupled from temperature by using external heating elements. As a result, it seems better to consider WGSR to be kinetically limited than to assume equilibrium. For this purpose, most modelers have used the kinetics presented in Table 14. This issue is discussed in detail below within the context of equilibrium and pseudo-equilibrium models.

In summary, it follows that a preliminary screening of the various homogeneous kinetics, especially the oxidation of CO and H_2, is a good practice in the modeling of FBBG because the reaction rate of these reactions varies widely depending on the choice of kinetics. The choice of the WGSR kinetics, in contrast, does not seem to be a concern because the same kinetics has been used in most publications. The uncertainty, instead, is whether equilibrium can be applied. It is expected that the choice of the oxidation

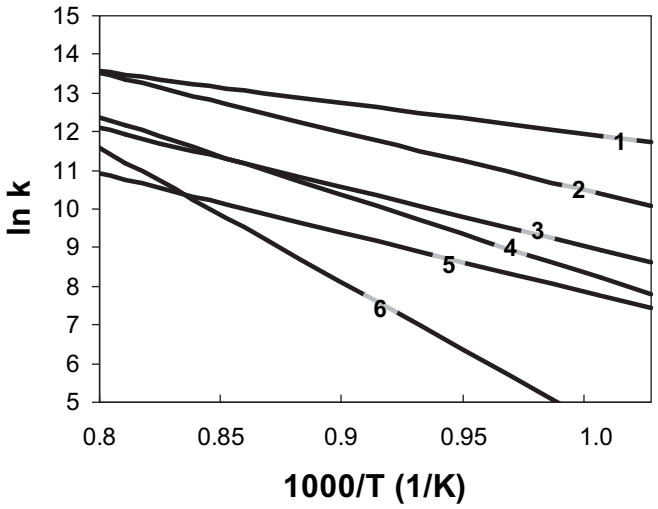

Fig. 22. Arrhenius graph for CO oxidation kinetics from (see Table 14): 1: Hottel et al. [291]; 2: Howard et al. [290]; 3: Jensen et al. [287]; 4: Dryer and Glassman [289]; 5: Hannes [21]; 6: Yetter et al. [292].

Table 14
Kinetics of the main homogeneous reactions (R in kmol.m^{-3}s^{-1}. c in kmol.m^{-3} in all reactions)

$CO + 0.5O_2 \rightarrow CO_2 \quad R_{CO} = Ae^{-E_a/(RT)} c_{CO}^{\alpha} c_{O_2}^{\beta} c_{H_2O}^{\nu}$

α	β	γ	E_a (kJ mol^{-1})	A [a]	Ref.
1	0.25	0.5	167	2.32×10^{12}	[289]
1	0.5	0.5	126	1.30×10^{11}	[290]
1	0.3	0.5	66.9	4.78×10^{8}	[291]
1	0.25	0.5	289	1.28×10^{17}	[292]
1	0.5	0.5	126	1.00×10^{10}	[21]
1	0.5	0.5	126	3.25×10^{10}	[287] [b]

$H_2 + 0.5O_2 \rightarrow H_2O \quad R_{H_2} = A\,T^{\delta} e^{-E_a/(RT)} c_{H_2}^{\alpha} c_{O_2}^{\beta}$

α	β	δ	E_a (kJ mol^{-1})	A [a]	Ref.
1	1	0	109	2.20×10^{9}	[293;294] [c]
1.5	1	−1.5	28.5	5.16×10^{13}	[24] [d]
1	1	0	125	1.08×10^{13}	[231] [e]
1	1	0	42	1.00×10^{14}	[295] [f]
$k_{H_2}/k_{CO} = 2.86$ [g]					[296]

(1) $CH_4 + 0.5O_2 \rightarrow CO + 2H_2$
(2) $CH_4 + 1.5O_2 \rightarrow CO + 2H_2O \quad R_{CH_4} = A\,T^{\delta} e^{-E_a/(RT)} c_{CH_4}^{\alpha} c_{O_2}^{\beta}$
(3) $CH_4 + 2O_2 \rightarrow CO_2 + 2H_2O$

Stoichiometry [h]	α	β	δ	E_a (kJ mol^{-1})	A [a]	Ref.
(1)	0.5	1.25	0	126	4.40×10^{11}	[300]
(2)	−0.3	1.3	0	203	2.80×10^{9}	[301]
(3)	−0.3	1.3	0	203	1.10×10^{9}	[301]
[i]	0.7	0.8	0	203	5.01×10^{11}	[289]
(3)	1	1	−1	130	5.16×10^{13}	[24] [j]

$CH_4 + H_2O \rightarrow CO + 3H_2 \quad R_{CH_4} = Ae^{-E_a/(RT)} c_{CH_4} c_{H_2O}$

E_a (kJ mol^{-1})	A (m^3 kmol^{-1}s^{-1})	Ref.
125	3.00×10^{8}	[300]

$CO + H_2O \leftrightarrow CO_2 + H_2 \quad R_{WGSR} = Ae^{-E_a/(RT)} (c_{CO} c_{H_2O} - c_{CO_2} c_{H_2}/\mathrm{K})$ [k]

E_a (kJ mol^{-1})	A (m^3 kmol^{-1}s^{-1})	Ref.
12.6	2.78×10^{3}	[302]

[a] A in (kmol.m^{-3})^m K$^{-\delta}$ s^{-1} with $m = 1 - \alpha - \beta - \gamma$.
[b] Jensen et al. [287] adapted the kinetics of Howard [290] by modifying A. Desroches-Ducarne et al. [288] adapted Jensen's equation to account for HCl effects on the observed kinetics.
[c] Mitani and Williams [293] is the original reference where the kinetics are only reported at one temperature as a function of elementary steps $k = (k_1 ? k_2)/k_5$. Groppi et al. [294] assumed that $(k_1\ k_2)/k_5$ equals $A\exp(-E_a/RT)$ (k_1, k_2 and k_5 follow the notation proposed by Mitani and Williams [293])
[d] Vilienskii and Hezmalian [297] is the original source (not verified)
[e] Kerinin and Shifrin [298] is the original source (not verified)
[f] not measured but assigned, assumed to be instantaneous, based on Bryden and Ragland [299]
[g] in the range of 900-1500°C
[h] See also Table 16
[i] not specified
[j] Vilienskii and Hezmalian [297] is the original source (not verified)
[k] K: Equilibrium constant with Eq. (94) [303]

reactions of CO and H_2 does not affect much the outlet gas composition, because it is dominated by the WGSR. However, the choice of reactions may have a strong influence on the char conversion predicted by the model. No publication has been found that clearly supports these statements. Other homogeneous reactions, such as the (non-catalytic) steam reforming of methane are so slow under normal FBBG conditions that the correct choice of kinetics seems to play a minor role. The presence of ash, char and other catalysts in the bed is known to influence the steam reforming of hydrocarbons and CO, and this should be taken into account. Homogeneous and heterogeneous reactions involving tar species are specifically discussed in the next section.

3.8. Secondary conversion of tar

Tar represents a large number of hydrocarbon species, usually heavier than benzene, whose properties differ widely among each other [304]. Operational factors, such as the ratios of air/oxygen, steam/biomass, catalyst/biomass, and design details, such as bed and freeboard height, have major effects on the amount and composition of the tar. These ratios affect the temperature and gas composition (especially oxygen and steam) in various regions of the reactor [305,306]. The presence of a catalyst in the bed may also affect the quantity and composition of tar [307]. Other design data, such as point of introduction of fuel, staging of the gasification agent (for instance secondary injection), determine the effective contact time of the tar and, thus, its final composition [308]. The following text is primarily devoted to secondary tar conversion, i.e. conversion of the tar after the pyrolysis vapor has been released from a fuel particle following the discussion in Section 3.1. In spite of the huge amount of work published on the kinetics of tar reactions under various operation conditions, the knowledge of tar formation and conversion in FBBG is still limited compared to other aspects surveyed in this work. Therefore, special concern is associated with data on the kinetics and the corresponding uncertainty in modeling.

3.8.1. Basis for modeling of the tar process

Secondary conversion of tar takes place on its way through the reactor by thermal cracking, reforming, and partial oxidation (R11–R15 in Table 3). The presence of an in-bed catalyst may have a great influence on the cracking and/or reforming reactions, affecting conversion and composition. Typical in-bed catalysts are calcined limestone and dolomite [309–311], olivine [311–313] and less frequently, Ni-based catalyst or catalysts made from a combination of the ones mentioned and other metals. Char itself is a catalyst, which has lately received attention, because it is cheap and generated within the process [314]. The performance of a variety of catalysts has been reviewed [315–318].

The modeling of tar conversion by secondary reactions encounters an additional difficulty compared to light gas compounds and char: tar is a mixture of compounds and changes its reactivity and chemical composition during conversion. Thus, accounting for tar conversion by mass tracking is not enough. This difficulty is formally also present in the modeling of char. However, char generated at high temperature consists mainly of carbon [215] and the conversion can be tracked by its relative mass change. Therefore, the approach of using one lump comprising all the tar compounds, despite being simple, is too limited in applications that aim at identifying the properties of the gas produced. In any case, the modeling of secondary tar conversion must be consistent with the kinetic data and the yields of primary tar employed as input to the modeling, as well as with the sampling and detection methods used for determination of tar. The latter can vary widely from one publication to another. Standardization of tar sampling and measurements has only been introduced a few years ago [304].

3.8.2. Tar classification and lumping

In the first attempt to distinguish tar components [319] the tar was split into classes (also called groups, families, or lumps) according to its thermal conversion behavior, using temperature and residence time as main criteria to establish tar groups. Class 1 consists of the products of primary pyrolysis, basically cellulose-derived products, released already at relatively low temperature (500 °C). Compounds measured in practical gasification operation are acetol, guaicol and acetic acid [320] and anisole [321]. Class 2 is phenolics and olefins, which are present in the temperature range of 500–1000 °C. Class 3, formed in the temperature range of 650–1000 °C, includes alkyl tertiary products (methyl derivatives of aromatics, such as toluene and indene). Class 4, formed above 750 °C, comprises aromatic compounds without substituents, such as benzene, naphthalene, anthracene and pyrene. For processes above 1000 °C, usually naphthalene is the primary component. This classification, despite being formally constrained to the experimental conditions of Ref. [319] (fine wood particles and a residence time in a gas-phase reactor of around 0.3–0.5 s), resulted in a first comprehensive experimental classification of the evolution of tar during its conversion. Recent work has refined and extended this idea, providing insight into the variation of tar species under different operation conditions [305,306,320,322].

A second established qualitative classification of tar has been made by ECN (Energy Centre of the Netherlands) [322], which grouped the individual tar compounds into five classes based on the behavior of the tar compounds in the downstream processes (mainly water solubility and condensing properties). The treatment of ECN has revealed the importance of the tar's dew point. They have shown that the dew point is dominated by the heavier tar (Group 5 or polyaromatic hydrocarbons, PAH, with 4 to 7 rings). Extensive reviews on these topics are available [307,308,315–318,320,323].

3.8.3. Scheme of reactions and kinetics using tar lumps and model compounds

The modeling of tar has been focused on making a simplified representation of tar formation and conversion. All the kinetic data for estimation of reaction rates are global and none of them represents elementary steps. Much work has been published to obtain practical kinetics of tar formation and secondary decomposition. This can be sorted up in three ways: by taking a generic lump of tar (not a specified compound) or by a tar indicator/model, i.e. a specific tar compound that is a quantitatively important representative for a class/group of tar compounds. The third way assumes a continuous representation of the tar mixture that evolves with time. The first approach has been widely applied in earlier models. The simplest procedure is to take one lump that represents the gravimetric tar, to describe the overall tar concentration [320]. Also the second approach has been widely used. Acetol ($C_3H_6O_2$) was chosen in [320] to represent the oxygenated compounds that constitute the primary tar, released during devolatilization. Other lumps representing primary tars are anisole (C_7H_8O) [321] and phenol (C_6H_6O) [324]. Toluene (C_7H_8) has been used to describe the behavior of the alkyl tertiary products class [325]. Naphthalene ($C_{10}H_8$) has been widely accepted as an indicator compound for PAH. Naphthalene has also been selected as an overall model compound, i.e. representative of all tars, because it is hard to destroy, giving a conservative estimate of the overall tar concentration (usually called gravimetric tar). Phenol is sometimes used as model compound for secondary tars, representing the thermal behavior of soluble tars [320].

In addition to the selection of one or various tar lumps, either specific or generic, the scheme of reaction and the interaction between the lumps in the gas atmosphere have to be established. The simplest scheme is to assume overall kinetics of formation and decomposition of the tar lumps. This approach gives a rough guidance about the behavior, but it does not provide sufficient information for the most practical targets. To refine this problem, tar lumps are assumed to interact in a more or less connected scheme of reaction. A common approach is to assume a series scheme, such as: primary tar lump → intermediate lump + gas → secondary lump + gas → soot + gas + lump. This has been used in [320] (gravimetric tar → intermediate lump → naphthalene → soot) providing kinetic constants adjusted by experiments in a two-stage process (primary pyrolysis in a fixed bed and secondary conversion in a pipe reactor located downstream). The kinetics of soot formation from tar was taken from [326]. In [321] the following scheme was assumed: gravimetric tar → naphthalene → gas + soot, taking the kinetics from literature and further introducing some simplifications. Interaction of one tar lump with another is possible, so superimposed reactions (parallel) have been considered [324,327,328]. In [327] two lumps represent the thermal and catalytic conversion of tar: an "easy-to-destroy" tar and a "hard-to-destroy" tar, resulting in four kinetic constants obtained by measurements made under specific operating conditions with silica sand and Ni catalyst in a laboratory FB. Later this treatment was extended to six lumps [328], yielding eleven kinetic constants. Values of these constants were calculated with data from a laboratory FB (the first stage: tar generation) and two fixed beds in series with a Ni-Based reforming catalyst for secondary conversion. These models provide deeper insight of the real tar conversion process, but their use in reactor models is limited. Evidence of this difficulty of application is that the authors themselves [110,329,330] did not use their own tar model when developing a model of a circulating FBBG, but they assumed a simplified treatment as discussed below.

The third approach mentioned regards tar as a continuous mixture of several species. A model consisting of two parts was proposed [331]. In the first part, tar destruction and/or formation is calculated, assuming that the reactivity of a given component depends on its molecular mass: the higher the molecular mass, the more reactive the component. In the second part, the tar compounds obtained in the first part are clustered into so-called discrete lumps, such as asphaltenes, corresponding to experimentally observed species. A similar approach was developed for catalytic cracking in a fixed bed [328]. Here, results were presented from measurements of the evolution of the distribution of the molecular mass of the continuous mixture during reaction in a catalytic bed. The models for the kinetics of continuous mixtures require a detailed molecular characterization of the mixture at different times of reaction. This approach is promising as demonstrated by its successful application in other branches of chemistry, but despite this, a considerable amount of work and measurements are still necessary for validation in the field of tar conversion. This model approach has therefore not been implemented in reactor models up to date.

3.8.4. Modeling of tar conversion in FBBG

The modeling of tar conversion in published FBBG models consists of two steps in series, following the strategy presented in Fig. 14b: (Step 1) the tar yield is obtained by a devolatilization model, either based on direct experiments or by applying kinetics or correlations taken from literature, and (Step 2) the secondary conversion is determined by thermal cracking, partial oxidation, and reforming. In the secondary tar conversion, two cases are distinguished, depending on the presence of external catalysts in the bed. When there is no external catalyst, a tar conversion model should be based on kinetics obtained in the presence of char and inert material at concentrations given by the FB application concerned. Also these materials, especially char from biomass, are known to have significant catalytic effects on tar reactions [314,327]. If the kinetic data in the experiments have been obtained in the absence of such materials, the model could predict at least the minimum tar conversion. This could be useful for conservative estimates [320]. On the other hand, when an external catalyst is added to the bed, tar conversion must be calculated using the kinetics obtained in the laboratory with the catalysts concerned. If the size of the catalyst in the bed is larger than that used in the lab, as it is usually the case, a catalytic particle model should be used, taking diffusion into account. Sometimes, kinetics tests in the lab are intentionally carried out to obtain an apparent kinetics for the catalyst size to be used in the FB. In such a case, the results from the lab can be used directly, but the reliability of scaling up results to other operating conditions is limited. In addition, attention has to be paid to processes like attrition and elutriation from the bed and poisoning of the catalyst. The model should account for these processes if they are significant.

Some well-known FBBG models have not even taken tar conversion into account at all [211]. The bulk of existing FBBG models employ one generic lump of tar to represent the overall conversion [219] taking the kinetics from various sources. Most published FBBG models have not considered (at least not explicitly) the presence of an external catalyst. Tar is assumed to be converted by thermal cracking in most cases. Oxidation is taken into account in some work, whereas it is not included in others with the motivation that the oxygen is consumed preferentially by light fuel volatiles [32]. Only a few FBBG reactor models include tar cracking, partial oxidation and reforming by assuming a variety of tar lumps integrated in a simple scheme of reactions [24,69,110,321]. The main features of these models are briefly discussed in the following paying attention to whether an external catalyst has been used or not in the bed.

3.8.4.1. FBBG models without external catalyst in the bed. It has been assumed [24,69] that the primary tar generated during devolatilization is converted by thermal cracking (secondary pyrolysis), generating light gas and inert (non-reactive) tar. In [69] the kinetics of [162] was used for thermal cracking with stoichiometric coefficients from [332] and the oxidation of tar was treated by the kinetics of [299]. In [24] various kinetics are reported for thermal conversion, depending on the biomass gasified and the operation temperature [162,191,320,333–336], while tar is oxidized according to the kinetics of [337].

3.8.4.2. FBBG models with external catalyst in the bed. The kinetics of tar cracking for anisole [338] were applied in [321] with reduction of the activation energy justified by the presence of olivine. In [321] reforming of naphthalene over olivine was treated with data from [311] and the stoichiometry of the reaction from [326]. In [110] instantaneous cracking of tar was assumed with a yield obtained by experiments depending on the biomass used. The oxidation kinetics were taken from [289] and/or [339]. Catalytic reforming of tar in the presence of calcined dolomite was included, using the kinetics of [340]. The tar resulting from oxidation was assumed to produce only light gas and steam and the tar from reforming to yield a different tar that could further react with secondary air in the freeboard with the same kinetics as the primary tar. The composition of the two secondary reacting tars was taken from [219], showing a dependence of the CHO content in the tar on temperature.

Table 15
Kinetics for thermal cracking of tar compounds.

Tar definition	E_a (kJ mol^{-1})	A (s^{-1})	Equipment	T (°C)	τ (s)	Reference
Tar	108	4.26E + 06	FB	450–600	0.4–0.7	[334]
Tar	87.6	1.55E + 05	–	–	–	[341]
Vapor	59	1.93E + 03	Pyrolyzer + Cracker	563–1030[a]	0.29–0.49	[342]
Acetol	99.9	5.00E + 05	Pyrolyzer + Cracker	500–1000[a]	0.4	[320]
Gravimetric tar	76.6	4.00E + 04	Pyrolyzer + Cracker	500–1000[a]	0.4	[320]
Tar1	66.3	3.08E + 03	TGA + Cracker	600–800[a]	0.49–2.12	[332]
Tar2	109	1.13E + 06	TGA + Cracker	600–800[a]	0.49–2.12	[332]
Tar	119	3.7E + 07	FB	700–950	–	[219]

– Unknown or not clearly indicated in the source paper.
[a] Temperature in the cracker (secondary converter).

Besides the more or less questionable simplifications of the kinetic scheme and tar lumps assumed in the models, it is evident from the above presentation that: (1) the tar kinetics and the mechanisms investigated in much of the existing work are still not used in FBBG reactor models, where, instead, very simple kinetics and reaction schemes are employed, and (2) the key factor of all reactor models is the choice of the kinetics. In the following, the kinetics of tar applied in FBBG models is discussed.

3.8.5. Discussion on the kinetics of tar

Most published kinetics of tar conversion, whether they are affected by thermal and catalytic cracking, reforming, or partial oxidation, are expressed in the form of a first order law with respect to tar, $R_{tar} = -kc_{tar}$, where k is the apparent kinetic coefficient (s^{-1}), assumed to follow an Arrhenius expression. In the following, we review the main kinetics applied in published FBBG models (further discussed in Section 4).

3.8.5.1. Thermal cracking of tar. The kinetics of thermal cracking has been taken from very different sources. Table 15 reports some of the cracking kinetics employed in the reactor models discussed. The table presents experimental equipment, operational range, biomass used in the experiments, and, when possible, the residence time of the gas. Great differences between the kinetics are evident, as plotted in Fig. 23. The practical implication of these differences is visualized in Fig. 24, where the conversion of tar vs. temperature is determined at a typical residence time of 0.5 s. As seen, the kinetics of [219] predicts almost complete conversion at 700 °C, whereas the rest of the kinetics give conversions in the range of 30–70%. At 800 °C the conversion ranges from 60 to 95% (except for the result of [219]).

3.8.5.2. Partial oxidation of tar. The sources of kinetics related to partial oxidation of tar are not as numerous as those of thermal cracking, as seen in Table 16. Many recent FBBG models have adopted the kinetics reported in [299], which are based on data from [7]. However, the original source leads to [343] from which the kinetics have been considerably changed according to the authors' interpretation and simplification. The kinetics of [289] which, in fact, was originally obtained for the oxidation of methane at high temperature, were used in [110]. In the latter work [110] first order with respect to both tar and oxygen was assumed and a correction factor was introduced to compensate for the uncertainty. Sometimes oxidation models and kinetics expressions for specific hydrocarbon compounds are used. An example related to benzene is given in the table for one and two-steps models with the kinetics of [301]. Oxidation kinetics for other light hydrocarbons is available [301].

3.8.5.3. Catalytic cracking and reforming of tar. Much work published on the determination of tar kinetics over catalyst materials has been conducted in fixed beds or in other laboratory devices. Many of the kinetics determined are effective/apparent/global, so they can be applied for the operation conditions used in the tests, mainly temperature and spatial time or velocity (in various units, as seen in Table 17). The main prospective catalysts for FBBG utilization are calcined limestone (calcite), calcined dolomite (magnesite + calcite) and olivine. Other materials, such as gamma-alumina, fluidized cracking catalysts or Ni-based catalysts, have been found less attractive for FBG, due to the high price of the catalyst, the difficulty in catalyst regeneration, and the contamination of the bed

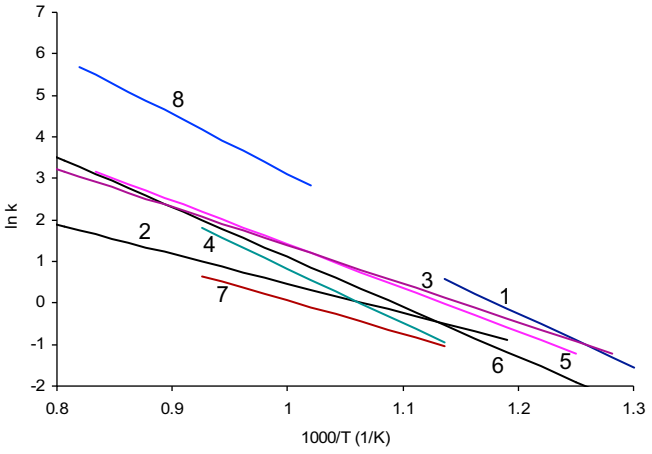

Fig. 23. Arrhenius plot for various kinetics of thermal cracking of tar (k is in s^{-1}). Kinetics from Table 15: 1 Liden et al. [334]; 2 Baumlin et al. [342]; 3 Morf (gravimeric tar) [320]; 4 Rath and Staudinger (tar 2) [332]; 5 Diebold (1985) [341]; 6 Morf (acetol) [320]; 7 Rath and Staudinger (tar "1") [332]; 8 van der Aarsen (1985) [219].

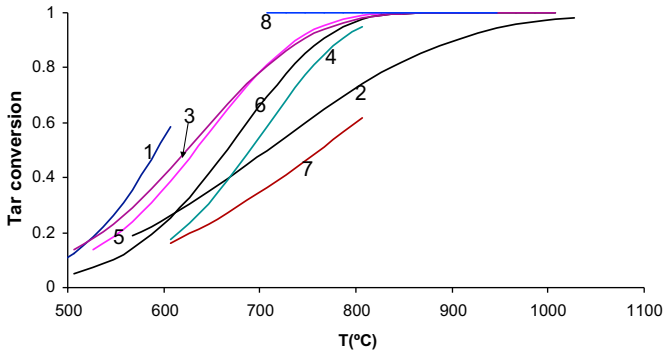

Fig. 24. Conversion of tar by thermal cracking as a function of temperature using various kinetics expressions at a residence time = 0.5 s. Kinetics from (see Table 15): 1 Liden et al. [334]; 2 Baumlin et al. [342]; 3 Morf (gravimeric tar) [320]; 4 Rath and Staudinger (tar 2) [332]; 5 Diebold (1985) [341]; 6 Morf (acetol) [320]; 7 Rath and Staudinger (tar 1) [332]; 8 van der Aarsen (1985) [219].

Table 16
Kinetics of partial oxidation of tar compounds.

Stoichiometry	Kinetics equation (R_{tar})	n_t	n_O	E_a (kJ mol^{-1})	A	Reference
$C_nH_m + 0.5nO_2 \rightarrow nCO + 0.5mH_2$	$Ae^{-Ea/RT} T\, p^{-0.825} c_{O_2}^{n_O} c_{tar}^{n_t}$	0.5	1	164.5	2.08×10^9 (units na)	[343]
$C_nH_m + 0.5nO_2 \rightarrow nCO + 0.5mH_2$	$Ae^{-Ea/RT} Tp^{0.3} c_{O_2}^{n_O} c_{tar}^{n_t}$	0.5	1	80.2	2.07×10^4 ($m^{1.5}$ kmol$^{-0.5}$ s^{-1} K^{-1} Pa$^{-0.3}$)	[7]
$CH_{1.522}O_{0.0228} + 0.867O_2 \rightarrow CO + 0.761H_2O$	$Ae^{-Ea/RT} T c_{O_2}^{n_O} c_{tar}^{n_t}$	0.5	1	80.2	9.2×10^6 ($m^{1.5}$ kmol$^{-0.5}$ s^{-1} K^{-1})	[299]
not specified	$Ae^{-Ea/RT} c_{O_2}^{n_O} c_{CH_4}^{n_t}$	0.7	0.8	202	5×10^{11}($m^{1.5}$ kmol$^{-0.5}$ s^{-1})	[289]
$CH_xO_y + zO_2 \rightarrow (x/2 - y - 2z + 2)CO + (y + 2z - \frac{x}{2} - 1)CO_2 + \frac{x}{2}H_2O$	$Ae^{-Ea/RT} c_{O_2}^{n_O} c_{tar}^{n_t}$	1	1	201	1.58×10^{10}(m^3 kmol^{-1} s^{-1})	[110]
$C_6H_6 + 4.5O_2 \rightarrow 6CO + 3H_2O$	$Ae^{-Ea/RT} c_{O_2}^{n_O} c_{C_6H_6}^{n_t}$	−0.1	1.85	125	1.35×10^9($m^{2.25}$ kmol$^{-0.75}$ s^{-1})	[301]
$C_6H_6 + 7.5O_2 \rightarrow 6CO_2 + 3H_2O$	$Ae^{-Ea/RT} c_{O_2}^{n_O} c_{C_6H_6}^{n_t}$	−0.1	1.85	125	9.55×10^8($m^{2.25}$ kmol$^{-0.75}$ s^{-1})	[301]

ash. Comparisons and kinetics of catalysts are reported in reviews [314–318]. In Table 17 some expressions, assuming first order with respect to tar, are presented. The table must be used with caution because of: (a) the different representations of the space time (s) in terms of catalyst volume/mass and volumetric feed flowrate at normal/reactor temperature, (b) many values of the kinetic coefficient were evaluated under mass transfer limitations, and (c) the treatment of different tars originating from different gasification conditions or model tar components. There are cases (not shown in Table 17) where an overall effective kinetic coefficient has been determined, including thermal cracking, reforming with catalysts, and oxidation by secondary air [339].

From this discussion, it seems that these kinetic data are difficult to extrapolate to the conditions of an FB, but a detailed comparison of different catalysts is out of the scope of this work. A graph, such as that presented in Fig. 24, is difficult to present for catalytic kinetics, based on the data of Table 17 or other sources. Instead, to give a rough idea on the effectiveness of distinct catalysts, experimental findings [314] have been drawn in Fig. 25. The conversion measurements comprised two model compounds: phenol and naphthalene. The figure shows the ranking of the activities of the catalysts for the conversion of naphthalene at 900 °C (a) and for phenol at 700 °C (b). At 900 °C the conversion of phenol is dominated by thermal cracking (all catalysts gave 100 wt% phenol conversion and more than 98 wt.% of the phenol was already thermally cracked), whereas the naphthalene is thermally stable at 900 °C (only 2% was converted over silica sand). Similar comparisons for tar compounds, catalyst material and operating conditions can be found in literature [317].

3.8.6. Conclusion and recommendations

Despite the great effort made to understand the mechanisms of reactions involving tar, the complexity of the process makes it difficult to develop comprehensive models. As a consequence, the tar conversion models are still implemented in FBBG models in an empirical way. To date, it has not been possible to predict the composition of tar in the outlet gas. Only a quantitative estimate of overall tar concentration has been achieved reasonably well. The tar models applied are of an empirical nature, based on the selection of the main reactions assumed to take place and global kinetics (experimentally obtained). In practical operation of FBBG the conversion of tar with oxygen is limited, because tar competes with light gases and char for the oxygen, and the light gases seem to be more reactive than tar. When there is no catalyst in the bed, thermal cracking partially converts the tar in the reactor. The kinetics reported in the literature for thermal cracking vary widely, and their selection is critical. When an external catalyst is used, the catalytic reaction is usually more rapid than thermal cracking, so the prediction of tar in the outlet gas is likely to depend on the choice of the catalytic kinetics. When diffusion effects within the catalyst particle are rate-controlling, detailed description of the heterogeneous model process at a particle level, i.e. a particle model, could be critical. The selection of the kinetics for thermal cracking should not be essential in this case. In both cases, the kinetics, the type of biomass, and the conditions for which the experimental data have been obtained, should be carefully analyzed.There are other factors, not discussed here, that can be influence tar conversion. For instance, the soot formation on char surfaces leads to loss of catalytic char activity (and also of the char reactivity) and has to be

Table 17
Kinetics of tar catalytic cracking and reforming for various materials.

Tar generation conditions	Catalyst bed (fixed)		Kinetic parameters [a]			Reference
	Type	T (°C)	E_a (kJ mol^{-1})	A (Nm^3 kg^{-1} h^{-1})	k (850 °C) [b] (Nm^3 kg^{-1} h^{-1})	
FB with air	Calcined dolomite	750–920	97	3.20×10^5	9.85	[344]
FB with steam	Calcined dolomite	782–912	42	1.96×10^3	21.81	[283]
FB with steam	Magnecite	803–882	42	1.46×10^3	16.24	[283]
FB with steam	Calcite	801–880	42	1.28×10^3	14.24	[283]
FB with air	Carbonate rocks	700–1000	160	9.24×10^7	3.34	[317]
FB with air	Olivine	800–900	114	8.75×10^5	4.35	[308]
FB with air	BASF G1-25 S	750–850	72	1.56×10^5	69.83	[345]
Steam + oxygen	BASF G1-25 S	785	58	4.02×10^4	80.70	[346]
FB with air	Nickel B	700–1000	210	2.16×10^{10}	3.68	[317]
Doped gas with naphthalene	Char	700–900	61	1.93×10^4	28.12	[314]

[a] In some cases the reported E_a and A have been recalculated by averaging the values given in the original reference. In order to calculate A in units (Nm^3 kg^{-1} h^{-1}), in some cases the values reported in (m^3 kg^{-1} h^{-1}) in the original references have been converted by the average temperature T given in the third column of the table to refer the volume flow rate to normal conditions (273 K).

[b] k is calculated as k (T) = A exp($-E_a$/RT) so that k (850 °C) = A exp($-E_a$/R(1173)).

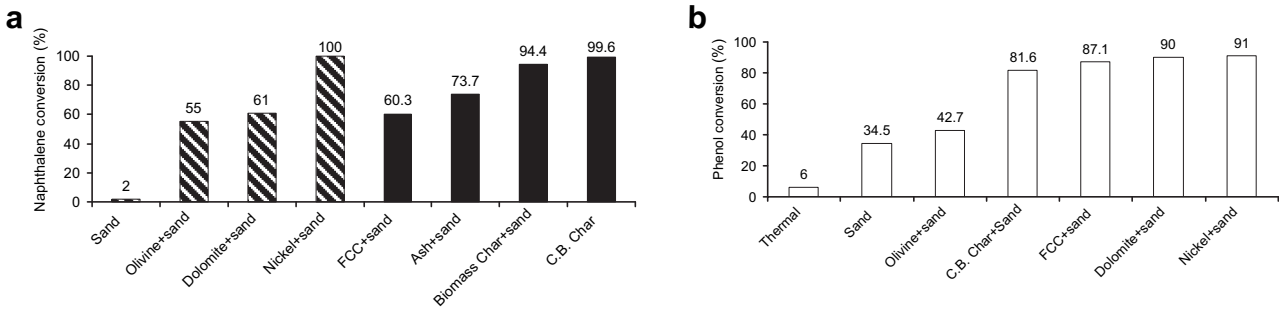

Fig. 25. (a) Effect of catalytic bed material on naphthalene conversion. T = 900 °C, τ = 0.3 s, feed gas composition: 6% v/v CO_2, 10% v/v H_2O, and balance N_2. The marking of the bars indicates the initial naphthalene concentration: 40 g/Nm^3 (back and white bars) and 90 g/Nm^3 (black bars). (b) Effect of catalyst bed material on phenol conversion. T = 700 °C, τ = 0.3 s, feed gas composition: 6% v/v CO_2, 10% v/v H_2O, and balance N_2, initial phenol concentration 8–12 g/Nm^3. Adapted from El Rub et al. [314].

taken into account. Despite there are a few studies, it has not been shown the influence on the tar conversion in FBBG.

The overall conclusion is the same as that for homogeneous reactions: in the development and validation of reaction models, it is not enough to report the assumptions made and the kinetic expression used. All reactor models taking "external" kinetics or using kinetics that have been obtained under conditions that may differ from those of the FBBG to be modeled, should include a sensitivity analysis to elucidate the degree of uncertainty in the tar concentration of the outlet gas. This is lacking in all FBBG models published up to date. A great deal of work is still needed in this area.

4. Survey of literature on FBBG models

In the following, existing models of FBG using the three approaches, CFDM, FM and BBM (Table 1), are reviewed, paying special attention to FM, as they are the most successful models applied up to date.

4.1. Computational fluid-dynamic (CFD) models

Over the last decade CFD has been applied to FB. There are still, however, relatively few models of this type compared to the many models of other classes. Existing work includes models for coal in bubbling [42], circulating [31], and spouted bed gasifiers [347]. Models have been published for biomass employing CFD tools for bubbling FBBG [348–350]. No work has been found using CFD to simulate biomass gasification in a CFBG. Entrained-flow CFD models of gasification are abundant for coal [351–353] because the solids flow is more disperse and this application is computationally less expensive. There are also some models for biomass conversion in entrained-flow gasifiers, although this is a relatively poorly developed technology for biomass [353]. In contrast to FB gasification, a great deal of models has been published applying CFD to simulate FB boilers burning biomass and wastes [23]. Some efforts have also been made to model pyrolysis in FB by CFD [354]. A recent review on CFD modeling, applied to thermochemical conversion of biofuel, has been published [352].

The essential distinction between CFDM and other kind of models is that the fluid mechanics are dealt with in detail in CFDM. The source terms are similar in all models. The momentum equations are solved for the gas and the solids phases. The gas phase is described by a continuum approach, adopting an Eulerian framework and modeled similar to single phase flow with an additional term, accounting for the interaction with the solid phase. The choice of turbulence model in the gas phase is a key issue. The solid phase is described by two distinct approaches: if the solid phase is treated as a continuum, an Eulerian framework is applied to describe the motion of the solids [41]; if the particles are individually tracked, the equation of motion of the particles is used. The two approaches are named Eulerian–Eulerian (EEM) and Eulerian–

Table 18
CFD models for FBBG.

Reference	Type of reactor	Model characteristics	Fuel	Simulated experiments	Remarks
Sofialidis and Faltsi [348]	BFB	Lagrangian for the particles in a prescribed porous medium	Eucalyptus and miscanthus	BFB 300 mm ID Comparison with outlet gas for one test Poor agreement	Space occupied by bubbles is prescribed. Bubbles are calculated by semi-empirical relations such as in FM. Solution with FLUENT
Wang et al. [358]	BFB	3D transient EEM k–ε turbulent model	Sorghum	BFB 40 mm ID 600–800 °C No detailed comparison made	Solution with homemade code
Wang and Yan [350]	BFB	3D ELM k–ε turbulent model	Sewage sludge	Experiments taken from literature BFB 38 mm ID Comparison with tests changing λ Reasonable agreement	Solution with FLUENT
Oevermann et al. [349]	BFB	2D EEM and ELM k–ε turbulent model	Beech and pine wood	BFB 95 mm ID Comparison with one test for each biomass	Solution with MFIX
Fletcher et al. [353]	Entrained flow	ELM k–ε turbulent model	Sawdust and cotton trash	No comparison Only sensitivity analysis made	Solution with CFX

Lagrangian (ELM) models. In the ELM, the discrete element/particle method (DEM/DPM) is commonly applied, inspired by molecular dynamics. In order to describe particle collisions and to predict the frequency of pressure fluctuations, bubble formation, and particle segregation, DEM is based on soft or hard sphere simulation [355]. Soft sphere simulation involves an empirical coefficient of restitution and friction, whereas the hard spheres are described by empirical spring stiffness and a friction coefficient. EEM, on the other hand, is solved by the so-called two-fluid model based on the assumption that the gas and particulate phases form two interpenetrating continua [40]. Closure relations needed are not simple: several equations with semi-empirical parameters have to be solved simultaneously. The kinetic theory of granular flow is used in the two-fluid model to simulate particle collision for closure. A comparative analysis of CFD models for FB has been made [356]. Whilst EEM needs to define a continuous solid particle phase for each diameter class, ELM handles variable and time dependent particle sizes in a natural way by tracking each individual particle with its physical properties [349].

Simplifications are needed also for CFD solutions, and experimental validation is necessary before using the models with confidence [357]. Table 18 presents the CFD models published for FBBG. The table indicates the type of model adopted for the simulations, the experimental rig used for validation, the fuel gasified, and the degree of agreement with experiments. From the works included in Table 18 the following conclusions are outlined:

1. Conversion of various biofuels in BFBG has been simulated by CFD tools: beech and pine wood [349], sewage sludge [350], eucalyptus and miscanthus [348] and sorghum [358]. In all cases, validation has been carried out in bench-scale FB with reasonable agreement with measurements. However, there is no indication of a better prediction than by the FM (discussed below). CFDM has not yet been applied to CFB biomass gasifiers.
2. In theory, in ELM the source terms, such as reactions and heat and mass transfer at a particle level, can be simulated in a more consistent way than in EEM. However, the demand for computational time puts ELM at a disadvantage because of the large number of particles to be simulated in a high-density bed. EEM is computationally less demanding and yields mean particle and gas flow-fields as result, which facilitates quantitative decisions for engineering design. For these reasons EEM seems to be currently more reliable for FBG simulations. Entrained-flow simulation seems to be adequate using ELM [353] because the flow is relatively disperse and the computational cost is less.
3. No matter the type of CFDM, there is no more precision in the modeling of the source terms than in an FM. The main advantage of ELM (the tracking each individual fuel particle, making it possible to include the changes in physico-chemical characteristics of the fuel particle during devolatilization and subsequent char conversion) has still not been exploited.
4. A preliminary comparison of the two methods (EEM vs. ELM), applied to a bubbling FB biomass gasifier, has been performed [349] but no conclusion is possible from that work because of the lack of measurements.

An interesting compromise between the EEM and ELM is to decouple the calculation of source terms from that of the flow field: the conversion of the individual particles is not calculated simultaneously with the flow solver, but it is parameterized, calculated a priory, and stored in a library. During the Euler–Lagrange simulation the source terms are taken from the library. This concept has been suggested recently [349], but no details are given or any trial applying it. This approach is an interesting way to simulate FBG within the ranges of the current computational capability, and it should be further explored.

4.2. Fluidization models (FM)

4.2.1. Comparison of FM for FBBG

A selection of FM for simulation of bubbling (a) and circulating (b) FBBG published up to date is presented in Tables 19a and b. The table is divided into the following parts: Part A informs about the degree of sophistication of the models, the hypotheses made by modelers, and compares the models with respect to the submodels; Part B gives a glance on the FBG systems (size, material and operating conditions) chosen for validation of the models; and Part C provides an overall perception about the ability of the models to predict measurements.

The criteria for selection of models to be included in the table are that they should be (1) fluidization models (FM), (2) applied to solid biomass fuels, (3) deal with stand-alone FBG, and (4) reported in detail. A further desirable condition is that a comparison between model results and measurements should be made, i.e. experimental validation. However, some CFBBG models in Table 19b have not been validated. The criteria mentioned exclude a number of otherwise relevant models: for liquid fuels such as black liquor gasification [367], for indirect steam FBBG in twin bed gasifiers [368], BFBG models that either have not been documented or validated in sufficient detail [369], FBG models that do not belong to FM [103,213,370–372] or those that have been developed for coal. Extensive reviews on coal FBG models have been published [25–28]. Finally, two models [28,188] and [24,62,145,373–375] have not been included in Table 19a, because these models have been developed in a more general way and the scope of application is wider, so they are discussed separately in more detail.

After analyzing Table 19a the following remarks can be made:

1. Most models are one-dimensional and steady state, and the fluid-dynamics are based on the two-phase theory of fluidization. Some modifications are made in the estimation of the diameter and velocity of the bubbles and the fraction of bubbles in the bed. The most common assumptions are perfect mixing of the solids in the bottom bed and plug flow of gas in the bubbles and emulsion, although sometimes the latter is taken as perfectly mixed, especially at high fluidization velocity.
2. The freeboard is not modeled in many BFBG models. When treated, it has been assumed homogeneous without any distribution of solids. For CFBG, however, the two-dimensional structure in the freeboard has been taken into account.
3. The most frequent assumption is that devolatilization is instantaneous. The authors treat the gases from devolatilization as an initial condition for further conversion in the bed. The composition of volatile species after devolatilization is not clearly reported by some authors. In some cases correlations are taken from other biomass materials or even from coal. The treatment of [219], also employed in [67], is unique in the sense that it considers a finite region (whose height is calculated as a function of fuel particle size) with a uniform rate of release of volatiles.
4. A majority of modelers have not paid particular attention to char conversion. The following features support this statement: (1) char reactivity is taken from coal or from other biomasses that could be different from the one under analysis. Sometimes the char reactivity is obtained from TGA or from other devices operated at low heating rate, (2) in models of char particle conversion, mass transfer and change in reactivity during

Table 19a
FM from literature for modeling of biomass gasification in BFB.

BFBBG	Nikoo [359]	Radmanesh et al. [69]	Sadaka et al. [147,360,361]	Fiaschi and Michelini [68]	Bilodeau et al. [212]	Jiang and Morey [67]	van den Aarsen [219]	Raman et al. [362]
A. Model characteristics								
Type of Reactor model	LM	LM	LM	LM	LM	LM	LM	LM
Dimensionality	SS 1D	SS 1D	*TM 1D*	SS 1D	SS 1D	SS 1D	SS 1D	*TM 2D*
Bottom bed model	Based on modified Two-Phase Theory with properties varying with height	- Based on KLM - CCBMM for the mixing of char in emulsion	Divided into three zones: jet, bubbling and slugging.	Based on Two-Phase Theory Reaction only in the emulsion phase	Based on Modified Two-Phase Theory	From [219]	Extended Two-Phase Theory with key parameters checked by own experiments	Based on modified Two-Phase Theory with properties varying with height
Freeboard model fuid-dynamics	Based on Eq. (27) with $a = 1.8/u$ and $\rho_\infty = 0$	No	No	Based on elutriation constants and Eq.(27)	Plug flow in an homogeneous emulsion	Based on Eq. (27) with measured parameter *a*.	No	No
Reactions in Freeboard	Char reactions assuming perfect mixing	No	No	No	The same as bottom bed with a single gas phase	Gas species determined by WGSR in equilibrium	No	No
Thermal balance	T imposed	No for reactor/Yes for particle	For reactor in each zone and also for the particle	For the bottom bed by lumping bubble and emulsion	For bottom bed and freeboard (compartments)	Overall. T_b is input to determine T_{fb} and biomass feed rate	T imposed (adjusted by airflow rate)	No
Devolatilization model	Instantaneous and equilibrium	Yes (2 models) Model 1: Tar generation model from [160,161]. Model 2: from their own tests.	Based on CHO balances with 3 adjustable parameters (values NR)	Instantaneous. NR gas distribution	Instantaneous (equilibrium assumed)	From [219]. Species distribution from own FB test with corncob	Pyrolysis takes place in a finite region determined by fuel particle size. Species distribution from own FB tests	Relative yield of gas and char from TGA (conducted by authors) Volatile yields distribution internal report
Char particle conversion model (PCM) and reactivity	No PCM Reactivity from coal	No PCM Char–CO_2 reactivity from coal. Langmuir–Hinshelwood kinetics for char–H_2O reactivity	No	PCM from [257].	Kinetic model from [363]	From [219].	Shrinking model with kinetics and physical parameters determined in own measurements in an FB	No PCM. Taken from [302] for coal
Fragmentation and attrition	No	No	No	Simplified model. Parameters NR	No	No	No	No
Population balance	No	No	No	No	No	No	No	No
Gas-phase reactions (kinetics)	Equilibrium is assumed	Oxidation of CH_4, CO, H_2, and tar	Equilibrium assumed for each zone	NR	Instantaneous volatile oxidation	From [219]	Oxidation at the bottom in a finite region. WGSR in equilibrium locally	Only WGSR kinetics considered
Tar model	No	Secondary tar cracking from [162,365]. Tar oxidation from [299]	Empirical cracking model from [364]	No	No	From [219]	One lump experimentally determined	No
B. Process conditions modeled for comparison with measurements								
Own measurements (If not, from where)	No (from Sadaka et al., 2003 [147,360,361])	Yes	Yes (FB with a dual distributor)	No (from 3 sources)	Yes	Yes	Yes	Yes

Fuel (size diameter if reported)	Pine sawdust Size: 0.25–0.75 mm	Beech wood	Wheat straw	Wood chips Almond shell Gass straw Corn stalk RDF pellets	Wood Mixture of wood/plastic	Corncob	Beech wood Size: 1–3 mm	Feedlot manure (2–40 meshes)
Biomass feed rate (kg/h)	0.45 – 0.50	5.5 – 18	0.6 – 1.5	NR	27 –46	14 –20	21–33	6.3 and 13.43
Bed Temperature (°C)	700–900		610–900	NR	740–857	650 and 780	800 – 885	596 and 710
External heating	Yes NR heat supply	Yes NR heat supply	Yes NR heat supply	NR	No (insulated)	No (insulated)	No (insulated)	No
Gasification agent	Air and steam	Air	Air and steam	Air and oxygen	Air	Air	Air	Air
Stoichiometric ratio (kg/kg)	0.19–0.27	0.13–0.66	NR	NR	0.27–0.33	0.25–0.45	NR	NR
Steam-to-biomass ratio (kg/kg)	0–3.5	0	0.20–0.33	NR	0	0	0	0
Fluidization agent temperature	Air: 60 °C Steam: 145 °C	Ambient	Air: NR Steam: 150 °C	NR	NR	60 °C	Ambient	NR
Fluidization velocity (in the bottom at bed T) (m/s)	NR	0.17–0.38	0.3–0.45	NR	NR	0.25–0.35	0.4– 1.2	0.4– 1.2
FB diameter (mm)	40 bed 60freeb.	78 bed 150 freeb.	NR	Three beds: 30/66/150	300 bed 460 freeb	160 bed 220 freeb	300 bed	229 bed 406 freeb
FB length (mm)	1400	750 bed 900 freeb.	NR	Three beds: 100/750/500	2900	690 bed 580 freeb	Bed material zone varied from 200 to 1000	864 bed 864 freeb
Bed material	Silica sand 30 g 0.275 mm	Silica sand 0.250 mm	Alumina sand 0.380 mm	Three diameters: 0.4/0.58/7 mm	Silica sand 0.500 mm	NR	Dense alumina 0.325 mm	Silica sand 0.55 mm 45 kg
Fuel feed point location	In bed at the bottom	Two levels: 1. In bed at 200 mm over the distributor 2. Top bed	In bed at the bottom	NR	In bed at 290 mm over the distribution	In bed at 80 mm over the distributor	In bed at the bottom	Top-fed (discharged over the bed surface)
C. Type of validation made between model and measurements.								
Gas composition Profiles/exit	No/Yes	Yes/Yes	No/Yes	No/Yes	No/Yes	No/Yes	No/Yes	No/Yes
Temperature Profiles/exit or average	No/Yes	Yes/Yes	No/Yes	No/No	No/Yes	No/Yes (only T_{fr})	No/No	No/No
Tar content[a]	No	No	No	No	No	No	Yes	No
Degree of agreement[b]	Reasonable-Poor	Reasonable	Good	Good	Reasonable	Good at 780 °C Poor at 650 °C	Good	Reasonable
Sensitivity analysis of model parameters [c]	Yes	Yes	Yes	Yes	Yes	Yes	Yes	*No*
Sensitivity analysis of model assumptions [d]	No	No	No	No	No	*Yes*	To some extent	No

Abbreviation: NR: not reported; LM: learning model; CM: Correlation model; DM: design model; SS: Steady state model; TM: Transient model; NV: not validated

[a] Different tar measurement methods have been used.

[b] Overall impression by present authors from the analysis made in the original work in terms of gas composition, carbon conversion, gasification efficiency and gas heating value (rank: Very Good, Good, Reasonable, Poor).

[c] Study of the effects of the various factors such as moisture, fuel composition, stoichiometric ratio, steam-to-biomass ratio, etc, on the main results such as gas composition, temperature, etc.

[d] Sensitivity analysis with respect to the key parameters (assumed) in the model, such as the reaction kinetics used, bubble size, steady state char size, etc.

Table 19b
FM from literature for modeling of biomass gasification in CFBG.

CFBBG	Corella and Sanz [110,329,330]	Petersen and Werther [43,231]	Liu and Gibbs [232]	Jennen et al. [146]
A. Model characteristics				
Type of Reactor model and target	LM	DM	LM–CM	LM–CM
Dimensionality	SS 1D	SS 1D	SS 1D	SS 1D
Bottom bed model	Constant solids porosity = 0.77	Modified TPM with some key parameters from own measurements	Treated as input from [73]	NR in detail Based on two-phase theory of fluidization
Freeboard model	Constant porosity in two zones: -Splash = 0.90 -Dilute = 0.99 Qualitative description of comminution but no modeling details reported	Core-annulus with some key parameters from own measurements	Treated as input from [73]	Based on core-annulus NR in detail
Thermal balance	Yes. 4 zones are defined. Overall heat balance in each	No	No T assumed as input (uniform long the bed.)	Yes. In each cell In the bottom uniform T in the bubble and the emulsion phase In the freeboard distinct T for the core and annulus
Devolatilisation model	Instantaneous (?) Gas distribution from literature data Tar and char chemical formula varying with T (from [219])	Instantaneous. Gas distribution from own measurements	N-compund from previous model [366] Rest of pyrolysis gas from [161]	NR
Char particle conversion	PM and kinetics from [219]	No	No	NR
Fragmentation and attrition	No	No	No	No
Population balance	No	No	No	*Yes* For the bottom bed and freeboard (with distinction between core and annulus)
Gas-phase reactions (kinetics)	Most reactions of Table 3 considered (kinetics from several sources with some ad-hoc corrections)	Most reactions of Table 3 considered (kinetics from several sources)	Most reactions of Table 3 considered (kinetics from several sources with some ad-hoc corrections) 28 reactions involve N-compounds	Most reactions of Table 3 considered NR the sources
Tar model	Two lumps reacting with O_2, H_2O and by thermal cracking. Effects of catalyst included	Benzene is taken as tar model Reaction with O_2 is considered	One lump reacting with O_2, H_2O and by thermal cracking. Effects of catalyst included by ad-hoc parameters	Reaction with O_2, H_2O and by thermal cracking. Sources NR.
B. Process conditions modeled				
Own measurements (If no, from where)	No measurements reported	Yes	No measurements reported (only trends from lab-scale results to assess the reasonabeness of model results)	Yes
Fuel	Pine wood chips 1–5 mm	Pelletised dried sewage sludge	Wood (38% moisture)	Wood
Biomass feed rate (kg/h)	11,800–23,700	NR	7200–14,400	110
Temperature (°C)	705–926 bed 805–1090 freeb.	Up to 800	750–900	Distributed along the riser from 900 to 950
External heating	No	Yes (NR heat supply)	No	NR
Gasification agent	Air	Air	Air	Air
Stoichiometric ratio	0.20 – 0.45	0.3 and 0.6	0.20 – 0.40	0.25 (estimated)
Steam-to-biomass ratio (kg/kg)	0	0	0	0
Fluidization agent preheating	Air 250 °C	to bed temperature	NR	82
Fluidization velocity (in the bottom at bed T) (m/s)	NR	3.5 and 5	NR	NR

Table 19b (*continued*).

CFBBG	Corella and Sanz [110,329,330]	Petersen and Werther [43,231]	Liu and Gibbs [232]	Jennen et al. [146]
Reactor diameter (mm)	Upper part 3.3×10^3	100	1760	200 bed 300 freeboard
Reactor length (mm)	Total 14.8×10^3	15,000	13,500	8000
Bed inventory (weight, average diameter)	Silica sand	Silica sand 0.2 mm approx.	Silica sand	NR
Secondary gas injection	Yes 0–40 (% of total air) (at height 6–10 m)	No	Yes 25 % of total air (at height 2.5 m)	NR
In-bed materials for tar reduction	dolomite	No	Limestone/dolomite	NR
C. Type of validation made between model and measurements				
Gas composition (Profiles/exit)	NV	Yes/Yes	NV	No/Yes
Temperature (Profiles/exit)	NV	No (T imposed)	NV	Yes/Yes
Tar content [a]	NV	No	NV	No
Degree of agreement[b]	NV	Reasonable	NV	Good (only one run is compared)
Sensitivity analysis of model parameters[c]	Yes	Yes	Yes	No
Sensitivity analysis of model assumptions[d]	No	No	Yes. Analysis of NH_3 emission varying selected reaction rates by a factor of 10	No

Abbreviations: NR: not reported; LM: learning model; CM: Correlation model; DM: design model; SS: Steady state model; TM: Transient model; NV: not validated.
[a] Different tar measurement methods have been used.
[b] Overall impression by present authors from the analysis made in the original work in terms of gas composition, carbon conversion, gasification efficiency and gas heating value (rank: Very Good, Good, Reasonable, Poor).
[c] Study of the effects of moisture, fuel composition, stoichiometric ratio, steam-to-biomass ratio, etc, on main results, such as gas composition, temperature.
[d] Sensitivity analysis with respect to the key parameters (assumed) in the model, such as the reaction kinetics used, bubble size, steady state char size, etc.

conversion have not been described, (3) the distribution of conversion in the bed has not been taken into account, for instance by a population balance as a function of particle size. These factors strongly affect the char conversion in FBG, as has been discussed in this review.

5. Reduction of fuel size by fragmentation and attrition of fuel and char has only been included in one model [68].
6. Tar conversion is usually not modeled at all or modeled as one or two lumped species reacting by oxidation, thermal cracking, or reforming with H_2O. The kinetics are taken from literature and, as it has been shown in this review, may differ greatly from one source to another. This is because the rate of tar conversion depends greatly on the kind of biomass, operating conditions, size of fuel particles, just to mention a few influencing parameters.
7. The effects of in-bed catalysts have been modeled by some authors [110,232], but the approach has been to use ad-hoc correction factors in the reaction kinetics. No comprehensive treatment has been applied. This is surprising, because huge amounts of measurements are available from FBGs with catalysts under a wide range of conditions.
8. Most experiments are validated, using the temperature and composition of the gas at the outlet stream. The species concentration profile along the gasifier has not been validated. Validation has been carried out in lab-scale FBs, where the fluid-dynamics can differ from full-scale gasifiers. Sometimes fluid-dynamic correlations are taken from tests with Group A particles (mainly from fluidized cracking catalyst studies) and can differ greatly from what is valid for Group B particles, normally employed in FB gasifiers.
9. In general, models predict the main gaseous species at the outlet reasonably well, but the validation is supported only by a few test runs (sometimes only one). The major disagreement is found in the concentrations of CO and H_2. Sometimes, all light hydrocarbons and tar are lumped into CH_4, which can explain the disagreement sometimes found in CH_4. Usually, tar has not been modeled, and when it has, the disagreement tends to be high. This could also be due to the many different methods for measuring the tar content of the gas from biomass gasifiers.
10. In almost all models a sensitivity analysis is made to study the effect of some variables, such as moisture, air ratio, and temperature on the gas composition, the gas production rate, and the heating value of the gas produced. This type of analysis increases the knowledge of the gasification process and is useful to explain observations under specific conditions.
11. In contrast, in many models the validity of the parameters assumed during the derivation of the model is not checked. There are many adjustable parameters, which are even varied from one case to another during the simulation. Some authors develop the model in a clear way, but others don't (for example the values employed for some parameters are not given). For instance, in [212] three adjustable parameters are introduced in the model and calibrated by fitting to four test runs with wood chips. However, the effect of the parameters on the results was not evaluated by a sensitivity analysis, applying the model to other operating conditions. Only a few authors have made a sensitivity analysis of the main parameters. For instance in [67], the importance of physical and chemical processes was checked by a sensitivity analysis of the processes, confirming the major importance of the pyrolysis step. A similar conclusion was drawn in [219], where it was experimentally verified that the fluid-dynamics and the mass transfer rate only influenced the results slightly, and consequently, that the chemical kinetics of the reactions were decisive for good model predictions. A sensitivity analysis was also made in [232] of the chemical kinetics network where NH_3 was involved. These examples show that the sensitivity of the results to variations in

parameters could be helpful to identify the ones representing the most important processes and the submodels that would need major modeling efforts.

12. Most models are "learning models" [50]. "Development-design-models" [50] are more rarely dealt with. Probably this type of model has been treated in private reports and is not available in the open literature. Only [43,231] could clearly be classified as development and design model. This model has been used for searching the best conditions for fuel feeding, air ratio and other operation variables for gasification of sewage sludge in a CFB. Moreover, it has been extended to 3D [43] making it possible to analyze the horizontal segregation of volatiles at the feed port of large CFBBG and other related issues of major importance for the design of industrial units. It is also possible that the model of [110] could be used for design purposes, but the published details are not sufficient to assess this ability. This work qualitatively considers several key processes and points out a variety of submodels that should be taken into account for proper description. However, it is not known if these features were actually incorporated in the model. Only the kinetics expressions are discussed in detail. Moreover, the model was not validated. Instead, the authors made a sensitivity study by analyzing the performance of an imaginary large-scale CFBBG under various operating conditions [329]. More recently they have used the model with ad-hoc modifications of kinetics for some reactions, studying the conditions under which a CFBBG should be operated to generate a gas with a tar concentration lower than 2 g/Nm^3 [330]. Again, the model was used without measurement support. Therefore, an assessment of the ability of the model is not possible.
13. A general conclusion is that it is not clear if a more sophisticated model is better because it contains more terms and submodels (for example improvement of the fluid dynamics), or if it just happened to improve the agreement because the pyrolysis was better modeled (for instance, as a result of experiments).

4.2.2. Advanced FM for FBBG

Two models [28,188] by Hamel and [24,62,145,373–375] by Souza-Santos, from now on abbreviated as HM and SSM, seem to be the most advanced FM developed up to date. They have been applied to a variety of BFBG and CFBG. They contain most of the submodels mentioned in the present review, thoroughly documented in the cited references. Only some details on the validation and the main issues for further improvements are commented here.

The SSM forms the basis for a commercial software [376], used to simulate a variety of fixed and fluidized bed equipment for coal and biomass gasifiers and combustors [24]. It has been used for simulation of several biomass gasification systems by SSM and also by other researchers [377]. It has been specifically validated by comparison with a number of FB biomass gasification systems with reasonable success, in particular: (1) the pressurized pilot scale BFBG at the Institute of Gas Technology in Illinois, the so-called RENUGAS process, using wood [24,373], (2) the BFBG at the University of California at Davis for gasification of almond shells and walnut pruning [374], (3) the pilot scale CFBBG at University of British Columbia for cypress and Hemlock biomasses [375], and (4) the pilot scale CFBBG at the State University of Campinas [375].

The HM has been validated mainly for coal. To validate the model with measurements from biomass FBG the authors have used two tests [378] with sawdust in a 500 kWth BFBG at moderate pressure (4 bar).

The main difficulties or weaknesses in the simulation of FBBG with these models are the following:

- The submodels for devolatilization kinetics in both SSM and HM are taken from coal. Adaptation to biomass is not clearly documented or not made because of lack of data.
- The devolatilization process in SSM is limited by mass transfer. This is inconsistent with measurements in biomass devolatilization experiments, which suggest a thermally limited process. The HM uses a model for coal drying and devolatilization [176]. The model input for simulation of biomass is uncertain.
- In SSM the freeboard model for CFBG does not consider the 2D nature of the flow. Recently [375] the SSM has been compared with the measurements made in CFBBG at the Universities of British Columbia and Campinas with reasonable agreement, but details of the freeboard model compared with the original BFBBG model are not presented.
- The char conversion reactivity and physical parameters affecting the gasification of char derived from biomass are not clearly reported for any of the simulated systems.
- In SSM the single char particle model is formulated mathematically in a coherent way, but the influence of the change of char reactivity with conversion is not explicitly treated for different biomasses, nor is it specifically reported for the biomass simulated. The effect of the state of conversion of different char particles in the bed seems not to have been taken into account in SSM.
- Some kinetic rates are given [24,28] but they have been obtained in dedicated systems and cannot be applied generally. In both models secondary tar conversion is not treated in detail, and the use of catalyst in the bed is not included.

4.2.3. Conclusions and recommendations

Formulation of a model naturally occupies the main attention of a modeller. However, validation is a necessary step before a model can be safely applied. The selected authors are all aware of this and have made efforts in this direction, but nevertheless one could desire more, as can be concluded from the information given in Table 19. The above items express the opinion that there are several incomplete features in the evaluation of the models, and, although sensitivity analyses are made, often the formal validation has not been sufficiently detailed, and there are still uncertainties about the model structure. Furthermore, Table 19a demonstrates that, despite the use of impressive laboratory installations in some cases, there is no validation against commercial-scale equipment.

Pyrolysis or devolatilization is demonstrated to be a key step, affecting greatly the model results. To support a reliable model, measurements are required of the gas composition and of the yield of pyrolysis at high heating rates with the biomass of interest, if such results are not available in literature. Char and tar conversion are the processes whose modeling in FBBG is least satisfactory. This is surprising, because the tar composition and the relatively poor carbon conversion are the two major problems in FBBG. A great effort is still needed to improve the tar submodels. The knowledge of the chemistry of tar generation and conversion, and of the effects of temperature, solids concentration and gas composition in the bed on the tar reactions has to be significantly improved. Char-conversion chemistry is, in contrast, well known for a large variety of chars from biomass and coals. However, published reactor models do not deal with this information. Char conversion by gasification is one of the main factors determining the performance of an FBG, and it should be modeled in a more rigorous way to

better know how operating conditions can be optimized to reduce the loss of char.

The SSM and HM seem to be the most advanced FM published up to date for simulation. The model structure of both models seems to be adequate for simulation of FBBG if proper kinetic data are given by the user of the model. In the case of SSM, the modeling of CFBBG is still uncertain and further details should be reported. The HM seems to be valid for both bubbling and circulating FBG, especially for coal. The HM has only been validated once for a biomass in a BFBG. The key items of improvement are the kinetics data for pyrolysis and the char and tar conversion processes: reliable devolatilization measurements should be selected as input to the models and char and tar conversion should be revised and expanded. The former is already possible with available knowledge by proper consideration of the char gasification processes. The simple model of char conversion developed in the present review could be applied as a first estimate. The development of a more reliable tar conversion submodel needs further knowledge and measurements in FBBG. Both SSM and HM have only been validated by measurements taken in lab-scale FBG. This is a common feature of the rest of the models too, and it is due to the lack of measurements in large FBBG. The reliability of these models for simulation of large-scale FBGs is therefore as much valid as the semi-empirical correlations employed for the fluid-dynamics.

4.3. Black-box models (BBM)

A set of models is called BBM because the processes inside the reactors are not resolved and the models consist of overall mass (species) and heat balances over the entire gasification reactor supported by assumptions to acquire the knowledge of the material distribution in the gasifier. The complexity of BBM and the type of assumptions vary widely from one BBM to another depending of the aim: from simple heat and mass balances to predict the overall performance to the prediction of the main gas and solids composition. Some models use equilibrium relationships (Equilibrium models, EM) or modified equilibrium models complemented by empirical correlations obtained from experiments (Pseudo-equilibrium models, pseudo-EM). Sometimes the gasifier is divided into black-box regions where specific processes are assumed to be dominant and different models, based on equilibrium or kinetics, are applied (Zone models). Other modelers simply use empirical correlations fit to experiments in a specific plant (Fitting-data models or empirical models). Sometimes, a model can consist of combinations of several of the indicated types, so it is difficult to classify. In the following we present the fundamental formulation of the various types of BBM and the applications to FBBG found in literature for each type.

4.3.1. Overall heat and mass-balance model

This is the simplest model, conceptually. It aims at predicting the overall performance of the gasifier, such as gas yield, heating value of the gas and gasification efficiency. The input required is readily obtained from a fuel analysis, but some assumptions have to be made. The gasification reactor is fed by a fuel quantity $F_{f,in}$ (kg/s). Only a part of the fuel is actually converted into gas, F_f, because some fuel, ξ_u kg/kg fuel converted, is lost, mostly in the form of non-reacted char. Another part of the fuel, ξ_b kg/kg fuel converted, has to be burned to heat the fuel and input gas from the surrounding temperature to the gasifier temperature T_b and to compensate for heat losses. This can be written as

$$F_{f,in} = F_f(1+\xi_u+\xi_b) \tag{87}$$

If subdivided into ashes a, moisture w and combustibles b, the three quantities in kg/kg fuel ($a+b+w=1$), it can expressed in the equivalent form

$$F_{f,in} = F_f a(1+\xi_u+\xi_b) + F_f w(1+\xi_u+\xi_b) + F_f b(1+\xi_u+\xi_b) \tag{88}$$

The quantity of gas produced F_g consists of: (1) volatiles that were not burned (those burned are included in ξ_b) and gas produced by gasification with H_2O of the char part of the fuel, both quantities representing the amount of fuel converted $F_f b$, (2) the fuel moisture w, and (3) the flue gases resulting from the combustion of part of the fuel. In summary, this quantity of gas can be written as

$$F_g = F_f b + F_{f,in} w + F_f b \xi_b g_0 \tag{89}$$

Here, g_0 is the flue gas produced by combustion of a kg of the part of the fuel that burns, $F_f b \xi_b$. The amount of fuel that has to be burned to operate the reactor at temperature T_b, ξ_b, can be obtained by a heat balance over the reactor:

$$\begin{aligned} F_f b \xi_b H_{u,b} = {} & F_{f,in} h_f(T_b) + F_{f,in} w H_w + F_f b \xi_b \ell_0 h_{air}(T_b) \\ & + F_f b x_c \varphi_g h_{H_2O}(T_b) MM_{H_2O}/MM_c \\ & + (\text{loss to surroundings}) \end{aligned} \tag{90}$$

where the terms on the right-hand side are the heat quantities required for: heating of the fuel to bed temperature, fuel (sensible and latent), air for combustion $F_f b \xi_b \ell_0$, steam for gasification, and losses from the reactor. The heating value of the fuel $H_{u,f}$ is here represented by the heating value of the fuel burned $H_{u,b}$ that depends on which part of the fuel that actually burns, volatiles or char, and this in turn depends on the type of gasifier, as will be defined below. The amount of gas, φ_g, produced by gasification, is not known and has to be treated as a parameter. The corresponding heating value, $H_{C,g}$, can be roughly estimated from a conventional gas composition. The char fraction (assumed to be pure carbon) x_c is obtained from the fraction of volatiles given by a standard analysis of the fuel's volatiles x_v, consequently $x_c + x_v = 1$. If there are additional input gases for fluidization of the bed they have to be added as well. The heating value of the fuel $H_{u,f}$ is given by the fuel analysis. Assuming that the heating value of char $H_{u,c}$ can be represented by that of carbon, the heating value of the volatiles can be expressed

$$H_{u,v} = \left(H_{u,f}/b - x_c H_{u,c}\right) \Big/ x_v \tag{91}$$

The energy in the producer gas is contained in the volatiles $F_f b(1 - x_c\varphi_g)$ and in the gas from gasification of char $F_f b x_c \varphi_g$. This defines the heating value of the produced gas

$$F_g H_{u,g} = F_f b\left(H_{u,v}\left(1 - x_c\varphi_g\right) + H_{c,g} x_c \varphi_g\right) \tag{92}$$

The simple formulation allows other useful quantities to be calculated, such as the air ratio λ, the amount of air burned compared with the stoichiometric air demand for combustion of all fuel,

$$\lambda = F_f b \xi_b \ell_0 / F_{f,in} b \ell_0 = \xi_b/(1+\xi_u+\xi_b) \tag{93}$$

Before the final calculation, it must be decided what burns and where. The two options, indirect (allothermal) or direct (autothermal) gasifiers are illustrated in Fig. 26. In a direct gasifier, Fig. 26a, part of the fuel is burnt directly by oxygen supplied by air. In this case, the product gas is diluted by nitrogen. In the indirect gasifier, see Fig. 26b, dilusion is avoided since the nitrogen escapes with the flue gases from the combustion reactor, whereas the product gas leaves the gasification reactor. In the direct gasifier it is assumed that the volatiles burn in the first place and char is

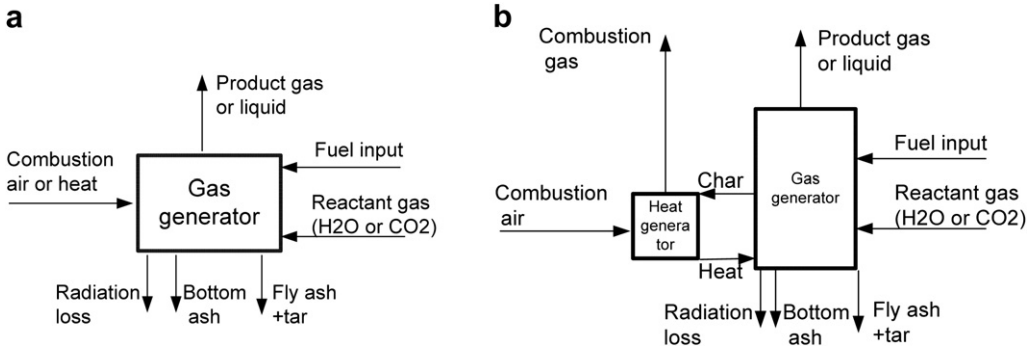

Fig. 26. Balances over gas generators: (a) Direct (b) Indirect.

consumed only after depletion of the volatiles. Then $H_{u,b} = H_{u,v}$ and all char that is not gasified is lost, $\xi_u = x_c(1 - \varphi_g)$. In the indirect gasifier, bed material is transported between the heat generator and the gas generator. In the heat generator only char is burned, and the heat generated is transported to the gas generator in the form of hot bed material. Hence, $H_{u,b} = H_{u,c}$ in Eq. (90) and the third term on the right-hand side disappears. Here, the char loss is $\xi_u = x_c(1 - \varphi_g) - \xi_b$. Only if the quantities of char or volatiles are not sufficient to satisfy the heat balance alone, a contribution from both components will be required.

Now, the desired quantities ξ_b, F_g, $H_{u,g}$ and the gas production efficiency $\eta_g = F_g H_{u,g}/(bF_{f,in}H_{u,f})$ can be calculated. The input necessary is the fuel analysis and the bed temperature. The amount of gas produced by steam and carbon dioxide gasification, φ_{gas}, also has to be given.

Some sample calculations with the model are illustrated in Fig. 27, showing a comparison between an autothermal (direct) and an allothermal (indirect) arrangement according to Fig. 26 in two extreme cases: a dry fuel ($w = 0$) subject to various degrees of char gasification ($0 < \varphi_g < 1$) or a case without char gasification ($\varphi_g = 0$) but with different moisture contents ($0 < w < 1$) (above a certain moisture content external fuel has to be added, but this is not shown). The two diagrams illustrate the higher conversion efficiency and gas heating value of the indirect arrangement. The great influence of moisture, resulting in a substantial reduction of both efficiency and heating value is also shown.

The simple modeling has obvious advantages, but there are also limitations: the amount of char gasified φ_g has to be assumed as an input, and the composition of the gas produced is not predicted, but the model has to be completed with other methods, such as the ones described in the following.

4.3.2. Equilibrium models (EM)

EM assume that equilibrium is attained in the outlet streams. A reacting system achieves the most stable composition at chemical equilibrium when its Gibbs free energy is minimized. Two formulations can be adopted for equilibrium modeling: stoichiometric and non-stoichiometric. The stoichiometric formulation requires a defined reaction mechanism, incorporating all chemical reactions and species concerned. In the non-stoichiometric formulation, no particular reaction mechanism is specified, and any species can be in the outlet gas, which should be a priori specified. Besides equilibrium data for the species considered, the only input needed in EM is the elemental composition of the fuel, which is readily obtained from the ultimate analysis [103]. The equilibrium formulations can be homogeneous or heterogeneous, the latter if there are solid species in the outlet stream, for instance, solid-phase carbon.

The non-stoichiometric formulation has been used to simulate biomass gasification systems for a large set of gaseous species as well as solid, usually carbon and inorganic species from minerals entering with biomass ash [103]. However, most EM for biomass gasification systems aim at predicting, at maximum, the composition of the outlet stream, involving the main gaseous species: CO, CO_2, H_2, H_2O, CH_4, O_2, N_2 and solid C, assumed to be graphite, and process temperature [33]. The bed temperature can be calculated if the heat loss is estimated, or, if the bed temperature is imposed,

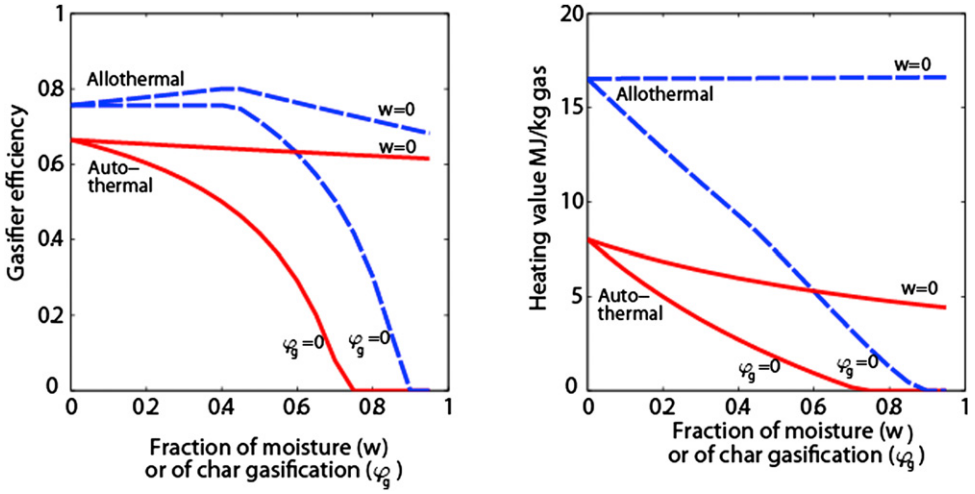

Fig. 27. Gas production efficiency of a gas generator and heating value of exit gas for various moisture contents in the fuel w and zero gasification of char ($\varphi_g = 0$) in auto- and allothermal gas generators. In the same diagram a case of zero moisture content ($w = 0$) and various degrees of gasification of char (φ_g) is shown.

Table 20
Examples of equilibrium models applied to FBG.

Ref.	T (K)	Feedstock	Remarks
[383]	1000–1060	Wood	BFB. Uses approach to equilibrium
[384]	873–1473	Various coals	Model of various types of coal gasifier. Predictions are poor for FB gasifiers
[385]	1023–1473	Biomass	BFB. Gasification of biomass for methanol synthesis
[386–388]	n.a.	Straw	BFB
[370–372]	n.a.	Rice husk	BFB
[381]	1023–1153	High-value and Pittsburgh seam coal	CFB. Kinetically-modified equilibrium model is proposed
[389]	920–1323	Biomass: beech chips	Dual fluidized-bed gasifier. Steam gasification
[390]	1053–1323	Wood	BFB. ASPEN PLUS model: Gibbs free energy
[147,360,361]	1273–1323	Agricultural waste	BFB. FB divided into three zones: jetting, bubbling and slugging.
[391]	1073–1573	Sewage sludge subbituminous coal	BFB
[103]	973–1123	Various biomasses	CFB

the heat loss is then calculated by the model. Reviews and analyses [33,103,379–382] have studied the influence of operating variables on biomass and coal gasification systems applying EM. The presence of heavy hydrocarbons or tar can be taken into account represented by a compound such as benzene, naphthalene or other [382], although this is rarely done in EM. We shall name this model with 10 unknowns (CO, CO_2, H_2, H_2O, CH_4, O_2, N_2, solid C, tar, and temperature), *EM-1*. In Table 20 a selection of equilibrium models for simulation of FBBG are presented, indicating the conditions of application. The discussion below is mainly based on these works, emphasizing stand-alone biomass FBG at atmospheric pressure.

Equilibrium simulations for FBG yield nearly no oxygen, solid carbon (above approximately 800 °C) or tar (no matter what compound is selected to represent it) [103,382]. The absence of oxygen is supported by measurements in FBBG, but the contents of tar and char in the gas are far from being null. In addition, gaseous N_2 is the most stable nitrogen species, and all nitrogen entering the system is usually assumed to be converted into N_2. It is known that some NH_3 as well as some other minor compounds, such as HCN and nitrogened tars are formed, originating from the fuel nitrogen; The amount of NH_3 and HCN is usually low compared to the N_2 in the gas produced, so the composition of the main species in the gas produced is not significantly altered by these components.

These observations allow formulating a simple EM to predict the six main gaseous species (CO, CO_2, H_2, H_2O, CH_4, N_2). The adoption of a homogeneous and non-stoichiometric equilibrium formulation is convenient in this case. The problem is solved by the atomic balances for C, H, O (N_2 is directly calculated by atomic balances without participating in the equilibrium equations) together with, for instance, the equations given by the equilibrium of water–gas shift reaction (WGSR) and steam reforming of methane:

$$K_{WGSR} = \frac{y_{H_2} y_{CO_2}}{y_{H_2O} y_{CO}} = 0.029\exp(4094/T) \quad (94)$$

$$K_{SRMR} = \frac{y_{H_2}^3 y_{CO}}{y_{CH_4} y_{H_2O}} = 6.14 \times 10^{13}\exp(-28116/T) \quad (95)$$

y being the molar fraction of the i species in the outlet gas. K_{WGSR} and K_{SRMR} are equilibrium constants. The selection of these two reactions has been shown to be useful because they include the key five gaseous reactants (CO, CO_2, H_2, H_2O, CH_4) and because measurements indicate directly the kinetic limitation of these two reactions [206]. A heat balance is made over the system to find the temperature if the heat loss is estimated. We shall name this model, with 7 unknowns (CO, CO_2, H_2, H_2O, CH_4, N_2 and T), *EM-2*.

Equilibrium and kinetic predictions were compared [206] and the conclusion is that steam reforming of methane is far from equilibrium under the operating conditions of interest for biomass gasifiers, and thus, there is a strong kinetic limitation. EM using air as gasification agent leads to a gas nearly free of CH_4 at atmospheric pressure [103,379,382], so the CH_4 concentration can be considered zero in practical application of EM (but it is not zero in the real gas) [103,379,382]. Exclusion of CH_4 from the calculations eliminates Eq. (95) in the EM, leading a simpler model that we shall call *EM-3*, containing 6 unknowns (CO, CO_2, H_2, H_2O, N_2 and T).

An even simpler model, called *EM-4*, is obtained by assuming a temperature *T*. Then, the heat balance is not coupled with the rest of the equations, but it separately serves to calculate the heat loss. For a given temperature, the solution becomes a single non-linear equation. Under the operating conditions of FBG, *EM-4* yields about the same result of CO, CO_2, H_2, H_2O as *EM-1*. In conclusion, *EM-4* is sufficient to give a first estimation of FBBG by EM. Char, tar and CH_4 are null and *T* is assumed. To estimate *T*, *EM-3* is applied taking the results of *EM-1* as a first estimate in the iteration (this makes the convergence rapid, and so the solution of *EM-3* is achieved with a simple data-sheet).

The question whether the equilibrium of the WGSR is attained in FBBG (and other biomass and coal systems) has been the subject of several investigations. Experimental investigations in FBBG [283,344,382,392] have evaluated the factor $f_{WGSR} = K_{exp}/K_{WGSR}$, where K_{WGSR} is calculated by Eq. (94) and K_{exp} by experimental data, $K_{exp} = (y_{CO2} y_{H2}/y_{CO} y_{H2})_{exp}$, y_i being the measured concentrations of the four gases involved in the WGSR. A comparison

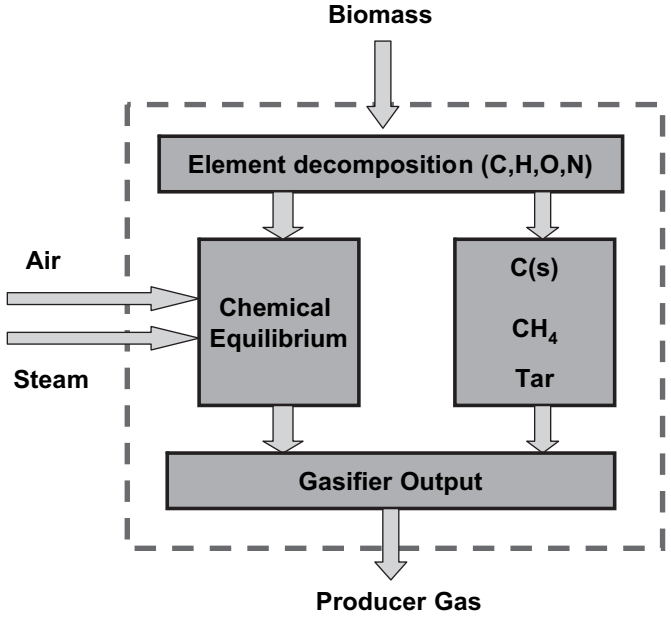

Fig. 28. Conversion processes in a gasifier. Basis for pseudo-equilibrium models: implementation accounting for non equilibrium factors (adapted from Li et al. [103]).

between the equilibrium and experimental values of K_{exp} and K_{WGSR} (or f_{WGSR}) with data taken from different sources [382] shows that f_{WGSR} is below unity in most cases, indicating the kinetic limitation of WGSR. f_{WGSR} depends mainly on temperature, size of reactor (residence time), presence of catalysts, and type of gasification agent. An assessment of the effect of equipment has been made [30] of the validity of EM applied to real biomass gasification units, concluding that chemical equilibrium is a good approach when simulating entrained-flow and down-draft fixed-bed gasifiers, in the latter case as long as high temperature and gas residence time are achieved in the throat of the gasifier. Updraft fixed bed, dual FB and stand-alone FB gasifiers have to be modeled by revised equilibrium models, i.e. pseudo-equilibrium models, or, in some extreme cases, by detailed flow models.

To sum up, for the proper application of EM, the temperature has to be high enough and the residence time larger than the time needed to complete the reactions. This does not usually occur in FBBG, because of the low temperature, between 750 and 900 °C. EM overestimates the yields of H_2 and CO, underestimates that of CO_2 and predicts an outlet stream free from CH_4, tars, and char. Therefore, EM does not seem to be accurate enough for design of FBBG. Despite this, EM is simple and useful for first estimates. The simplest EM version discussed (named *EM-4*) is often enough for this aim. To improve this model, pseudo-equilibrium models (or more advanced models) have to be applied.

4.3.3. Pseudo-equilibrium models

Pseudo-EM aim at making the equilibrium calculations more realistic by supporting the EM with empirical relations. Fig. 28 shows the essential idea behind pseudo-EM. It allows solid carbon, methane and tar to be contained in the outlet gas, and the corresponding quantities of carbon and hydrogen are discounted from the input fuel. The remaining fuel elements and the gasification agent react to attain equilibrium. The outlet gas is then obtained by summing the gas components given by the equilibrium and the carbon, methane and tar taken off initially. The underlying reason for this approach is that decomposition of CH_4, tar, and char conversion by gasification is kinetically limited, as discussed above. This type of pseudo-EM needs as input the concentrations of CH_4, solid carbon and tar in the outlet stream. It is necessary, therefore, to estimate these species in the reactor. Usually, these estimates are made by experiments in the same plant where the model will be applied [103], or they are somehow estimated according to experience [382]. This fact makes pseudo-EM quite sensitive to such estimates, and this type of model is less predictive.

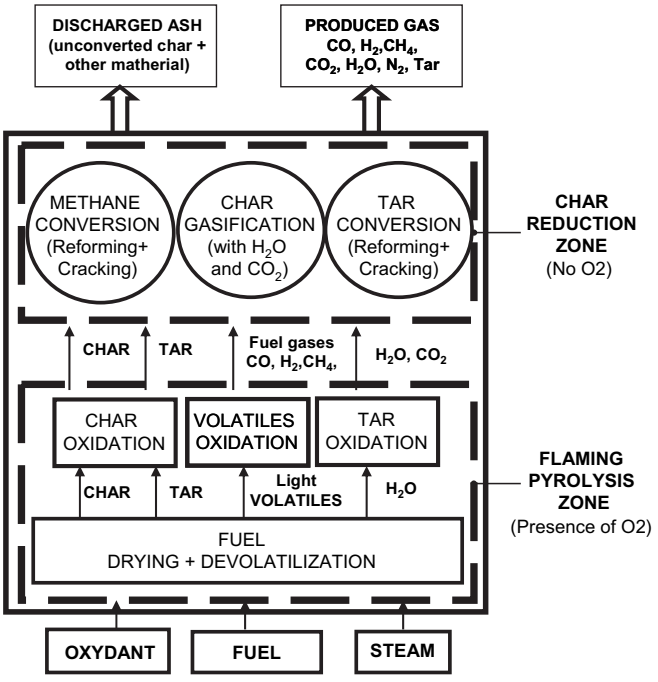

Fig. 29. Outline of a zone model for FBBG: devolatilization of fuel, oxidation of light fuel gases, tar and char define the flaming pyrolysis zone (where there is O_2), and conversion of the tar, methane and char in the char reduction zone, where there is no oxygen. Adapted from Gómez-Barea et al. [394].

The simplest pseudo-EM extends *EM-4* described above by accounting for the methane in the outlet stream (tar and char are still assumed zero in the outlet gas). It is assumed that all the methane from the initial devolatilization is found in the product gas, without being converted in the bed. Empirical yields of methane (kg methane/kg of dry fuel) are obtained from devolatilization experiments for each biomass or taken from literature [382]. This simple pseudo-EM is useful for preliminary predictions of the gas composition and often gives reasonably good agreement with experimental results. However, the method should only be applied if the process temperature is high and/or there is a catalyst in the bed; otherwise, the equilibrium of the WGSR is not attained and the quantities of char and tar would be significant, making the calculation of the gas composition more uncertain.

A variety of more sophisticated pseudo-EM have been published, based on the scheme (or some variant) of Fig. 28, [103,382,390,393,394]. Tar has been included as a model compound in the gas only in some cases. The essentials of pseudo-EM have been summarized [382] and a model was formulated introducing three correction parameters: carbon conversion, methane conversion and the yield of methane after devolatilization. The value of these parameters are influenced by the type of gasification agent (steam vs. air-blown), the use of catalysis, type of catalyst (natural rocks vs. synthetic), and process temperature [382]. It is stated [382] that: (1) carbon conversion ranges from 0.8 to 0.9; (2) The methane yield from devolatilization is only marginally affected by the operating conditions and the value of 8.8×10^{-2} kg/kg dry and ash-free biomass was chosen for wood, based on previous experiments with beech wood; (3) The conversion of methane through the reactor (X_{CH4}) can be considered zero for air gasification using no synthetic catalyst in the bed. In contrast, X_{CH4} is in the range of 0–1 for steam reforming of methane using metal-based catalyst (Ni or similar): $X_{CH4} = 1/3–2/3$, when very active reforming catalysts are employed in steam gasification, whereas $X_{CH4} \leq 1/4$ is recommended in air gasification. However, other conversions and yields have been reported, depending on the nature of fuel, operating mode, design and size of gasifier. Therefore, the recommendations above [382] should be taken as rough guides for first estimates.

A pseudo-EM was developed [394] employing simple kinetic models to estimate the conversion of char, methane and tar, which well predicted the gas composition and carbon conversion measured in a pilot-scale FBBG. The input to the model came from measurements of the kinetics in a lab-scale FBBG for the same biomass and char. This kind of model has shown to increase the prediction capability compared with the pseudo-EM discussed, but dedicated experiments for biomass devolatilization and char gasification have to be conducted in a laboratory FB to provide the necessary data.

Another approach for correcting EM was proposed [395] where the equilibrium of the reactions is evaluated at a lower temperature, a "quasi-equilibrium temperature", than the actual process temperature. This approach is not, in fact, a pseudo-EM like the others discussed above. In a similar way [384] the discrepancies of

the equilibrium prediction were attributed to temperature gradients from the gasification zone to the outlet zone. Therefore, the temperature was modified to obtain a reasonable correlation to data from semi-commercial and commercial coal gasifiers. For operating temperatures in the range of 740–910 °C [393] the measured unconverted carbon in the ash, was only compatible with equilibrium of the char gasification reactions with H_2, CO_2, and H_2O, evaluated at much lower temperatures (450–580 °C). This demonstrates that char conversion was extremely kinetically limited [393].

To sum up, pseudo-EM improves considerably the EM because the inclusion of empirical parameters leads to a better agreement with experimental data. However, the model looses much of its predictive capability. For instance, the corrections developed [103] were based on air-factor correlations obtained from a CFB pilot plant, and so they are not applicable to other systems. The method presented in [382] is useful if the estimation of the parameters required is available or can be extracted from past experiences. The recommendations given above [382] can be useful as rough guidelines. Refinements, such as that in [394], require reliable kinetics. In general, pseudo-EM leads to more or less precise estimates of the gas composition but they do not generally predict the char and tar contents in the outlet gas. For proper prediction of these quantities more advanced models are necessary.

4.3.4. Zone models

In a zone model an FBBG is represented by various zones in series where dominant processes are treated in each zone. The solution of each zone is then made by a variety of methods: from equilibrium to kinetic rates, where some process is rate-controlling, or simply by assuming empirical relations. An illustrative example of zone models in FBBG is shown in Fig. 29 adapted from [394]. This model describes the situation in Fig. 6b in a simplified case ($Da_{py,V} > 1$), by distinguishing two zones, characterized by the presence or the absence of oxygen. Devolatilization and oxidation occur in the flaming pyrolysis zone where oxygen is present, whereas char conversion by gasification as well as tar and methane conversion take place in the char reduction zone, where there is no oxygen. The model is greatly simplified because the two zones are assumed to be in series, and the flaming pyrolysis zone is very small compared to the char reduction zone, the latter occupaying most of the bed. This assumption is made because the processes in the flaming pyrolysis zone are rapid compared to those in the char reduction zone. The release of volatile gases in the flaming pyrolysis zone needs to be predicted for the estimation of the gas produced in the reduction zone, where conversion of char, tar and methane takes place. In the char reduction zone simple kinetic models are developed for each process, giving the performance of the FBG.

A zone model was developed [213] to simulate the processes in air-blown FBGs. Two steps were assumed: the first step calculates the concentration of the four species participating, assuming the WGSR to be in equilibrium at bed temperature. In the second step, a pseudo-homogeneous model was applied for the char reduction zone, where only the CO_2 and H_2O–char gasification reactions were assumed to occur. This approach is simple, but the short contact time and the relatively low temperature of the pyrolysis stage in an FBG make the assumption of the attainment of equilibrium of the gas species unrealistic.

Some of the FM of Table 19 could be considered zone models. In particular, devolatilization is assumed to be rapid compared to char conversion by gasification in most FM. In [219] a model was applied in a finite pyrolysis zone, where the height of the zone was calculated on the basis of the time of devolatilization and vertical dispersion of the fuel.

5. Summary and conclusions

Modeling of biomass gasification in fluidized-bed reactors was reviewed. The most relevant phenomena considered in modeling of FBBG were formulated and discussed in detail, including fluid-dynamics and chemical conversion processes. Fields for further research have been identified: devolatilization and conversion of tar and char are recognized as the processes that require major modeling efforts. The knowledge of the chemistry of tar generation and conversion has to be significantly improved, as well as the effects of temperature, solids concentration and gas composition in the bed on the tar reactions. Char conversion is, in contrast, well known but, published FBBG models have not dealt with the available information. Devolatilization and comminution of fuel particles is still treated in a semi-empirical way and much has to be done to develop reliable computational models.

The various approaches applied for reactor modeling, from black-box models to computational fluid-dynamic models, were described, illustrating their state of development and the usefulness of each approach depending of the aim of the model. The fluidization model, where the fluid-dynamics of the FB is simplified by semi-empirical correlations, is the most common approach up to date, used with major success. The survey presented of published mathematical reactor models for biomass and waste gasification in FB allows the overall conclusion that most of the FBBG models from the simplest to the most advanced formulation fit reasonably well the selected experiments, despite the various formulations and input data. However, there are few measurements available for detailed comparison with the models. Validation of models with data from full-scale FBBG units is necessary. Much experimental work is required before detailed models can be validated with sufficient confidence, to make them useful for process optimization and hardware design. Two additional issues need the focus of future FBG models: the scale-up of results obtained in laboratory FBG to large-scale units, and better consideration of the specific characteristics of waste and biomass fuels.

Acknowledgment

The authors acknowledge the European Commission, the Commission of Science and Technology of Spain, and Junta de Andalucía for their financial support. Comments and suggestions from PhD students and colleagues are acknowledged. The help of Paco Bueno in figures and tables is acknowledged.

References

[1] Maniatis K. Progress in biomass gasification: an overview. In: Bridgwater AV, editor. Progress in thermochemical biomass conversion. London: Blackwell Science; 2001. p. 1–31.
[2] Kurkela E, Nieminen M, Simell, P. Development and commercialisation of biomass and waste gasification technologies from reliable and robust co-firing plants towards synthesis gas production and advanced cycles. 2nd World Conference on Biomass for Energy, Industry and Climate Protection, Rome; 2004, pp. 10–5.
[3] Gómez-Barea A, Leckner B. Gasification of biomass and waste. In: Winter F, editor. Handbook of combustion, vol. 4. Wiley; 2009.
[4] Oka SO. Fluidised bed combustion. New York: Marcel Dekker; 2004.
[5] Anthony DB, Howard JB. Coal devolatilisation and hydrogasification. AIChE J 1976;22:625–56.
[6] Laurendeau NM. Heterogeneous kinetics of coal char gasification and combustion. Prog Energy Combust Sci 1978;4:221–70.
[7] Smoot LD, Smith PJ. Coal combustion and gasification. New York: Plenum Press; 1985.
[8] Annamalai K, Ryan W. Interactive processes in gasification and combustion-II. Isolated carbon, coal and porous char particles. Prog Energy Combust Sci 1993;19:383–446.
[9] Saxena SC. Devolatilization and combustion characteristics of coal particles. Prog Energy Combust Sci 1990;16:55–94.
[10] Kristiansen A. Understanding of coal gasification. Gemini House, London: IEA Coal Research; 1996.

[11] Niksa S, Liu GS, Hurt RH. Coal conversion submodels for design applications at elevated pressures. Part I. Devolatilization and char oxidation. Prog Energy Combust Sci 2003;29:425–77.
[12] Liu GS, Niksa S. Coal conversion submodels for design applications at elevated pressures. Part II. Char gasification. Prog Energy Combust Sci 2004;30:679–717.
[13] Li CZ. Some recent advances in the understanding of the pyrolysis and gasification behaviour of Victorian brown coal. Fuel 2007;86:1664–83.
[14] Agarwal PK, La Nauze RD. Transfer processes local to the coal particle. A review of drying devolatilization and mass transfer in fluidized bed combustion. Chem Eng Res Design 1989;67:457–80.
[15] Thunman H, Leckner B. Mathematical modeling of combustion in bio-fuelled small boilers. Report A05-227. Department of Energy Conversion, Chalmers University of Technology; 2005.
[16] Moghtaderi B. The state-of-the-art in pyrolysis modelling of lignocellulosic solid fuels. Fire and Materials 2006;30:1–34.
[17] Di Blasi C. Modeling chemical and physical processes of wood and biomass pyrolysis. Prog Energy Combust Sci 2008;34:47–90.
[18] La Nauze RD. Fundamentals of coal combustion in fluidized beds. Chem Eng Res Design 1985;63:3–33.
[19] Leckner B. Fluidized bed combustion: mixing and pollutant limitation. Prog Energy Combust Sci 1998;24:31–61.
[20] Hobbs ML, Radulovic PT, Smoot LD. Combustion and gasification of coals in fixed-beds. Prog Energy Combust Sci 1993;19:505–86.
[21] Hannes JP. Mathematical modeling of circulating fluidized bed combustion PhD Thesis, RWTH Aachen, Germany; 1996.
[22] Eaton A, Smoot LD, Hill SC, Eatough CN. Components, formulations, solutions, evaluation and application of comprehensive combustion models. Prog Energy Combust Sci 1999;25:387–436.
[23] Ravelli S, Perdichizzi A, Barigozzi G. Description, applications and numerical modelling of bubbling fluidized bed combustion in waste-to-energy plants. Prog Energy Combust Sci 2008;34:224–53.
[24] Souza-Santos ML. Solid fuels combustion and gasification. New York: Marcel Dekker; 2004.
[25] Buekens AG, Schoeters JG. Modelling of biomass gasification. In: Overend RP, Milne TA, Mudge KL, editors. Fundamentals of thermochemical biomass conversion. London: Elsevier Applied Science Publishers; 1985. p. 619–89.
[26] Gururajan VS, Agarwal PK, Agnew JB. Mathematical modelling of fluidized bed coal gasifiers. Trans IChemE 1992;70:211–38.
[27] Moreea-Taha R. Modeling and simulation for coal gasification. IEA Greenhouse Gas R&D Programme; 2000.
[28] Hamel S. Mathematische Modellierung und experimentelle Untersuchung der Vergasung verschiedener festen Brennstoffe in atmosphärischen und druckaufgeladenen stationären Wirbelschichten. Ph.D. dissertation, Universität Siegen; 2001.
[29] Newstov DA, Zabaniotou A. Mathematical modelling and simulation approaches of agricultural residues air gasification in a bubbling fluidized bed reactor. Chem Eng J 2008;143:10–31.
[30] Villanueva A, Gómez-Barea A, Revuelta E, Campoy M, Ollero P. Guidelines for selection of gasifiers modelling strategies. Proc. 16th European Biomass Conference; Valencia, Spain; 2008, pp. 980–6.
[31] Grabner M, Ogriseck S, Meyer B. Numerical simulation of coal gasification at circulating fluidised bed conditions. Fuel Proc Technol 2007;88:948–58.
[32] van der Drift A, Boerrigter H, Coda B, Cieplik MK, Hemmes K. Entrained flow of gasification of biomass: Ash behavior, feeding issues and system analyses. ECN Report ECN-C-04-039; 2004.
[33] Higman C, van der Burgt M. Gasification. Amsterdam: Gulf Professional Publishers/Elsevier Science; 2008.
[34] Rauch R, Hofbauer H, Bosch K, Siefer I, Aichernig C, Tremmel H, et al. Steam gasification of biomass at CHP plant in güssing – Status of the Demonstration Plant. Proc 2nd World Conf on Biomass for Energy, Industry and Climate Protection, Rome; 2004, Vol. II, pp. 1687–90.
[35] Paisley MA, Overend RP. The SylvaGas process from future energy resources – a commercialization success. In: Palz W, Spitzer J, Maniatis K, Kwant K, Helm P, Grassi A, editors. Proc 12th European Conference on Biomass for Energy. Amsterdam: Industry and Climate Protection; 2002. p. 975–8.
[36] Di Felice R, Coppola G, Rapagna S, Jand N. Modeling of biomass devolatilization in a fluidized bed reactor. Can J Chem Eng 1999;77:325–32.
[37] Wu SY, Baeyens J. Segregation by size difference in gas fluidized beds. Powder Technol 1998;98:139–50.
[38] Wirsum M, Fett F, Iwanowa N, Lukjanow G. Particle mixing in bubbling fluidized beds of binary particle systems. Powder Technol 2001;120:63–9.
[39] Ge W, Wang W, Dong W, Wang J, Lu B, Xiong Q, et al. Meso-scale structure – a challenge of computational fluid dynamics for circulating fluidized bed risers. In Werther J, Nowak W, Wirth K-E, Hartge E-U, editors. Proc Int Conf on Circulating Fluidised Beds, Hamburg; 2008, pp. 19–37.
[40] Ranade VV. Computational flow modelling for chemical reactor engineering. London: Academic Press; 2002.
[41] Enwald H, Peirano E, Almstedt AE. Eulerian two-phase flow theory applied to fluidization. Int J Multiphase Flow 1996;22(Suppl. 1):21–66.
[42] Yu L, Lu J, Zhang X, Zhang S. Numerical simulation of the bubbling fluidized bed coal gasification by the kinetic theory of granular flow (KTGF). Fuel 2007;86:722–34.
[43] Petersen I, Werther J. Three-dimensional modeling of a circulating fluidized bed gasifier for sewage sludge. Chem Eng Sci 2005;60:4469–84.
[44] Kunii D, Levenspiel O. Fluidization engineering. 2nd ed. Amsterdam: Elsevier; 1991.
[45] Grace JR. Fluid beds as chemical reactors. In: Geldart D, editor. Gas fluidization technology. Chichester: Wiley; 1986. p. 285–339.
[46] Toomey RD, Johnstone HF. Gaseous fluidization of solid particles. Chem Eng Prog 1952;48:220–6.
[47] Davidson JF, Harrison D. Fluidised particles. Cambridge: Cambridge University Press; 1963.
[48] Chavarie C, Grace JR. Performance analysis of a fluidized bed reactor II. Observed reactor behavior compared with simple two-phase models. Ind Eng Chem Fund 1975;14:79–86.
[49] Horio M, Wen CY. An assessment of fluidized-bed modelling. AIChE Symp Ser 1977;73:9–21.
[50] van Swaaij WPM. Chemical reactors. In: Davidson JF, Clift R, Harrison D, editors. Fluidization. 2nd ed. London: Academic Press; 1985. p. 595–629. Chapter 18.
[51] Yates JG. Fundamentals of fluidized-bed chemical processes. London: Butterworths; 1983.
[52] Grace JR. High-velocity fluidized bed reactors. Chem Eng Sci 1990;45: 1953–66.
[53] Kato K, Wen CY. Bubble assemblage for fluidized bed catalytic reactors. Chem Eng Sci 1969;24:1351–69.
[54] Fryer C, Potter OE. Countercurrent backmixing model for fluidized bed catalytic reactors. Applicability of simplified solutions. Ind Eng Chem Fund 1972;11:338–44.
[55] Overturf BW, Reklaitis GV. Fluidized-bed reactor model with generalized particle balances. Part I: formulation and solution. AIChE J 1983;29:813–20.
[56] Overturf BW, Reklaitis GV. Fluidized-bed reactor model with generalized particle balances. Part II: coal combustion application. AIChE J 1983;29:820–9.
[57] Yoshida K, Kunii D. Complex reaction in fluidised beds-simulation of gasification. J Chem Eng Jpn 1974;7:34–9.
[58] Matsui I, Kunii D, Fursuawa T. Study of fluidized bed steam gasification of char by thermogravimetrically obtained kinetics. J Chem Eng Jpn 1985;18: 105–13.
[59] Weimer AW, Clough DE. Modeling a low pressure steam-oxygen fluidized bed coal gasification reactor. Chem Eng Sci 1981;36:549–67.
[60] Saffer M, Ocampo A, Laguerie C. Gasification of coal in a fluidized bed in the presence of water vapor and oxygen; an experimental study and a first attempt at modeling the reactor. Int Chem Eng 1988;28:46–61.
[61] Ma RP, Felder RM, Ferrell JK. Modelling a pilot-scale fluidised bed coal gasification reactor. Fuel Proc Technol 1988;19:265–90.
[62] Souza-Santos ML. Modeling and simulation of fluidized-bed boilers and gasifiers for carbonaceous solid. PhD thesis, Department of Chemical Engineering and Fuel Technology, University of Sheffield; 1987.
[63] Caram HS, Amundson NR. Fluidized bed gasification reactor modeling 1. Model description and numerical results for a single bed. Ind Eng Chem Proc Des Dev 1978;18:80–96.
[64] Yan HM, Heidenreich C, Zhang DK. Mathematical modelling of a bubbling fluidised-bed coal gasifier and the significance of net flow. Fuel 1997;77: 1067–79.
[65] Yan HM, Heidenreich C, Zhang DK. Modelling of bubbling fluidised bed coal gasifiers. Fuel 1999;78:1027–47.
[66] Ross DP, Yan HM, Zhong Z, Zhang DK. A non-isothermal model of bubbling fluidised-bed coal gasifier. Fuel 2005;84:1469–81.
[67] Jiang H, Morey RV. A numerical model of a fluidized bed biomass gasifier. Biomass Bioenergy 1992;3:431–47.
[68] Fiaschi D, Michelini M. A two-phase one-dimensional biomass gasification kinetics model. Biomass Bioenergy 2001;21:1211–32.
[69] Radmanesh R, Chaouki J, Guy C. Biomass gasification in a bubbling fluidized bed reactor: experiments and modeling. AIChE J 2006;52:4258–72.
[70] Kersten SRA, Prins W, van der Drift A, van Swaaij WPM. Experimental fact-finding in CFB biomass gasification for ECN's 500 kWth pilot plant. Ind Eng Chem Res 2003;42:6755–64.
[71] Xiang Q, Huang G, Ni M, Cen K, Tao T. Lateral dispersion of large coal particles in an industrial-scale fluidized bed combustor. Proc Int Conf Fluid Bed Combust 1987;9:546–53.
[72] Niklasson F, Thunman H, Johnsson F, Leckner B. Estimation of solids mixing in a fluidized bed combustor. Ind Eng Chem Res 2002;41:4663–73.
[73] Pallarès D. Fluidised bed combustion: modelling and mixing. PhD thesis. Chalmers University of Technology, Göteborg, Sweden; 2008.
[74] Couturier M, Doucette B, Stevens D, Poolpol S, Razbin V. In: Anthony EJ, editor. Proc Int Conf Fluidized Bed Combustion; 1991, 11, pp. 107–14.
[75] Luecke H, Hartge EU, Werther J. 3D model of combustion in large-scale circulating fluidized bed boilers. Int J Chem Reactor Eng 2004;2. article A11.
[76] Kersten SRA, Moonen RHW, Prins W, van Swaaij WPM. Gas mixing in pilot scale (500 kWth) air blown circulating fluidised bed biomass gasifier. In: Bridgwater AV, editor. Progress in thermochemical biomass conversion. Cambridge (MA): Blackwell Science; 2001. p. 452–64.
[77] Adánez J, Gayán P, de Diego LF, García-Labiano F, Abad A. Combustion of wood chips in a CFBC. Modeling and validation. Ind Eng Chem Res 2003;42:987–99.
[78] Damköhler G. Einfluesse der Strömung, Diffusion und des Wärmeueberganges auf die Leistung von Reaktionsöfen. Zeitschrift der Elektrochemie 1936;42:846–62.

[79] van Deemter JJ. In: Davidson JF, Clift R, Harrison D, editors. Fluidization. 2nd ed. London: Academic Press; 1985.
[80] Baeyens J, Geldart D. Solids mixing. In: Geldart D, editor. Gas fluidization technology. Chichester: Wiley; 1986. p. 97–122.
[81] Shen L, Zhang M, Xu Y. Solids mixing in fluidized beds. Powder Technol 1995;84:207–12.
[82] Fitzgerald TJ. Cold modeling of fluidized bed combustors. Report EPRI CS-1476, RP315-1; 1980.
[83] Nienow AW, Rowe PN, Chiba T. Mixing and segregation of a small proportion large particles in gas fluidized beds of considerably smaller ones. AIChE Symp Ser 1978;74:45–53.
[84] Tran KD, Masson H, Rios GM. Free object motion in a gas fluidized bed. Chem Eng Commun 1986;47:247–72.
[85] Aznar MP, Garcia-Gorria FA, Corella J. Minimum and maximum velocities for fluidization for mixtures of agricultural and forest residues with a second fluidized solid. Preliminary data and results with sand-sawdust mixtures. Int Chem Eng 1989;32:95–102.
[86] Shen L, Xiao J, Niklasson F, Johnsson F. Biomass mixing in a fluidized bed biomass gasifier for hydrogen production. Chem Eng Sci 2007;62: 636–43.
[87] Zhang Y, Jin B, Zhong W. Experimental investigation on mixing and segregation behavior of biomass particle in fluidized bed. Chem Eng Process 2009;48:745–54.
[88] Borghi G, Sarofim F, Beér JM. A model of coal devolatilization and combustion. Combust Flame 1985;61:1–16.
[89] Palchonok G. Heat and mass transfer to a single particle in fluidised bed. Ph.D. dissertation, Chalmers University of Technology, Gothenburg, Sweden; 1998.
[90] Geldart D. Particle entrainment and carryover. In: Geldart D, editor. Gas fluidization technology. New York: Wiley; 1986. p. 123.
[91] Fiorentino M, Marzocchella A, Salatino P. Segregation of fuel particles and volatile matter during devolatilization in a fluidized bed reactor-I. Model development. Chem Eng Sci 1997;52:1893–908.
[92] Fiorentino M, Marzocchella A, Salatino P. Segregation of fuel particles and volatile matter during devolatilization in a fluidized bed reactor-II, Experimental. Chem Eng Sci 1997;52:1909–22.
[93] Schlichthärle P, Werther J. Axial pressure profiles and solids concentration distributions in the CFB bottom zone. In: Werther J, editor. Proc Circulating Fluidized Bed Technology VI, Frankfurt/Main: DECHEMA e.V; 1999, pp. 185–200.
[94] Hirschberg B, Werther J. Factors affecting solids segregation in circulating fluidized-bed riser. AIChE J 1998;44:25–34.
[95] Koenigsdorff R, Werther J. Gas and solids mixing in and flow structure modelling of the upper dilute zone of a circulating fluidized bed. Powder Technol 1995;82:317–29.
[96] Johansson A. Solids flow pattern in circulating fluidized-bed boilers PhD. thesis. Chalmers University of Technology, Göteborg, Sweden; 2005.
[97] Miccio F, Moersch O, Spliethoff H, Hein KRG. Generation and conversion of carbonaceous fine particles during bubbling fluidized bed gasification of a biomass fuel. Fuel 1999;78:1473–81.
[98] Sternéus J, Johnsson F, Leckner B. Gas mixing in circulating fluidized bed risers. Chem Eng Sci 2000;55:129–48.
[99] Werther J. Fluidized-bed reactors. In: Ullmann's encyclopedia of industrial chemistry. Weinheim: Wiley-VCH Verlag GmbH; 2007. doi:10.1002/14356007.b04_239.pub2.
[100] Leckner B, Werther J. Scale-up of circulating fluidized bed combustion. Energy Fuels 2000;14:1286–92.
[101] Arena U. Gas mixing. In: Grace JR, Avidan AA, Knowlton TM, editors. Circulating fluidized beds. London: Chapman and Hall; 1997. p. 86–118.
[102] Kruse M, Schönfelder H, Werther J. A two-dimensional model for gas mixing in the upper dilute zone of a circulating fluidized bed. Can J Chem Eng 1995;73:620–34.
[103] Li X, Grace JR, Lim CJ, Watkinson AP, Chen HP, Kim JR. Biomass gasification in a circulating fluidized bed. Biomass Bioenergy 2004;26:171–93.
[104] Gómez-Barea A, Leckner B, Campoy M. Conversion of char in CFB gasifiers. In: Werther J, Nowak W, Wirth K-E, Hartge E-U, editors. Proc 9th Int Conf on circulating fluidized beds. Hamburg: Germany; 2008. p. 727–32.
[105] Liu DY, Chen XP, Liang C, Zhao CS. Solids mixing in the bottom zone of fluidized beds. In: Yue GX, Zhang H, Zhao CS, Luo ZY, editors. Proc. 20th Int. Conf. on Fluidized Bed Combustion, Xian; 2009, pp. 459–63.
[106] Na Y, Yan C, Sun X, Cui P, He J, Karlsson M, et al. Large and small particles in CFB combustors. In: Kwauk M, Li J, editors. Proc Fifth Int Conf on circulating fluidized bed. Beijing: Science Press; 1997. p. 194–9. isbn 7-03-006111-X/TQ.
[107] Win K, Nowak W, Matsuda H, Hasatani M, Bis Z, Krzywanski J, et al. Transport velocity of coarse particles in multi-solid fluidized bed. J Chem Eng Jpn 1995;28:535–40.
[108] Palchonok GI, Breitholtz C, Thunman H, Leckner B. Impact of heat and mass transfer on combustion of a fuel particle in CFB boilers. Proc Int Conf on FBC 1997;14:871–88.
[109] Haider A, Levenspiel O. Drag coefficient and terminal velocity of spherical and nonspherical particles. Powder Technol 1989;58:63–70.
[110] Corella J, Sanz A. Modeling circulating fluidized bed biomass gasifiers. A pseudo-rigorous model for stationary state. Fuel Proc Technol 2005;86: 1021–53.
[111] Yan HM, Heidenreich C, Zhang DK. Modelling of fluidised – bed coal gasifiers: elimination of the combustion product distribution coefficient by considering homogeneous combustion. Chem Eng Process 1999;39:229–37.
[112] Leckner B, Lyngfelt A. Optimization of emissions from fluidized bed combustion of coal, biofuel and waste. Int J Energy Res 2002;26:1191–202.
[113] Gómez-Barea A, Nilsson S, Vidal-Barrero FD, Campoy M. Devolatilization behavior of wood and wastes under fluidized bed conditions, submitted for publication.
[114] Davidson JF, Harrison D, editors. Fluidization. 2nd ed. London: Academic Press; 1985.
[115] Basu P. Combustion and gasification in fluidized beds. Boca Raton (FL): Taylor and Francis; 2005.
[116] Gogolek PEG, Grace JR. Fundamental hydrodynamics related to pressurized fluidized bed combustion. Prog Energy Combust Sci 1995;21:419–51.
[117] Pallarès D, Johnsson F. Macroscopic modelling of fluid dynamics in large-scale circulating fluidized beds. Prog Energy Combust Sci 2006;32:539–69.
[118] Svensson A, Johnsson F, Leckner B. Bottom bed regimes in a circulating fluidized bed boiler. Int J Multiphase Flow 1996;22:1187–204.
[119] Wen CY, Yu YH. A generalized method for predicting the minimum fluidization velocity. AIChE J 1966;12:610–2.
[120] Ergun S. Fluid flow through packed columns. Chem Eng Prog 1952;48: 89–94.
[121] Darton RC, LaNauze RD, Davidson JF, Harrison D. Bubble-growth due to coalescence in fluidized beds. Trans Inst Chem Eng 1977;55:274–80.
[122] Mori S, Wen CY. Estimation of bubble diameter in gaseous fluidized beds. AIChE J 1975;21:109–15.
[123] Stubington JF, Barret D, Lowry G. Bubble size measurements and correlation in a fluidized bed at high temperature. Chem Eng Res Design 1984;62:173–8.
[124] Horio M, Nonaka AA. Generalized bubble diameter correlation for gas-solid fluidized beds. AIChE J 1987;33:1865–72.
[125] Johnsson F, Andersson S, Leckner B. Expansion of a freely bubbling fluidized bed. Powder Technol 1991;68:117–23.
[126] Grace JR, Clift R. On the two-phase theory of fluidization. Chem Eng Sci 1974;141:53–62.
[127] Werther J. Influence of the bed diameter on the hydrodynamics of gas fluidized beds. In: Keairns DL, editor. Fluidization and fluid-particle systems, vol. 70; 1974. p. 53–62.
[128] Zijerveld RC, Koniuta A, Johnsson F, Marzocchella A. Axial solids distribution and bottom bed dynamics for CFBC application. AIChE Symp Ser 1997;93: 97–102.
[129] Babu P, Shah B, Talwalker A. Fluidization correlations for coal gasification materials—minimum fluidization velocity and fluidized bed expansion ratio. AIChE Symp Ser 1978;74:176–86.
[130] Delvosalle C, Vanderschuren J. Gas-to-particles and particle-to-particle heat transfer in fluidized beds of large particles. Chem Eng Sci 1985;40: 769–79.
[131] Partridge BA, Rowe PN. Chemical reaction in a bubbling gas-fluidized beds. Trans Inst Chem Eng 1966;44:335–47.
[132] Sit SP, Grace JR. Effect of bubble interaction on interphase mass transfer in gas fluidized beds. Chem Eng Sci 1981;36:327–35.
[133] Werther J, Wein J. Expansion of gas fluidized beds in the turbulent regime. AIChE Symp Ser 1994;90:31–44.
[134] Solimene R, Marzocchella A, Salatino P. Hydrodynamic interaction between a coarse gas-emitting particle and a gas fluidized bed of finer solids. Powder Technol 2003;133:79–90.
[135] Bruni G, Solimene R, Marzocchella A, Salatino P, Yates JG, Lettieri P, et al. Self-segregation of high-volatile fuel particles during devolatilisation in a fluidized bed reactor. Powder Technol 2002;128:11–21.
[136] Wen CY, Chen LH. Fluidized bed freeboard phenomena entrainment and elutriation. AIChE J 1982;28:117–28.
[137] Colaykan M, Levenspiel O. Elutriation from fluidized beds. Powder Technol 1984;38:223–32.
[138] Johansson A, Johnsson F, Leckner B. Solids back-mixing in CFB boilers. Chem Eng Sci 2007;62:561–73.
[139] Johnsson F, Leckner B. Vertical distribution of solids in a CFB-furnace. Int Conf FBC 1995;13:266–73.
[140] Johnsson F, Zhang W, Leckner B. Characteristics of the formation of particle wall layers in CFB boilers. In: Serizawa A, Fukano T, Battaille J, editors. Proc second int conf on multiphase flow. Kyoto: Japan Society of Multiphase Flow; 1995. p. 3. p. FB1-25.
[141] Zhang W, Johnsson F, Leckner B. Characteristics of the lateral particle distribution in CFB boilers. In: Avidan AA, editor, 4th Int Conf on CFB; 1993, pp. 266–73.
[142] Leith D, Licht W. The collection efficiency of cyclone type particle collectors—a new theoretical approach. AIChE Symp Ser 1972;68:196–206.
[143] Zhang R, Basu P. A simple model for prediction of solid collection efficiency of a gas–solid separator. Powder Technol 2004;147:86–93.
[144] Cortés C, Gil A. Modeling the gas and particle flow inside cyclone separators. Prog Energy Combust Sci 2007;33:409–52.
[145] Souza-Santos ML. Comprehensive modelling and simulation of fluidized bed boilers and gasifiers. Fuel 1989;68:1507–21.
[146] Jennen T, Hiller R, Koneke D, Weinspach PM. Modeling of gasification of wood in a circulating fluidized bed. Chem Eng Tech 1999;22:822–6.
[147] Sadaka SS, Ghaly AE, Sabbah MA. Two phase biomass air–steam gasification model for fluidized bed reactors: Part I – model development. Biomass Bioenergy 2002;22:439–62.

[148] Bazardorj B, Sonoyama N, Hayashi J-I, Hosokai S, Li C-Z, Chiba T. Inhibition of steam gasification of char in a fluidized-bed under continuous feeding of a Victorian brown coal. Fuel 2006;85:340–9.
[149] Leckner B. Heat and mass transfer. In: Crowe C, editor. Multiphase flow handbook. Boca Raton (FL): CRC Press; 2006 [chapter 5.2].
[150] Roberts Af A. Review of kinetics data for the pyrolysis of wood and related substances. Combust Flame 1970;14:261–72.
[151] Shafizadeh F. Introduction to pyrolysis of biomass. J Anal Appl Pyrolysis 1982;3:283–305.
[152] Antal Jr MJ. Effects of reactor severity on the gas-phase pyrolysis of celulose- and kraft lignin-derived volatile matter. Ind Eng Chem Prod Res Dev 1983;22:366–75.
[153] Hansson KM. Principles of biomass pyrolysis with emphasis on the formation of the nitrogen-containing gases HNCO, HCN and NH_3. PhD thesis. Chalmers University of Technology; 2003.
[154] Kersten SRA, Wang X, Prins W, van Swaaij WPM. Biomass pyrolysis in a fluidized bed reactor. Part 1: Literature review and model simulations. Ind Eng Chem Res 2005;44:8773–85.
[155] Shafizadeh F, Chin PPS. Thermal deterioration of wood. ACS Symp Ser 1977;43:57–81.
[156] Pitt GJ. The kinetics of the evolution of volatile products from coal. Fuel 1962;41:267–74.
[157] Anthony DB, Howard JB, Hottel HC, Meissner HP. Rapid devolatilisation of pulverised coal. Proc Combust Inst 1975;15:1303–17.
[158] de Diego LF, García-Labiano F, Abad A, Gayán P, Adánez J. Modeling of the devolatilization of nonspherical wet pine wood particles in fluidized beds. Ind Eng Chem Res 2002;41:3642–50.
[159] Loison R, Chauvin R. Pyrolyse rapide du charbon. Chemie Indust 1964;91:269–75.
[160] Hajaligol MR, Howard JB, Longwell JP, Peters WA. Product compositions and kinetics for rapid pyrolysis of cellulose. Ind Eng Chem Process Des Dev 1982;21:457–65.
[161] Nunn TR, Howard JB, Longwell JP, Peters WA. Product compositions and kinetics in the rapid pyrolysis of sweet gum hardwood. Ind Eng Chem Proc Des Dev 1985;24:836–44.
[162] Boroson ML, Howard JB, Longwell JP, Peters WA. Product yields and kinetics from the vapor phase cracking of wood pyrolysis tars. AIChE J 1989;35:120–8.
[163] Jand N, Foscolo PU. Decomposition of wood particles in fluidized beds. Ind Eng Chem Res 2005;44:5079–89.
[164] Gavalas GR, Cheong PH, Jain R. Model of coal pyrolysis. 1. Qualitative development. Ind Eng Chem Fund 1981;20:113–22.
[165] Gavalas GR, Cheong PH, Jain R. Model of coal pyrolysis. 2. Quantitative formulation and results. Ind Eng Chem Fund 1981;20:122–32.
[166] Niksa S, Kerstein AR. On the role of macromolecular configuration in rapid coal devolatilization. Fuel 1987;66:1389–99.
[167] Solomon PR, Hamblen DG, Carangelo RM, Serio MA, Deshpande GV. General model of coal devolatilization. Energy Fuels 1988;2:405–22.
[168] Niksa S, Kerstein AR. Flashchain theory for rapid coal devolatilization kinetics. 1: Formulation. Energy Fuels 1991;5:647–65.
[169] Niksa S. Flashchain theory for rapid coal devolatilization kinetics. 2: Impact of operating conditions. Energy Fuels 1991;5:665–73.
[170] Grant DM, Pugmire RJ, Fletcher TH, Kerstein AR. A chemical model of coal devolatilization using percolation lattice statistics. Energy Fuels 1989;3:175–86.
[171] Chen Y, Charpenay S, Jensen A, Wojtowicz MA, Serio MA. Modeling of biomass pyrolysis kinetics. Proc Combust Inst 1998;27:1327–34.
[172] Niksa S. Predicting the rapid devolatilization of diverse forms of biomass with bio-flashchain. Proc Combust Inst 2000;8:2727–33.
[173] de Jong W, Di Nola G, Venneker BCH, Spliethoff H, Wojtowicz MA. TG-FTIR pyrolysis of coal and secondary biomass fuels: determination of pyrolysis kinetic parameters for main species and NO_x precursors. Fuel 2007;86:2367–76.
[174] Ranzi E, Cuoci A, Faravelli T, Frassoldati A, Migliavacca G, Pierucci S, et al. Chemical kinetics of biomass pyrolysis. Energy Fuels 2008;22:4292–300.
[175] Sheng C, Azevedo JLT. Modeling biomass devolatilization using the chemical percolation devolatilization model for the main components. Proc Combust Inst 2002;29:407–14.
[176] Agarwal PK, Genetti WE, Lee YY. Coupled drying and devolatilization of wet coal in fluidized beds. Chem Eng Sci 1986;41:2373–83.
[177] Saastamoinen J, Richard JR. Simultaneous drying and pyrolysis of solid fuel particles. Combust Flame 1996;106:288–300.
[178] Miller RS, Bellan J. Analysis of reaction products and conversion time in the pyrolysis of cellulose and wood particles. Combust Sci Technol 1996;119:331–73.
[179] Peters B, Bruch C. Drying and pyrolysis of wood particles: experiments and simulation. J Anal Appl Pyrolysis 2003;70:233–50.
[180] Di Blasi C. The state of the art of transport models for charring solid degradation. Polym Int 2000;49:1133–46.
[181] Bryden KM, Ragland KW, Rutland CJ. Modeling thermally thick pyrolysis of wood. Biomass and Bioenergy 2002;22:41–53.
[182] Wurzenberger JC, Wallner S, Raupenstrauch H, Khinast JG. Thermal conversion of biomass: comprehensive reactor and particle modeling. AIChE J 2002;48:2398–411.
[183] Thunman H, Leckner B, Niklasson F, Johnsson F. Combustion of wood particles—a particle model for Eulerian calculations. Combust Flame 2002;129:30–46.
[184] Sreekanth M, Kolar AK, Leckner B. Transient thermal behaviour of a cylindrical wood particle during devolatilization in a bubbling fluidized bed. Fuel Proc Technol 2008;89:838–50.
[185] Sreekanth M, Kolar AK, Leckner B. A semi-analytical model to predict primary fragmentation of wood in a bubbling fluidized bed combustor. J Anal Appl Pyrolysis 2008;83:88–100.
[186] Sreekanth M, Renu K, Kolar AK, Leckner B. Estimation of wood char size at the end of devolatilization in a bubbling fluidized bed combustor. Fuel 2008;87:3393–402.
[187] Sreekanth M, Sudhakar DR, Prasad BVSSS, Kolar AK, Leckner B. Modelling and experimental investigation of devolatilizing wood in a fluidized bed combustor. Fuel Proc Technol 2008;89:838–50.
[188] Hamel S, Krumm W. Mathematical modelling and simulation of bubbling fluidised bed gasifiers. Powder Technol 2001;120:105–12.
[189] Dupont C, Chen L, Cances J, Commandre JM, Cuoci A, Pierucci S, et al. Biomass pyrolysis: kinetic modelling and experimental validation under high temperature and flash heating rate conditions. J Anal Appl Pyrolysis 2009;85:260–7.
[190] Pyle DL, Zaror CA. Heat transfer and kinetics in the low temperature pyrolysis of solids. Chem Eng Sci 1984;39:147–58.
[191] Font R, Marcilla A, Devesa J, Verdu E. Kinetic study of the flash pyrolysis of almond shells in a fluidized bed reactor at high temperatures. J Anal Appl Pyrolysis 1993;27:245–73.
[192] Davidsson KO, Pettersson JBC, Bellais M, Liliedahl T, Sjöström K. The pyrolysis kinetics of a single wood particle. In: Bridgwater AV, editor. Progress in thermochemical biomass conversion. NJ: Blackwell Science; 2001. p. 1129–42.
[193] Brink DL, Massoudi MS. A flow reactor technique for the study of wood pyrolysis. I. Experimental. J Fire Flammab 1978;9:176–88.
[194] Biagini E, Fantozzi C, Tognotti L. Characterization of devolatilization of secondary fuels in different conditions. Combust Sci Technol 2004;176:685–703.
[195] Lewellen PC, Peters WA, Howard JB. Cellulose pyrolysis kinetics and char formation mechanism. Proc Inst Combust 1977;16:1471–80.
[196] Kosstrin HM. Direct formation of pyrolysis oil from biomass. In Proc Specialists Workshop on Fast Pyrolysis of Biomass, Copper Mountain, Colorado; 1980. pp. 105–21.
[197] Richard N, Thunman H. Report. Available from, www.entek.chalmers.se/~heth/; 2002.
[198] Thunman H, Davidsson K, Leckner B. Separation of drying and devolatilization during conversion of solid fuels. Combust Flame 2004;137:242–50.
[199] Heisler MP. Temperature charts for induction and constant – temperature heating. ASME Trans 1947;69:227–36.
[200] Gröber H, Erk S, Grigull U. Fundamentals of heat transfer. 3rd ed. New York: McGraw-Hill; 1961.
[201] Ostrogorsky AG, Mikic BB. Explicit equations for transient heat conduction in finite solids for $Bi > 2$. Heat Mass Transfer 2009;45:375–80.
[202] Ostrogorsky AG. Simple explicit equations for transient heat conduction in finite solids. J Heat Trans 2009;131(1):011303. doi:10.1115/1.2977540. 11 pages.
[203] Scott SA, Davidson JF, Dennis JS, Hayhurst AN. The devolatilisation of particles of a complex fuel (dried sewage sludge) in a fluidised bed. Chem Eng Sci 2007;62:584–98.
[204] Leckner B, Hansson KM, Tullin C, Borodulya AV, Dikalenko VI, Palchonok GI. Kinetics of fluidized bed combustion of wood pellets. Proc Int Conf on Fluidized Bed Combustion; 1999;15:Paper 47.
[205] Grønli M. A theoretical and experimental study of the thermal degradation of biomass, Doctoral Thesis, Norwegian University of Science and Technology, Trondheim; 1996.
[206] Dupont C, Boissonnet G, Seiler JM, Gauthier P, Schweich D. Study about the kinetic processes of biomass steam gasification. Fuel 2006;86:32–40.
[207] Ross DP, Heidenreich CA, Zhang DK. Devolatilisation times of coal particles in a fluidised-bed. Fuel 2000;79:873–83.
[208] de Diego LF, García-Labiano F, Abad A, Gayán P, Adánez J. Effect of moisture content on devolatilization times of pine wood particles in a fluidized bed. Energy Fuels 2003;17:285–90.
[209] Kumar RR, Kolar AK, Leckner B. Effect of fuel particle shape and size on devolatilization time of Casuarina wood. In: Bridgwater AV, Bookock DGB, editors. Proceeding on science in thermal and chemical biomass conversion. Newbury Burks: CPL Press; 2004. p. 1251–64.
[210] de Diego LF, García F, -Labiano, Abad A, Gayán P, Adánez J. Coupled drying and devolatilisation of non-spherical wet pine wood particles in fluidised beds. Journal of Analytical and Applied Pyrolysis 2002;65:173–84.
[211] Wang Y, Kinoshita CM. Kinetic model of biomass gasification. Solar Energy 1993;51:19–25.
[212] Bilodeau JF, Thérien N, Proulx P, Czernik S, Chornet E. A mathematical model of fluidized bed biomass gasification. Can J Chem Eng 1993;71:549–77.
[213] Konttinen J, Hupa M, Moilanen A, Kurkela E. Carbon conversion predictor for fluidized bed gasification of biomass fuels–model concept. In: Bridgwater AV, Boocock DGB, editors. Science in thermal and chemical biomass conversion. Newbury, Berks, UK: CPL Press; 2006. p. 590–604.
[214] Thunman H, Niklasson F, Johnsson F, Leckner B. Composition of volatile gases and thermochemical properties of wood for modeling of fixed or fluidized beds. Energy Fuels 2001;15:1488–97.

[215] Neves D, Thunman H, Seemann M, Ideias P, Matos A, Tarelho L, et al. Proc 17th European Biomass Conference and Exhibition. Hamburg: Germany; 2009. 1018–1028.
[216] Di Blasi C. Combustion and gasification rates of lignocellulosic chars. Prog Energy Combust Sci 2009;35:121–40.
[217] Bhatia SK, Perlmutter DD. A random pore model for fluid-solid reactions: I. Isothermal, kinetic control. AIChE J 1980;26:379–86.
[218] Adschiri T, Shiraha T, Kojima T, Furusawa T. Prediction of CO_2 gasification rate of char in fluidized-bed gasifier. Fuel 1986;65:1688–93.
[219] van den Aarsen FG. Fluidised bed wood gasifier. Performance and modelling, Ph.D. dissertation, Twente University Publication, University of Twente; 1985.
[220] Zhang Y, Ashizawa M, Kajitani S, Miura K. Proposal of a semi-empirical kinetic model to reconcile with gasification reactivity profiles of biomass chars. Fuel 2008;87:475–81.
[221] Simons GA. The unified coal-char reaction. Fuel 1980;59:143–4.
[222] Johnson JL. Kinetics of coal gasification. New York: Wiley; 1979.
[223] Dutta S, Wen CY, Belt RJ. Reactivity of coal and char, 1: carbon dioxide in atmosphere. Ind Eng Chem Proc Des Dev 1977;16:20–30.
[224] Gardner N, Samuels E, Wilks K. Catalysed hydrogasification of coal chars. Adv Chem Ser 1974;131:217–36.
[225] Kasaoka S, Sakata Y, Tong C. Kinetic evaluation of the reactivity of various coal chars for gasification with carbon dioxide in comparison with steam. Int Chem Eng 1985;25:160–75.
[226] Ollero P, Serrera A, Arjona R, Alcantarilla S. The CO_2 gasification kinetics of olive waste. Biomass and Bioenergy 2003;24:151–61.
[227] Gómez-Barea A, Ollero P, Arjona R. Reaction-diffusion model of TGA gasification experiments for estimating diffusional effects. Fuel 2005;84: 1695–704.
[228] Rensfelt E, Blomkvist G, Ekström C, Engström S, Espenäs BG, Liinanki L. Basic gasification studies for development of biomass medium-btu gasification processes. In: Klass DL, Waterman WW, editors. Energy from biomass and wastes III. Chicago: Institute of Gas Technology; 1978. p. 465–94.
[229] Luo C, Watanabe T, Nakamura M, Uemiya S, Kojima T. Gasification kinetics of coal chars carbonized under rapid and slow heating conditions at elevated temperatures. J Energy Resources Technol 2001;123:21–6.
[230] Matsui I, Kunii D, Furusawa T. Study of char gasification by carbon dioxide. 1. Kinetic study by thermogravimetric analysis. Ind Eng Chem Res 1987;26: 91–5.
[231] Petersen I, Werther J. Experimental investigation and modeling of gasification of sewage sludge in the circulating fluidized bed. Chem Eng Process 2005;44:717–36.
[232] Liu H, Gibbs BM. Modeling NH_3 and HCN emissions from biomass circulating fluidized biomass gasifiers. Fuel 2003;82:1591–604.
[233] Luo C, Aoki K, Uemiya S, Kojima T. Numerical simulation of a jetting fluidized bed gasifier and the comparison to the experimental data. Fuel Proc Technol 1998;55:193–218.
[234] Gómez-Barea A, Ollero P, Leckner B. Mass transport effects during measurements of gas–solid reaction kinetics in a fluidised bed. Chem Eng Sci 2007;62:1477–93.
[235] Zanzi R, Sjöström K, Björnbom E. Rapid pyrolysis of agricultural residues at high temperature. Biomass and Bioenergy 2002;23:357–66.
[236] Fushimi C, Araki K, Yamaguchi Y, Tsutsumi A. Effect of heating rate on steam gasification of biomass. 1 Reactivity of char. Ind Eng Chem Res 2003;42: 3922–8.
[237] Srinivas B, Amundson NR. A single-particle char gasification model. AIChE J 1980;26:487–96.
[238] Bliek A, Lont JC, van Swaaij WPM. Gasification of coal-derived chars in synthesis gas-mixtures under intraparticle mass-transfer-controlled conditions. Chem Eng Sci 1986;41:1895–909.
[239] Doraiswamy LK, Sharma MM. Heterogeneous reactions. Analysis, examples and reactor design, vol. 1. New York: Wiley; 1984.
[240] Mantri VB, Gokarn AN, Doraiswamy LK. Analysis of gas–solid reactions: formulation of a general model. Chem Eng Sci 1976;31:779–85.
[241] Levenspiel O. Chemical reaction engineering. 3rd ed. New York: Wiley; 1999.
[242] Wen CY. Noncatalytic heterogeneous solid fluid reactions. Ind Eng Chem 1968;60:34–54.
[243] Szekely J, Evans JW, Sohn HY. Gas–solid reactions. New York: Academic Press; 1976.
[244] Froment GF, Bischoff KB. Chemical reactor analysis and design. 2nd ed. New York: Wiley; 1990.
[245] Yang YB, Sharifi VN, Swithenbank J, Ma L, Darvell LI, Jones JM, et al. Combustion of a single particle of biomass. Energy Fuels 2008;22: 306–16.
[246] Lu H, Robert W, Peirce G, Ripa B, Baxter LL. Comprehensive study of biomass particle combustion. Energy Fuels 2008;22:2826–39.
[247] Winter F, Prah ME, Hofbauer H. Temperatures in a fuel particle burning in a fluidized bed: the effect of drying, devolatilization, and char combustion. Combust Flame 1997;108:302–14.
[248] Canò G, Salatino P, Scala F. A single particle model of the fluidized bed combustion of a char particle with a coherent ash skeleton: application to granulated sewage sludge. Fuel Proc Technol 2007;88:577–84.
[249] Hurt RH, Calo JM. Semi-global intrinsic kinetics for char combustion modeling. Combust Flame 2001;125:1138–49.
[250] Dennis JS, Lambert RJ, Milne AJ, Scott SA, Hayhurst AN. The kinetics of combustion of chars derived from sewage sludge. Fuel 2005;84:117–26.
[251] Basu P. Combustion of coal in circulating fluidized-bed boilers: a review. Chem Eng Sci 1999;54:5547–57.
[252] Arthur JR. Reactions between carbon and oxygen. Trans Faraday Soc 1950;47: 164–78.
[253] Ashman PJ, Mullinger PJ. Research issues in combustion and gasification of lignite. Fuel 2005;84:1195–205.
[254] Kulasekaran S, Linjewile TM, Agarwal PK, Biggs MJ. Combustion of a porous char particle in an incipiently fluidized bed. Fuel 1998;77:1549–60.
[255] Chang YH. A mathematical model for the gasification of a single char article of coal. Int Chem Eng 1988;28:520–6.
[256] Morell JI, Amundson NR, Park SK. Dynamics of a single particle during char gasification. Chem Eng Sci 1990;45:387–401.
[257] Fiaschi D, Bettagli N, Desideri U. A Biomass combustion—gasification model: validation and sensitivity analysis. J Energy Resources Technol 1995;117:329–36.
[258] Barrio M, Hustad JE. CO_2 gasification of birch and the effect of CO inhibition on the calculation of chemical kinetics. In: Bridgwater AV, editor. Proc Conf: progress in thermochemical biomass conversion; 2000. Tyrol, Austria.
[259] Mermoud F, Golfier F, Salvador S, Van de Steene L, Dirion JL. Experimental and numerical study of steam gasification of a single charcoal particle. Combust Flame 2006;145:59–79.
[260] Britten JA. Extinction phenomena in countercurrent packed-bed coal gasifiers: a simple model for gas production and char conversion rates. Ind Eng Chem Res 1988;27:197–203.
[261] Gómez-Barea A, Leckner B. Char gasification model for circulating fluidized beds. Proc 16th European Biomass Conference, Valencia, Spain; 2008, pp. 747–55.
[262] Gómez-Barea A, Leckner B, Santana D, Ollero P. Gas–solid conversion in fluidised beds. Chem Eng J 2008;141:151–68.
[263] Heesink ABM, Klaus J, van Swaaij WPM. Influence of particle residence time distribution on the reactivity in fluidized bed reactors. Chem Eng Sci 1994;49:2243–61.
[264] Caram HS, Amundson NR. Fluidized bed gasification reactor modeling 2. Effect of the residence time distribution and mixing of particles. Staged bed modelling. Ind Eng Chem Proc Des Dev 1978;18:96–102.
[265] Gómez-Barea A, Leckner B. Evaluation of char reaction rate in a fluidised bed gasifier: from reactivity determination to reactor simulation. Proc 17th European Biomass Conference; 2009. Hamburg, Germany.
[266] Chirone R, Massimilla L, Salatino P. Comminution of carbons in fluidized bed combustion. Prog Energy Combust Sci 1991;17:297–326.
[267] Marban G, Pis JJ, Fuertes AB. Characterizing fuels for atmospheric fluidized bed combustion. Combust Flame 1995;103:41–58.
[268] Scala F, Salatino P, Chirone R. Fluidized bed combustion of a biomass char (*Robinia pseudoacacia*). Energy Fuels 2000;14:781–90.
[269] Scala F, Chirone R, Salatino P. Combustion and attrition of biomass chars in a fluidized bed. Energy Fuels 2006;20:91–102.
[270] Chirone R, Salatino P, Scala F. The relevance of attrition on the fate of ashes during fluidized-bed combustion of a biomass. Proc Combust Inst 2000;28: 2279–86.
[271] Scala F, Chirone R. Characterization and early detection of bed agglomeration during the fluidized bed combustion of olive husk. Energy Fuels 2006;20: 120–32.
[272] Thunman H. Principles and models of solid fuel combustion. Ph.D. dissertation, Chalmers University of Technology, Gothenburg, Sweden; 2001.
[273] Feng B, Bhatia SK. Percolative fragmentation of char particles during gasification. Energy Fuels 2000;14:297–307.
[274] Donsi G, Massimilla L, Miccio M. Carbon fines production and elutriation from the bed of a fluidized coal combustor. Combust Flame 1981;41:57–69.
[275] Halder PK. Combustion of single coal particles in circulating fluidized bed, Ph.D. thesis, Technical University of Nova Scotia; 1989.
[276] Merrick D, Highley J. Particle size reduction and elutriation in a fluidized bed process. AIChE Symp Ser 1974;70:366–78.
[277] Salatino P, Massimila L. A descriptive model of carbon attrition in the fluidized combustion of coal char. Chem Eng Sci 1985;40:1905–16.
[278] Arena U, Chirone R, D'Amore M, Miccio M, Salatino P. Some issues in modelling bubbling and circulating fluidized-bed coal combustors. Powder Technol 1995;82:301–16.
[279] Salatino P, Scala F, Chirone R. Fluidized bed combustion of a biomass char: the influence of carbon attrition on fixed carbon conversion. Proc Symp Combust 1996;27:3103–10.
[280] Palchonok GI, Leckner B, Tullin C, Martinsson L, Borodulya A. Combustion characteristics of wood pellets. The 1st World Pellets Conference, Jönköping; 2002.
[281] Saastamoinen JJ, Shimizu T. Attrition-enhanced sulfur capture by limestone particles in fluidized beds. Ind Eng Chem Res 2007;46:1079–90.
[282] Salatino P. Survey of particle attrition phenomena relevant to fluidized bed combustion and gasification of solid fuels. Leslie J Ford Lecture – 8th Particle Technology Forum, Cambridge; 2007.
[283] Delgado J, Aznar MP, Corella J. Biomass gasification with steam in fluidized bed: effectiveness of CaO, MgO, and CaO–MgO for hot raw gas cleaning. Ind Eng Chem Res 1997;36:1535–43.
[284] Reed TB, Levie B, Markson ML, Graboski MS. A mathematical model for stratified downdraft gasifiers. ACS Div Fuel Chem 1983;28(5):410–20.
[285] Chen WJ, Sheu FR, Savage RL. Catalytic activity of coal ash on steam methane reforming and water–gas shift reactions. Fuel Proc Technol 1987;16:279–88.

[286] Valk M, de Jong P. Fluid bed combustion of coal: a film. Proc Int Conf Fluid Bed Combust 1989;10:1363–5.
[287] Jensen A, Johnsson JE, Andries J, Laughlin K, Read G, Mayer M. Formation and reduction of NO_x in pressurized fluidized bed combustion of coal. Fuel 1995;74:1555–69.
[288] Desroches-Ducarne E, Dolignier JC, Marty G, Martin E, Delfosse L. Modelling of gaseous pollutants emissions in circulating fluidized bed combustion of municipal refuse. Fuel 1998;77:1399–410.
[289] Dryer FL, Glassman I. High-temperatue oxidation of CO and CH_4. Proc 14th Symp (Int) Combust; 1973, pp. 987–1003.
[290] Howard JB, Williams GC, Fine DH. Kinetics of carbon monoxide oxidation in postflame gases. Proc 14th Symp (Int) Combust; 1973, pp. 975–86.
[291] Hottel HC, Williams GC, Nerheim NM, Schneider GR. Kinetic studies in stirred reactors: combustion of carbon monoxide and propane. Proc 10th Symp (Int) Comb; 1965, pp. 111–21.
[292] Yetter RA, Dryer FL, Rabitz H. Complications of one-step kinetics for moist CO oxidation. Proc 21st Symp (Int) Comb; 1986, pp. 749–60.
[293] Mitani T, Williams FA. Studies of cellular flames in hydrogen-oxygen-nitrogen mixtures. Combust Flame 1980;39:169–90.
[294] Groppi G, Tronconi E, Forzatti P, Berg M. Mathematical modelling of catalytic combustors fuelled by gasified biomasses. Catalysis Today 2000;59:151–62.
[295] Di Blasi C. Dynamic behaviour of stratified downdraft gasifiers. Chem Eng Sci 2000;55:2931–44.
[296] Haslam RT. The simultaneous combustion of hydrogen and carbon monoxide. Ind Eng Chem 1923;15:679–81.
[297] Vilienskii TV, Hezmalian DM. Dynamics of the combustion of pulverized fuel. Energia 1978;11:246–51.
[298] Kerinin EV, Shifrin EI. Mathematical model of coal combustion and gasification in a passage of an underground gas generator. Combustion, explosion and shock waves. Russian Academy of Sciences; 1993. pp. 148–54.
[299] Bryden KM, Ragland KW. Numerical modeling of a deep, fixed bed combustor. Energy Fuels 1996;10:269–75.
[300] Jones WP, Lindstedt RP. Global reaction schemes for hydrocarbon combustion. Combust Flame 1988;73:233–49.
[301] Westbrook CK, Dryer FL. Chemical kinetic modeling of hydrocarbon combustion. Prog Energy Combust Sci 1984;10:1–57.
[302] Biba V, Macak J, Klose E, Malecha J. Mathematical model for the gasification of coal under pressure. Ind Eng Chem Process Des Dev 1978;17:92–8.
[303] Yoon H, Wei J, Denn MM. A model for moving bed coal gasification reactors. AIChE J 1978;24:885–903.
[304] Good J, Ventress L, Knoef H, Zielke U, Hansen PL, van de Kamp W, et al. Sampling and analysis of tar and particles in biomass producer gases. CEN BT/TF 143 ''Organic Contaminants (''Tar'') in Biomass''.
[305] Kinoshita CM, Wang Y, Zhou J. Tar formation under different biomass gasification conditions. J Anal Appl Pyrolysis 1994;29:169–81.
[306] Brage C, Yu Q, Chen G, Sjöström K. Tar evaluation profiles obtained from gasification of biomass and coal. Biomass Bioenergy 2000;18: 87–91.
[307] Milne TA, Abatzoglou N, Evance RJ. Biomass gasifire ''tars'': their nature, formation and conversion. NREL/TP-570-25357; 1998, pp. 1–68.
[308] Devi L, Ptasinski KJ, Janssen FJJG. A review of the primary measures for tar elimination in biomass gasification processes. Biomass and Bioenergy 2002; 24:125–40.
[309] Corella J, Herguido J, Alday FJ. Pyrolysis and steam gasification of biomass in fluidized beds: influence of the type and location of the biomass feeding point on the product distribution. In: Bridgwater AV, Kuester JL, editors. Research in thermochemical biomass conversion. London: Elsevier Applied Science; 1988. p. 384–98.
[310] Olivares A, Aznar MP, Caballero MA, Gil J, Frances E, Corella J. Biomass gasification: produced gas upgrading by in-bed use of dolomite. Ind Eng Chem Res 1997;36:5220–6.
[311] Devi L. Catalytic removal of biomass tars; olivine as prospective in-bed catalyst for fluidized-bed biomass gasifiers. PhD thesis. Technical University of Eindhoven, Eindhoven, The Netherlands; 2005.
[312] Rapagna S, Jand N, Kiennemann A, Foscolo PU. Steam-gasification of biomass in a fluidised-bed of olivine particles. Biomass Bioenergy 2000;19:187–97.
[313] Corella J, Toledo JM, Padilla R. Olivine or dolomite as in-bed additive in biomass gasification with air in a fluidized bed: which is better? Energy Fuels 2004;18:713–20.
[314] Abu El-Rub Z, Bramer EA, Brem G. Experimental comparison of biomass chars with other catalyst for tar reduction. Fuel 2008;87:2243–52.
[315] Abu El-Rub Z, Bramer EA, Brem G. Review of catalysts for tar elimination in biomass gasification processes. Ind Eng Chem Res 2004;43:6911–9.
[316] Sutton D, Kelleher B, Ross JRH. Review of literature on catalysts for biomass gasification. Fuel Proc Technol 2001;73:155–73.
[317] Simell P. Catalytic hot gas cleaning of gasification gas. No 330. VTT Publication; 1997.
[318] Dayton D. A review of the literature on catalytic biomass tar destruction. National Renewable Energy Laboratory, NREL/TP-510-32815; 2002.
[319] Evans RJ, Milne TA. Molecular characterization of the pyrolysis of biomass. 1. Fundamentals. Energy Fuels 1987;1:123–37.
[320] Morf P. Secondary reactions of tar during thermochemical biomass conversion. Ph.D. thesis. Swiss Federal Institute of Technology, Zurich; 2002.
[321] Fiorenza G, Canonaco J, Galvagno G, Braccio S. An advanced model for the prediction of tar content in the product gas from biomass steam gasification. In: Bridgwater AV, editor. Success and visions for bioenergy. Newbury: CPL Press, ISBN 978-1-872691-28-2; 2007.
[322] Kiel JHA, van Paasen SVB, Neeft JPA, Devi L, Ptasinski KJ, Janssen FJJG, et al. Primary measures to reduce tar formation in fluidized-bed biomass gasifiers. Report ECN-C-04-014, The Netherlands; 2004.
[323] Han J, Kim H. The reduction and control technology of tar during biomass gasification/pyrolysis: an overview. Renew Sustain Energy Rev 2008;12: 397–416.
[324] Gerun L, Paraschiv M, Vijeu R, Bellettre J, Tazerout M, Gobel B, et al. Numerical investigation of the partial oxidation in a two-stage downdraft gasifier. Fuel 2008;87:1383–93.
[325] Taralas G, Kontominas M, Kakatsios X. Modeling the thermal destruction of toluene as tar-related species for fuel-gas cleanup. Energy Fuels 2003;17:329–37.
[326] Jess A. Catalytic upgrading of tarry fuel gases: a kinetic study with model components. Chem Eng Process 1996;35:487–94.
[327] Corella J, Toledo JM, Aznar MP. Improving the modeling of the kinetics of the catalytic tar elimination in biomass gasification. Ind Eng Chem Res 2002;41:3351–6.
[328] Corella J, Caballero MA, Aznar MP, Brage C. Two advanced models for the kinetics of the variation of the tar composition in its catalytic elimination in biomass gasification. Ind Eng Chem Res 2003;42:3001–11.
[329] Sanz A, Corella J. Modeling circulating fluidized bed biomass gasifiers. Results from a pseudo-rigorous 1-dimensional model for stationary state. Fuel Proc Technol 2006;87:247–58.
[330] Corella J, Toledo JM, Molina G. Calculation of the conditions to get less than 2 g tar/mn3 in a fluidized bed biomass gasifier. Fuel Proc Technol 2006;87: 841–6.
[331] van Riessen GJ. Reactions in continuous mixtures: modelling tar behaviour during biomass gasification. Report R 2001/130. Apeldoorn: TNO Environment, Energy and Process Innovation; 2001.
[332] Rath J, Staudinger G. Cracking reactions of tar from pyrolysis of spruce wood. Fuel 2001;80:1379–89.
[333] Antal Jr MJ, Varhegyi G. Cellulose pyrolysis kinetics: the current state of knowledge. Ind Eng Chem Res 1995;34:703–17.
[334] Liden AG, Berruti F, Scott DS. A kinetic model for the production of liquids from the flash pyrolysis of biomass. Chem Eng Commun 1988;65: 207–21.
[335] García AN, Font R, Marcilla A. Kinetic study of the flash pyrolysis of municipal waste in a fluidized bed at high temperature. J Anal Appl Pyrolysis 1995;31: 101–21.
[336] Caballero JA, Conesa JA, Font R, Marcilla A. Pyrolysis kinetics of almond shells and olive stones considering their organic fractions. J Anal Appl Pyrolysis 1997;42:159–75.
[337] Sergeant GD, Smith IW. Combustion rate of bituminous coal char in the temperature range 800 to 1700 K. Fuel 1973;52:52–77.
[338] Friderichsen AV, Shin EJ, Evans RJ, Nimlos MR, Dayton DC, Barney EG. The pyrolysis of anisole ($C_6H_5OCH_3$) using a hyperthermal nozzle. Fuel 2001;80: 1747–55.
[339] Lammers G, Beenackers AACM, Corella J. Catalytic tar removal from biomass producer gas with secondary air. In: Bridgwater AV, Boocock DGB, editors. Development in thermochemical biomass conversion, vol. 2. London: Blackie Academic; 1997. p. 1179–93.
[340] González-Sáiz J. Advances in biomass gasification in fluidized bed. Ph.D. thesis, University of Saragossa, Spain. Dept Chem Eng; 1988.
[341] Diebold JP. The cracking kinetics of depolymerized biomass vapors in a continuous tubular reactor. MS thesis, Colorado School of Mines; 1975.
[342] Baumlin S, Broust F, Ferrer M, Meunier N, Marty E, Lédé J. The continuous self stirred tank reactor: measurement of the cracking kinetics of biomass pyrolysis vapours. Chem Eng Sci 2005;60:41–55.
[343] Siminski VJ, Wright FJ, Edelman R, Econmos C, Fortune O. Research on methods of improvising the combustion characteristics of liquid hydrocarbons fuels. General Applied Science Laboratories; 1972.
[344] Orío A, Corella J, Narváez I. Performance of different dolomites on hot raw gas cleaning from biomass gasification with air. Ind Eng Chem Res 1997;36:3800–8.
[345] Narváez I, Corella J, Orío A. Fresh tar (from a biomass gasifier) elimination over a commercial steam-reforming catalyst. Kinetics and effect of different variables of operation. Ind Eng Chem Res 1997;36:317–27.
[346] Aznar MP, Caballero MA, Gil J, Martín JA, Corella J. Commercial steam reforming catalysts to improve biomass gasification with steam–oxygen mixtures. 2. Catalytic tar removal. Ind Eng Chem Res 1998;37:2668–80.
[347] Deng Z, Xiao R, Jin B, Huang H, Shen L, Song Q, et al. Computational fluid dynamics modeling of coal gasification in a pressurized spout-fluid bed. Energy Fuels 2008;22:1560–9.
[348] Sofialidis D, Faltsi O. Simulation of biomass gasification in fluidized beds using computational fluid dynamics approach. Thermal Science 2001;5:95–105.
[349] Oevermann M, Gerber S, Behrendt F. Euler–Euler and Euler–Lagrange modeling of wood gasification in fluidized beds. In Werther J, Nowak W, Wirth K-E, Hartge E-U, editors, Proceedings of 9th Circulating Fluidized Bed Technology; 2008, pp. 733–40.
[350] Wang Y, Yan L. CFD modeling of a fluidized bed sewage sludge gasifier for syngas. Asia-Pacific J Chem Eng 2008;3:161–70.

[351] Chen C, Horio M, Kojima T. Use of numerical modeling in the design and scale-up of entrained flow coal gasifiers. Fuel 2001;80:1513–23.
[352] Wang Y, Yan L. Review CFD studies on biomass thermochemical conversion. Int J Mol Sci 2008;9:1108–30.
[353] Fletcher DF, Haynes BS, Christo FC, Joseph SD. A CFD based combustion model of an entrained flow biomass gasifier. Appl Math Model 2000;24: 165–82.
[354] Papadikis K, Gu S, Bridgwater AV, Gerhauser H. Application of CFD to model fast pyrolysis of biomass. Fuel Proc Technol 2009;90:504–12.
[355] Hoomans BPB, Kuipers JAM, van Swaaij WPM. Granular dynamics simulation of segregation phenomena in bubbling gas-fluidized beds. Powder Technol 2000;109:41–8.
[356] van Wachem BG, Schouten JC, van den Bleek CM, Krishna R, Sinclair JL. Comparative analysis of CFD models of dense gas–solid systems. AIChE J 2001;47:1035–51.
[357] Grace JR, Taghipour F. Verification and validation of CFD models and dynamic similarity for fluidized beds. Powder Technol 2004;139:99–110.
[358] Wang L, Weller CL, Hanna MA. An integrated mathematical model of fluid dynamics, heat transfer and reaction kinetics for fluidized bed gasification of sorghum DDG. Proc AIChE Annual Meeting; 2005, pp. 4206–22.
[359] Nikoo MB, Mahinpey N. Simulation of biomass gasification in fluidized bed reactor using ASPEN PLUS. Biomass Bioenergy 2008;32:1245–54.
[360] Sadaka SS, Ghaly AE, Sabbah MA. Two phase biomass air-steam gasification model for fluidized bed reactors: Part II – model sensitivity. Biomass Bioenergy 2002;22:463–77.
[361] Sadaka SS, Ghaly AE, Sabbah MA. Two phase biomass air–steam gasification model for fluidized bed reactors: Part III – model validation. Biomass Bioenergy 2002;22:479–87.
[362] Raman P, Walawender WP, Fan LT, Chang CC. Mathematical model for the fluid-bed gasification of biomass materials. Application to feedlot manure. Ind Eng Chem Process Des Dev 1981;20:686–92.
[363] Thérien N, Marchand P, Chamberland A, Gravel G. Computer modeling and simulation of a biomass fluidized bed gasifier. Proc XVIII Congress on the use of computers in chemical engineering, CEF87, Gianardi Naxos, Italy; 1987, pp. 187–92.
[364] Corella J, Herguido J, Gonzalez-Saiz J. Steam gasification of biomass in fluidized bed-effect of the type of feedstock. In: Ferrero GL, Maniatis K, Buekens A, Bridgwater AV, editors. Pyrolysis and gasification. London: Elsevier Applied Science; 1989. p. 618–23.
[365] Rath J, Steiner G, Wolfinger MG, Staudinger G. Tar cracking from fast pyrolysis of large beech wood particles. J Anal Appl Pyrolysis 2002;62:83–92.
[366] Liu H, Gibbs BM. Modelling of NO and N_2O emissions from biomass-fired circulating fluidized bed combustors. Fuel 2002;81:271–80.
[367] Chen Z, Sarofim AF, Bockelie MJ, Whitty KJ. Modeling of black liquor gasification in a bubbling fluidized bed. The 21st Annual Int Pittsburgh Coal Conference. Pittsburgh, Pennsylvania USA, Paper G3; 2003.
[368] Kaushal P, Pröll T, Hofbauer H. Model for biomass char combustion in the riser of a dual fluidized bed gasification unit: Part 1 – model development and sensitivity analysis. Fuel Proc Technol 2008;84:651–9.
[369] Chen G, Spliethoff H, Andries J, Glazer MP, Yang LB. Biomass gasification in a circulating fluidized bed–Part I: preliminary experiments and modelling development. Energy Sources 2004;26:485–98.
[370] Mansaray KG, Al-Taweel AM, Ghaly AE, Hamdullahpur F, Ugursal VI. Mathematical modeling of a fluidized bed rice husk gasifier: Part III – model verification. Energy Sources 2000;22:281–96.
[371] Mansaray KG, Al-Taweel AM, Ghaly AE, Hamdullahpur F, Ugursal VI. Mathematical modeling of a fluidized bed rice husk gasifier: Part I – model development. Energy Sources 2000;22:83–98.
[372] Mansaray KG, Al-Taweel AM, Ghaly AE, Hamdullahpur F, Ugursal VI. Mathematical modelling of a fluidized bed rice husk gasifier: Part II – model sensitivity. Energy Sources 2000;22:167–85.
[373] Souza-Santos ML. A new version of CSFB, comprehensive simulator for fluidised bed equipment. Fuel 2007;86:1684–709.
[374] Souza-Santos ML. CSFB applied to fluidized-bed gasification of special fuels. Fuel 2008;88:826–33.
[375] Souza-Santos ML. Comprehensive simulator (CSFMB) applied to circulating fluidized bed boilers and gasifiers. Open Chem Eng J 2008;2:106–18.
[376] CSFMB: www.csfmb.com.
[377] van den Enden PJ, Silva E. Design approach for a biomass fed fluidized bed gasifier using the simulation software CSFB. Biomass Bioenergy 2004;26: 281–7.
[378] Kurkela E, Ståhlberg P. Air gasification of peat, wood and brown coal in a pressurized fluidized-bed reactor. I. Carbon conversion, gas yields and tar formation. Fuel Proc Technol 1992;31:1–21.
[379] Desrosiers R. Thermodynamics of gas-char reactions. In: Reed TB, editor. A survey of biomass gasification. Colorado: Solar Energy Research Institute; 1979.
[380] Prins MJ. Thermodynamic analysis of biomass gasification and torrefaction. PhD thesis. Technische Universiteit Eindhoven; 2005.
[381] Li X, Grace JR, Watkinson AP, Lim CJ, Ergüdenler A. Equilibrium modelling of gasification: a free energy minimization approach and its application to a circulating fluidized bed coal gasifier. Fuel 2001;80:195–207.
[382] Jand N, Brandani V, Foscolo PU. Thermodynamic limits and actual product yields and compositions in biomass gasification processes. Ind Eng Chem Res 2006;45:834–43.
[383] Bacon DW, Downie J, Hsu JC, Peters J. Modeling of fluidized bed gasifiers. In: Milne TA, Mudge KL, editors. Fundamentals of thermochemical biomass conversion. London, UK: Elsevier Applied Science; 1985. p. 717–32.
[384] Watkinson AP, Lucas JP, Lim CJ. A prediction of performance of commercial coal gasifiers. Fuel 1991;70:519–27.
[385] Kinoshita CM, Wang Y, Takahashi PK. Chemical equilibrium computations for gasification of biomass to produce methanol. Energy Sources 1991;13: 361–8.
[386] Ergüdenler A, Ghaly AE, Hamdullahpur F, Al-Taweel AM. Matematical modelling of fluidized bed straw gasifier: Part I – model development. Energy Sources 1997;19:1065–84.
[387] Ergüdenler A, Ghaly AE, Hamdullahpur F, Al-Taweel AM. Matematical modelling of fluidized bed straw gasifier: Part II – model sensitivity. Energy Sources 1997;19:1085–98.
[388] Ergüdenler A, Ghaly AE, Hamdullahpur F, Al-Taweel AM. Mathematical modelling of fluidized bed straw gasifier: Part III – model verification. Energy Sources 1997;19:1099–121.
[389] Schuster G, Löffler G, Weigl K, Hofbauer H. Biomass steam gasification an extensive parametric modeling study. Bioresource Technol 2001;77:71–9.
[390] Mathieu P, Dubuisson R. Performance analysis of a biomass gasifier. Energ Conv Manag 2002;43:1291–9.
[391] Scott SA, Harris T, Dennis JS, Hayhurst AN, Davidson JF. Gasification of biomass: the consequences of equilibrium. Proc Int Conf on Fluidized Bed Combustion 2003;17:1–13.
[392] Gómez-Barea A, Arjona R, Ollero P. Pilot plant gasification of olive stone: a technical assessment. Energy Fuels 2005;19:598–605.
[393] Kersten SRA, Prins W, van der Drift A, van Swaaij WPM. Interpretation of biomass gasification by ''quasi''-equilibrium models. In: Palz W, Spitzer J, Maniatis K, Kwant K, Helm P, Grassi A, editors. Amsterdam: Proc 12th European Conf on Biomass for Energy, Industry and Climate Protection, vol. 1; 2002. p. 777–80.
[394] Gómez-Barea A, Thunman H, Leckner B, Campoy M, Ollero P. Prediction of gas composition in biomass gasifiers. 2nd Int Congress of Energy and Environment Engineering and Management (IICIIEM2007). Badajoz, Spain. Paper ref. ER-030; 2007.
[395] Gumz W. Gas producers and blast furnaces. New York: John Wiley and Sons; 1950.